ISAS INTERNATIONAL SCHOOL FOR ADVANCED STUDIES

NON THERMAL RADIATIVE PROCESSES IN COMPACT SOURCES

by

Gabriele Ghisellini

A thesis submitted for the degree

of *Doctor Philosophiae*

Trieste – December 1987

Supervisors

Roland Svensson

Marek A. Abramowicz

TABLE OF CONTENTS

Acknowledgments

My greatest debt of gratitude is owed to Roland Svensson: from him I learned almost everything I know about pairs. He steadily fought against my ignorance, and fortunately, sometimes won.

I benefitted from daily conversations and discussions with him, and with Marek Abramowicz, Laura Maraschi and Aldo Treves, and, more important, they helped me to find my way to research.

Special thanks are due to to my friend and colleague Piero Madau, with whom I enjoyed a fruitful collaboration and never ending day and night long discussions.

Paul Guilbert offered me his knowledge and experience (and his personal hospitality, too) for the better understanding of the synchrotron reheating problem.

I acknoweledge the constant encouragement of Dennis Sciama, director of the Astrophysics Sector of SISSA. He also allowed me to partecipate to interesting meetings, and in particular to a stimulating program on AGNs at the Institute for Theoretical Physics in Santa Barbara.

I thank Chris Pethick, director of Nordita, where I have been for several months, supported by a Della Riccia fellowship.

Thanks are due to my colleagues Roberto Scaramella, sharp in focussing my confused problems, and to Tomaso Belloni and Silvano Molendi for fruitful interactions.

This thesis is dedicated to the memory of my mother.

"Che fai tu, luna, in ciel? dimmi, che fai,
Silenziosa luna?"

Giacomo Leopardi (*Canto notturno di un pastore errante dell'Asia*)

INTRODUCTION

The regions sorroundings black holes can be the site of the most spectacular phenomena in the Universe. From these regions, electromagnetic waves extending from the radio to the γ−ray band have been detected, covering more than ten decades in frequency.

Active galactic nuclei (AGNs) emit, very approximately, constant luminosity per logarithmic bandwidth and a power law can fit their continuum in restricted frequency ranges. A subclass of AGNs (BL Lac objects and highly polarized quasars, HPQs) show high polarization in the radio to optical band, suggesting that the emission is due to the synchrotron process. This requires the presence of a population of a magnetic field and of relativistic electrons with a power law distribution in energy. If the source is compact, prediction of this model is that synchrotron photons will be boosted to X- and γ-ray energies by inverse Compton scattering with the relativistic electrons. This model, briefly called synchrotron self Compton (SSC), has been the object of extensive and detailed studies soon after the discovery of quasars and the conviction of their extragalactic nature. Since then, the SSC has been widely adopted for interpreting at least in part the continuum of AGNs.

The key assumption of the SSC model in its "standard" version (e.g. Ginzburg & Syrovatskii 1965, Jones, O'Dell & Stein 1974) is that the energy distribution of the relativistic particles is a power law.

A more consistent approach is to solve the kinetic equation for the relativistic particles (a continuity equation in the energy space), assuming e.g. a power law or monoenergetic distribution of *injected* particles, and to follow its time evolution or deriving the particle distribution function in the case of steady state.

In extended radio sources, the lifetime of a relativistic population of particles against radiative energy losses can be long, compared to other timescales, the shortest of which is the light crossing time of the source. Hence the assumed energy distribution will not be substantially modified. Cavaliere & Morrison (1980) found

that the luminosity to size ratio L/R is the key parameter measuring the ratio of the cooling time to the light crossing time. The dimensionless version of L/R, is the so called *compactness* parameter ℓ (Guilbert, Fabian & Rees 1983)

$$\ell \equiv \frac{L}{R}\frac{\sigma_T}{mc^3}$$

where σ_T is the Thomson cross section, and m is the electron rest mass. When $\ell > 1$, the inverse Compton cooling timescale is shorter than the light crossing time R/c for any relativistic particle energy. In this case in order to mantain a stationary energy distribution new energetic particles must be continuously supplied to the source, or the cool ones must be reaccelerated to relativistic energies. For ℓ approaching one, the effects of radiation on the particles which produce it start becoming important, and the study of the possible self consistent equilibria for the particle distribution function is essential. Three points have to be stressed:

1) Low frequency synchrotron radiation is self absorbed by the lowest energy electrons present in the source, modifying their *net* cooling rate, as a result of emission and absorption.

2) The scattering probability *decreases* as the product of the interacting photon and particle energies is increased, due to the decline of the Klein Nishina cross section. Then for a particle of given energy γmc^2 only a *fraction* of the radiation energy density, smaller for larger γ, is effective in the Compton cooling process.

3) In non thermal models where the inverse Compton is an efficient cooling process, photons are produced with energy up to the maximum energy of the emitting particles. The $\gamma-$rays produced inside the source can collide with target photons of lower energy, producing electron-positron pairs, which share the energy of the original photons. These pairs have to be considered as an extra injection of relativistic particles, besides the primary ones.

If the ultimate source of power in compact sources is accretion onto a black hole, the compactness ℓ can be rewritten in terms of the Eddington luminosity L_E and the

Schwarzschild radius R_s

$$\ell = \frac{2\pi}{3}\frac{3R_s}{R}\frac{m_p}{m_e}$$

Then the (pair free) Eddington limit corresponds to $\ell_E \sim 4000$ and defines the upper limit of the values of ℓ considered in this thesis.

On the observational side the compactness ℓ can be derived from the *observed* luminosity and the shortest variability timescale. Both these quantities may not be indicative of the intrinsic ones, if the emission is not isotropic and/or relativistic effects due to bulk motion of the source are important. However, values of ℓ derived by short term variability in X-rays seem to correlate with those indirectly found assuming Keplerian motion of the emission line clouds sorrounding the compact core of an AGN (Wandel & Mushotzky 1986), and an average value of $\ell \sim 10^{-2}\ell_E$ (Lightman & Zdziarski 1987) is suggested for a sample of non blazar sources. Note that the value of ℓ derived from variability in a particular band does not necessarily extend to other bands of the spectrum. For instance transparent radio emission must be produced in a much larger volume than that responsible for the rapidly variable high energy radiation of the sources considered by the above authors.

The plan of the thesis is the following:

In the first chapter I critically review the basic theory of synchrotron radiation and inverse Compton emission in the astrophysical context. In particular, the energy balance of an electron emitting and absorbing synchrotron radiation and the consequences on the particle kinetic equation are discussed, deriving new results contrasting earlier studies (Rees 1967a, McCray 1969).

The second chapter is devoted to the application of the standard SSC model to blazars. The homogeneous model is used as a tool to derive the Doppler enhancement factor, due to relativistic bulk motion, for a sample of BL Lac and HPQ sources. More complicated jet inhomogeneous geometries are then considered, and a specific model constructed, to explain the different spectra observed for blazars selected either by radio means or by their X-ray emission.

In the third chapter the particle kinetic equation is considered. Solutions are discussed under the assumption of steady state and neglecting pair production processes. Synchrotron self absorption is found to play a major role when the source term of relativistic particles is a steep power law. In this case multiple Compton scatterings are always important and provide the bulk of the emission in the whole energy range even if the magnetic to radiation energy density ratio is much greater than one. In these models, the emitted $\gamma-$ray luminosity is small, and pair production can be consistently neglected.

The fundamental processes acting in plasmas in which pair production play a dominant role are reviewed in the fourth chapter. Both thermal and non thermal plasmas are considered, and an overview of the most important work on the subject is given.

The fifth chapter deals with the effects of pair production in SSC models. A full set of equations is given (which is solved for analytically when possible, and numerically in other cases), to find the steady equilibrium distributions of particles and photons.

It is shown that models in which synchrotron photons can reach $\gamma-$ray energies, and produce pairs, can be described in a way similar to models in which pairs are created by photons produced by inverse Compton scattering on a soft external radiation field. Important differences are however found, and enphasized.

A second class of models which has been considered assumes the synchrotron process as the dominant cooling mechanism, even if extending at energies below the pair production threshold. Here pairs created by inverse Compton photons can be handled as a perturbation carrying a small fraction of the total luminosity, but with important consequences in restricted energy intervals, particularly in X- and γ-rays.

Finally, the third class of models assumes inverse Compton as the dominant cooling mechanism. Here most of the luminosity is emitted at γ-ray energies. Then pair production processes are very important and reprocess the entire spectrum. Con-

trary to earlier investigations (Bonometto & Rees 1971, Kazanas 1984), the steady equilibrium photon spectrum is characterized by a spectral index flatter than unity up to hard X-rays, which is therefore the energy band where most of the luminosity emerges. Furthermore the spectrum flattens when the ratio of the magnetic to radiation energy density decreases.

A discussion of the relevance of the obtained results on observations concludes the thesis.

CHAPTER ONE

SYNCHROTRON RADIATION AND INVERSE COMPTON EMISSION

The basic synchrotron and inverse Compton formulae are discussed. The problem of synchrotron self absorption is discussed in detail, and new results are found for the absorption rate of the emitting and absorbing particles. Photon spectra produced by the inverse Compton process using an approximated form for the Klein Nishina cross section are compared to more exact results, and the approximation made is found to be acceptable.

1.1 Synchrotron radiation

A relativistic electron of energy γmc^2 and Lorentz factor γ spiraling in a magnetic field B emits a power

$$p(\gamma,\theta) = 2\sigma_T c U_B \gamma^2 \beta^2 \sin^2\theta \tag{1.1}$$

where σ_T is the Thomson cross section, θ is the pitch angle, U_B is the magnetic energy density $B^2/8\pi$. For $\gamma \gg 1$, the spectrum of the emitted radiation becomes continuous and can be described by

$$p(\nu,\gamma,\theta) = \frac{\sqrt{3}e^3 B}{mc^2}\frac{\nu}{\nu_c}\sin\theta\int_{\nu/\nu_c}^{\infty} dx K_{5/3}(x) \tag{1.2}$$

$$\nu_c = \frac{3}{2}\nu_B\gamma^2\sin\theta \equiv \frac{3}{2}\frac{eB}{2\pi mc}\gamma^2\sin\theta \tag{1.3}$$

Here $K_{5/3}(x)$ is the modified Bessel function of order 5/3. This spectrum peaks at $\nu = 0.29\nu_c$, while the mean frequency is $<\nu> \simeq (4/3)\nu_c$. The function $F(x) = x\int_x^\infty dy K_{5/3}(y)$, with $x = \nu/\nu_c$, can be approximated by $F'(x)$ =const$\times x^{1/3}e^{-x}$, which peaks at $\nu = \nu_c/3$ and has $<\nu> = (4/3)\nu_c$. The two (normalized) functions are plotted in fig. 1.1.

The synchrotron emissivity produced by a power law of relativistic electrons of differential energy spectrum

$$N(\gamma) = K\gamma^{-p}, \quad \gamma_{min} < \gamma < \gamma_{max} \tag{1.4}$$

is, far from the endpoints, and for $p > -1/3$ (see, e.g. Ginzburg & Syrovatskii 1965, Rees 1967a)

$$\epsilon_s(\nu,\theta) = \frac{1}{4\pi}\int d\gamma N(\gamma) p(\nu,\gamma,\theta)$$

$$= \frac{3\sigma_T c K U_B}{8\pi^2\nu_B}\left(\frac{\nu}{\nu_B}\right)^{-\frac{p-1}{2}} (\sin\theta)^{\frac{p+1}{2}} 3^{p/2}\frac{\Gamma(\frac{3p-1}{12})\Gamma(\frac{3p+19}{12})}{p+1} \tag{1.5}$$

For $p < -1/3$ the highest energy electrons dominate the emission, and the spectrum resembles the spectrum of the single electron at energy γ_{max}. For frequencies smaller than $\frac{3}{2}\nu_B\gamma_{min}^2$ the emission come from the lowest energy electrons and has a slope of 1/3. Above $\frac{3}{2}\nu_B\gamma_{max}^2$ the spectrum has an exponential cutoff.

Averaging eq. (1.5) over angles, for a random distribution of pitch angles we have (e.g. Ginzburg & Sirovatskii 1965, Blumenthal & Gould 1970)

$$\epsilon_s(\nu) = \frac{3\sigma_T c K U_B}{16\pi\sqrt{\pi}\nu_B}\left(\frac{\nu}{\nu_B}\right)^{-\frac{p-1}{2}} 3^{\frac{p}{2}}\frac{\Gamma(\frac{p+5}{4})}{\Gamma(\frac{p+7}{4})}\frac{\Gamma(\frac{3p-1}{12})\Gamma(\frac{3p+19}{12})}{p+1} \tag{1.6}$$

An accurate expression for $\epsilon_s(\nu)$ can be obtained using a $\delta-$ function approximation for $p(\nu,\gamma)$. Choosing $p(\nu,\gamma) = p(\gamma)\delta(\nu - \frac{4}{3}\nu_B\gamma^2)$, and for a random pitch angle distribution we have

$$\epsilon_s(\nu) = \frac{1}{4\pi}\frac{\tau_c}{2}\frac{1}{R/c}\frac{U_B}{\nu_B}\left(\frac{3\nu}{4\nu_B}\right)^{-\frac{p-1}{2}} \tag{1.7}$$

which agrees with eq. (1.6) to within 20% for $2 < p < 4$. Here $\tau_c \equiv KR\sigma_T$. As suggested by Blumenthal & Gould (1970), the synchrotron process can be thought as an inverse Compton scattering against the virtual magnetic photons of frequency ν_B. In eq. (1.7) $(U_B/\nu_B)/(R/c)$ can be thought as the production rate of these virtual photons, of which a fraction $\sim \tau_c/2$ undergoes scattering being boosted in energy by the factor $\frac{4}{3}\gamma^2$.

1.2 Synchrotron self absorption

If the source is compact enough, the absorption of synchrotron photons by the same electrons which produced them must be considered. Due to the non thermal nature of the process, the absorption coefficient cannot be derived by the Kirchoff law, but must be computed by means of the Einstein coefficients and their relations. In the presence of a radiation field $I(\nu)$, the net power absorbed by a single electron is

$$\dot{\gamma}_{abs}(\nu) = I(\nu)\frac{h\nu}{mc^2}(B_{23} - B_{21}) \tag{1.8}$$

where the Einstein coefficients A_{ij}, B_{ij} are related by (in energy space)

$$B_{21} = \left[\frac{\gamma - h\nu/(mc^2)}{\gamma}\right]^2 B_{12} = \frac{c^2}{2h\nu^3}A_{21} = \frac{c^2}{2h^2\nu^4}p(\nu,\gamma) \tag{1.9}$$

These relations only hold for $\gamma \gg 1$ (i.e. if the linear momentum can be approximated with γmc). The contribution of the single electron to the absorption coefficient κ_ν is $\dot{\gamma}_{abs}/I(\nu)$. Integrating over the electron distribution function $N(\gamma)$ we have

$$\kappa_\nu(\theta) = \frac{1}{8\pi h\nu^3}\int_{\gamma_1}^{\gamma_2} d\gamma \frac{N(\gamma)}{(\gamma mc^2)^2}\left[(\gamma + \frac{h\nu}{mc^2})^2 p(\nu, \gamma + \frac{h\nu}{mc^2}, \theta) - \gamma^2 p(\nu,\gamma,\theta)\right] \tag{1.10}$$

In the frequency range where self absorption is important we always have $h\nu \ll mc^2$. Then

$$\kappa_\nu(\theta) = \frac{1}{8\pi m\nu^2}\int_{\gamma_1}^{\gamma_2} d\gamma \frac{N(\gamma)}{\gamma^2}\frac{d}{d\gamma}[\gamma^2 p(\nu,\gamma,\theta] \tag{1.11a}$$

In this form the absorption coefficient can be computed for any $N(\gamma)$ distribution (i.e. not continuous). It reduces to the usual expression (e.g. Ginzburg & Sirovatskii 1965) when the limit of integration can be taken one and infinity. But it must be kept in mind that at low energies the emission function $p(\nu,\gamma)$ consists of the superposition of discrete cyclotron harmonics, and eq. (1.2) is no longer valid. Furthermore, the momentum p is no longer proportional to the energy, and the γ^2 terms should be replaced by γp.

For power law electron distribution of the form of eq. (1.4), and in a frequency range such that $\nu \gg \frac{3}{2}\nu_B\gamma_{min}^2$, $\gamma_{min} \gg 1$, we have

$$\kappa_\nu(\theta) = \frac{3^{\frac{p+1}{2}}}{4}\Gamma\left(\frac{3p+22}{12}\right)\Gamma\left(\frac{3p+2}{12}\right)\frac{e^2K}{mc}(\nu_B\sin\theta)^{\frac{p+2}{2}}\nu^{-\frac{p+4}{2}} \qquad (1.11b)$$

The average over the pitch angle distribution (if isotropic) yields another factor

$$< (\sin\theta)^{\frac{p+2}{2}} >= \frac{\sqrt{\pi}}{2}\frac{\Gamma(\frac{p+6}{4})}{\Gamma(\frac{p+8}{4})} \qquad (1.12)$$

in the same frequency range the source function $S(\nu) = \epsilon_s(\nu)/\kappa_\nu$ is

$$S(\nu,\theta) = \frac{2m}{\sqrt{3}}\frac{\nu^{5/2}}{(\nu_B\sin\theta)^{1/2}}f(p) \qquad (1.13)$$

$$f(p) = \frac{\Gamma(\frac{3p-1}{12})\Gamma(\frac{3p+19}{12})}{(p+1)\Gamma(\frac{3p+2}{12})\Gamma(\frac{3p+22}{12})} \qquad (1.14)$$

$$S(\nu) = \frac{2m}{\sqrt{3}}\frac{\nu^{5/2}}{\nu_B^{1/2}}f'(p) \qquad (1.15)$$

$$f'(p) = f(p)\frac{\Gamma(\frac{p+5}{4})\Gamma(\frac{p+8}{4})}{\Gamma(\frac{p+7}{4})\Gamma(\frac{p+6}{4})} \qquad (1.16)$$

Eqs. (1.13) and (1.15) are valid for $p > -2/3$. For $p < -2/3$ the main contribution to both the emission and the absorption coefficients comes from electrons of energy close to γ_{max}, and the source function becomes proportional to ν^2 (Rees 1967a). This always happens when the intensity at different frequencies comes from electrons of the same energy. The characteristic behaviour $\nu^{5/2}$ of the synchrotron self absorbed radiation can in fact be found identifying the brightness temperature T_b with the electron energy $\gamma(\nu)mc^2$ of the electrons mainly radiating at the frequency ν. From the Raleigh Jeans law one has

$$S(\nu) \sim 2kT_b\frac{\nu^2}{c^2} = 2m\gamma(\nu)\nu^2 \sim 2m\nu^{5/2}\nu_B^{-1/2} \qquad (1.17)$$

If instead $\gamma(\nu)$ is constant, the ν^2 dependence is found.

For $-2/3 < p < 1/3$ the emission comes from electrons of the highest energies at all frequencies, while electrons of energy $\gamma \sim (\nu/\nu_B)^{1/2}$ gives the dominant contribution to the absorption coefficient at the frequency ν. In this case $S(\nu) \propto \nu^{\frac{3p+14}{6}}$

(Rees 1967a). The same result can be found using the approximate form for the single electron spectrum $[F'(x) \propto x^{1/3}e^{-x}]$.

For $p > 1/3$, the coupling between photons of energy ν and electrons of energy $\gamma \sim (\nu/\nu_B)^{1/2}$ is tight both for the emission and the absorption process. Then the source function is remarkably insensitive to the slope of the electron distribution, being slightly lower for steeper electron spectra, as can be seen from fig. 1.2, where $f(p)$ and $f'(p)$ are plotted.

From the equation of energy transfer, assuming a slab geometry, one has

$$I(\nu) = S(\nu)(1 - e^{-\tau_\nu}) = \epsilon_s(\nu)R\frac{1 - e^{-\tau_\nu}}{\tau_\nu} \tag{1.18}$$

where $\tau_\nu = \kappa_\nu R$ is the absorption optical depth, and R is the size of the source. The self absorption frequency has not a unique definition in the literature. One can define the self absorption frequency ν_t as the one for which the optical depth is unity

$$\nu_t = \left[\frac{3^{p/2}\sqrt{3\pi}}{8}\frac{\Gamma(\frac{3p+22}{12})\Gamma(\frac{3p+2}{12})\Gamma(\frac{p+6}{4})}{\Gamma(\frac{p+8}{4})}\frac{e^2KR\nu_B^{\frac{p+2}{2}}}{mc}\right]^{\frac{2}{p+4}} \tag{1.19}$$

or define ν_m as the frequency where a maximum in the spectrum occurs. This defines the optical depth $\tau_m = \tau(\nu_m)$

$$e^{\tau_m} = 1 + \tau_m\frac{p+4}{5} \tag{1.20}$$

(Pacholczyk, 1970). Furthermore, one can assume geometries different from the slab (see Urry 1984 for an extensive review on this subject). Solving eq. (1.20) for τ_m and sobstituting in eq. (1.18), we can find the value of the magnetic field B in terms of the angular diameter θ_d of the source, its self absorption frequency ν_m and the flux at this frequency $F_m = S(\nu_m)\pi\theta_d^2/4$

$$B = \frac{\pi^3 m^3 c}{6e}f'^2(p)(1 - e^{-\tau_m})^2 F_m^{-2}\theta_d^4\nu_m^5$$

$$= 1.34 \times 10^{-3}f'^2(p)(1 - e^{-\tau_m})^2\left(\frac{F_m}{\text{Jy}}\right)^{-2}\left(\frac{\theta_d}{\text{mas}}\right)^4\left(\frac{\nu_m}{\text{GHz}}\right)^5 \text{G} \tag{1.21}$$

From eq. (1.18) we can find the parameter τ_c in terms of the same observables. As will shown later, τ_c directly measures the importance of the inverse Compton effect

$$\tau_c = \frac{F_m \nu_m^{\frac{p-1}{2}} B^{-\frac{p+1}{2}}}{\theta_d^2} \frac{\tau_m}{1-e^{-\tau_m}} \left(\frac{2\pi mc}{e}\right)^{\frac{p-3}{2}} \frac{8^3 \pi \sqrt{\pi}(p+1)\Gamma(\frac{p+7}{4})}{3^{p/2} 3c \Gamma(\frac{p+5}{4})\Gamma(\frac{3p-1}{12})\Gamma(\frac{3p+19}{12})} \quad (1.22)$$

As for B, also τ_c strongly depends on the observables [$\tau_c \propto F_m^{2\alpha+3} \nu_m^{-4\alpha-5} \theta_d^{-6-4\alpha}$, with $\alpha = (p-1)/2$]. In addition, many authors have used in the past different definition of the self absorption frequency, different approximations, or made some mistakes, so that at least a dozen of different formulae exist in the literature for deriving the magnetic field and the particle density in a source of known parameters (Urry 1984).

1.3 Synchrotron self absorption: energy balance

If Compton losses can be neglected, eq. (1.18) assures that all the power emitted in the self absorbed regime must be reabsorbed. However, this *does not* imply, as noted by Rees (1967a), that each electron is in detailed balance with the photon field, emitting and absorbing the same amount of energy, even if a strong coupling exists between electrons of energy γmc^2 and photons of frequencies $\sim \gamma^2 \nu_B$, both for the emission and the absorption process. The spectrum of radiation absorbed by the single electron, in fact, depends on the radiation field, which in turn depends on the slope of the electron distribution. This can be seen directly from eq. (1.8) which becomes

$$\dot{\gamma}_{abs}(\nu,\gamma,\theta) = \frac{1}{2m\gamma^2} \frac{I(\nu,\theta)}{\nu^2} \frac{d}{d\gamma}[\gamma^2 p(\nu,\gamma,\theta)] \quad (1.23)$$

For $\tau_\nu \gg 1$, and for power law electron distributions, $I(\nu,\theta)$ is described by eqs.

(1.13), (1.14). Then

$$\dot{\gamma}_{abs}(\nu,\gamma,\theta) = \frac{4\pi\sqrt{3}}{\sqrt{2}}\frac{e^2\nu_B\sin\theta}{c}f(p)\left(\frac{\nu}{\nu_c}\right)^{5/2}K_{5/3}\left(\frac{\nu}{\nu_c}\right) \qquad (1.24)$$

which can be compared with $p(\nu,\gamma,\theta)$ (eq. 1.2). Since the behaviour of $x^{5/2}K_{5/3}(x)$ is approximately $x^{-1/6}e^{-x}$, most of the radiation absorbed by an electron of energy γ has frequencies close to ν_c.

The total absorption rate is the integral of $\dot{\gamma}_{abs}(\nu,\gamma,\theta)$ over frequency, but can be found only for electrons with $\gamma \gg 1$, for the reasons outlined when describing the absorption coefficient. Then for power law electron distribution we have [setting $\dot{\gamma}_e(\gamma,\theta) = p(\gamma,\theta)$]

$$\dot{\gamma}_{abs}(\gamma,\theta) = \frac{9\sqrt{3}}{4\pi\sqrt{2}}\dot{\gamma}_e(\gamma,\theta)f(p)\int_0^\infty dx x^{5/2}K_{5/3}(x)\left[1-e^{-\tau(x)}\right] \qquad (1.25)$$

When $\tau(x) \gg 1$, so for $\gamma \ll \gamma_t$ (where $\gamma_t \equiv [3\nu_t/(4\nu_B)]^{1/2}$), we have the result of Rees (1967a) (correcting for a misprint in his numerical coefficient)

$$\dot{\gamma}_{abs}(\gamma,\theta) = \frac{9\sqrt{3}}{2\pi}f(p)\Gamma\left(\frac{31}{12}\right)\Gamma\left(\frac{11}{12}\right)\dot{\gamma}_e(\gamma,\theta), \quad 1 \ll \gamma \ll \gamma_t \qquad (1.26)$$

Since $f(p)$ is a decreasing function of p, $\dot{\gamma}_{abs} > \dot{\gamma}_e$ for flat electron distributions, while the opposite is true for electron spectrum slopes steeper than the critical index $p_{crit} = 3$. The electrons absorb more photons for higher radiation intensities, while their emission rate remains fixed. However it must be stressed that eq. (1.26) is valid only in the allowed range of energies. The electrons with $\gamma \sim \gamma_t$ will always loose rather than gain energy, due to the decreasing radiation intensity above ν_t. On the other extreme, the electrons with γ close to unity experience a net heating, independently on the slope p, as can be suggested by energy conservation arguments. An example can clarify the last statement. Consider a steady electron distribution $N(\gamma) \propto \gamma^{-p}$ with $p = 5$, $\gamma_{min} = 1$. Eq. (1.26) in this case yields $\dot{\gamma}_{abs}(\gamma) \simeq 0.5\dot{\gamma}_e(\gamma)$. If this were true for all electrons, including the low energy ones, the total emitted luminosity would be a factor $\gamma_t^2/2$ greater than the absorbed one. Then the energy lost by the electrons with $1 \ll \gamma_{crit} \leq \gamma \leq \gamma_t$ must be absorbed by the lowest

energy electrons present, with $1 \leq \gamma \leq \gamma_{crit}$, where γ_{crit} is some critical energy for which gains and losses balance. This will be true independently of the details of the emission and absorption processes (synchrotron or cyclo-synchrotron), since directly follows from the radiative transfer equation (eq. 1.18). The *value* of γ_{crit} must, however, be found by a detailed treatment of the cyclo-synchrotron process, unless the $N(\gamma)$ distribution has a low energy cutoff $\gamma_{min} \gg 1$, which allows to use standard synchrotron formulae. In this case the source function $S(\nu)$ is not a unique power law, being proportional to ν^2 below $\nu_{c,min} = \frac{3}{2}\gamma_{min}^2 \nu_B \sin\theta$, where electrons of energy γ_{min} predominantly contribute to the emission and absorption. Thus these electrons can absorb more photons with respect to the $S(\nu) \propto \nu^{5/2}$ case, and consequently gain rather than loose energy. In the case of $\gamma_{min} \gg 1$ the source function $S(\nu, \theta)$ is

$$S(\nu,\theta) = \frac{m\nu^{5/2}}{(\frac{3}{2}\nu_B \sin\theta)^{1/2}} \frac{\int_0^{\nu/\nu_{c,min}} dx x^{\frac{p-1}{2}} \int_x^\infty dy K_{5/3}(y)}{\int_0^{\nu/\nu_{c,min}} dx x^{\frac{p+2}{2}} K_{5/3}(x)} \tag{1.27}$$

Eq. (1.27) reduces to the usual form (eq. 1.13) for $\nu \gg \nu_{c,min}$, while, for $\nu < \nu_{c,min}$, taking the asymptotic behaviours of the integrands we have

$$S(\nu) \simeq \frac{3}{2} m \frac{3p+2}{3p-1} \gamma_{min} \nu^2, \quad \nu < \nu_{c,min} \tag{1.28}$$

Eq. (1.27) can be used to compute the absorption rate at any energy

$$\dot{\gamma}_{abs}(\gamma,\theta) = \dot{\gamma}_e(\gamma,\theta) \frac{9\sqrt{3}}{8\pi} \int_{\frac{2}{3\gamma^2}}^\infty dx x^{5/2} K_{5/3}(x)(1 - e^{-\tau(x)}) \times \frac{\int_0^{x(\gamma/\gamma_{min})^2} dy y^{\frac{p-3}{2}} F(y)}{\int_0^{x(\gamma/\gamma_{min})^2} dy y^{\frac{p+2}{2}} K_{5/3}(y)} \tag{1.29}$$

In fig. 1.3 the function $\dot{\gamma}_{abs}(\gamma,\theta)/\dot{\gamma}_e(\gamma,\theta)$ is plotted for different values of p, choosing $\gamma_t = 50$ and $\gamma_{min} = 2$. As can be seen, the functions have a plateau for intermediate energies, where they have the value of eq. (1.26). But for any value of p there is a range $\gamma_{min} < \gamma < \gamma_{crit}$ where electrons gain energy. The value of γ_{crit} is a function of p and γ_{min} for $p > 3$, while for $p < 3$ it becomes function of p and γ_t. For $\gamma_{min} = 2$ and $\gamma_t = 50$ we have

p	1.0	1.5	2.0	2.5	3.0	3.5	4.0	4.5	5.0
γ_{crit}	49	40	30	23	17	3.7	3.2	2.7	2.6

One can then compute the total power absorbed P_a and the total power emitted P_e by the electrons emitting in the self absorbed region of the spectrum

$$\frac{P_a - P_e}{P_e} = \frac{\int_{\gamma_{min}}^{\gamma_t} d\gamma \gamma^{-p} \dot{\gamma}_{abs}(\gamma)}{\int_{\gamma_{min}}^{\gamma_t} d\gamma \gamma^{-p} \dot{\gamma}_e(\gamma)} - 1 \tag{1.30}$$

Due to the complexity of the function $\dot{\gamma}_{abs}(\gamma)$, the integration was performed numerically for different values of p. The results are in all cases close to zero. The scatter around this value is due to the somewhat arbitrary choice of γ_t as the energy separating the thin and the thick regime. Another approximate derivation, due to Guilbert (private communication) is as follows. The total power absorbed from the radiation field is

$$P_a = \int_0^\infty \kappa_\nu I(\nu) d\nu = \int_0^\infty \epsilon_s(\nu) \left[1 - e^{-\tau(\nu)}\right] d\nu \tag{1.31}$$

This expression includes the power absorbed by the electrons with $\gamma > \gamma_t$, but this contribution is negligible. The power emitted by the electrons with $\gamma < \gamma_t$ is

$$\begin{aligned} P_e &= \int_0^\infty d\nu \int_{\gamma_{min}}^{\gamma_{max}} p(\nu, \gamma) N(\gamma) d\gamma \\ &= \int_0^\infty \epsilon_s d\nu - \int_{\gamma_t}^{\gamma_{max}} p(\nu, \gamma) N(\gamma) d\gamma \end{aligned} \tag{1.32}$$

so that the difference is

$$P_a - P_e = \int_0^\infty \left[\epsilon_s(\nu) e^{-\tau(\nu)} - \int_{\gamma_t}^{\gamma_{max}} N(\gamma) p(\nu, \gamma) d\gamma \right] d\nu \tag{1.33}$$

The emitted and absorbed power are thus equal if all the radiation that escapes the source is provided by those electrons with $\gamma > \gamma_t$, which is approximately true, since the spectrum radiated by the single electron is peaked. Note that this derivation is independent on the specific emission mechanism (synchro or cyclo- synchrotron) and hence is valid even for $\gamma_{min} = 1$.

So far Compton losses have been neglected, requiring $U_B \gg U_r$, but eq. (1.26) can be easily extended to the case of arbitrary value of the ratio U_B/U_r. Furthermore, the influence of averaging over pitch angles can be seen, using $f'(p)$ instead of $f(p)$ (eqs. 1.14, 1.15). Now the cooling rate $\dot{\gamma}_e(\gamma)$ is the sum of the synchrotron and the inverse Compton one (see section 1.5 below)

$$\dot{\gamma}_e(\gamma) = \dot{\gamma}_e^s(\gamma) + \dot{\gamma}_e^c(\gamma) = \dot{\gamma}_e^s(\gamma)\,(1 + U_r/U_B)$$

The value of p_{crit} for which gains and losses balance is given by solving

$$\frac{9\sqrt{3}}{2\pi} f'(p_{crit}) \Gamma\left(\frac{31}{12}\right) \Gamma\left(\frac{11}{12}\right) = 1 + \frac{U_r}{U_B} \tag{1.34}$$

In fig. 1.4 p_{crit} is plotted vs. U_B/U_r. Due to the differences between $f(p)$ and $f'(p)$, p_{crit} for $U_r/U_B = 0$ is now 3.15 and not 3. As before, p_{crit} is an approximate solution only in the range $1 \ll \gamma \ll \gamma_t$. We can easily understand the general behaviour of $p_{crit}(U_r/U_B)$, reminding that the self absorbed radiation intensity is higher for smaller p. Thus inclusion of Compton losses requires an increased radiation field to let the absorption rate balance the increased total loss rate.

1.4 Initial relaxation of the electron distribution

Suppose that at the time t_0 a power law electron distribution $N(\gamma, t)$ is emitting and absorbing synchrotron radiation. This distribution will be modified by energy losses and gains, and eventually by injection and escape of particles. This problem has been discussed by McCray (1969), who neglected Compton losses and the escape and the source terms in the kinetic equation for $N(\gamma, t)$. In his paper, furthermore, eq. (1.24) and (1.25) are supposed to hold even at low energies, down to $\gamma = 1$, and this leads to uncorrect results for what concerns low energy electrons.

Considering transitions between the energy levels γ, $\gamma + h\nu/mc^2$, $\gamma - h\nu/mc^2$, expanding in Taylor series about γ, and integrating over all possible levels, one has (McCray 1969, including the escape term)

$$\frac{\partial N(\gamma,t)}{\partial t} = \frac{\partial}{\partial \gamma}[\dot{\gamma}_c(\gamma)N(\gamma)] + \frac{\partial}{\partial \gamma}\left[\gamma^2 C(N,\gamma)\frac{\partial}{\partial \gamma}\left(\frac{N(\gamma,t)}{\gamma^2}\right)\right] + Q(\gamma,t) - \frac{N(\gamma,t)}{t_{esc}} \tag{1.35}$$

where $Q(\gamma,t)$ is the source function, and the coefficient $C(N,\gamma)$ is given by

$$C(N,\gamma) = \frac{1}{2m}\int d\nu \frac{I(\nu)}{\nu^2} p(\nu,\gamma) \tag{1.36}$$

In this notation, $\dot{\gamma}_{abs}(\gamma)$ is given by

$$\dot{\gamma}_{abs}(\gamma) = \frac{1}{\gamma^2}\frac{\partial}{\partial \gamma}[\gamma^2 C(N,\gamma)] \tag{1.37}$$

Rearranging terms, one can write eq. (1.35) in the form of a Fokker Planck equation

$$\frac{\partial N(\gamma,t)}{\partial t} = -\frac{\partial}{\partial \gamma}[<\dot{\gamma}> N] + \frac{\partial^2}{\partial \gamma^2}[N\frac{1}{2}\frac{d}{dt} <(\Delta\gamma)^2>] + S(\gamma,t) - \frac{N(\gamma,t)}{t_{esc}} \tag{1.38}$$

where $<\dot{\gamma}> = -\dot{\gamma}_c(\gamma) + \dot{\gamma}_{abs}(\gamma)$ is the systematic term for the net energy loss rate, while $\frac{1}{2}\frac{d}{dt} <(\Delta\gamma)^2> = C(N,\gamma)$ is the stochastic term. Several approximations must be made in order to find an analytical solution for the initial relaxation $\frac{\partial N(\gamma,0)}{\partial t}$ of the distribution:

1) Consider a power law initial distribution of slope p

2) Neglect the escape and the source terms

3) Consider electrons of $\gamma_{min} \ll \gamma \ll \gamma_t$. With these assumptions the radiation field is described by eq. (1.13) or (1.15). In the paper of McCray the pitch angle is fixed and equal to $\pi/2$, so that eq. (1.13) is used. We can easily extend his results including Compton losses in an isotropic radiation field, for which $\dot{\gamma}_c^c = \dot{\gamma}_c^s(2U_r/3U_B)$

$$\frac{\partial N(\gamma,0)}{\partial t} = g(p)\gamma N(\gamma,0)\frac{2\sigma_T}{mc} U_B \sin^2\theta \tag{1.39}$$

$$g(p) = (2-p)\left[1 + \frac{2U_r}{3U_B} - \frac{p+2}{5}\frac{9\sqrt{3}}{2\pi}\Gamma\left(\frac{31}{12}\right)\Gamma\left(\frac{11}{12}\right) f(p)\right] \tag{1.40}$$

Fig. 1.5 shows $g(p)$ for different values of U_r/U_B. For comparison, the line $g(p) = 2-p$, corresponding to free relaxation (the optically thin limit), is also plotted. As expected, inclusion of Compton losses causes the steady solutions of eq. (1.39) to be flatter than 3. For strong Compton losses only $p = 2$ is a solution. For this value of p, however, the flux of particles in energy space is not zero.

Charugin & Tsvetanov (1980) discussed the same problem treated here, using a δ-function approximation for the emission rates, and deriving the function $p_{crit} = (3 - 6.6U_r/U_B)$ in the limit of small U_r/U_B. However, their eq. 12 does not follow from their eq. 9, which insted yields $g(p) = (2-p)U_r/U_B$, and so does not define any p_{crit}.

It is important to note that the steady solutions of eq. (1.39) defining p_{crit} are not stable. Any departure from the power law distribution of index p_{crit} will grow, even in the range $\gamma_{min} < \gamma < \gamma_t$ where the solution is valid. Furthermore, as discussed before, the low energy electrons are always heated at the expences of the electrons above γ_{crit}, the energy exchange being mediated by the radiation field. This can also be suggested by the kinetic equation: in fact, without injection and escape, the total number of particles must be conserved, so that $\frac{\partial N(\gamma,0)}{\partial t}$ must change sign at some γ. Neglecting Compton losses, and for $p < 3$, the change of sign is provided by the radiative transfer term, which makes $g(p)$ (eq. 1.40) negative for γ close to γ_t. For steeper distribution, instead, $g(p)$ has to become positive for the lowest energy electrons. In both cases $g(p)$ is function of the electron energy.

These considerations suggest that the only stable solution of eq. (1.35) for self absorbed sources, without injection, escape, and Compton losses, is a Maxwellian distribution, with temperature of the order of the mean energy of the initial distribution function. Strong Compton losses ($U_r > U_B$) will make the reabsorption term unimportant, and will let the initial $N(\gamma,0)$ distribution relax as in a thin source.

A general discussion of the steady solutions of eqs. (1.35) or (1.38) will appear elsewhere (Ghisellini, Guilbert, & Svensson, in preparation), but some features can

be suggested in the simple case of monoenergetic electron injection at an energy $\gamma_{max} > \gamma_t$. Solving for steady state, and integrating once, eq.(1.38) becomes

$$N(\gamma) < \dot{\gamma} > -\frac{\partial}{\partial \gamma}\Big[N(\gamma)C(N,\gamma)\Big] + Q_0 - \frac{\int_\gamma N(\gamma)d\gamma}{t_{esc}} = 0 \qquad (1.41)$$

where a monoenergetic electron source function is assumed: $Q(\gamma) = Q_0\delta(\gamma - \gamma_{max})$. Steady state requires particle conservation: $Q_0 t_{esc} = \int_1^{\gamma_{max}} N(\gamma)d\gamma$, and if $N(\gamma)$ is peaked at some energy γ_p, as the previous consideration suggest, we have $\gamma_p N(\gamma_p) \sim Q_0 t_{esc}$ =const. Above γ_t, the distribution will have the usual form: $N(\gamma) = Q_0/\dot{\gamma}_e \propto \gamma^{-2}$, since reabsorption and escape are unimportant. We can estimate the value of γ_p from a luminosity balance condition. Neglect for the moment the luminosity emerging from the self absorbed region of the spectrum, assuming that all these photons are reabsorbed to mantain a peaked energy distribution of particles. The escaping luminosity is in this case in the form of kinetic energy of escaping electrons, synchrotron and inverse Compton photons produced by particles with $\gamma > \gamma_t$, and photons produced by the inverse Compton process by particles with $\gamma < \gamma_t$. Very crudely, approximate the latter luminosity with

$$L_c(\gamma < \gamma_t) \approx N(\gamma_p)\gamma_p\dot{\gamma}_c(\gamma_p)\,Vol\,mc^2 \approx Q_0 t_{esc} Vol\,mc^2\dot{\gamma}_c(\gamma_p)$$

where $\dot{\gamma}_c(\gamma)$ is the Compton cooling rate. Balancing the injected with the total escaping luminosity gives

$$\gamma_{max} \approx (\gamma_{max} - \gamma_t) + t_{esc}\dot{\gamma}_c(\gamma_p) + \frac{\int \gamma N(\gamma)d\gamma}{Q_0 t_{esc}}$$

Defining $t_{cool} \equiv \gamma/\dot{\gamma}_e$ we have

$$\gamma_p \approx \gamma_t\left[1 + \frac{t_{esc}}{t_{cool}(\gamma_p)}\right]^{-1} \qquad (1.42)$$

Then for small Compton losses the peak energy γ_p is below, but close to, γ_t. Increasing the ratio U_r/U_B should let γ_p move towards lower energies, until it reaches values close to unity for $U_r \geq U_B$ The value of $N(\gamma_p)$ can be found by (Svensson, private communication)

$$\frac{N(\gamma_p)}{N(\gamma_t)} \simeq \frac{t_{esc}}{t_{cool}(\gamma_t)}\frac{\gamma_t}{\gamma_p} \qquad (1.43)$$

If the injected distribution is steeper than γ^{-2}, most of the power lies at small energies, and an appropriate treatment of the cyclo-synchrotron emission is necessary. The actual shape of the steady $N(\gamma)$ distribution has to be found numerically. But since very low energy electrons experience a net gain of energy, a peaked distribution is expected to develop also in this case, with γ_p close to γ_{min}. In this case the luminosity in escaping electrons can be a sizeable fraction of the injected one, but the escaping *kinetic* luminosity has to be a negligible fraction of the injected one, as it will be argued in Chapter 3.

For $U_B \gg U_r$, the electron cooling cannot proceed down to very subrelativistic energies, and form a cool population of thermal electrons through Coulomb collisions. Instead, a peaked distribution of relativistic electrons is expected to form through photon exchanges, the peak energy being function of U_B/U_r and the shape of the distribution of the injected electrons.

1.5 Compton emission

Consider an electron of energy γ moving at an angle θ with respect to photons of dimensionless energy $x = h\nu/mc^2$ in the (unprimed) lab frame. In the (primed) electron's frame the corresponding angle θ' is given by

$$\tan\theta' = \frac{\sin\theta}{\gamma(\cos\theta - \beta)}\underset{\gamma\gg 1}{\longrightarrow} - \frac{1}{\tan(\theta/2)} \tag{1.44}$$

Thus, due to aberration, the electron sees pactically all photons coming from a narrow cone around its direction of motion. In its frame the photon energy becomes

$$x' = \gamma x(1 - \beta\cos\theta) \tag{1.45}$$

After the scattering, the photon energy x'_1 is

$$x'_1 = \frac{x'}{1 + x'(1 - \cos\theta'_1)} \tag{1.46}$$

where θ_1' is the angle between the directions of the photon before and after the scattering. Transforming back to the lab frame

$$x_1 = \gamma x_1' \Big[1 + \beta \cos(\pi - \theta_1')\Big] = \gamma^2 x \frac{(1 - \beta\cos\theta)(1 - \beta\cos\theta_1')}{1 + \gamma x(1 - \beta\cos\theta)(1 - \beta\cos\theta_1')} \tag{1.47}$$

For $\gamma \gg 1$, the maximum and minimum energies of the scattered photon are

$$x_{1max} = \frac{4\gamma^2 x}{1 + 4\gamma x}; \qquad x_{1min} = \frac{x}{4\gamma^2} \tag{1.48}$$

When the incoming photon energy as seen by the electron is less than its rest mass ($\gamma x \ll 1$), the electron recoil is negligible and the Thomson cross section σ_T can be used to compute the scattering rate, and the energy distribution of the scattered photon of initial energy x. In this limit, and for an isotropic distribution of photons of energy density U_r, the cooling rate of the single electron is (e.g. Rybicki & Lightman 1979)

$$\dot{\gamma}_c = \frac{4}{3}\frac{\sigma_T c}{mc^2}\gamma^2\beta^2 U_r \tag{1.49}$$

The energy distribution function of initially monochromatic photons after the scattering with monoenergetic electrons is given in this limit by (e.g. Blumenthal & Gould 1970)

$$f_T(y) = 2y\ln y + y + 1 - 2y^2 \tag{1.50}$$

where $y = x_1/(4\gamma^2 x)$ is the photon energy in units of its maximum value. From this function, the average energy of the scattered photon is $< x >= (4/3)\gamma^2 x$.

When $\gamma x \geq 1$, the exact Klein Nishina (hereafter KN) cross section must be used, and the electron recoil becomes important. The total cooling rate is reduced with respect to eq. (1.49), due to the decline of the KN cross section. The energy transfer in each collsion is described by the energy distribution function (e.g. Blumenthal & Gould 1970)

$$f_{KN}(q) = 2\ln q + q + 1 - 2q^2 + \frac{1-q}{2}\frac{(4\gamma x q)^2}{1 + 4\gamma x q} \tag{1.51}$$

where $q = x_1/\big[4\gamma x(\gamma - x_1)\big]$ is again the photon energy in units of its maximum. For $\gamma x \ll 1$ eq. (1.51) reduces to eq. (1.50), but for $\gamma x \gg 1$ the function $f_{KN}(q)$ peaks

at q close to one. In this case the electron looses almost all its kinetic energy in the process and $x_1 \sim \gamma$, independent of the initial photon energy.

The inverse Compton (IC) emissivity produced by an isotropic distribution of electrons and photons in the general case must be computed numerically. However, useful formulae can be derived in the Thomson limit and in the extreme KN limit. In the firmer case, following Zdziarski (1986), we have

$$\epsilon_c(x_1) = \frac{1}{4\pi}\frac{\sigma_T c}{2}\int_{x_{min}}^{x_{max}} dx n(x)\gamma N(\gamma), \quad \gamma = \left(\frac{3x_1}{4x}\right)^{1/2} \tag{1.52}$$

where $n(x)$ is the photon density distribution before scattering. If $N(\gamma)$ is a power law of the form of eq. (1.4), and setting $\tau_c \equiv \sigma_T RK$, we have

$$\epsilon_c(x_1) = \frac{1}{4\pi}\frac{\tau_c}{2}\frac{(4/3)^{\frac{p-1}{2}}}{R/c} x_1^{-\frac{p-1}{2}} \int_{x_{min}}^{x_{max}} dx n(x) x^{\frac{p+1}{2}} \tag{1.53}$$

The evaluation of the limits of integration follows from fig. 1.6. In this figure, and in eqs. (1.52), (1.53), a δ-function approximation for the energy of the scattered photon is used, and the emission from collisions in the KN regime is completely neglected, by using a step function for the cross section

$$\sigma_{KN} = \begin{cases} \sigma_T & \text{for} \quad \gamma x \leq 3/4 \\ 0 & \text{for} \quad \gamma x > 3/4 \end{cases} \tag{1.54}$$

In the energy range for which x_{min} and x_{max} are constant, the IC emissivity is a power law of index $\alpha = (p-1)/2$, just the same of the synchrotron emission, both cooling rates being dependent on the square of the electron energy. The energy range where the IC emission is a power law depends however on the extension in energy of the incident photon and electron distribution. As an example, consider $n(x)x \propto x^{-\alpha}$, up to $x = 1$. In this case $x_{max} \sim \min(x_1, 1/x_1)$ is never constant. If α is flatter than $(p-1)/2$, the slope of the scattered spectrum α_1 is equal to α, independent on p, up to $x = 1$, breaking to $\alpha_2 = p - \alpha - 1$ above $x = 1$. Steep power law electron distributions scattering flat photon distributions produce a broken power law spectrum, with the break at the maximum energy of the incident radiation.

In the extreme KN limit the emissivity is (e.g. Blumenthal & Gould 1970)

$$\epsilon_{KN}(x_1) = \frac{1}{4\pi}\frac{3\tau_c}{8}\frac{1}{R/c}x_1^{-p}\int\frac{dx}{x}n(x)\Big[\ln(xx_1)+C(p)\Big] \tag{1.55}$$

where the function $C(p)$ (of order unity) is plotted in Blumenthal & Gould (1980). Comparing with $\alpha_2 = p-\alpha-1$ derived before, it can be concluded that emission in the extreme KN limit is important if $\alpha < -1$.

The exact formula for the IC emissivity has been derived, for the general case, by Jones (1968), including the contribution of those photons which are downscattered by the Compton process. He also calculated a series expansion of the exact formula to first order in the terms $1/\gamma^2$ and x/γ. From his approximate formula, assuming $n(x) = n_0 x^{-\alpha-1}$ between x_{min} and $x_{max} \leq 1$, we have

$$\epsilon_c(x_1) = \frac{1}{4\pi}\frac{3\tau_c}{4R/c}2^p n_0\left[\frac{x_1}{2^{p+2}}\int_{\max(x_1,x_{min})}^{x_{max}} A(x,x_1)x^{-\alpha-2}dx + \right.$$

$$\left. x_1^{-\frac{p-1}{2}}\int_{x_{min}}^{x_{max}} x^{\frac{p-3}{2}}x^{-\alpha}dx\int_0^1 dqf(q)\right] \tag{1.56}$$

where

$$\begin{aligned} A(x,x_1) =& 2\left[\frac{2}{(p+3)^2}+\frac{1}{p+3}\ln\left(\frac{4x_1}{x}\right)\right]\left[\gamma_{max}^{-p-3}-\gamma_1^{-p-3}\right]+ \\ &+4\left[\frac{\ln\gamma_{max}}{\gamma_{max}^{p+3}}-\frac{\ln\gamma_1}{\gamma_1^{p+3}}\right]-\frac{4x_1}{x}\frac{1}{p+1}\left[\gamma_{max}^{-p-1}-\gamma_1^{-p-1}\right]+ \\ &+\frac{x}{2x_1(p+5)}\left[\gamma_{max}^{-p-5}-\gamma_1^{-p-5}\right] \end{aligned} \tag{1.57}$$

$$\gamma_1 = \max\left\{\gamma_{min}, \min\left[\gamma_{max}, \left(\frac{x}{4x_1}\right)^{1/2}\right]\right\} \tag{1.58}$$

$$f(q) = q^{\frac{p-1}{2}}\frac{2q\ln q+1+q+2qxx_1-2q^2(1+xx_1)}{(1+qxx_1)^{\frac{p+3}{2}}\left[1+\left(\frac{qxx_1}{1+qxx_1}\right)^{1/2}\right]^{p+2}} \tag{1.59}$$

$$q = \frac{x_1}{4\gamma x(\gamma-x)}$$

The first term in eq. (1.56) refers to the emission from the downscattered photons, the second term to emission from photons whose energy is increased in the scattering process.

In fig. 1.7 the emissivity (1.56) is plotted for $\gamma_{min} = 1$, $\gamma_{max} = 10^3$, $x_{min} = 10^{-4}$, $x_{max} = 1$, $p = 3$, and for different value of α (solid lines). The dashed line refers to eq. (1.53) for the same parameters, and for $\alpha = 0$. From this figure is apparent that the step function approximation for the cross section (eq. 1.54) overestimates the contribution of the emission in the Thomson regime, rather than underestimate the emission from the extreme KN limit. For all values of α, the spectrum breaks at the same energy $x_b \approx 0.6$, somewhat smaller than unity. Above the break, the analytical estimate of α_2 is in good agreement with the numerical results for $\alpha = 0.5$ and $\alpha = 0$. For rising spectra the emission from the KN regime is significant, and the spectrum is slightly flatter than $\alpha_2 = p - 1 - \alpha$, and has approximately the same slope for the cases $\alpha = -0.5$ and $\alpha = -1$, according to eq. (1.55), which gives $\epsilon_c(x) \propto x^{-p} \ln x$.

Fig. 1.7 shows an extreme case, with the spectrum of incident photons extending up to $x_{max} = 1$. If x_{max} is smaller, then the scattered spectrum has the usual slope $(p-1)/2$ between x_{max} and γ_{min}. Note, however, that when multiple Compton scatterings are important (Zdziarski & Lamb 1986) the final spectrum is the superposition of many IC orders, contributing at the same frequency. For τ_c of order unity, it can be approximated with a unique power law up to $x \sim 1$. In this case the first order IC spectrum resulting from the scattering with the final photon distribution coincides with the superposition of the spectra of all IC orders. In other words, the spectrum is scattered into itself. When multiple Compton is important, the final spectrum does not depend on the electron distribution slope for energies below the break, since most of the contribution to the emission comes from the lowest energy electron present. This resembles the case of unsaturated thermal Comptonization, where the spectral shape of the emerging radiation is a power law up to $x = kT/mc^2$, whose slope depends on the electron density and temperature.

It must be noted that for relativistic multiple scattering the break in the spectrum occurs at $x_b \sim \gamma_{min}$. Then for γ_{min} of order unity x_b coincides with the threshold

for photon-photon pair production.

In the following the approximated cross section of eq. (1.54) will be adopted. This choice leads to a Compton cooling rate

$$\dot{\gamma}_c = \frac{4}{3}\frac{\sigma_T c}{mc^2}(\gamma^2-1)g(\gamma)\,U_r \tag{1.60}$$

where the factor $g(\gamma)$ is the fraction of radiation energy density available for scattering in the Thomson regime, for an electron of energy γ. For power law spectra of index α

$$g(\gamma) = \frac{\left(\frac{3}{4\gamma}\right)^{1-\alpha} - x_0^{1-\alpha}}{x_{max}^{1-\alpha} - x_0^{1-\alpha}} = \begin{cases} \sim 1, & \alpha > 1 \\ \left(\dfrac{3}{4\gamma x_{max}}\right)^{1-\alpha}, & \alpha < 1 \end{cases} \tag{1.61}$$

For steep ($\alpha > 1$) spectra most of the radiation energy density is at low energies, so that $g(\gamma)$ is constant and $\dot{\gamma}_c \propto \gamma^2$ for any γ, provided that $\gamma_{max}x_0 < 3/4$. For spectral slopes flatter than unity $\dot{\gamma}_c \propto \gamma^{1+\alpha}$, and the cooling rate is reduced with respect to the Thomson regime (Rees 1967b). For this reason, the luminosity produced by higher orders IC scatterings becomes negligible, and no Compton Catastrophe exists, in the sense of a dramatic cooling of the electrons. For a monoenergetic soft photon production rate at the energy x_0, and for flat ($p < 3$) $N(\gamma)$ distributions, the successive IC orders contribute to the total luminosity up to the N_{th} order, with N given by

$$N = \mathrm{Int}\left\{1 - \frac{\ln[(4/3)\gamma_{max}x_0]}{\ln[(4/3)\gamma_{max}^2]}\right\} \tag{1.63}$$

For lower orders, the luminosity ratio of two successive IC orders is

$$\frac{L_{c,i+1}}{L_{c,i}} \approx \tau_c \gamma_{max}^{3-p}, \qquad p < 3 \tag{1.64}$$

where a logarithmic term has been neglected.

If the electron distribution is steep, ($p > 3$), and $\tau_c \ll 1$, only the first order scattering is important, even if the KN regime is not reached, because the resulting spectrum is steep. However, for τ_c approaching unity, successive IC orders dominate the emission in slightly different energy ranges. Defining $<\gamma> = (p-1)/(p-2)\gamma_{min}$, Compton emission becomes unimportant above the N_{th} order, where N is given by eq. (1.63) with $<\gamma>$ replacing γ_{max}.

For $\tau_c \geq 1$ and $\gamma_{min} \sim 1$, care must be taken of the radiative tranfer equation, which can be written as (e.g. Zdziarski & Lamb 1986)

$$\dot{n}_{esc}(x) = \dot{n}_{prod}(x) - \dot{n}_{abs}(x) \tag{1.65}$$

The scattering process here acts as an absorption process, decreasing the number of escaping photons in a given energy bin, with respect to those that are produced. For homogeneous distributions of photons and electrons, we have

$$\dot{n}_{esc}(x) = \dot{n}_{prod}(x)\left[\frac{1-e^{-\tau_c(x)}}{\tau_c(x)}\right] \tag{1.66}$$

with $\tau_c(x)$ given by

$$\tau_c(x) = \int_{\gamma_{min}}^{3/(4x)} d\gamma \sigma_T R N(\gamma) \simeq \frac{\tau_c}{p-1}\gamma_{min}^{1-p}\left[1-\left(\frac{4x\gamma_{min}}{3}\right)^{p-1}\right], \quad x < \frac{3}{4\gamma_{min}}$$

$$\tau_c(x) = 0, \qquad x > \frac{3}{4\gamma_{min}} \tag{1.67}$$

Eq. (1.67) follows from the approximated form of the KN cross section (eq. 1.54). Note that $\tau_c(x) \sim$ constant until x becomes close to $3/(4\gamma_{min})$, and then rapidly drops. If the source is optically thick to pair production by photon absorption above $x \sim 1$, then only those photons produced just below the pair production threshold can freely escape. At these energies the observed spectrum will show an *excess of radiation* with respect to the extrapolation of the spectrum from lower energies.

Figs. 1.9 and 1.10 show the IC spectrum computed for a source of size $R = 10^{15}$ cm, monochromatic soft photon luminosity at the energy $x_0 = 10^{-6}$, $\gamma_{min} = 1$, $\gamma_{max} = 100$. In fig. 1.9 $\tau_c = 0.01$, $p = 2$, while in fig. 1.10 $\tau_c = 1$ and $p = 3$. As can be seen, only the first and second order contribute to the spectrum in fig. 1.9, in agreement with the estimate of eq. (1.63), while 7 orders significantly contributes to the spectrum in fig. 1.10, where the overall spectral index $\alpha \sim 0.66$ below $x \sim 1$ is not related to the slope p of the electron distribution. Note also the break at $x = 3/4$, above which $\alpha_\gamma \sim 1.4 \sim p - 1 - \alpha$.

1.6 Thermal Comptonization

A Maxwellian distribution of electrons of dimensionless temperature $\Theta = kT/mc^2$ and scattering optical depth τ_T can produce a power law spectrum scattering off a soft photon distribution with typical energy $x \ll \Theta$ (Katz 1976, Shapiro, Lightman, & Eardley 1976, Pozdnyakov, Sobol, & Sunyaev 1979, Sunyaev & Titarchuk 1980), if the Comptonization y parameter is of the order of unity. This parameter measures the average increase in energy of the soft photon and can be defined as

$$y = 4\tau_T^2\Theta\left(1+\frac{1}{\tau_T}\right)(1+4\Theta)$$

For large values of y (and τ_T), the Comptonization is *saturated* and a Wien ($\propto x^3e^{-x}$) spectrum is established. For $y \ll 1$ Comptonization is unimportant. In the interesting case of y of order unity and for monochromatic soft photon emission rate $\dot{n}_s(x) = A\delta(x-x_0)$ the corresponding scattered spectrum can be approximated with a power law ending in an exponential tail

$$\dot{n}_c(x) \simeq Bx^{-\alpha_{th}-1}e^{-x/\Theta} \tag{1.68}$$

whose normalization can be found from photon conservation. In the case $\tau_T > 3$ and $\Theta < 1$ the slope α_{th} is given by (Shapiro, Lightman, & Eardley 1976)

$$\alpha_{th} \simeq \left[\frac{9}{4} - \frac{\pi^2}{3(\tau_T+2/3)^2\Theta}\right]^{1/2} - \frac{3}{2} \tag{1.69}$$

For more general soft photon emission rates, extending from x_0 and x_{max}, we have

$$\dot{n}_c(x) \sim \alpha_{th}x^{-\alpha_{th}-1}\int_{x_0}^{\tilde{x}} dx' x'^{\alpha_{th}}\dot{n}_s(x') \tag{1.70}$$

where $\tilde{x} = \min(\Theta, x_{max}, x)$, and the exponential tail has been neglected for simplicity. If $\dot{n}_s(x) = n_0x^{-\alpha_0-1}$, eq. (1.70) yields

$$\dot{n}_c(x) \simeq \frac{\alpha_{th}}{\alpha_{th}-\alpha_0}\dot{n}_s(x)\left[\left(\frac{\tilde{x}}{x}\right)^{\alpha_{th}-\alpha_0} - \left(\frac{x_0}{x}\right)^{\alpha_{th}-\alpha_0}\right] \tag{1.71}$$

which coincides with the result of Zdziarski (1986) if $x < x_{max} < \Theta$. The spectral slope of the scattered spectrum is thus the flattest between α_0 and α_{th}, with a break at x_{max} (if $x_{max} < \Theta$ and $\alpha_{th} > \alpha_0$). Note that these expressions are only valid for $\tau_T > 3$ and $\Theta < 1$. For $\tau_T < 3$ and subrelativistic temperatures the spectral index resulting from Comptonization of monochromatic photons is given by Pozdnyakov,Sobol, & Sunyaev (1977). The validity of their formula has been extended by Zdziarski (1985) to any value of Θ and τ_T less than a few

$$\alpha_{th} \simeq -\frac{\ln P_\tau}{\ln(1+4\Theta+16\Theta^2)} \tag{1.72}$$

$$P_\tau = 1 - \frac{3}{\tau_T^3}\left[(2\tau_T^2-1) + e^{-2\tau_T^2}(2\tau_T+1)\right] \tag{1.73}$$

The factor $P_\tau \sim 3/(4\tau_T)$ in the limit of $\tau_T \ll 1$. For extremely small optical depths and larger temperatures, the resulting spectrum is bumpy, reflecting the shape of each order.

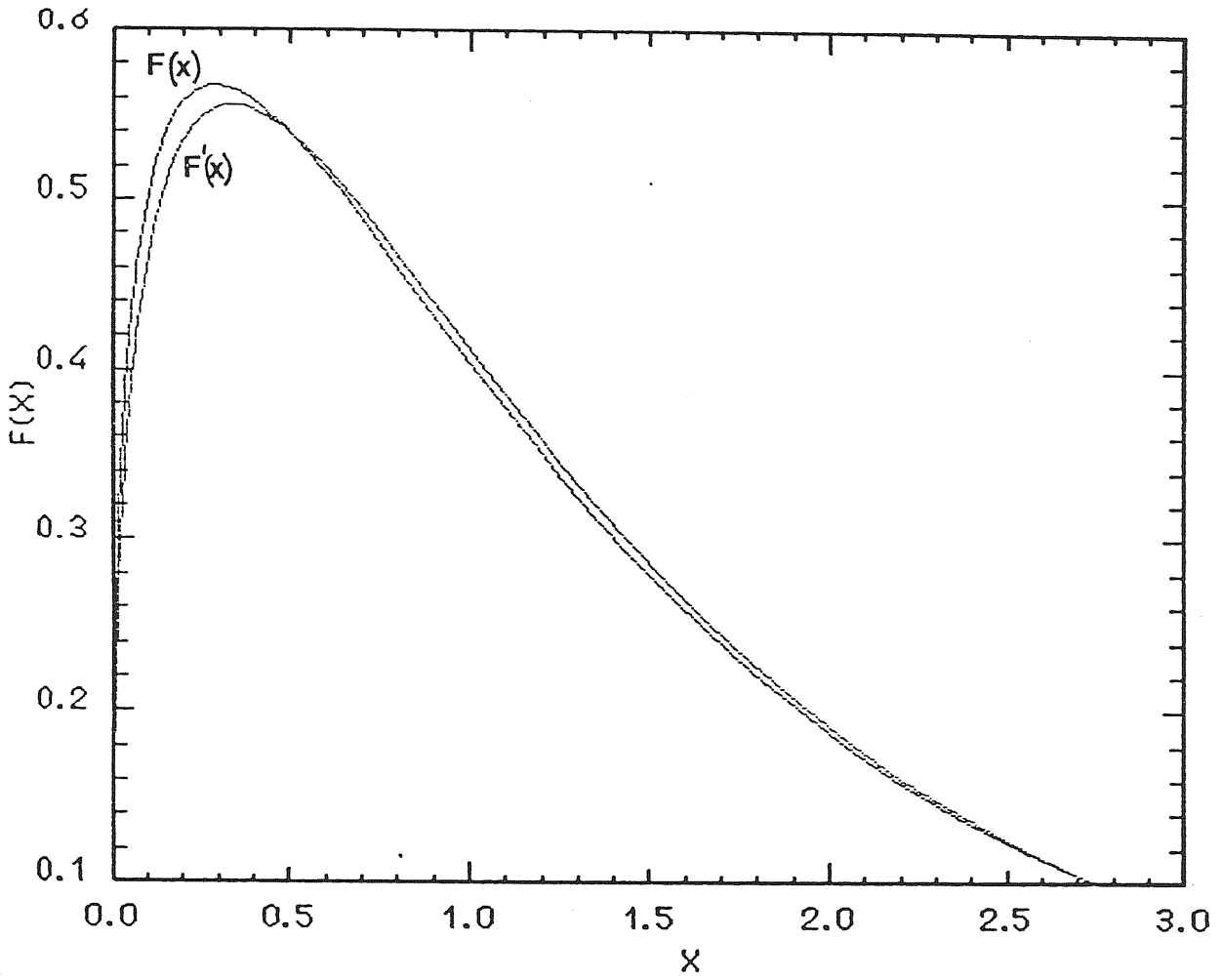

Figure 1.1. The function $F(x) = x \int_x^\infty dx K_{5/3}(x)$ describing the synchrotron emission of a relativistic electron is compared to $F'(x) = x^{-1/3}e^{-x}$. Both functions are normalized.

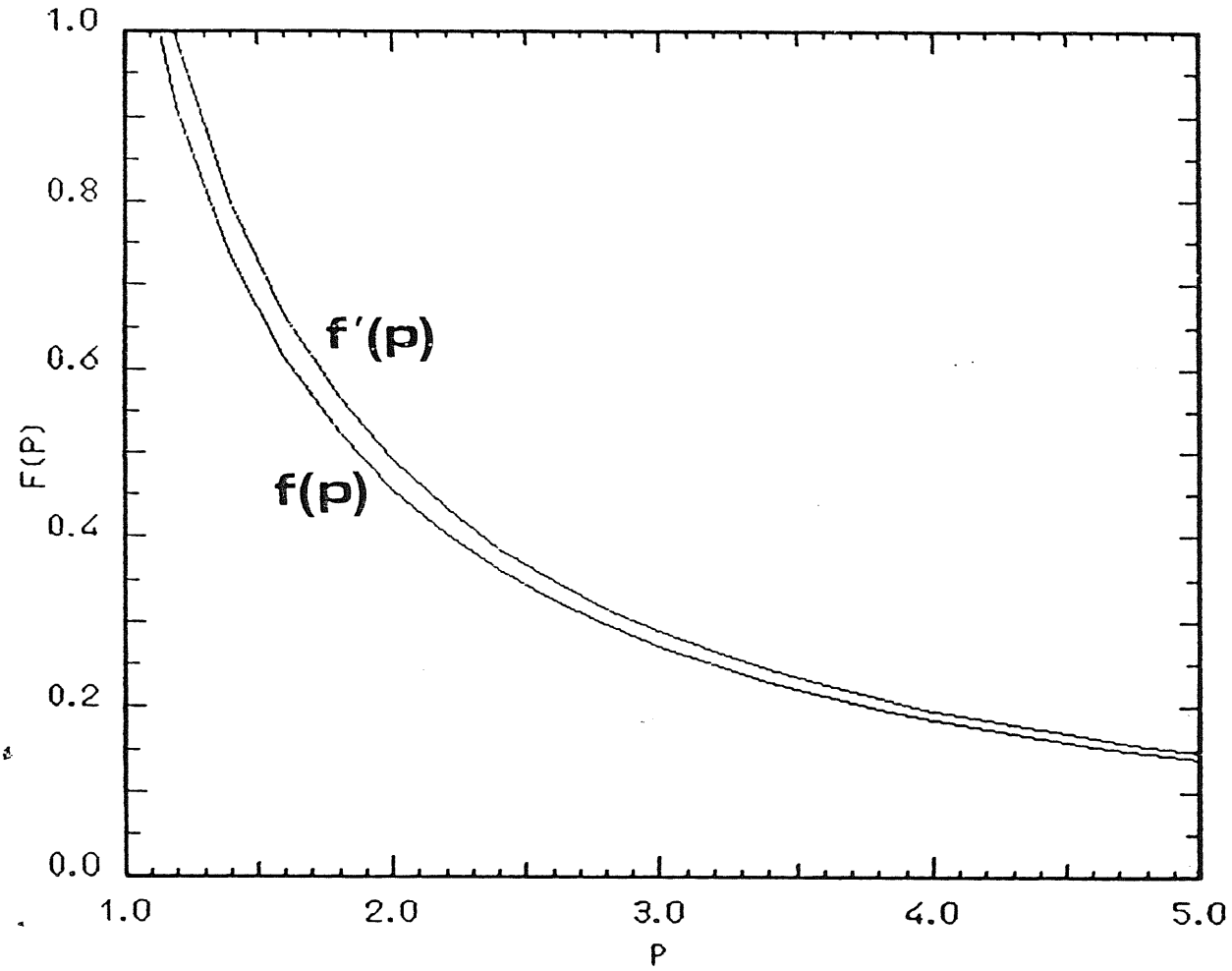

Figure 1.2. The coefficients $f(p)$ (eq. 1.13) and $f'(p)$ (eq. 1.15) of the synchrotron source function $S(\nu)$. $f(p)$ refers to emission at a given pitch angle, while $f'(p)$ refers to emission with a random distribution of pitch angles.

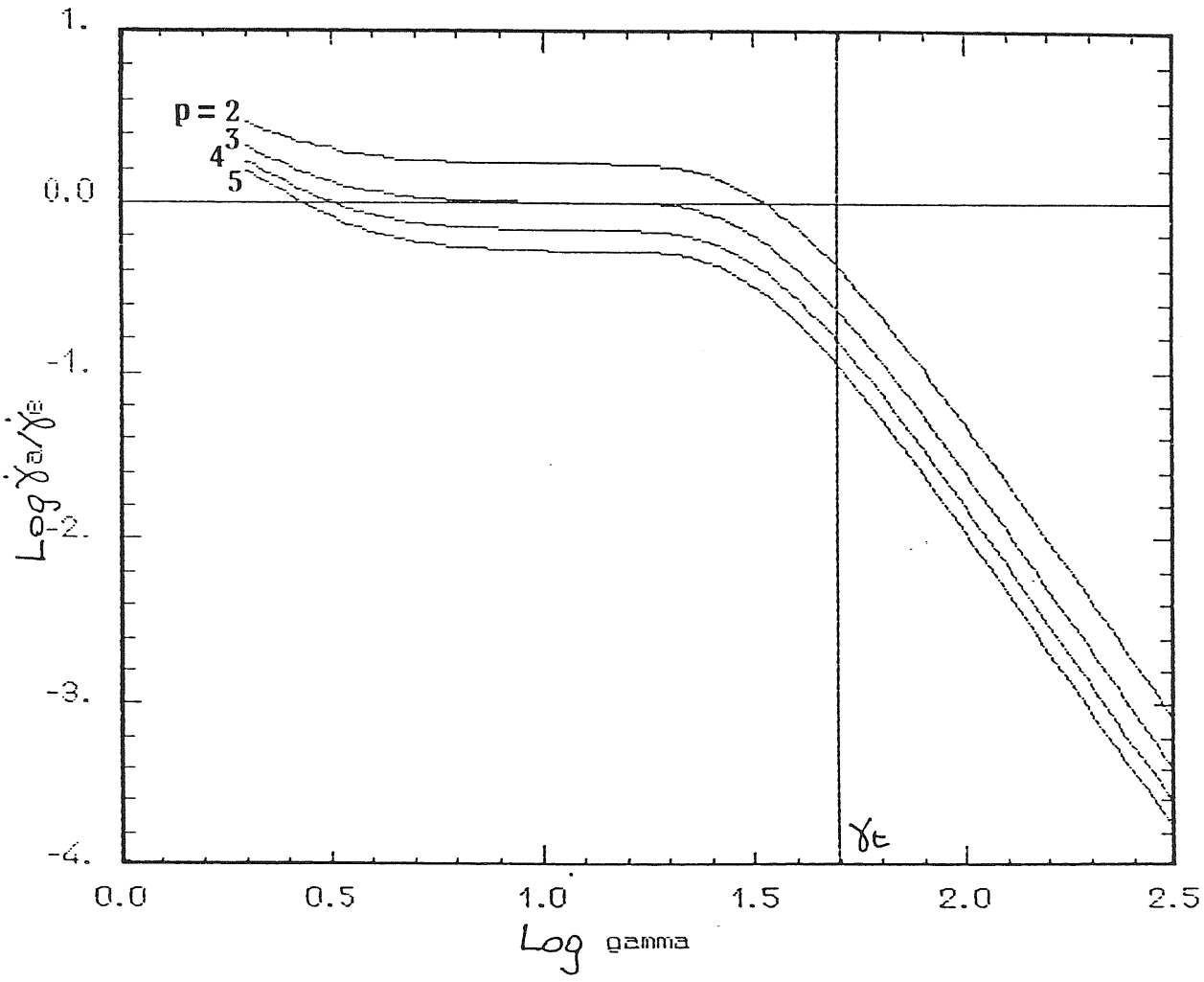

Figure 1.3. The function $\dot{\gamma}_{abs}(\gamma,\theta)/\dot{\gamma}_e(\gamma,\theta)$ for different values p of the slope of the electron distribution (eq.1.29). From top to bottom: p =1, 2, 3, 4, 5. The self absorption energy $\gamma_t = 50$ (indicated by the vertical line), and $\gamma_{min} = 2$ have been used for all curves. The horizontal line indicates $\dot{\gamma}_{abs} = \dot{\gamma}_e = 1$. Low energy electrons always *gain* rather *loose* energy.

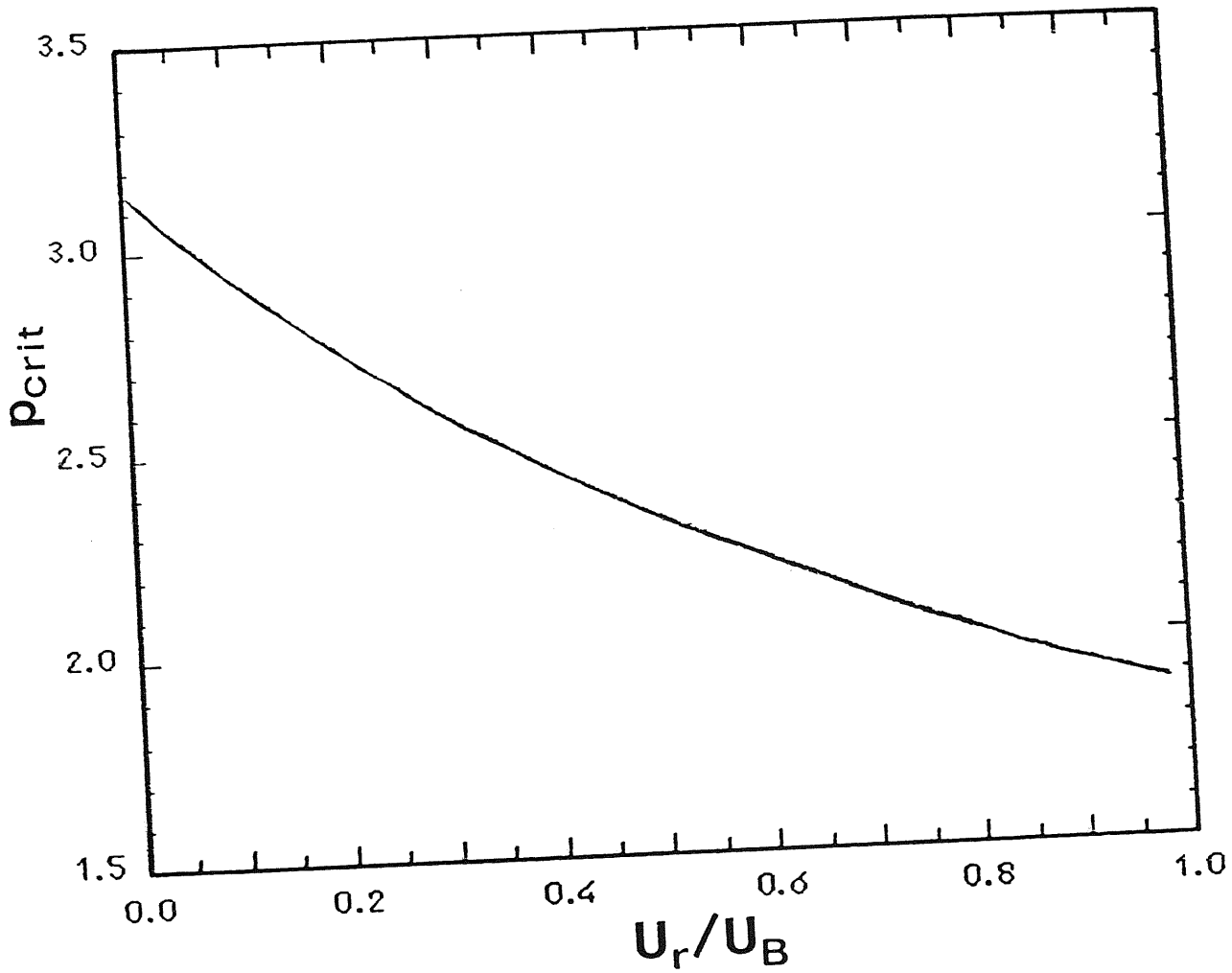

Figure 1.4. The critical value p_{crit} of the electron distribution slope at which radiative (Compton and synchrotron) losses equal energy gains due to synchrotron reabsorption, as a function of U_r/U_B (eq. 1.34). A power law electron distribution of slope p is assumed, and the synchrotron emission and absorption coefficients have been averaged over pitch angles. Note that the solutions of eq. (1.34) here plotted are only valid in the range $1 \ll \gamma \ll \gamma_t$

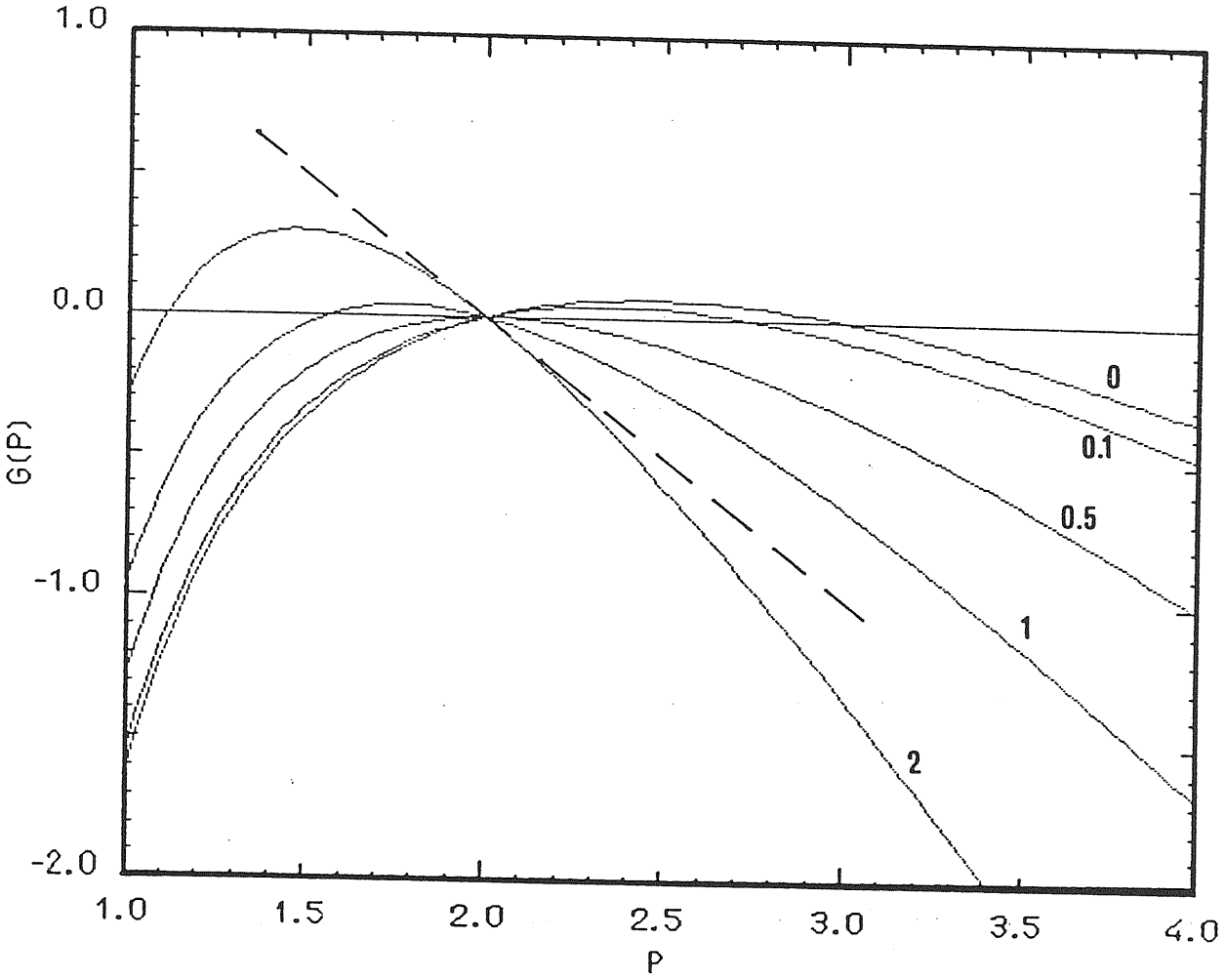

Figure 1.5. The function $g(p)$ (eq. 1.40) for different values of the ratio U_r/U_B, determining the initial relaxation behaviour of the power law electron distribution of index p, at energies $1 \ll \gamma \ll \gamma_t$. The dashed line $g(p) = 2 - p$ corresponds to free relaxation for $U_r/U_B = 0$. Each curve is labelled by the value of U_r/U_B.

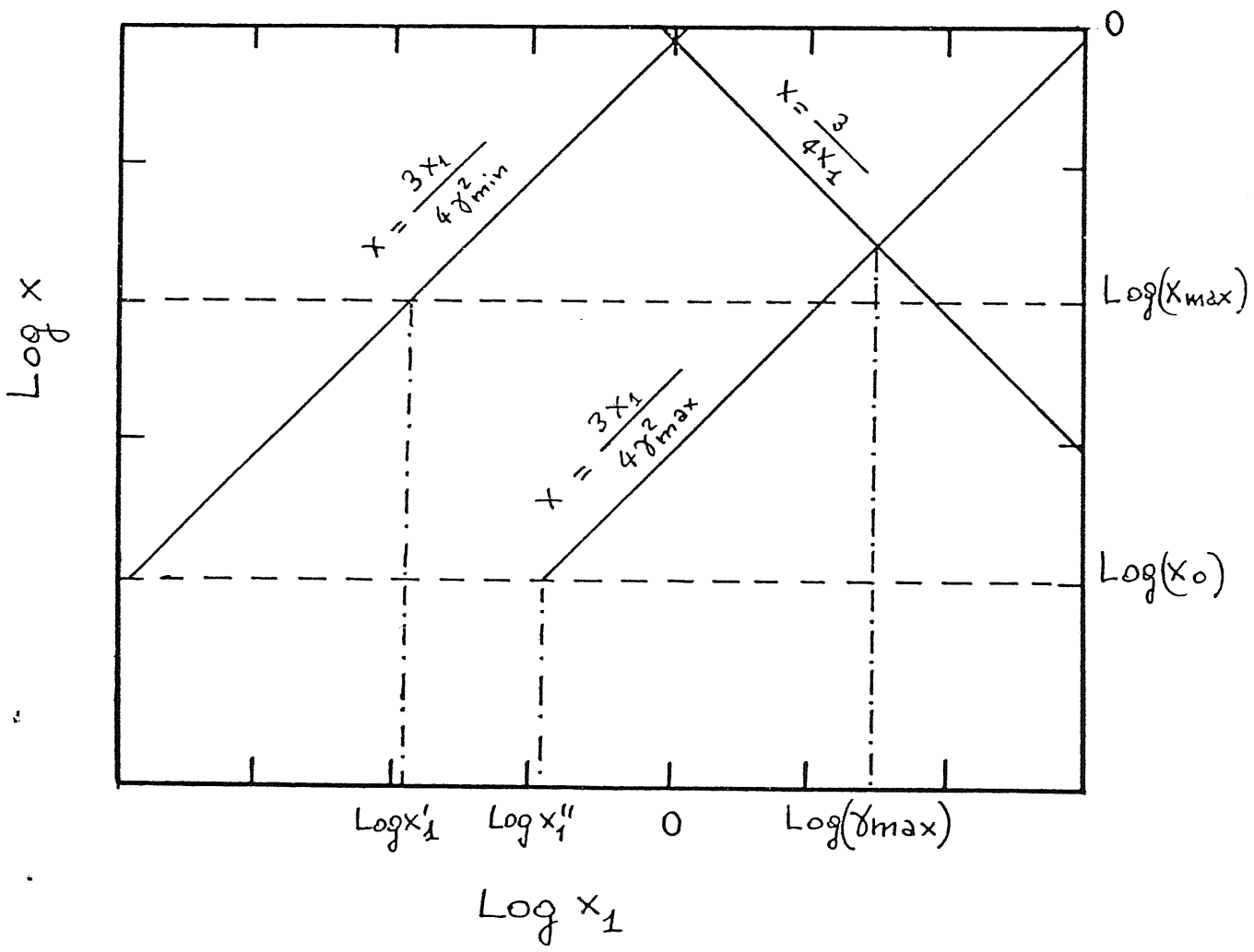

Figure 1.6. Schematic diagram for computing the Compton characteristic energies and the limits of integration in eq. (1.53). A $\delta-$approximations is assumed for the energy of the scattered photon x_1. For a given x_1, only a fraction of incident photons energies is available.

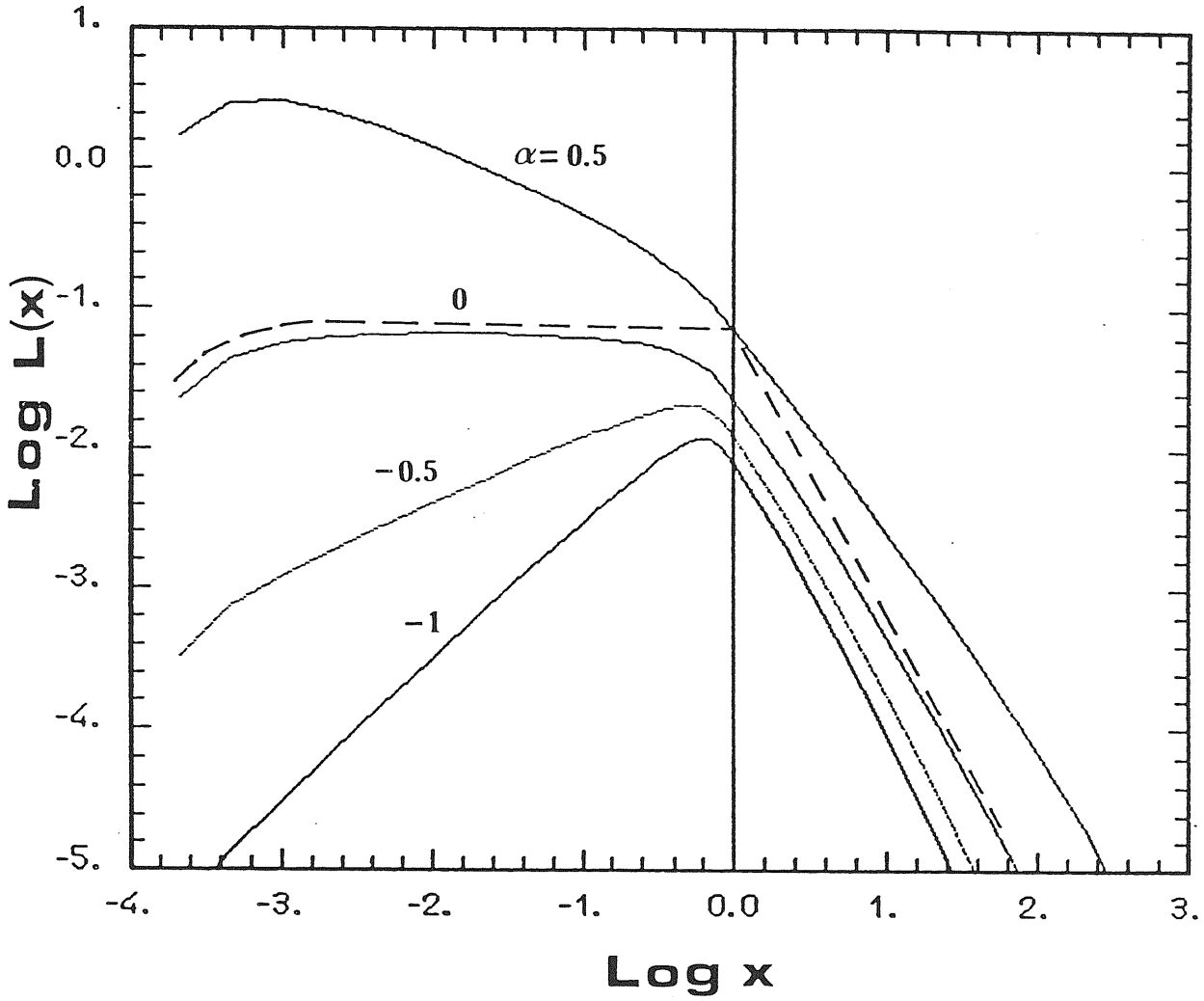

Figure 1.7. *Solid lines:* Inverse Compton spectra computed through eq. (1.56) for different values of the spectral index α of the incident radiation. From top to bottom: $\alpha = 0.5, 0, -0.5, -1$. *Dashed line:* Inverse Compton spectrum for $\alpha = 0$ computed through eq. (1.53). For all calculations, the electron distribution is assumed to be a power law of slope $p = 3$, with $\gamma_{min} = 1$ and $\gamma_{max} = 10^3$. The minimum and maximum energy of the incident spectra are $x_{min} = 10^{-4}$ and 1, respectively.

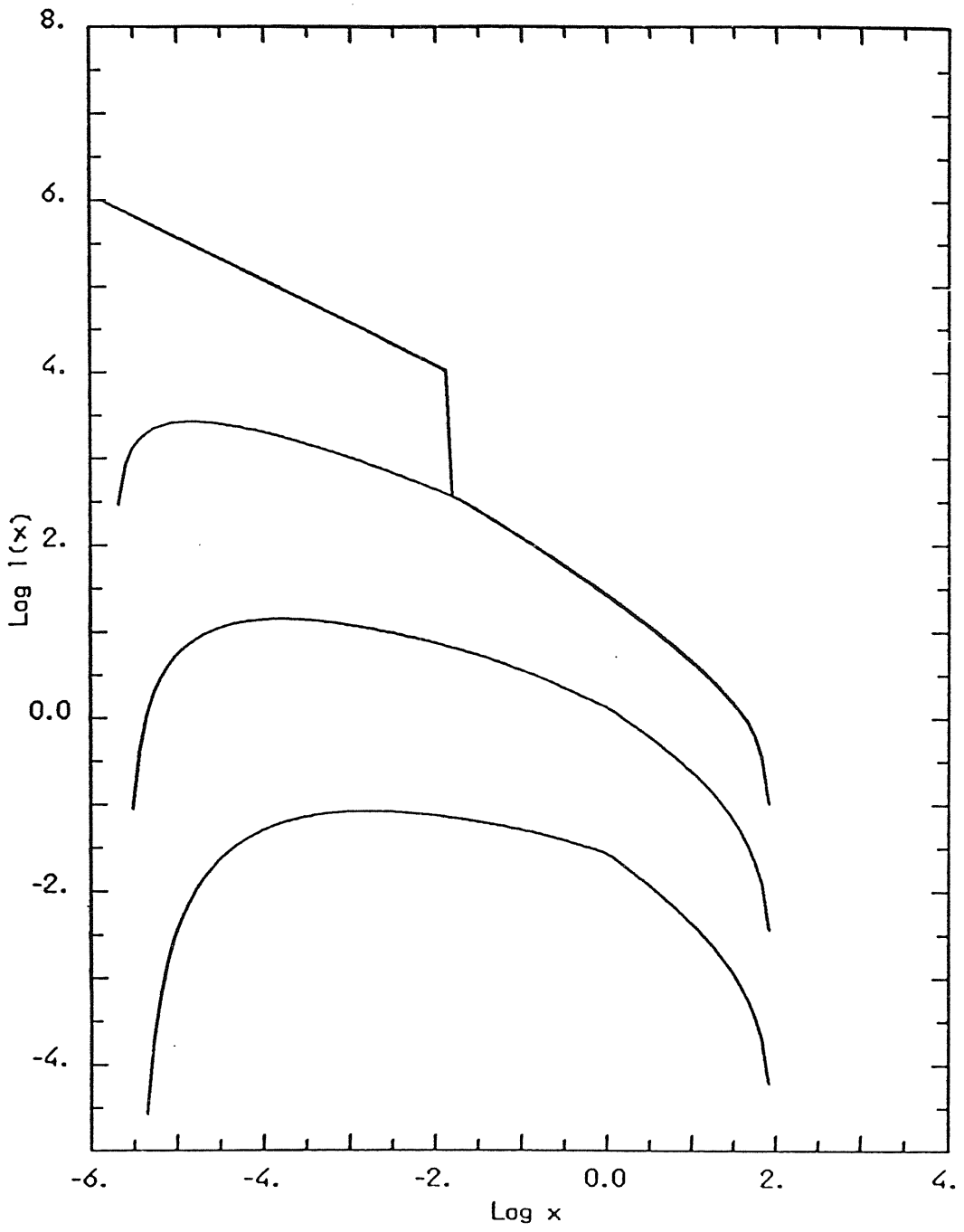

Figure 1.8. Inverse Compton spectrum computed for monochromatic soft photon incident radiation of energy $x_0 = 10^{-6}$ scattered by a power law electron distribution of slope $p = 2$ and normalization $\tau_c = 10^{-2}$, extending from $\gamma_{min} = 1$ to $\gamma_{max} = 100$. The first four orders are shown.

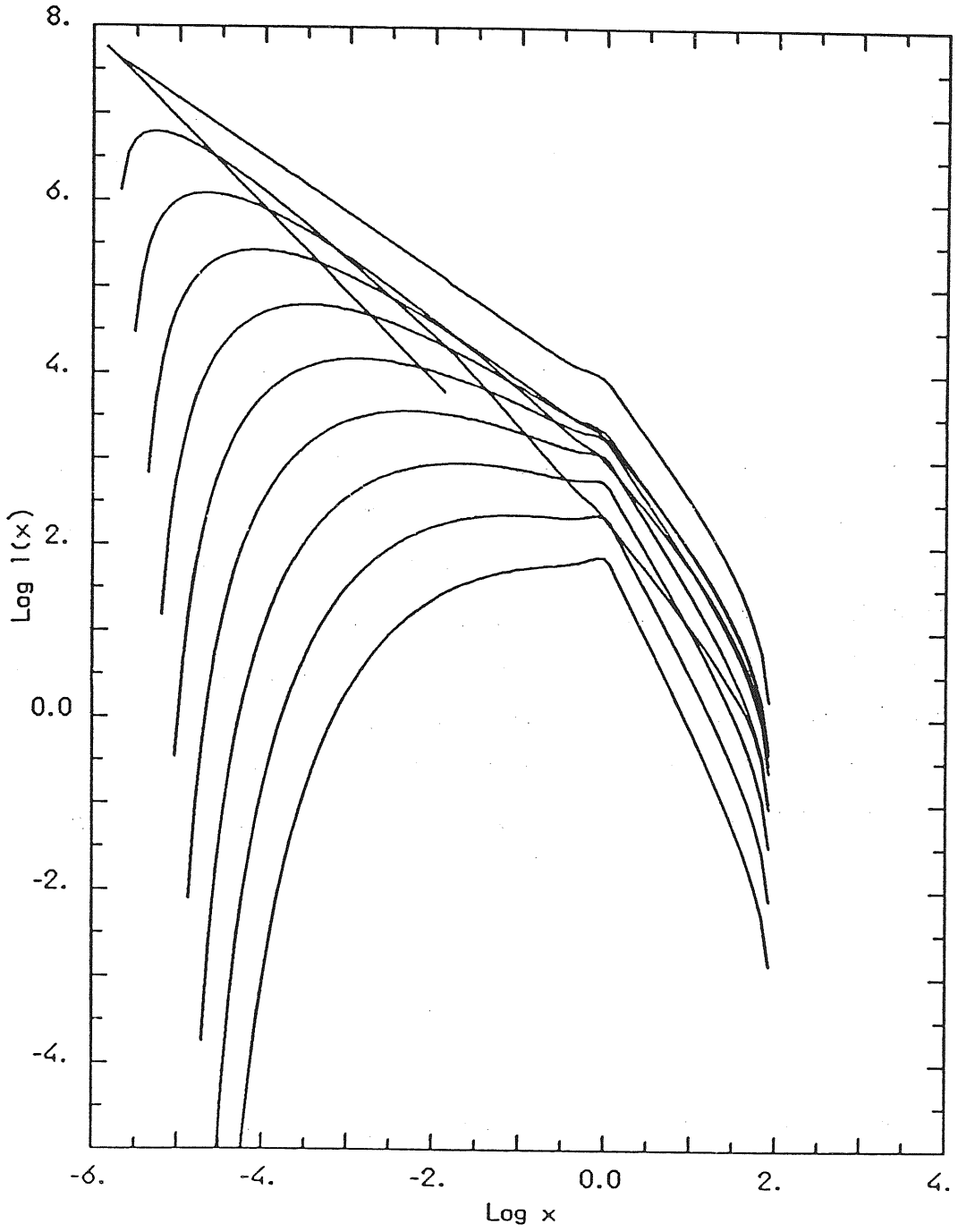

Figure 1.9. Inverse Compton spectrum computed for monochromatic soft photon incident radiation of energy $x_0 = 10^{-6}$ scattered by a power law electron distribution of slope $p = 3$ and normalization $\tau_c = 1$, extending from $\gamma_{min} = 1$ to $\gamma_{max} = 100$. The overall spectrum and the spectrum of the first ten orders are shown.

CHAPTER TWO

THE STANDARD SYNCHROTRON SELF COMPTON MODEL

In this chapter I will summarize the main features of the standard synchrotron self Compton (SSC) model, as formalized by Jones, O'Dell & Stein (1974). In this widely used version of the model, the electron distribution function is assumed, regardless of the details of the (energy dependent) cooling rates. Furthermore, only the first order Compton spectrum will be taken into account, and the Compton cooling is assumed to be always in the Thomson regime. Beaming effects due to relativistic bulk motion of the source will be considered and discussed. The homogeneous model standard model will be used as a tool for deriving the beaming factor for a sample of BL Lac and HPQ sources. Bulk acceleration of the emitting plasma in inhomogeneous jet geometries is the distinctive feature of a constructed and proposed model for explaining the spectral differences of blazars selected either by radio means or by their X-ray emission.

2.1 The homogeneous SSC model

Consider a spherical source of radius R, embedded in a tangled magnetic field B and containing a power law distribution of relativistic electrons

$$N(\gamma) = K\gamma^{-p} \equiv \frac{\tau_c}{\sigma_T R}\gamma^{-p}, \quad 1 \leq \gamma \leq \gamma_{max} \tag{2.1}$$

isotropic in the rest frame of the emitting plasma. These electrons produce synchrotron photons with a power law spectrum, and scatter them to higher frequencies by the IC mechanism. Neglecting self absorption and Klein Nishina (KN) effects, the ratio of the synchrotron to the first order IC cooling rates equals the corresponding luminosity

ratio and the ratio between the magnetic to synchrotron radiation energy density

$$\frac{\dot{\gamma}_s(\gamma)}{\dot{\gamma}_{c,1}(\gamma)} = \frac{U_B}{U_r^s} = \frac{\int d\gamma N(\gamma)\dot{\gamma}_s(\gamma)}{\int d\gamma N(\gamma)\dot{\gamma}_{c,1}(\gamma)} = \frac{L_s}{L_{c,1}} \tag{2.2}$$

where U_r^s is the energy density of synchrotron radiation. To derive the spectral emissivities in very simple way, a δ-function approximation can be assumed for the spectrum emitted by the single electron. For synchrotron emission

$$\nu_s = \frac{4}{3}\gamma^2 \frac{eB}{2\pi mc} = \frac{4}{3}\gamma^2 \nu_B \tag{2.3}$$

This approximation leads to the synchrotron emissivity given by eq. (1.7). For Compton emission

$$\nu_c = \frac{4}{3}\gamma^2 \nu_s \tag{2.4}$$

Rewriting eq. (1.53) for SSC radiation we have

$$\epsilon_{c,1}(\nu_c) = \left(\frac{3}{4}\right)^{1-\alpha} \frac{\tau_c}{2} \ln \Lambda \epsilon_s(\nu_c) \tag{2.5}$$

where Λ is a function of ν_c near the extremes of the possible values of ν_c, and it is constant and equal to $(\gamma_{max}/\gamma_t)^2$ otherwise, as can be derived by fig. 1.6. Note that, at a given frequency, the synchrotron thin emission (or its extrapolation) is a factor $\sim (2\ln\Lambda\tau_c)^{-1}$ above the Compton spectrum (for $\tau_c \ll 1$). Since the synchrotron emissivity is proportional to τ_c, the first order IC emission is proportional to τ_c^2, reflecting the fact the the same electrons work twice. In a similar way, the second order IC emissivity is proportional to τ_c^3 and so on. For complete Thomson cooling, the energy density ratio of photons produced in the $(i+1)_{th}$ IC order to that of the i_{th} one is

$$\frac{U_{r,i+1}}{U_{r,i}} = \left(\frac{U_{r,1}}{U_B}\right)^{i+1} \tag{2.6}$$

where $U_{r,0} = U_B$. However, eq. (2.6) is valid only for i less than a few, since, as we have seen in the previous chapter, only few orders IC spectra can contribute to the emission. For flat electron distribution the KN limit is reached after only one or two IC orders for any reasonable choice of the parameters. This was suggested as early as

1967 by Rees, and solves the *Compton Catastrophe* problem posed by Hoyle, Burbidge and Sargent (1966). Sources with $U_r \gg U_B$ can actually exist in steady state, and they do not suffer the dramatic Compton cooling implied by the (erroneous) use of eq. (2.6). However, the Compton Catastrophe or Compton limit can be thought as the prediction of X-ray fluxes much exceeding the observed ones. The two interesting physical quantities: the magnetic field B, and the relativistic particle density or optical depth τ_c, can be derived by the observed synchrotron spectrum and the source angular size θ_d (eqs. 1.21, 1.22), in a distance independent way. By eq. (2.5) the IC flux can then be predicted to be

$$F_c(\nu_x) \propto \tau_c F_s(\nu_x) \propto \tau_c^2 B^{1+\alpha} \theta_d^2$$

$$\propto F_m^{2(2+\alpha)} \theta_d^{-2(3+2\alpha)} \nu_m^{-(5+3\alpha)} \nu_x^{-\alpha} \qquad (2.7)$$

2.2 Relativistic beaming

Although the predicted X-ray flux depends on high powers of the poorly determinable observables, and is thus highly uncertain, there are cases of irriducible disagreement between the predicted and the observed X-ray flux. Usually, this is ascribed to relativistic beaming effects, that is, to the enhancement of the observed flux produced by the emitting plasma relativistically moving towards the observer. Blushift, time contraction and aberration, enhancing the observed flux, decreasing the apparent source size if measured by variability timescales, and shifting the observed frequencies, lead the observer to highly overestimate the electron and photon densities effectively present in the source, and thus to overestimate the scattering probability.

All these effects can be described introducing the Doppler or beaming factor δ

$$\delta = \left[\Gamma - (\Gamma^2 - 1)^{1/2} \cos\phi\right]^{-1} \qquad (2.8)$$

where Γ is the bulk Lorentz factor of the plasma, and ϕ is the angle between the velocity and the line of sight. Beaming factors greater than unity occur for angles smaller than ϕ_c

$$\phi_c = \arcsin\Big[2/(\Gamma+1)\Big]^{1/2} \tag{2.9}$$

and the possible δ-values range from $\delta_{max} \sim 2\Gamma$ ($\phi = 0^o$, $\Gamma \gg 1$), to $\delta_{min} = 1/\Gamma$ ($\phi = 90^o$, corresponding to a two sided jet). The observed flux density coming from a thin source is enhanced by the factor δ^p

$$F(\nu) = \delta^p F'(\nu) \tag{2.10}$$

with respect to the flux in a comoving frame. If the plasma flows in a volume at rest in the observer frame, the flux transforms as the emissivity, and thus $p = 2 + \alpha$ (two powers for aberration, the factor α for blushift). For a source in ballistic motion, volume transformation gives an extra power, and $p = 3 + \alpha$.

Note also that the observed shape of a moving spherical blob is a disc with the same radius, due to the balancig effects of length contraction and different light travel times (Terrel 1959). Different source elements emit photons at different times (and thus at different positions), to let them arrive at the observer simultaneously. The source is observed rotated, not contracted, even if its volume obeys Lorentz transformation.

The beaming hypothesis is the most economic way of explaining the otherwise disparate phenomena of superluminal motion, rapid variability, one sided jets, strong jet bending, weak X-ray emission and highly super-Eddington luminosities.

These extremes properties can be produced by observing at small viewing angles sources otherwise "normal". It is then tempting to order different classes of active galactic nuclei in a unified picture, the viewing angle being the most important parameter. Several attempts have been made in the past (amongst others: Orr & Browne 1982, Scheuer & Readhead 1979, Blandford & Rees 1978), to unify radio quiet and radio loud quasars, radio galaxies and BL Lacs, and blazars with and without strong emission lines.

Beaming poses a statistical problem, because for an isotropic distribution of jet directions in the sky, the misaligned sources (with different spectra, luminosities, and behaviours), are much more numerous than the aligned sources, even if an obvious selection effect works in favour of the latter, more luminous ones. To quantify this statement, Urry & Shafer (1984) analized the effects of beaming on the luminosity function of a population of sources, assuming random orientation, two sided jets, and the same value of the bulk Lorentz factor Γ for all sources. The result is that, if the intrinsic luminosity function is $\Phi(\ell) = \ell^{-\beta}$, between ℓ_{min} and ℓ_{max}, the observed one $\Phi(L)$ is a broken power law, having the same slope β above $\ell_{min}\delta^p$ and the *flat* slope $(1 + 1/p)$ below.

We can simply derive the value of the flat part of the observed luminosity function, considering that any value of the intrinsic luminosity ℓ corresponds to a range of observed luminosities L, distributed as the probability to observe a particular value of δ:

$$P(L,\ell) = P(\delta)d\delta = d\cos\phi$$

since $d\cos\phi/d\delta = \left[(\Gamma^2-1)^{1/2}\delta^2\right]^{-1}$ and $d\delta/dL = (L/\ell)^{1/p}/(pL)$, we have

$$P(L,\ell) = \frac{\ell^{1/p}}{p(\Gamma^2-1)^{1/2}} L^{-1-1/p} \tag{2.11}$$

In this picture the sources of intrinsic lower luminosities give rise to the flat part of the observed luminosity function, and the most aligned sources gives the major contribution to $\Phi(L)$ above $\ell_{min}\delta^p_{max}$. This simple derivation can be generalized to include the case of a distribution of Γ factors. As an example, suppose a power law Γ-distribution $N(\Gamma) \propto \Gamma^{-n}$. Then

$$P(\delta) = \frac{1}{\delta^2}\int_{\Gamma_{min}(\delta)}^{\Gamma_{max}} \frac{N(\Gamma)}{(\Gamma^2-1)^{1/2}}\, d\Gamma \tag{2.12}$$

where $\Gamma_{min}(\delta) = 1/\delta$ for $\delta < 1$ and $(\delta + 1/\delta)/2$ for $\delta > 1$. In the particular case of $n = 2$, we have

$$P(\delta) = \frac{\Gamma_{max}}{\delta^2(\Gamma_{max}-1)} \times \begin{cases} \dfrac{\sqrt{\Gamma^2_{max}-1}}{\Gamma_{max}} - \sqrt{1-\delta^2}, & \delta \le 1 \\ \dfrac{\sqrt{\Gamma^2_{max}-1}}{\Gamma_{max}} - \dfrac{\delta^2-1}{\delta^2+1}, & \delta \ge 1 \end{cases} \tag{2.13}$$

The resulting $P(L,\ell)$ is a broken power law having slopes $\beta_1 = 1-1/p$ for $L < \ell$, and $\beta_2 = 1+3/p$ for $L > \ell$. For $L > \ell$, the slope is thus steeper than before, since only a small fraction of sources are beamed with $\Gamma \sim \Gamma_{max}$. Convolving with $\Phi(\ell)$, the observed $\Phi(L)$ has the same slope β of the intrinsic distribution above $\ell_{min}\left[\delta(\Gamma_{max})\right]^p$, while below this value it keeps the two slopes derived before.

If all sources are characterized by the same value of Γ, the resulting flat part of the corresponding $\Phi(L)$ has important consequences on source counts, in the sense that a log$N$-log$S$ slope flatter than 1.5 can be possible even if the population of sources evolves (Cavaliere *et al.* 1985?). Note however that if there is a distribution of Γ-values, this may not be possible (Ghisellini & Madau, in preparation).

These models, besides being important for the statistics of beamed sources, make the prediction of a break in the observed luminosity function. The slope below this break can carry informations on the probability of an object to undergo relativistic motion. Taking $p = 2+\alpha$, $\alpha = \alpha_x \sim 1$, the predictions of the two possibilities examined above are significantly different, being $\beta_2 = 2$ for $N(\Gamma) \propto \Gamma^{-2}$ and $\beta_2 = 4/3$ if all sources have the same Γ.

Independently on the Γ-distribution, the enhancement due to beaming depends on the slope of the spectrum, and thus the flat portion of the luminosity function of beamed objects is steeper for flatter spectra (i.e. the X-ray luminosity function should be flatter than the radio one).

The picture outlined before could be an oversimplification. In fact it is reasonable to assume that only a fraction f of the intrinsic luminosity ℓ is beamed (Urry & Shafer 1984). If f is constant, the slopes of the observed $\Phi(L)$ remains unchanged, but in different ranges of luminosities. However, both f and Γ can be functions of the intrinsic luminosity ℓ, or of the ratio ℓ/ℓ_E, where ℓ_E is the Eddington luminosity. As an example, radiation pressure can accelerate a wind of electron positron pairs up to a maximum Lorentz factor (Phinney 1983)

$$\Gamma_{max} \sim 5\left(\frac{\ell}{\ell_E}\frac{R}{3r_g}\right)^{1/4} \qquad (2.14)$$

where R is the size of the emitting region, $r_g = GM/c^2$ is the gravitational radius,

and where the limit to Γ is due to Compton drag (aberrated photons in the forward emisphere balance the radiation pressure of photons in the backward emisphere).

2.3 Beaming in blazars

High polarization quasars (HPQs) and BL Lac objects are often grouped toghether under the common denomination of blazars. They share many peculiar features such as flat radio spectra, rapid radio and optical variability, steep non-thermal continuum, high and strongly variable optical polarization. The clearest observational distinction between the two classes is the presence, in HPQs, of broad emission lines. When available, redshifts of BL Lac objects indicate a smaller luminosity than HPQs. The most popular model for interpreting the spectral and variability properties of blazars invokes highly relativistic bulk motion of the plasma at small angles to the observer's line of sight (Blandford & Rees 1978). In this scenario, the core emission is strongly anisotropic, while, owing to its relaxed diffuse morphology and large linear scale, off-nuclear emission is very likely to be isotropic. Thus the ratio of the core to extended radio emission is a possible indicator of viewing aspect and beaming intensity (Antonucci & Ulvestad 1985). Madau, Ghisellini, & Persic 1987 have attempted to directly test the beaming hypothesis in blazars, applying the simplest SSC homogeneous model to derive the beaming factor δ for 41 objects of known VLBI size and X-ray flux. In fact eq. (2.7) can easily generalized to include beaming effects. Viceversa, knowing the X-ray flux, a *minimum* Doppler factor δ can be derived (Gould 1979, Urry 1984)

$$\delta = f(\alpha)\left(\frac{F_m}{Jy}\right)\left(\frac{F_x}{Jy}\right)^{-\frac{1}{2(2+\alpha)}}\left(\frac{\nu_x}{2.42\times 10^8 GHz}\right)^{-\frac{\alpha}{2(2+\alpha)}}\left(\frac{\nu_m}{GHz}\right)^{-\frac{5+3\alpha}{2(2+\alpha)}}\times$$

$$\left(\frac{\theta_d}{mas}\right)^{-\frac{3+2\alpha}{2+\alpha}}\left[\ln\left(\frac{\nu_b}{\nu_m}\right)\right]^{\frac{1}{2(2+\alpha)}}(1+z) \qquad (2.15)$$

with $f(\alpha)\simeq 0.2$ for $\alpha = 0.75$ [$f(\alpha)\simeq 0.08\alpha + 0.14$]. The observables appearing in eq. (2.15) are the X-ray flux density F_x at the frequency ν_x, the self absorption frequency

ν_m and the flux density F_m at this frequency, the high energy synchrotron cut-off ν_b, the optical thin spectral index α, the redshift z and the angular diameter measured by VLBI techiques. Estimates of δ based on variability time scales of the optical and X-ray fluxes, besides being distance dependent, are misleading, because the region responsible for flux variations may not be coincident with the radio emission region which is relevant here (see below for inhomogeneous SSC models).

Our sample is not complete, nevertheless it is a large subset of all the blazars known, and it is substantially larger than the sample of 16 BL Lacs studied by Madejski & Schwartz (1983), who used a less accurate formula for δ. We found published data for 11 out of 22 definite HPQs listed in Moore & Stockman (1984), and for 30 BL Lacs listed in Maraschi *et al.* (1986), Weiler & Johnston (1980), and Ledden & O'Dell (1985). Table 2.1 lists the objects under study. Column 3 gives the redshift, when no redshift is available, we adopted an average value of $z = 0.4$ (Ghisellini *et al.* 1986), Madejski & Schwartz 1983, note that $\delta \propto 1 + z$). Angular diameters are given in column 4, while in column 5 and 6 are listed the frequency of the VLBI measurements and the corresponding flux density. The measured X-ray fluxes at 1 KeV are given in column 7. The δ-factors computed by eq. (2.15) are given in column 8. Column 9 gives the overall spectral index α_{RX} defined between 5 GHZ and 1 KeV

$$\alpha_{RX} = \frac{\ln(F_m/F_x)}{\ln(2.42 \times 10^{17}/5 \times 10^9)}$$

Finally, column 10 gives the core dominance parameter R, defined as the compact to extended radio flux density ratio. All values of R are taken from Antonucci & Ulvestad (1985) and refers to a frequency of 1.5 GHz. Note also that the radio flux of the compact component was measured with VLA, and thus corresponds to typical angular sizes of 1 arsec.

To estimate ν_b we have considered the observed steepening of the blazar spectra between infrared and optical frequencies (Ghisellini *et al*, 1986, Cruz-Gonzales & Huchra 1984) as an indication of the synchrotron high energy cut-off and consequently adopted $\nu_b = 10^5$ GHz for all sources. The synchrotron turnover frequency ν_m is not observed in any source. We assume that the flat radio spectra (up to $\sim$ 300 GHz, Gear

et al. 1985) indicates an inhomogeneous synchrotron source (see next section). This hypothesis is supported by multifrequency VLBI observations (Unwin *et al.* 1983, 1985) which show the presence of several discrete radio blobs and a compact, partially opaque, flat spectrum core. In inhomogeneous synchrotron models, the VLBI frequency corresponds to the self absorption frequency of the observed component. In other words, the observed angular size θ_d is a function of wavelength. Hence, a lower limit on δ can be computed at any frequency of the flat radio spectrum, provided that the angular size is determined at the same frequency. Inhomogeneous models are more realistic than an homogeneous sphere model, but unfortunately have many parameters that cannot be simply or uniquely constrained. However, we checked that for reasonable values of these parameters, the derived δ-factors are in good agreement with those computed in the homogeneous model that we adopt here for simplicity. The biggest uncertainty in the determination of δ comes from θ_d, since it is difficult to determine accurately and it is raised to the largest exponent in eq. (2.15). For all sources, we assume a spectral index $\alpha = 0.75$ for the optically thin emission. Repeating the calculations for $\alpha = 0.5$ and $\alpha = 1$ the computed δ-factors change by no more than 30%.

In fig. 2.1a, b the δ-factor distributions for BL Lacs and HPQs are shown. For BL Lacs, the δ-values range from 10^{-2} to 15, half of the sources do not require relativistic beaming ($\delta < 1$). On the other hand, all HPQs have δ-values greater than unity, up to $\delta \sim 19$. Such values indicate a Γ factor of the order of 5 or 10, consistent with estimates derived independently from models of superluminal motion (Cohen & Unwin 1984). Indeed, we found that the possible and definite superluminal BL Lacs and HPQs listed in Cohen & Unwin (1984) and Bååth (1984) (shaded areas in fig. 1) are actually characterized by δ-values greater than unity.

It is important to stress that δ-values lower than unity do not necessarily mean misaligned beaming of radiation ($\phi > \phi_c$, eq. 2.9), since other regions of the source can contribute to the X-ray flux by SSC or other emission mechanisms. On the other hand, if the VLBI component is responsible for only 1% of the observed X-ray flux, the derived values of δ correspondingly increase only by a factor ~ 2.3. Suppose

that an isotropic component is also contributing to the X-ray flux, and that the radio component dominates X-ray emission only if its radiation is beamed with $\delta > 1$. As a consequence the average α_{RX} for sources with $\delta > 1$ would reflect the typical F_m/F_x ratio of the radio component we are observing, while $< \alpha_{RX} >$ for the low- δ sources reflects the ratio between the (misaligned) radio and the isotropic X-ray fluxes. On average, a smaller $< \alpha_{RX} >$ for low δ sources is predicted, as observed. In fact we have

	$\delta < 1$ BLLacs	$\delta > 1$ BLLacs	HPQs
$< \alpha_{RX} >$	0.756 ± 0.025	0.876 ± 0.012	0.875 ± 0.022

Continuing the argument a little further, a better determination of δ for those BL Lacs with $\delta < 1$ can be derived supposing that all these objects have the same ratio of the anisotropic radio to X-ray flux of the $\delta > 1$ sources. This gives a value of $\tilde{F}_x$ (not related to the observed one), and a new value for δ. Calling δ_{new} this new value and δ_{old} the ones listed in table 1, we have

$$\delta_{new} = \delta_{old} \left[\frac{F_m}{F_x} \left(\frac{\nu_m}{\nu_x} \right)^{\alpha_{RX}} \right]^{-\frac{1}{4+2\alpha}} \tag{2.16}$$

where F_x is the observed X-ray flux and α_{RX} refers to the average value for the $\delta > 1$ BL Lacs. Eq. (2.16) was applied for the sources with $\delta < 1$ and α_{RX} flatter than $< \alpha_{RX} >_{\delta>1}$. Derived values of δ_{new} are slightly larger than δ_{old}, but remains lower than unity for all sources but 1101+384 ($\delta_{new} = 1.39$). This qualitative argument argues in favour of $\delta < 1$ values being indicative of misaligned radio emission.

Since the core dominance parameter R has been suggested as beaming indicator, a correlation between R and δ should exist. In fig. 2.2 R is plotted versus δ for BL Lac objects. As can be seen, the two quantities are well correlated. A linear fit analysis gives $\log R = 0.9 \log\delta + 1.29$, with correlation coefficient $r = 0.66$ (which improves to $r = 0.77$ neglecting ON 231). Again, the fact that this correlation holds even including sources with value of δ less than unity argues in favour that some BL Lacs exist, whose radio emission is beamed at large angles to the line of sight.

The low-δ tail of the BL Lac distribution is mostly contributed by non radio selected or low redshift sources, or both. This supports the picture of Maraschi *et al.* (1986) in which X-ray selected BL Lacs are supposed to have misaligned radio jets, but more isotropic X-ray emission.

The δ-distributions in fig. 2.1 indicate, on average, a large Doppler boosting for HPQs than for BL Lacs. This is stricly valid for radio emission. However, by continuity arguments, it is reasonable to expect the same trend for the optical continuum as well. In other words if δ_{opt} is monotonically related with δ_{radio}, even if different in absolute value, one expects the polarized optical continuum to be more relativistically enhanced in HPQs than in BL Lac objects. If this is true, the lack of strong emission lines in BL Lacs cannot be attributed to Doppler boosting of the continuum. This is at variance with the conventional scenario in which the presence or absence of emission lines in blazars is explained by purely geometric effects (Blandford & Konigl 1979, Antonucci & Ulvestad 1985). Within this hypothesis, as the angle of observation decreases, the contribution of the beamed, polarized component increases relative to the isotropic unpolarized one. Hence the distribution in line to continuum ratios in blazars would reflect their orientation with respect to the line of sight. BL Lac objects would represent the extreme case, in which the Doppler boost is so large that the emission lines are washed out by the beamed continuum. Instead, we find lower (radio) Doppler factors in objects with weak lines so that the conventional scenario could be restored only if the $\delta-$distributions at optical frequencies were reversed to those of fig. 2.1.

We suggest that orientation effects are not the primary cause which distinguished weak from strong line blazars and that the emission lines are intrinsically weak in BL Lac objects.

A possible explanation for the truncated $\delta-$distribution of HPQs can also be put forward: in normal low polarization quasars the isotropic component is intrinsically so strong that the polarized "blazar" continuum is observable only when highly boosted. On average, the luminosity in the beam, since it does not swamp the emission lines,

is only a small fraction of the quasars' energy budget when Doppler enhancement is accounted for. Only occasionally sources like 3C 446, during bursts, have their polarized continuum so boosted that the object would be classified as a liness BL Lac.

Finally, since in our sample five sources are found to be definite superluminal with published values of β_{obs} (Cohen & Unwin 1984), we can compute the corresponding values of Γ and ϕ in the framework of the simple ballistic model

$$\beta_{obs} = \beta \frac{\sin\phi}{1 - \beta\cos\phi} \tag{2.17}$$

$$\Gamma = \frac{\beta_{obs}^2 + \delta^2 + 1}{2\delta} \tag{2.18}$$

$$\sin\phi = \frac{\beta_{obs}}{\delta(\Gamma^2 - 1)^{1/2}} \tag{2.19}$$

Note that $\beta_{obs} \propto H_0^{-1}$, H_0 being the Hubble constant. For $H_0 = 100\,\mathrm{Km\,s^{-1}\,Mpc^{-1}}$, we find

	0735+178	2200+420	1253-055	1641+399	2251+158
β_{obs}	3.0	2.4	3.5	8.0	9.0
δ	7.2	4.4	4.2	5.2	5.9
Γ	4.3	3.0	3.7	8.8	9.9
ϕ	5.7	11.3	13.8	10	8.9

2.4 Inhomogeneous models

More realistic models of active galactic nuclei invoke the presence of a jet, also supported by high resolution radio observations, which is supposed to be a scaled version of the radio jets seen at the arcminute scale. It is natural to hipothesize that, in these structures, the magnetic field and the particle density are functions of position

within the source. The simplest approach is to parametrize these behaviours through power laws

$$B = B_0(r_0/r)^m \tag{2.20}$$

$$K = K_0(r_0/r)^n, \quad \tau_c \equiv \sigma_T r K = \tau_{c,0}(r_0/r)^{n-1} \tag{2.21}$$

where r_0 is some fiducial minimum size, and r is the radius of the jet section, which will depend on the distance from the apex of the jet R

$$r = aR^\epsilon \tag{2.22}$$

The ϵ parameter controls the geometry of the jet, $\epsilon = 1$ corresponding to a truncated cone, while $\epsilon < 1$ describes a paraboloid. For semplicity, we can take $r_0 = R_0$ for $\epsilon < 1$, and so $a = R_0^{1-\epsilon}$. Models with these assumptions has been developped, among others, by Marscher (1977), Konigl (1981), Marscher (1980), Reynolds (1982), and Ghisellini, Maraschi & Treves (1985). The main differences between these models concern the assumptions about the maximum energy of the electrons being an increasing or decreasing function of distance, the calculation of the self Compton flux, lacking in some models, the assumed shape of the electron distribution, the adopted geometry, and the degree of beaming. Here I will follow the formalism and the assumptions of Ghisellini, Maraschi & Treves (1985) to generalize that model in order to include the possibility of bulk acceleration of the emitting plasma (Ghisellini & Maraschi, in preparation, see also Maraschi 1987). In other words, the Lorentz factor of the bulk motion is assumed to be function of position

$$\Gamma = (R/R_0)^g \tag{2.23}$$

A radial dependence is also assumed for the maximum electron energy

$$\gamma_{max}(R) = \gamma_{max}(R_0)(r_0/r)^e \tag{2.24}$$

with these hypotheses the maximum synchrotron frequency becomes

$$\nu_{max}(R) = \nu_{max}(R_0)(R_0/R)^\eta \tag{2.25}$$

where $\eta = \epsilon(2e + m)$ is taken to be positive, corresponding to the largest frequencies being produced in the base of the jet. Thus different frequencies are produced in different regions, of different bulk velocities. Lower frequencies come from the outer parts, where the higher values of Γ can highly enhanced (or dim) the observed flux, depending on the viewing angle. The overall observed synchrotron spectrum will be viewing-angle dependent, being steeper for aligned sources. By eqs. (1.6) and (2.20)-(2.24), the synchrotron luminosity is

$$L_s(\nu) = \int_{R_1(\nu)}^{R_2(\nu)} dR\pi r^2 \epsilon_s(r,\nu)\delta(r)^{2+\alpha_0}$$

$$\propto \nu^{-\alpha_0} \int_{x_1(\nu)}^{x_2(\nu)} dx x^{\xi-1}\delta(x)^{2+\alpha_0} \qquad (2.26)$$

where a power law electron distribution with the same index $p = 2\alpha + 1$ all over the source is assumed, $x = R/R_0$, and $\xi = 1 + 2\epsilon - \epsilon[n + m(1 + \alpha_0)]$ is an important parameter, whose sign controls if most of the radiation is produced in the inner ($\xi < 0$) or outer ($\xi > 0$) parts of the jet, for constant δ-factor (without acceleration).

Ghisellini Maraschi & Treves (1985), with a costant δ-factor, found that a possible model for interpreting blazar spectra requires two components: the inner one with $\xi > 0$, for which the upper limit of the integral $R_2(\nu) = R_0(\nu_{max}(R_0)/\nu)^{1/\eta}$ is important, and a second, more external one, with $\xi < 0$, for which the lower limit is important. In this case the limit is given by the radial dependence of the self absorption frequency

$$\nu_m(R) = \nu_m(R_0)(R_0/R)^{k_m} \qquad (2.27)$$

where k_m can be derived by eqs. (1.19), (2.20), (2.22), which yield

$$k_m = \frac{2\epsilon}{5 + 2\alpha_0}[n + m(1.5 + \alpha_0) - 1] \qquad (2.28)$$

In a way analogous to the synchrotron luminosity, the self Compton (hereinafter IC) luminosity can be found from

$$L_c(\nu) \propto \nu^{-\alpha_0} \int_{x_1(\nu)}^{x_2(\nu)} dx x^{l-1}\delta(x)^{2+\alpha_0} \qquad (2.29)$$

where $l = 1 + 3\epsilon - \epsilon[2n + m(1+\alpha_0)]$ has the same meaning of ξ: $l > 0$ means that the outer regions of the jet are mostly contributing at the frequency ν, if $\delta(x)$ is constant. Note that, for the frequency range we are interested (1-10 keV), the limit of integration are usually constant, corresponding to the minimum and maximum size of the jet.

As an example, let's explore the case of $\alpha_0 = 0.5$, (corresponding to a monoenergetic injection of electrons, see next chapter), $\epsilon = 0.5$ for the inner zone, $m = 1$, $n = 2$, corresponding to a constant ratio of magnetic to particle energy density throughout the source, $e = 0$, corresponding to constant $\gamma_{max}(R)$, and no beaming.

For the inner, paraboloidal zone, $\xi = 0.25$ and, by eq. (2.26), $L_s(\nu) \propto \nu^{-(\alpha_0+\xi/\eta)}$ for $\nu > \nu_b$ where ν_b is the maximum frequency emitted by the larger regions of the paraboloid. This is the region mostly contributing at frequencies $\nu < \nu_b$, for which $L_s(\nu) \propto \nu^{-\alpha_0}$, down to the self absorption frequency of this region. Since $\eta = 0.5$, the spectrum is steepened by $\Delta\alpha = 0.5$ above ν_b. Going over towards the conical zone, we have $\xi = -0.5$, so that the inner regions dominate the emission up to their self absorption frequency. From eqs. (2.26) and (2.27) we have

$$L_s(\nu) \propto \nu^{-(\alpha_0+\xi/k_m)} \tag{2.30}$$

which, for $m = 1$, $n = 2$, and $\epsilon = 1$ gives a flat spectrum of index zero. Thus the overall synchrotron spectrum is characterized by three spectral indices: $\alpha_{thick} = 0$, $\alpha_0 = 0.5$, and $\alpha_1 = 1$, with the breaks at the self absorption and the maximum emitted frequency of the intermediate regions at the jet, connecting the paraboloid and the cone. Variability timescales should, in this model, decrease with increasing frequency, since only the smallest regions emit the highest frequencies.

For the assumed values of the parameters, we find $l = -0.25$ for the paraboloid, and $l = -1.5$ for the cone. Contrary to the synchrotron emission, the IC flux thus mostly comes from the inner jet, and in the range 1-10 keV, is characterized by the spectral index $\alpha_0 = 0.5$ for any reasonable choice of the magnetic field and the electron density.

Now let the plasma be accelerated according to eq. (2.23). In this case the spectrum is viewing-angle dependent, and some analytical results can be derived if

the viewing-angle $\theta = 0^0$ or $\theta = 90^0$, since in this case $\delta(0^0) \sim \Gamma$ and $\delta(90^0) \sim 1/\Gamma$, for $\Gamma \gg 1$. Then eq. (2.26) yields

$$L_s(\nu) \propto \nu^{-\alpha_0} \frac{x_2(\nu)^{\xi \pm g(2+\alpha_0)} - x_1(\nu)^{\xi \pm g(2+\alpha_0)}}{\xi \pm g(2+\alpha_0)} \tag{2.31}$$

where the + sign corresponds to $\theta = 0^0$, and the − sign to $\theta = 90^0$. Setting $\xi > g(2+\alpha_0)$ for the paraboloid, and for frequencies $\nu > \nu_b$, (with ν_b defined as before) the spectral slopes corresponding to $\theta = 0^0$ and $\theta = 90^0$ are

$$\alpha(\theta = 0^0) = \alpha_0 + \frac{\xi + g(2+\alpha_0)}{\eta}, \quad \nu \gg \nu_b \tag{2.32}$$

$$\alpha(\theta = 90^0) = \alpha_0 + \frac{\xi - g(2+\alpha_0)}{\eta}, \quad \nu \gg \nu_b \tag{2.33}$$

The hypothesis $\xi > g(2+\alpha_0)$ assures that larger regions dominate the emission at lower frequencies even for $\theta = 90^0$. However their contribution is enhanced for $\theta = 0^0$ and dimmed for $\theta = 90^0$, and correspondingly the two spectral indices are respectively steeper and flatter than in the case of constant Γ, for which $\alpha = \xi/\eta$. The flux density ratio at ν_b obviously depends on the Lorentz factor Γ_2 reached in the outer part of the paraboloid R^p_{max}

$$\frac{L_s(\nu_b, 0^0)}{L_s(\nu_b, 90^0)} \sim \left[\frac{R^p_{max}}{R_0}\right]^{2g(2+\alpha_0)} = {\Gamma_2}^{2(2+\alpha_0)} \tag{2.34}$$

in the hypothesis of negligible isotropic components, and if $\xi > g(2+\alpha_0)$.

In this scheme the flux at the largest synchrotron frequencies, coming from regions of small Lorentz factor, is nearly isotropic, and is the same for any viewing angle. Only at lower frequencies beaming effects become important, modifying the observed flux density, its slope, and the minimum variability timescale observable at a given frequency

$$t_{var}(\nu) \sim \frac{R(\nu)}{c} \frac{1}{\delta(R(\nu))} \tag{2.35}$$

If the bulk acceleration continues in the conical region, for which $\xi < 0$, the observed luminosity is in any case given by eq. (2.31), but reasonable values of g,

m, n now give $\xi < g(2+\alpha_0)$. Depending on the value of ξ, the enhancement due to beaming can let the outer regions be dominant for small viewing angles, up to the point where bulk acceleration is eventually halted and Γ becomes constant. The flat radio spectra observed in blazars in fact suggest the presence of a superposition of partially opaque regions, self absorbing at different frequencies. If the bulk acceleration let the outer regions dominate the emission in the radio band, the resulting spectrum would reflect that of the largest emitting zone, and no flat spectrum would be possible.

One can then envisage at least three components of different characteristics: an inner zone, with bulk acceleration of the plasma and paraboloidal shape, an intermediate zone, with bulk acceleration and conical shape, and the outer zone, with constant Γ-factor and conical shape. In the following, the model is applied to blazar spectra.

2.5 Application to blazars

All blazars (33 objects) observed in the UV band before December 1983 with the IUE satellite have been studied by Ghisellini *et al.* (1986), who presented a collection of data including radio, optical, UV and X-ray flux densities, and infrared, optical and UV slopes. In an accompanying paper, Maraschi *et al.* considered all blazars (75 objects) observed in the X-ray band, 52 of which of known redshift. Due to the large percentage of sources of known distance, the luminosity distribution in different bands could be studied. Both samples contain objects discovered by radio surveys (radio selected objects) and a minority of sources that has been or could have been discovered from X-ray observations (X-ray selected objects). In table 2.2 the mean spectral indices and luminosities are given. Overall spectral indices are defined from flux density ratios at the following frequencies: 5 GHz, 2500 Å, and 2 keV. UV luminosities are derived directly from the observed flux density at 2500 Å or extrapolating the optical flux with the optical spectral index. K-corrections are taken into account, using average values of α and redshift z when these quantities were not

available, and assuming $\alpha_{radio} = 0$ and $\alpha_x = 1$ for all objects.

Two main conclusion can be drawn from table 2.2:

1) *X-ray selected objects have significantly flatter spectral indices than radio selected blazars.* Both classes of objects show a gradual steepening from the radio to the optical band, less pronounced for X-ray sel. sources. A large change in shape occurs between radio and IR frequencies (compare α_{IR} with α_{RU}) as expected if the radio spectrum remains flat up to $3 \times 10^{11} \sim 10^{12}$ Hz (Ennis, Neugebauer, and Werner 1982, Landau *et al.* 1983, Gear *et al.* 1985). A further steepening occurs between the IR and the UV bands. The average $\Delta\alpha =< \alpha_{UV} - \alpha_{IR} >$ is about 0.5 for radio sel. objects, and ~ 0.35 for X-ray sel. ones. Note, however, that $\Delta\alpha$ values for individual sources are widely spread (see table 1 in Ghisellini *et al.* 1986). Comparing α_{UV} and α_{UX}, the 2 keV flux lies on average above the extrapolation from the UV for radio sel. sources, and below for X-ray sel. objects. In the SSC model, this can be interpreted as a greater contribution of the IC flux in radio sel. sources.

2) *X-ray and radio sel. blazars have the same mean X-ray luminosity, the former class being underluminous at UV and radio frequencies.* A phenomenological distinction between them can be made on the basis of α_{RX}: values less than 0.7 corresponds to radioweak, X-ray sel. sources. X-ray selection does not a priori introduce any bias toward one class. Through X-ray surveys is thus possible to infer the relative space densities of the two classes. The X-ray survey of Wood *et al.* (1984), complete at the flux limit of 1.5 μJy at 5 keV picked up 6 objects, and all of them are radioweak. Furthermore all X-ray serendipitously discovered BL Lacs turned out to be radioweak. Thus one is forced to conclude that radioweak objects have a larger space density than that of radio loud ($\alpha_{RX} > 0.7$) objects with the same X-ray luminosity.

The basic facts that have to be interpreted are:

a) The "classical" radio loud blazar may not be the tipical member of the class of blazars as a whole, representing only a minority of sources.

b) Radio loud have steeper spectra than radioweak blazars.

c) Both classes have the mean X-ray luminosity, but they differ by two orders of magnitude in the mean radio luminosities.

The jet model with bulk acceleration of the emitting plasma is able to qualitatevely account for all these facts. In this model, synchrotron emission produces X-rays in the inner regions of the jet, characterized by a small values of the Lorentz factor Γ. Being isotropically emitted, the X-ray luminosity appears the same for any viewing angle. Optical emission is preferentially produced in the intermediate zone, with intermediate values of Γ. It is moderately boosted, and appears slightly greater for head on observers. Finally, the radio emission coming from the outer regions of the jet is Doppler boosted with the maximum value of Γ (Γ_{max}). Then the same source viewed at differing angles appears with different shapes, steeper for smaller angles. The probability to see the source within an angle $1/\Gamma_{max}$ is of the order of $(2\Gamma_{max})^{-2}$, thus accounting for the inferred different space densities of radio loud and radio weak blazars.

To constrain the many parameters which the model requires, we are guided by the following considerations.

The minimum size R_0 of the inner jet can be suggested by the minimum variability timescale, which in this model should occur in the X-rays. Analogously, variability timescales at frequencies just below ν_b can fix the size of the intermediate regions. Setting $\nu_{max} \sim 10^{18}$ Hz and $\nu_b \sim 10^{14}$ Hz, from eq. (2.25) we derive η (applying eq. 2.25 to observed quantities, care must be taken to different Doppler shifts and time contractions of different frequencies and timescales). To proceed further, let assume that eqs. (2.32) and (2.33) apply to radio sel. and X-ray sel. blazars respectively

$$\alpha_{UX}(\theta = 0^0) - \alpha_{UX}(\theta = 90^0) \sim \frac{2g(2+\alpha_0)}{\eta}$$

If the infrared flux comes from the same, intermediate, region of the jet (the outer paraboloid) then $\alpha_0 \sim \alpha_{IR}$ and

$$(\alpha_{UV} - \alpha_{IR})_{\theta=0^0} \sim \frac{\xi}{\eta} + \frac{g}{\eta}(2+\alpha_0)$$

$$(\alpha_{UV} - \alpha_{IR})_{\theta=90^0} \sim \frac{\xi}{\eta} - \frac{g}{\eta}(2+\alpha_0)$$

but note that also the outer regions of the jet can contibute to the infrared, particularly for $\theta = 0^0$. The difference in the average optical luminosities between X-ray

and radio sel. sources can fix the value of Γ corresponding to the regions emitting frequencies close to ν_b. Then the g parameter can be derived by eq. (2.34). Since optical luminosities differ only by a factor of 10, g is small, of the order of 0.1 for $R^p_{max}/R_0 = 100$ and $\alpha_0 = 0.5$. To let the radio emission differ by a factor ~ 200, as table 2.2 indicates, bulk acceleration has to continue even if the jet geometry changes at R^p_{max}. A new set of parameters: η_2, ξ_2, g_2 is assumed for this conical region ($\epsilon = 1$). Bulk acceleration is halted at some radius R_2, and further on g_2 is set to zero, while the other parameters are not allowed to change. Throughout the whole jet, the same value of $\alpha_0 = 0.5$ is assumed. For the inner, paraboloidal region, $\epsilon = 0.5$.

Further constraints derive by the self Compton emission, which it is computed assuming that the radiation field is isotropic in the rest frame and that the scattering between electrons at a given position in the jet and photons produced in different regions can be neglected (local approximation, see Ghisellini, Maraschi & Treves 1985). A first constrain is that IC emission has not to overproduce X-rays. This limits the values of the magnetic field and of the electron density. Furthermore, to be viewing-angle independent, the observed X-rays have to be produced in the inner regions of the jet. This automatically happens for the synchrotron emission, but not for the IC one. Thus, assuming that the X-ray flux is mostly synchrotron in origin, we have to further limit the contribution of the IC flux.

Fig. 2.3, 2.4, and 2.5 show the SSC spectra computed with different choices of the parameters, listed in table 2.3. Stars denote the mean observed luminosities of the radio and X-ray sel. blazars in the radio, UV, and X-ray bands. The first model (fig. 2.3) adopts $n = 2$, $m = 1$ for the whole jet, and the emitting plasma is accelerated with $g = 0.2$ up to $R/R_0 = 100$, above which the plasma bulk velocity is constant. This choice of m and n corresponds to a constant ratio of particle to magnetic energy density. As fig. 2.3 shows, this model is underluminous at IR and radio frequencies, can account for the UV and X-ray luminosities, and does not show any break between the IR and UV bands for large viewing angles. In the second and

third model the parameters have been chosen following the prescriptions discussed above. They require larger values of ξ than that of fig. 2.3, and in the models of fig. 2.4 and 2.5 $\xi = 1$ for the paraboloid, and $\xi = 0$ for the cone. In both models bulk acceleration (with $g = 0.15$) is assumed to continue up to $x = 10^3$. The models differ only by the choice of m and n for the inner region. As fig 2.4 and 2.5 show, the IC flux becomes overluminous at X-ray frequencies as m increases. This is to be expected, because larger values of m correspond to smaller values of n ($cf.$ the definitions of ξ and l) and then to a greater dominance of the IC flux of the outer region of the paraboloid. Both models qualitatively account for the UV fluxes and slopes. In the radio band, the luminosity ratio between small to large viewing-angle sources is smaller than required by observations. In the X-ray band, the contribution of the IC flux is larger for smaller viewing-angles.

This model is necessarily highly idealized. In reality, the emission regions of the jet may be associated with discrete shocks, even if the regularity of the observed spectra suggests that, at least on average, a continuous model may be an acceptable representation of a succession of shocks. Although many parameters are involved, they are rather well constrained by the observed properties of blazars. Then, if the different spectra of radio and X-ray selected objects are solely due to orientation effects, stringent conditions on the properties of the relativistic jet are found. In particular, maximum Lorentz factor of the order of $3 \sim 4$ are indicated, achieved with a modest acceleration over a very extended spatial scale, a factor $100 \sim 1000$ of the inner dimension of the jet. Furthermore, in the paraboloidal region, the requirements that the synchrotron flux be mostly produced in the outer regions implies a weak radial dependence of the magnetic field, not to overproduce X-rays by the IC emission. The latter one contributes more for smaller viewing-angles. Coming from the intermediate regions, the associated time variability is less rapid than that of synchrotron radiation at the same frequencies. This can explain the peculiar behaviour of some BL Lac object, like 0735+178 (Bregman *et al.* 1984), which shows faster variability in the UV band than in X-rays. If the proposed model is correct, the IC flux coming from the intermediate regions can give a sizeable contribution to the X-ray band only for

radio sel. sources, which, on average, are then predicted to show less rapidly X-ray variability than X-ray sel. sources.

Table 2.1

Name		z	$\theta_d^{(b)}$ mas	ν_m GHz	F_m Jy	F_X Jy	δ	α_{RX}	R	Ref.
BL Lac objects										
0048–097	OB 081	...	0.4	5	0.71	6.6 (-8)	3.24	0.914	8.1	1,2
0212+73		...	0.6	5	1.5	2.3 (-7)	2.82	0.887	—	3,2
0219+428	3C 66A	0.444	1.5	5	0.2	1.6 (-7)	0.09	0.793	0.6	1,2
0235+164	AO	0.852	0.5	5	1.75	1.7 (-7)	6.19	0.9125	59.7	1,2
0306+102	PKS	...	0.5	5	0.73	1.1 (-7)	2.11	0.888	—	1,2
0316+41	NGC1275	0.018	0.3	22	1.2	1.8 (-5)	0.3	0.628	<2.9	4,2
0454+84		...	0.55	5	1.3	5. (-8)	3.71	0.965	—	3,2
0521–365	PKS	0.055	1.8	5	0.86	6.8 (-7)	0.16	0.794	0.3	5,2
0716+714		...	0.35	5	0.5	2.2 (-7)	2.28	0.827	—	3,2
0735+178	OI 158	0.424	<0.3	5	1.29	3.2 (-7)	7.2	0.859	>808	6,2
0754+100	OI 090	...	0.6	5	0.53	1.7 (-7)	1.06	0.845	12.1	1,2
0818–128	OJ 131	...	0.8	5	0.47	7. (-8)	0.68	0.888	1.5	1,2
0829+046	OJ 049	...	0.9	5	0.26	1.9 (-7)	0.26	0.798	8.	1,2
0851+202	OJ 287	0.306	0.3	5	2.3	1.7 (-6)	8.7	0.798	>995	7,2
1101+384	Mkn 421	0.03	<0.3	5	0.24	1.4 (-5)	0.49	0.55	2.8	6,2
1147+245	B2	...	0.9	5	0.39	8. (-8)	0.46	0.87	22.7	1,2
1215+303	ON 235	...	0.7	5	0.33	8.5 (-7)	0.38	0.727	1.6	1,2
1219+285	ON 231	0.102	0.5	5	0.13	4.2 (-7)	0.23	0.714	>866	8,2
1400+162	MC3	0.244	1.4	5	0.08	1. (-7)	0.04	0.768	0.4	1,2
1538+149	4C14.60	...	0.6	5	0.56	1.5 (-7)	1.14	0.855	7.8	9,2
1652+398	Mkn 501	0.034	<0.5	5	0.4	1.7 (-7)	0.35	0.829	19.9	9,2
1727+502	I Zw186	0.055	1.2	5	0.04	2.1 (-6)	0.01	0.557	<3.4	1,2
1749+096	4C 09.57	...	0.2	5	1.43	3.5 (-7)	15.0	0.860	>585	1,2
1803+78		...	0.4	5	1.8	1.6 (-7)	7.0	0.917	—	3,2
1807+698	3C 371	0.05	1.4	5	1.21	6. (-7)	0.36	0.82	1.3	10,2
2007+776		...	0.4	5	1.17	1.1 (-7)	4.87	0.914	—	3,2
2200+420	BL Lac	0.069	0.35	5	1.6	8.2 (-7)	4.39	0.818	78.4	7,2
2201+044	PKS	0.028	0.7	5	0.16	2.1 (-7)	0.17	0.765	—	1,11
2254+074	OY 091	...	1.0	5	0.14	1. (-7)	0.13	0.800	23.5	1,2
2335+031	PKS	...	1.7	5	0.03	<2.3 (-8)	0.02	>0.796	—	1,2

Table 2.1
(continued)

Name		z	$\theta_d^{(b)}$ mas	ν_m GHz	F_m Jy	F_X Jy	δ	α_{RX}	R	Ref.
HPQs										
0106+013	PKS	2.107	<0.4	5	2.3	2.2 (-7)	18.76	0.913	—	12,2
0336–019	CTA 26	0.852	<1.0	5	2.1	4.7 (-8)	3.02	0.995	—	12,2
0420–014	PKS	0.915	<0.7	5	1.5	5.2 (-7)	2.57	0.84	35.6	12,2
1253–055	3C 279	0.538	0.3	5	0.9	1.4 (-6)	4.15	0.756	1.9	7,2
1308+326	B2	0.996	0.5	5	1.97	3. (-7)	6.76	0.887	17.3	1,2
1641+399	3C 345	0.595	0.3	22	6.9	6.6 (-7)	5.22	0.913	5.9	13,2
2223–052	3C 446	1.404	0.4	10.7	2.2	1.1 (-6)	3.74	0.82	0.14	14,2
2230+114	CTA 102	1.037	<0.5	5	0.54	3.4 (-7)	1.85	0.807	7.8	9,2
2234+282	B2	0.795	<0.5	5	1.21	5. (-8)	5.17	0.961	—	9,2
2251+158	3C 454.3	0.859	<0.3	5	0.9	5.6 (-7)	5.93	0.808	6.6	7,2
2345–167	PKS	0.6	<0.4	5	2.5	1.8 (-7)	10.9	0.929	8.1	12,2

a) References:

1 Weiler and Johnston 1980
2 Ledden and O'Dell 1985
3 Eckart *et al.* 1982
4 Lawrence *et al.* 1985
5 Preuss and Fosbury 1983
6 Bååth *et al.* 1981
7 Kellerman *et al.* 1977
8 Weistrop *et al.* 1985
9 Zensus *et al.* 1984
10 Pearson and Readhead 1981
11 Madejski and Schwartz 1983
12 Kellerman *et al.* 1971
13 Unwin *et al.* 1983
14 Brown *et al.* 1981

b) When the minor and major axes a and b of the source are given we adopt $\theta_d = \sqrt{ab}$

*) Superluminal sources

Table 2.2

	All	X–ray sel.	Radio sel.	Strong line obj.
α_{IR}	0.94 ± 0.07 (28)	0.51 ± 0.10 (6)	1.06 ± 0.06 (22)	1.25 ± 0.09 (5)
α_o	1.38 ± 0.10 (31)	0.83 ± 0.14 (6)	1.51 ± 0.10 (25)	1.42 ± 0.15 (6)
α_{UV}	1.43 ± 0.11 (31)	0.87 ± 0.12 (6)	1.56 ± 0.11 (25)	1.52 ± 0.28 (7)
α_{RU}	0.59 ± 0.02 (75)	0.37 ± 0.03 (13)	0.63 ± 0.02 (62)	0.69 ± 0.02 (22)
α_{UX}	1.25 ± 0.03 (72)	1.03 ± 0.05 (13)	1.30 ± 0.03 (59)	1.23 ± 0.04 (21)
α_{RX}	0.80 ± 0.01 (72)	0.59 ± 0.02 (13)	0.85 ± 0.01 (59)	0.86 ± 0.01 (21)
$\log L_R$	33.44 ± 0.20 (53)	31.57 ± 0.09 (10)	33.87 ± 0.19 (43)	33.43 ± 0.19 (22)
$\log L_{UV}$	30.19 ± 0.14 (53)	29.51 ± 0.19 (10)	30.35 ± 0.16 (43)	30.71 ± 0.18 (22)
$\log L_X$	27.01 ± 0.13 (52)	26.85 ± 0.16 (10)	27.07 ± 0.16 (42)	27.54 ± 0.15 (21)

Average spectral indices and monochromatic luminosities (in *cgs* units) of blazars. Parentheses enclose number of objects for each entry (from Ghisellini *et al.* 1986 and Maraschi *et al.* 1986).

Table 2.3

Model number	1	2	3
B_0 (G)	200	100	100
$\tau_{c,0}$	2×10^{-3}	10^{-3}	10^{-3}
R_0 (cm)	3×10^{14}	3×10^{14}	3×10^{14}
x_1	100	50	50
x_2	10^3	10^3	10^3
x_3	10^5	10^5	10^5
g_1	0.2	0.15	0.15
g_2	0	0.15	0.15
m_1	1	0.5	1
n_1	2	1.25	0.5
m_2	1	1	1
n_2	2	1.5	1.5
η_1	1.8	1.8	1.8
η_2	1.2	1.2	1.2
ξ_1	0.25	1	1
ξ_2	-0.5	0	0
ρ_1	-0.25	0.9	1.25
ρ_2	1.5	-0.5	-0.5

Input and derived parameters for the models shown in Figs. 2.3-2.5. The radial extension of the paraboloid (x_1), the point at which bulk acceleration is halted (x_2), and the maximum radial extension of the cone (x_3) are in units of the inner size R_0.

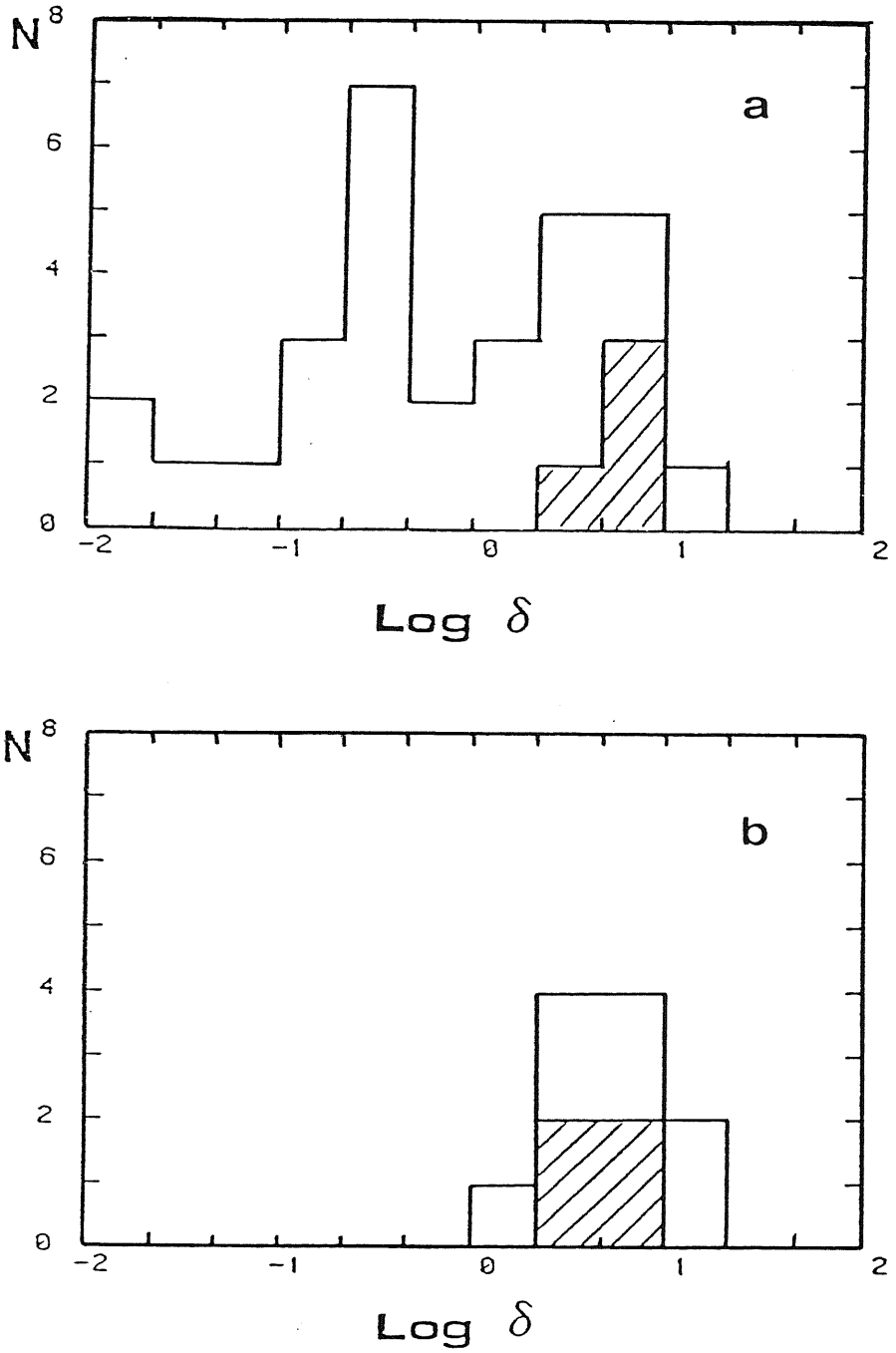

Figure 2.1. The distribution of the derived values of δ for BL Lac objects (*a*) and HPQs (*b*). Shaded areas corresponds to superluminal sources.

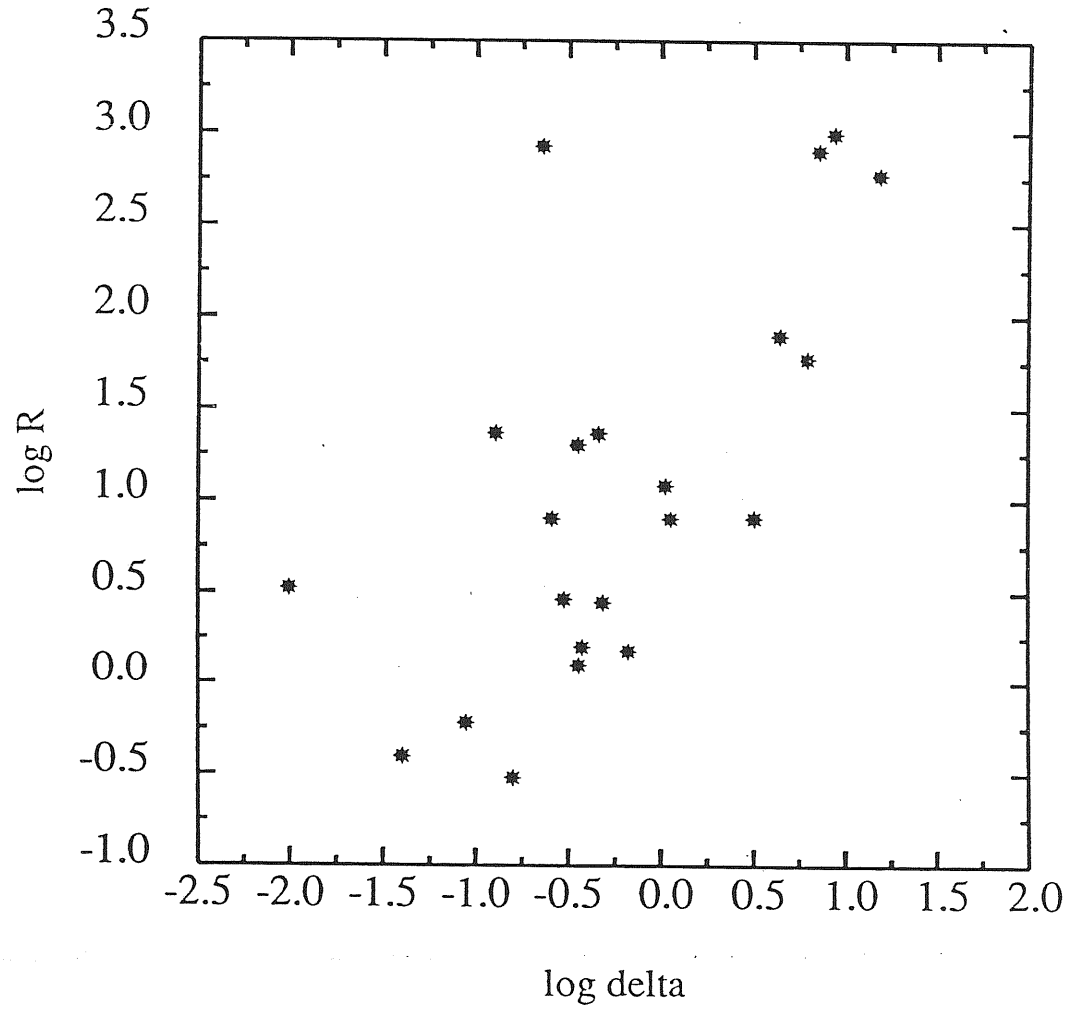

Figure 2.2. The core dominance parameter R (from Antonucci & Ulvestad 1985) vs. the value of the Doppler factor δ for BL Lac objects. The isolated point at the top of the diagram is ON 231.

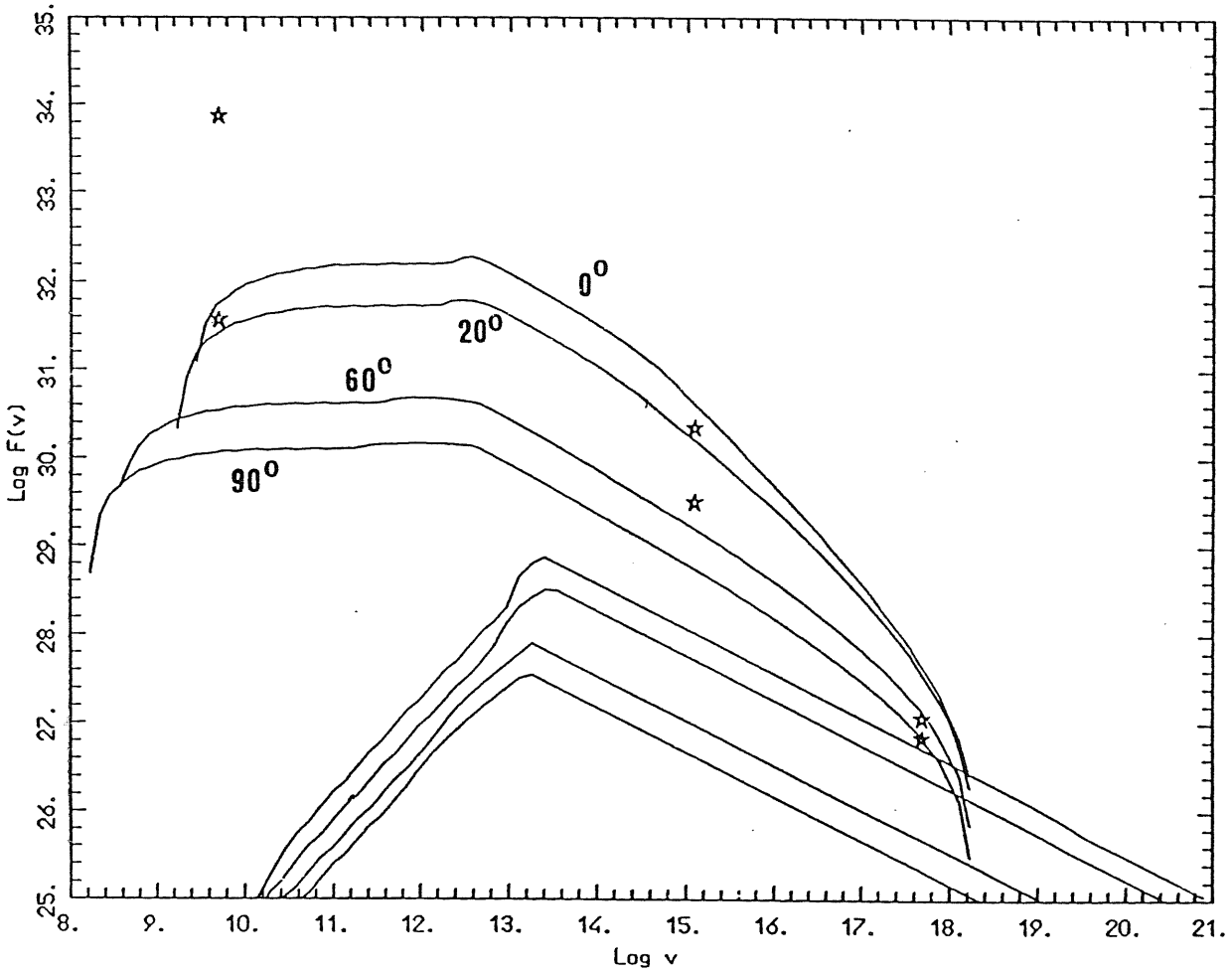

Figure 2.3. Overall synchrotron and self Compton spectra for the parameters listed in table 2.3 (*model* 1) corresponding to viewing angles $\theta = 0^0$, 20^0, 60^0, and 90^0 (from top to bottom).

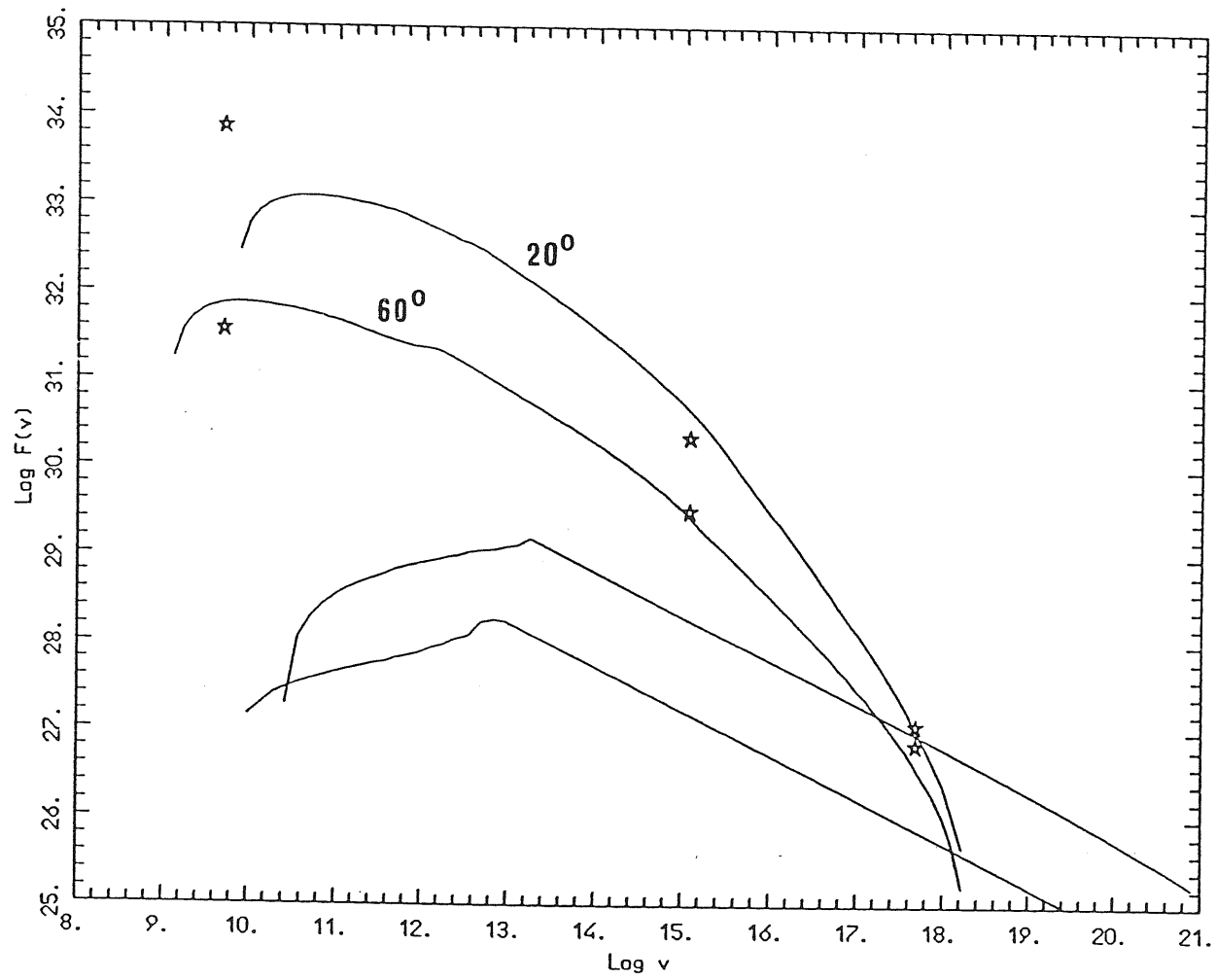

Figure 2.4. Overall synchrotron and self Compton spectra for the parameters listed in table 2.3 (*model* 2) corresponding to viewing angles $\theta = 20^0$, and 60^0 (from top to bottom).

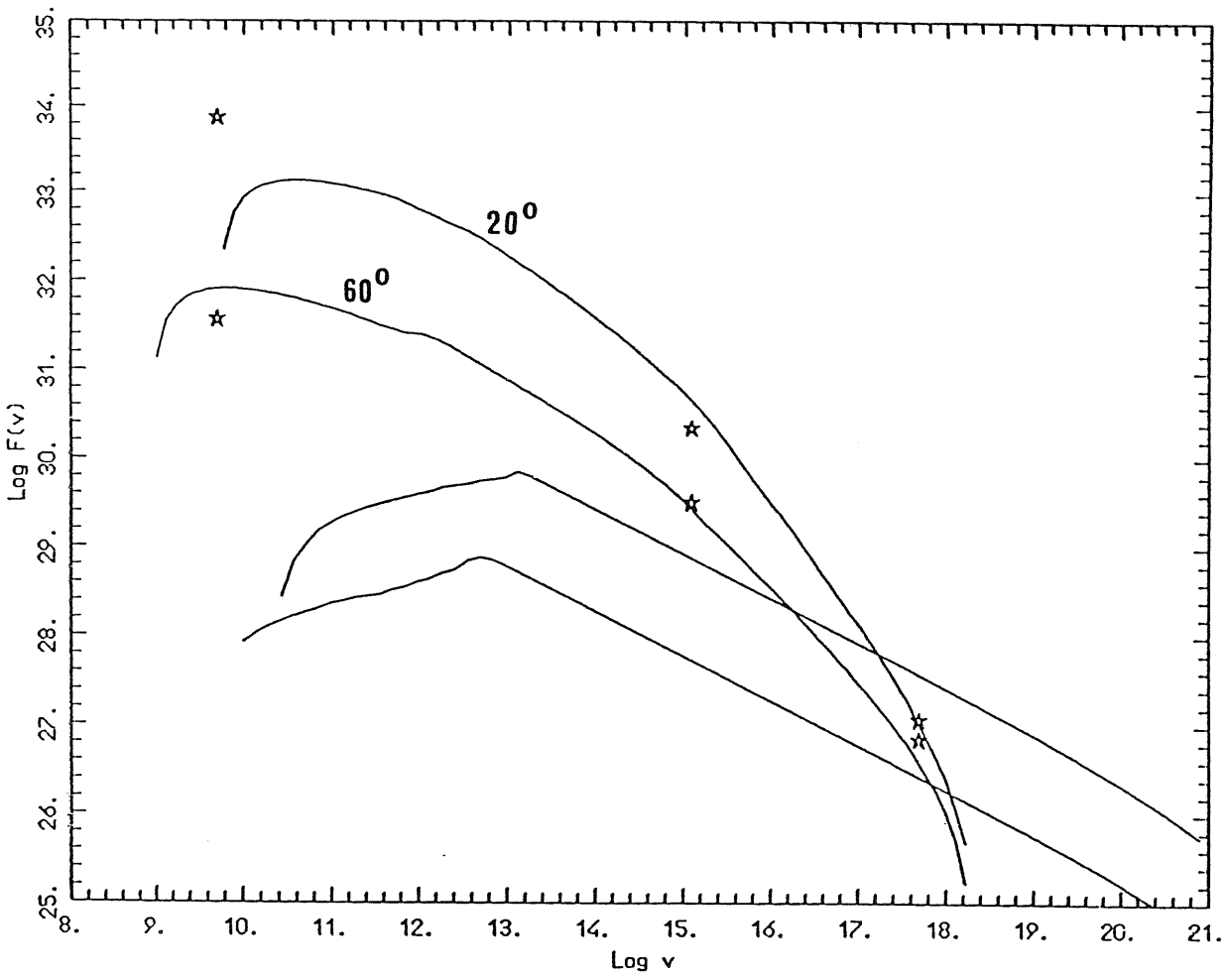

Figure 2.5. Overall synchrotron and self Compton spectra for the parameters listed in table 2.3 (*model* 3) corresponding to viewing angles $\theta = 20^0$, and 60^0 (from top to bottom).

CHAPTER THREE

THE SSC MODEL REVISITED

A crucial assumption of the standard model is that the electron distribution function is given a priori. If it is a power law of index p, than the standard theory predicts that the spectral index of the radiation is $\alpha = (p-1)/2$ both for the synchrotron and the self Compton spectrum, and any value of the spectral index can be accounted for by choosing an appropriate value of p. On the other hand, the steady electron distribution can be derived, on theoretical grounds, considering the kinetic equation for the electrons. This approach is a natural further step towards the understanding of the properties of the underlying acceleration mechanism. In this chapter the particle distribution function is self consistently derived considering a given electron source term, and the particle cooling and escape rates. Pair production is here neglected, being discussed in the next chapters.

This approach is not new (Kardashev 1962, Rees 1967b, Zdziarski 1986), but in this chapter previous results are extended and important consequences on the final spectra are found. The main point is that, for relativistic electrons, the cooling rate is not always proportional to the square of their energy, being inhibited by synchrotron reabsorption on one hand, and by the Klein Nishina decline of the scattering cross section on the other hand.

3.1 Characteristic timescales

Consider a source of radius R, magnetic field B and luminosity L. Define the

dimensionless parameter ℓ (Guibert, Fabian & Rees 1983)

$$\ell = \frac{L}{R}\frac{\sigma_T}{mc^3} \simeq 27\frac{L_{45}}{R_{15}} \tag{3.1}$$

which measures the compactness of the source. In terms of ℓ, the inverse Compton (IC) cooling timescale $t_c \equiv |\gamma/\dot{\gamma}_c|$ is given by

$$t_c = \frac{4\pi}{3}\frac{R/c}{\gamma\ell} \tag{3.2}$$

deriving eq. (3.2), I have implicitly assumed that all photons making the luminosity ℓ can be scattered with the Thomson cross section. The escape time t_{esc} of the electrons is a poor known quantity, and I will define it by a mean escape velocity $c\beta_{esc}$

$$t_{esc} = \frac{R/c}{\beta_{esc}} \tag{3.3}$$

Obviously, t_{esc} is always longer than the light crossing time $t_{cross} \equiv R/c$. Then a clear distinction between compact and non-compact sources can be made on the basis of the inverse Compton cooling timescale. Sources with $\ell > 1$ will be called compact, because in these sources the electrons of any relativistic energy Compton cool before escaping. The synchrotron cooling time t_s is given, neglecting self absorption, by

$$t_s = t_c\frac{U_r}{U_B} \tag{3.4}$$

If the source is optically thick to electron scattering, with optical depth τ_T, then t_c is shorter by the factor $\sim (1+\tau_T/3)$, due to the increased radiation energy density with respect to an optically thin source. The photon escape timescale t_{ph} in thin sources equals t_{cross}. Diffusion will increase t_{ph} by the factor $\sim (1+\tau_T/3)$.

3.2 The electron kinetic equation

The general form of the kinetic equation for relativistic electrons emitting synchrotron and self Compton radiation is given by eq. (1.35). To find a steady state

solution a numerical treatment is required, due to the presence of an heating term, corresponding to synchrotron reabsorption. However electrons of energy greater than γ_t do not reabsorb photons, and in this regime the kinetic equation has the steady solution

$$\frac{\partial}{\partial\gamma}\left[\dot{\gamma}N(\gamma)\right] + Q(\gamma) - \frac{N(\gamma)}{t_{esc}} = 0 \tag{3.5}$$

where $\dot{\gamma}$ is the total (synchrotron plus IC) cooling rate and $Q(\gamma)$ is the source term. For energies $\gamma < \gamma_t$, eq. (3.5) is approximately valid if $U_B < U_r$, since in this case Compton losses overcome synchrotron heating, in the self absorbed regime. If the particles can escape, and $\ell < 1$, a particular value γ_b will exist, for which the cooling time equals the escape time

$$\gamma_b = \frac{4}{3}\frac{\beta_{esc}}{\ell} \tag{3.6}$$

Electrons with $\gamma > \gamma_b$ radiatively cool rather than escape, while the opposite is true for $\gamma < \gamma_b$. Then the electron distribution is

$$N(\gamma) = \dot{\gamma}^{-1}\int_{\gamma}^{\gamma_{max}} d\gamma' Q(\gamma'), \quad \gamma > \gamma_b \tag{3.7}$$

$$N(\gamma) = Q(\gamma)t_{esc}, \quad \gamma < \gamma_b \tag{3.8}$$

Neglecting KN effects, the cooling rate is proportional to γ^2. For power law injection rates $Q(\gamma) = Q_0\gamma^{-s}$, the steady $N(\gamma)$ distribution will thus have a *stationary* break at γ_b, where the slope steepens by unity. For equipartition magnetic fields, the synchrotron frequency corresponding to γ_b is

$$\nu_b = 1.6\times 10^{12}\left(\frac{\ell}{0.01}\right)^{-3/2}\left(\frac{R}{10^{14}\mathrm{cm}}\right)^{1/2}\ \mathrm{Hz} \tag{3.9}$$

which, incidentally, is too small to explain the change in spectral slopes between the IR and the UV spectra of (beamed) blazars.

From now on, only the case $\ell > 1$ is considered. If the particles radiatevely cool down to $\gamma = 1$, the steady state condition implies that the injected kinetic luminosity must balance the luminosity coming out from the source in the form of radiation. Then the radiation energy density can be related to the injected luminosity L_i

$$U_r = \frac{3R}{4c}\frac{L_i}{(4/3)\pi R^3} \tag{3.10}$$

where the factor 3/4 is appropriate for spherical sources, and L_i given by

$$L_i = Vol\, mc^2 \int_{\gamma_{min}}^{\gamma_{max}} d\gamma Q(\gamma)(\gamma - 1) \tag{3.11}$$

For power law injection rates $\propto \gamma^{-s}$, and setting $\gamma_{min} = 1$, eq. (3.7) yields, for those electrons with $\gamma > \gamma_t$

$$\tau_c(\gamma) \equiv \sigma_T R N(\gamma) = \frac{\gamma^{-(s+1)}}{(s-1)\left[\frac{U_B}{U_r} + g(\gamma)\right]} \frac{\left[1 - (\gamma/\gamma_{max})^{s-1}\right]}{\left[\frac{1-\gamma_{max}^{2-s}}{s-2} - \frac{1-\gamma_{max}^{1-s}}{s-1}\right]} \tag{3.12}$$

For a monoenergetic injection $Q(\gamma) = Q_0 \delta(\gamma - \gamma_{max})$ we have

$$\tau_c(\gamma) = \frac{\gamma^{-2}}{\gamma_{max}\left[\frac{U_B}{U_r} + g(\gamma)\right]} \tag{3.13}$$

The function $g(\gamma)$ is defined by eq. (2.62). It is a constant and equal to unity if the scattering process occurs in the Thomson regime, and it is unimportant if $U_B > U_r$.

Several comments are in order. First, note that $\tau_c(\gamma)$ depends on the injected luminosity L_i only through the ratio U_B/U_r. If this ratio is smaller than $g(\gamma)$, then $\tau_c(\gamma)$ depends on the *shape* of the emitted spectrum, and eqs. (3.12), (3.13) become non linear. For $U_r > U_B$ and if KN effects are not important, the steady energy distribution of electrons is nearly independent of the injected power. If the number of injected particles (and hence the luminosity) is increased, the IC cooling rate increases also, and the steady $N(\gamma)$ remains constant.

Second, note that these equations are valid for $\gamma > \gamma_t$. Their validity can be extended to lower energies only for $U_B < U_r$. This is however not important when computing the synchrotron emission, whose self absorbed radiation [emitted by the unknown part of $N(\gamma)$] is usually a negligible fraction of the total luminosity. A more serious complication would occur if a fraction of the injected luminosity could escape in the form of kinetic energy of the electrons reheated by synchrotron reabsorption. This fraction will certainly be negligible in the case of flat ($s < 2$) injected distributions, since in this case most of the injected power is radiated in the thin part of the

spectrum. It will be negligible also in the case of $U_B < U_r$, for any injection slope s, since in this case Compton cooling dominates. Then it can be substantial only for $U_B > U_r$ and $s > 2$, but qualitative arguments can put strong limits on the escaping kinetic luminosity even in this case (see below). We confidently conclude that the radiation energy density will always corresponds to the injected luminosity L_i, so that eqs. (3.12) and (3.13) can be used in any case, at least for $\gamma > \gamma_t$.

Third, note that for $s > 2$, eq. (3.12) becomes indipendent on γ_{max}

$$\tau_c(\gamma) \simeq \gamma^{-(s+1)}(s-2)\left[\frac{U_B}{U_r} + g(\gamma)\right]^{-1}, \qquad \gamma > \gamma_t \tag{3.14}$$

For $\gamma < \gamma_t$, we face the same problems of point 2 above. Zdziarski (1986) used a step function for the synchrotron cooling rate, neglecting it for $\gamma < \gamma_t$, and thus deriving the $N(\gamma)$ distribution in the whole energy range. Zdziarki's assumption essentially means that the energy gains and losses of the electrons in the self absorbed regime exactly balance for each particle. As discussed in chapter 1, this is not true for any power law distribution of electrons. However, eq. (3.12) is valid below γ_t if $U_B < U_r$. In this case, since $g(\gamma) \sim 1$, $\tau_c(1) \simeq s - 2$, and the integrated Compton optical depth of the *relativistic* electrons is of the order of unity. Note that $\tau_c(1)$ has the same meaning of τ_c of the first chapter. Even if the electron distribution self consistently derived is not a unique power law (due to KN effects), $\tau_c(1)$ still measure the relative importance of the Compton flux with respect to the synchrotron one *at the same frequency* (eq. 2.5). The important consequences on the observed spectra will be discussed below.

Fourth: eq. (3.12) and (3.13) are also valid in the case of IC scattering off a given (externally produced) radiation field U_s, without magnetic field, provided that U_B is replaced with U_s. This was the case considered by Zdziarski & Lamb (1986), in which U_s is assumed to be blackbody radiation, and the injected electrons have a steep ($s > 2$) energy distribution. Without the complications introduced by synchrotron self absorption, the most important parameter of this model is the ratio U_s/U_r, which controls the overall shape of the emitted spectrum. For $U_s \gg U_r$, $\tau_c(1) \sim U_r/U_s \ll 1$, and the spectrum of the radiation reflects the shape of the

electron distribution ($\alpha \sim s/2$). In the opposite case, for $U_s \ll U_r$, $\tau_c(1) \sim g(1) \sim 1$, multiple Compton is important, and the overall spectrum is the superposition of many IC orders. Its spectral slope is flatter than the canonical value $\alpha = s/2$, and can be determined by general considerations of luminosity balance and conservation of photons, for any value of the injected power. A similar approach will be given below for SSC models.

Neglecting KN effects, the steady $N(\gamma)$ distribution cannot be flatter than γ^{-2}, corresponding to a spectral index of the emitted radiation $\alpha = 0.5$. Flatter slopes can be achieved, in limited energy ranges, only if KN effects become important. To quantify this statement, a dimensionless notation is useful, for which photon energies are measured in electron rest mass unit

$$x \equiv \frac{h\nu}{mc^2}$$

$$x_B \equiv \frac{h\nu_B}{mc^2} = \frac{B}{B_c}$$

$$B_c \equiv \frac{m^2c^3}{\hbar e} \simeq 4.4 \times 10^{13}\mathrm{G}$$

The approximated scattering cross section (eq. 1.54) is adopted. For simplicity, a monoenergetic injection of particles of energy γ_{max} is assumed, of luminosity L_i such that, by eq. (3.10), $U_r \gg U_B$. The radiation energy density is the sum of the synchrotron (U_r^s) and IC (U_r^c) contributions. Since $\tau_c(1) = \left[\gamma_{max}\left(g(1) + U_B/U_r\right)\right]^{-1} \ll 1$, U_r^s is dominant for energies below the maximum emitted synchrotron energy $x^s_{max} = (4/3)x_B\gamma^2_{max}$. The function $g(\gamma)$ can now be written as

$$g(\gamma) = \frac{\int_{x_t}^{x^s_{max}} U_r^s(x)dx + \int_{x^s_{max}}^{3/(4\gamma)} U_r^c(x)dx}{U_r}, \qquad \gamma < \frac{9}{16x_B\gamma^2_{max}} \tag{3.15}$$

$$g(\gamma) = \frac{\int_{x_t}^{3/(4\gamma)} U_r^s(x)dx}{U_r}, \qquad \gamma > \frac{9}{16x_B\gamma^2_{max}} \tag{3.16}$$

If, in eq. (3.15), the first integral is greater than the second one, KN effects introduce a flattening (with respect to γ^{-2}) in the $N(\gamma)$ distribution only for $\gamma >$

$9/(16 x_B \gamma_{max}^2)$. Requiring γ_{max} be above this limits yields

$$\gamma_{max} > \left(\frac{9B_c}{16B}\right)^{1/3} = 2.9 \times 10^4 B^{-1/3} \tag{3.17}$$

While the condition $U_B > U_r$ reads

$$B < \frac{3}{R}\left(\frac{L_i}{2c}\right)^{1/2} \simeq 390\, L_{45}^{1/2} R_{15}^{-1}\ \mathrm{G} \tag{3.18}$$

Fig. 3.1 shows a SSC spectrum numerically computed for $L_i = 10^{45}$ erg/s, $R = 10^{15}$ cm, $B = 100$ G, and $\gamma_{max} = 10^4$. For these parameters $U_r/U_B \simeq 15$. Note that the synchrotron spectrum flattens at the highest energies, as a result of the corresponding flattening of the $N(\gamma)$ distribution. Due to the high value of γ_{max}, the first order IC emission already reaches the maximum possible energy, and consequently the second order is unimportant (dashed line). It is important to realize, as fig. 3.1 shows, that the IC to the synchrotron luminosity ratio is about 3, despite the much greater value of the ratio U_r/U_B. The decline of the scattering cross section has in fact strongly suppressed the IC emission, increasing the steady particle number densities at high energies, and thus ultimately enhancing the synchrotron luminosity. From eq. (3.15), the flattening in $N(\gamma)$ is expected for $\gamma \geq 2500$, corresponding to synchrotron frequencies $x \geq 2 \times 10^{-5}$, in agreement with the numerical result of fig. 3.1. At these energies, the slope is $\alpha \sim 0.3$.

3.3 Injection of a steep distribution of particles

Consider to inject a power law distribution of relativistic electrons $Q(\gamma) = Q_0 \gamma^{-s}$, with $s > 2$. Most of the injected power is in the lowest energetic electrons, which will radiate self absorbed synchrotron photons and thin IC emission. The power absorbed substantially modifies the particle distribution if $U_B > U_r$ with respect to the optically thin case (Ghisellini, Guilbert & Svensson, in preparation). For the same range of energies the net cooling (losses minus gains) timescale becomes longer than the escape

time, even for $\ell > 1$. A fraction of the injected power will escape in the form of a wind, whose kinetic energy depends on the average energy γ_p of the steady energy distribution function. The value of γ_p in turn depends on on the ratio U_r/U_B, the slope s, and on the escape time. If the particles are electrons, steady state requires that the total numbers of injected and escaping electrons, per unit time, balance. Then the particle density is fixed, and the scattering optical depth τ_e is known

$$\tau_e = \frac{3}{4\pi} \frac{s-2}{s-1} \frac{\ell_i}{\beta_{esc}} \tag{3.19}$$

where ℓ_i is the total injected power, including particle rest mass, and it is assumed that the injected $Q(\gamma)$ distribution is a power law of index s from $\gamma_{min} = 1$. If the injected particles are pairs, eventually their annihilation timescale is shorter than the escape time, and in this case a minimum optical depth τ_p can be found balancing the injection with the annihilation rate (see next chapter). It is a lower limit since it is derived assuming that pairs annihilate at very low energies, where the cross section is maximized

$$\tau_p = \left(\frac{4}{\pi} \frac{s-2}{s-1} \ell_i \right)^{1/2} \tag{3.20}$$

From eqs. (3.19) and (3.20) we conclude that the optical depth is inevitably greater than unity, for $\ell_i > 1$, and if reacceleration of the lowest energetic particles is not at work.

The ratio of the rest mass to the total power is

$$\frac{\ell_{rest\ mass}}{\ell_i} = \frac{s-2}{s-1} = \frac{1}{\gamma_i} \tag{3.21}$$

where γ_i is the mean energy of the injected electron distribution function. To self consistently derive the spectrum of the outgoing emission we have to know the fraction of the injected power available for radiation. In other words, we have to know the kinetic luminosity of the wind, $\ell_{w,k}$. Assuming electrons, the ratio of escaping and injected kinetic luminosities is

$$\frac{\ell_{w,k}}{\ell_{i,k}} = \frac{\gamma_p - 1}{\gamma_i - 1} \tag{3.22}$$

General arguments suggest that this ratio is much less than unity, independently of the ratio U_B/U_r. Consider in fact the Compton y parameter for $\ell \gg 1$

$$y = \tau_e^2\left[(\gamma_p - 1) + (\gamma_p - 1)^2\right] = \tau_e^2\gamma_p(\gamma_p - 1) \tag{3.23}$$

the y parameter is constrained to be, at most, of the order of a few, because the Compton luminosity ℓ_c must be obviously less than $\ell_i/(s-1)$. Then, for $\ell_i \gg 1$

$$\gamma_p - 1 = \frac{y}{\tau_e^2\gamma_p} \ll 1 \tag{3.24}$$

and consequently $\ell_{w,k}$ is negligible with respect to $\ell_{i,k}$. For $\ell_i \gg 1$, all the kinetic injected luminosity produces radiation, rather than power a wind.

The bulk of the radiation is produced by the IC process, which becomes the dominant emission mechanism even for $U_B \gg U_r$. The ratio of the synchrotron to the Compton luminosity L_s/L_c is no more equal to U_B/U_r, but it is instead determined by the fraction of power injected above or below γ_t. From eq. (1.19), approximating the (slowly varying) gamma functions with a constant value

$$\gamma_t \simeq \frac{3}{4}\left[\left(\frac{3}{2}\right)^{s+1}\frac{\sqrt{\pi}}{2\sqrt{3}}\frac{\tau_c(\gamma_t)}{x_B\alpha_f}\right]^{1/4} \tag{3.25}$$

where α_f is the fine structure constant.

To find L_c/L_s, I assume that the synchrotron self absorbed luminosity is negligible with respect to the thin synchrotrone one, and neglect the kinetic luminosity in the escaping particles. Then

$$\frac{L_c}{L_s} = \frac{\int_1^{\gamma_{max}} d\gamma Q(\gamma)(\gamma-1)}{\int_{\gamma_t}^{\gamma_{max}} d\gamma \dot{\gamma}_s N(\gamma)} - 1 \tag{3.26}$$

If $U_B \gg U_r$, this expression simplifies into

$$\frac{L_c}{L_s} \simeq \gamma_t^{s-2} - 1 \tag{3.27}$$

which is independent on the Compton cooling regime (KN or Thomson). For $U_r > U_B$ this ratio approximately increases by the factor $(U_B + U_r)/U_B$. It also increases for steeper injections, since more power is injected at energies smaller than γ_t. Even if

$U_B \gg U_r$, higher order IC scatterings are important, since the total radiation energy density greatly exceeds that in synchrotron photons.

In order to find the resulting spectrum analytically, without computing each IC contribution, further considerations have to be made.

1) Eqs. (3.19) and (3.20) indicate that the scattering optical depth, for $\ell \gg 1$, is large. However, it can be reduced if reacceleration of subrelativistic particles occurs, in a timescale shorter than the escape time. If the reacceleration process is active also for relativistic particles, then the injected kinetic luminosity is not totally radiated, and eq. (3.26) is not valid.

2) Our ignorance of the actual shape of the $N(\gamma)$ distribution for the $U_B \gg U_r$ case prevents us to know the shape of the individual IC contributions to the overall spectrum, although general arguments are sufficient to fix the overall spectral index.

3) The KN limit $\dot{\gamma}_c = 0$ for $\gamma x > 3/4$ will play a double important role: first, it constrains the number of IC scatterings to be finite, and second, it fixes the slope of the γ-ray spectrum, which, as shown below, is always greater than unity.

I will consider, in turn, two cases. In the first one I will neglect the effects of subrelativistic particles, assuming that they are reaccelerated and reinjected. In the second case the overall spectrum is found taking into account the effects of cool particles, with the optical depth given by eq. (3.19) or (3.20).

Starting with the first case, I will assume that the overall spectrum is a power law with index α_c from x_t to $x = 1$, and α_γ above. It is easy to realize that α_c must be less than one, since for photon conservation the IC radiation cannot be greater than the synchrotron one at energies close to x_t, while the integrated luminosity has to exceed the synchrotron one. The spectral index α_γ in the case of multiple Compton scatterings by a steep electron distribution of index p off an externally produced radiation field of index α has been derived by Zdziarski & Lamb (1986) and discussed in chapter one. For $x > 1$ eq. (1.52) reads

$$\ell(x) \propto \int_{3x/(4\gamma_{max})}^{3/(4x)} dx' n(x') \gamma N(\gamma), \quad \gamma = \left(\frac{3x}{4x'}\right)^{1/2} \tag{3.28}$$

Since $n(x') \propto (x')^{-\alpha_c - 1}$, the upper limit of the integral will be important if $p >$

$2\alpha_c + 1$. In this case the IC radiation at a given x mainly comes from electrons of energy $\gamma \sim x$ scattering photons of energy $1/x$. If $U_r > U_B$, $p = s + \alpha_c$, yielding $\alpha_\gamma = s - 1$. On the other hand, for $U_r < U_B$, the $N(\gamma)$ distribution will be steeper than $s + \alpha_c$ for $\gamma < \gamma_t$, yielding $\alpha_\gamma > s - 1$ up to $x \sim \gamma_t$. Above γ_t, KN effects are not important if $U_B > U_r$, and $p = s + 1$, yielding $\alpha_\gamma \sim s + \alpha_c$ above $x \sim \gamma_t$.

Since $\alpha_c < 1$ and $s > 2$, we conclude that $\alpha_\gamma > 1$ in any case. As a consequence, only a small fraction of the injected luminosity is channeled into γ-ray radiation.

Assuming that the overall spectrum begins at x_t with the synchrotron luminosity $L_s(x_t)$ and that it is described with the two slopes α_c and α_γ, we can derive α_c balancing the injected and the emerging luminosities

$$\frac{L_i}{s-1} = L_r(x_t \leq x \leq 1) + L_\gamma \tag{3.29}$$

The first term of the RHS is the integrated luminosity (including the synchrotron one) up to $x = 1$, while the second term refers to the integrated luminosity above $x = 1$. Solving for α_c we have

$$\alpha_c \simeq 1 - \frac{1}{\ln(1/x_t)} \ln\left[\frac{2(1-\alpha_c)}{s-2}\frac{L_c}{L_s}\left(1 - \frac{L_\gamma}{L_c}\right) + \frac{s-2\alpha_c}{s-2}\right] \tag{3.30}$$

Since $L_\gamma/L_c \ll 1$, eq. (3.30) can be used also when $U_B \gg U_r$, and only a lower limit for α_γ is known.

When $U_B < U_r$, the steady electron distribution can be found from eq. (3.12), which becomes valid for all energies. In this special case, I have numerically derived the final spectrum, shown in fig. 3.2, for $R = 10^{15}$ cm, $L_i = 10^{45}$ erg/s, $s = 3$ and for $B = 274$ G, corresponding to $U_B/U_r \simeq 1$. This spectrum has been computed using a code constructed following the prescriptions given by Zdziarski (1986a).

As can be seen, the overall emission is the convolution of the synchrotron and many orders IC radiation, giving rise to a smooth power law up to $x = 1$. The γ-ray spectral index is $\alpha_\gamma \sim 2 \sim s - 1$, while $\alpha_c \sim 0.81$. Eqs. (3.25), (3.27) and (3.30) yield $\alpha_c = 0.80$, in good agreement with the value found numerically.

It must be noted that the break at $x \sim 1$ is caused by KN effects, and not by $\gamma - \gamma$ collisions and pair production. In these computations, pair production is

completely neglected. It can be taken into account, but pairs are expected to play a negligible role here, due to the steepness of the γ-ray spectrum. Furthermore, in the saturated pair production regime, when all γ-rays get absorbed, and for $U_B < U_r$, the pair production rate $P(\gamma)$ has the same slope as the primary injected particles, i.e. $P(\gamma) \propto \gamma^{-s}$, so that pairs will not change the derived spectral index α_c (Zdziarski & Lamb 1986).

So far the effects of cool, subrelativistic particles have been neglected. If they are not reaccelerated at relativistic energies, they provide an important source of opacity. Our previous condition $\ell > 1$ yields scattering optical depths $\tau_T > 1$ in any case. If the source is optically thick for scattering, we must take into account photon diffusion, enhancing photon and radiation energy densities by the factor $\sim 1 + \tau_T/3$, and thermal Comptonization of soft radiation, which will approximately increase the energy of photons below the thermal particle energy by the factor e^y (Guilbert, Fabian, & Rees 1983).

Finally, hard radiation will be down scattered by cool particles, and the spectrum should break at $x = 1/\tau_T^2$. Above this break, the spectral index is approximately $\alpha_c' = \alpha_c + 0.5$ (Sunyaev & Titarchuck 1980). I will use this spectral index up to $x = 1$, but it must be stressed that this assumes a crude approximation of the exact KN cross section. Consequently, I will assume that the photon density $n(x) \propto x^{-\alpha_c - 2}$ between $1/\tau_T^2$ and 1.

In the special case of $\alpha_c > 0.5$, most of the radiation energy density is at energies close to $1/\tau_T^2$. Furthermore, repeating the arguments above concerning the possible values of α_γ, it can be found that α_γ is always greater than unity. Neglecting the γ-ray luminosity, the luminosity balance equation can now be written

$$L_r = L(1/\tau_T^2 \geq x \geq x_t) + L(1 \geq x \geq 1/\tau_T^2) \tag{3.31}$$

which yields

$$\alpha_c \approx 1 - \frac{1}{\ln[1/(\tau_T^2 x_t)]} \ln\left[\frac{2(1-\alpha_c)(2-\alpha_c-1)}{s-2}\left(\frac{L_c}{L_s}+1\right)\right] \tag{3.32}$$

valid for $\alpha_c > 0.5$. Comparing eq. (3.30) with eq. (3.32) we can see that α_c will now be flatter, since most of the luminosity must now be emitted in a restricted range of energies.

Fig. 3.3 shows a spectrum numerically computed for the same parameters of fig. 3.2, but taking into account cool particle effects. The Thomson optical depth is $\tau_T = 4.15$ (eq. 3.20) and the Compton equilibrium dimensionless temperature $\Theta = kT/mc^2 \approx 0.01$. Comptonization has been included, following the equations discussed in section 1.5. To take down scattering into account, a steepening of $\Delta\alpha = 0.5$ between $1/\tau_T^2$ and 1 has been assumed. The kink in the spectrum at $x \sim 10^{-2}$ is due to the abrupt cut off assumed for the Comptonized spectrum. For easy comparison, fig. 3.2 also shows the overall spectrum for the same parameters, without cool particle effects. As can be seen, the resulting spectral index is now flatter, being $\alpha_c = 0.74$ between x_t and $1/\tau_T^2$. Using eq. (3.32) we can derive, for the chosen parameters, $\alpha_c \approx 0.75$.

3.4 Discussion

The synchrotron and the IC spectra emitted by relativistic electrons injected with a power law distribution of index s can be characterized by spectral indices very different from the canonical value $\alpha = s/2$. This result was obtained assuming no reacceleration of relativistic particles, and requiring that the radiative cooling timescale is shorter than any other relevant timescale (escape, annihilation, thermalization).

For flat injections ($s < 2$) and for $U_r \gg U_B$, we have argued that the synchrotron spectrum flattens towards high energies, due to KN effects on the electron cooling rate.

When the injected power law is steep ($s > 2$), the Compton process always dominates the cooling, independent on the ratio U_B/U_r. In this case, higher order Compton scatterings are important and the overall spectrum is always flatter than unity up to $x \sim 1$ (or up to $x = 1/\tau_T^2$ if no reacceleration of thermal particles occurs).

The detailed knowledge of the electron distribution function below γ_t is not necessary to find the overall shape of the spectrum, even if $U_B \gg U_R$. The overall behaviuor can be derived by the requirement of steady state and by considerations about KN effects.

In order to illustrate, at least partially, the dependence of the spectral index α on the injection slope s, numerical computations were performed for different values of s, for fixed luminosity, size, and magnetic field. Fig. 3.4 shows the results of these computations for $U_r \sim U_B$ (upper line) and $U_B \sim 10^{-2}U_r$ (lower line). For $s < 2$, the plotted spectral index refers to the synchrotron emission at energies just above x_t, while for $s > 2$ it describes the overall spectrum from x_t to $x \sim 1$. Cool particle effects are neglected.

As can be seen, for $1 < s < 2$, α is somewhat steeper than the canonical value $\alpha = s/2$, due to the steepening of the electron distribution for γ approaching γ_{max} (*cf.* eq. 3.12). However, the usual relation $\alpha = s/2$ can be recovered if a larger γ_{max} is used. The steepest spectrum is obtained for $s \sim 2$, for which $\alpha \sim 0.95$ in the equipartition case. For $s > 2$, α flattens for steeper injections, due to the increasing dominance of L_c with respect to L_s. In the equipartition case, for $0 < s < 4$, the spectral index α, as defined above, is constained in the narrow range $0.5 < \alpha < 1$. Taking into account cool particle effects introduces a steepening above $1/\tau_T^2$. The condition of fixed total luminosity would then flatten the spectrum between x_t and $x = 1/\tau_T^2$, to compensate the steepening at higher energies. Spectral indices flatter than 0.5 can be obtained only for $U_r \gg U_B$ and $s > 2$.

In fig. 3.5 the behaviour of α for different values of U_B/U_r is shown for the particular case $s = 3$, again neglecting cool particle effects. As fig. 3.5 shows, even for $U_B \gg U_r$, the spectral index is smaller than unity, since also in this case the Compton luminosity exceeds the synchrotron one. For smaller magnetic fields, the ratio L_c/L_s increases, yielding flatter overall spectral indices.

The crucial assumption of this work is that no reacceleration of relativistic particles occurs. In the steep injection case, this always implies $L_c/L_s > 1$, even when

$U_B > U_r$. If, instead, low energy electrons with $\gamma < \gamma_t$ are reaccelerated before loosing a substantial fraction of their energy, than the ratio L_c/L_s reflects the ratio U_r/U_B, and spectra steeper than unity can be obtained if $U_B > U_r$. Thus steep broad band spectra should indicate magnetic dominated sources in which an efficient reacceleration mechanism is at work. On the other hand, steep spectra in narrow frequency bands can be produced in the flat injection case, either by the high energy cut off of the electron distribution, or if $U_B > U_r$, by the electrons with $\gamma_t < \gamma$ radiating in X-rays by the IC mechanism.

As already remarked, the SSC model with steep injection is analogous to the pure Compton model discussed by Zdziarski & Lamb (1986) which was applied to γ-ray burst sources, assumed to be weakly magnetized neutron stars. According to the result of the present study, synchrotron emission can be the source of soft radiation in γ-ray bursts, but in order to obtain flat spectra ($\alpha < 0.5$), the magnetic field has to be weak, well below the equipartition value with U_r, as can be seen from fig. 3.5.

It is worth noting that the break at $x \sim 1$ (0.5 MeV) strongly resembles the break that should occur in models where $\gamma - \gamma$ collisions and pair production is important (see next chapters). Here, the break has a completely different origin, being due only to Klein Nishina effects. If cool particles are not reaccelerated, but can only escape or annihilate, another break at $x = 1/\tau_T^2$ is present in both models, due to down scattering by the cooled electrons or pairs, respectively. Thus these spectral features alone can not be used as diagnostic in favour of the importance of pair production. Instead, they can give informations on the presence of a reacceleration mechanism. Furthermore, as shown in this work and, in a different context, by Zdziarski & Lamb (1986), a flat X-ray spectrum breaking at $x \sim 1$ into a steep γ-ray spectrum is suggestive of a steep electron distribution and of small magnetic fields or small external soft radiation fields.

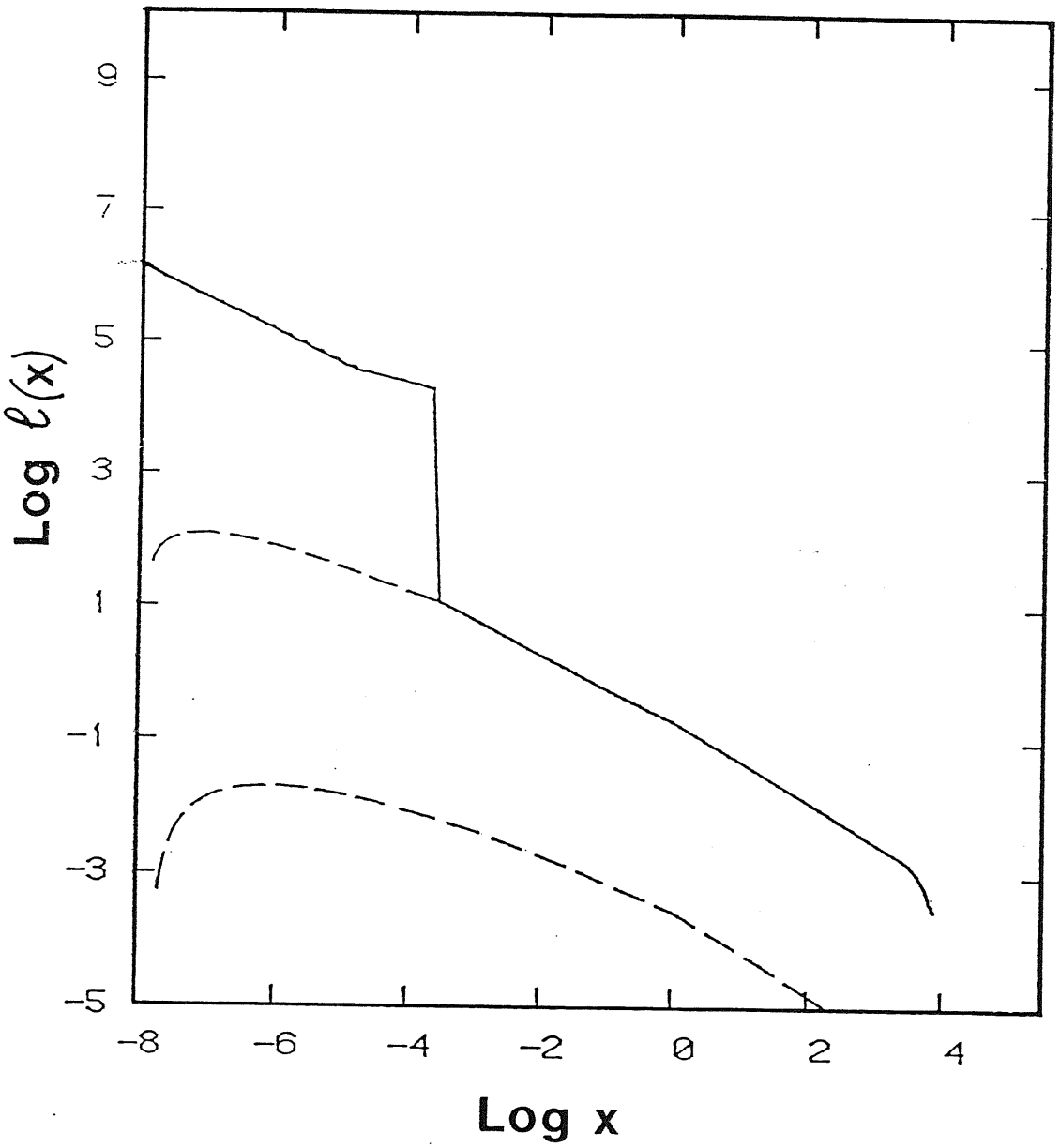

Figure 3.1. SSC spectrum computed numerically for $L_i = 10^{45}$ erg/s, $R = 10^{15}$ cm, $B = 100$ G, and monoenergetic particle injection at $\gamma_{max} = 10^4$. For these parameters, $U_r/U_B \sim 15$. The flattening at high synchrotron energies is due to Klein Nishina dimming. The lower dashed line corresponds to the second order Compton scattering.

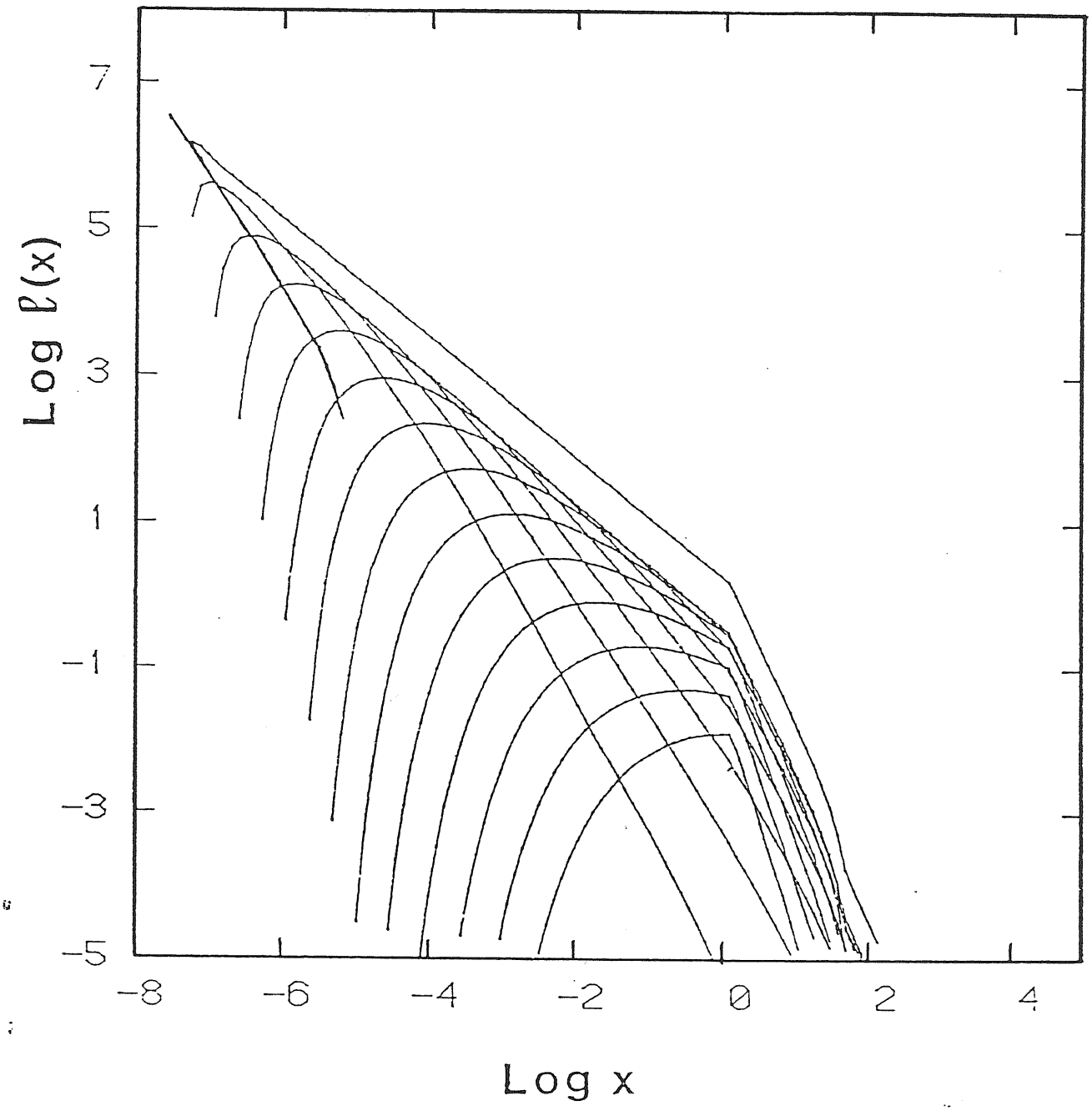

Figure 3.2. SSC spectrum, computed numerically for a power law particle injection rate with slope $s = 3$. The other input parameters are $L_i = 10^{45}$ erg/s, $R = 10^{15}$ cm, and $B \sim 275$, corresponding to $U_B \sim U_r$ and $\ell_i \sim 27$. The slopes of the overall spectrum are $\alpha_c \sim 0.81$ and $\alpha_\gamma \sim 2$. Cool particle effects are here neglected.

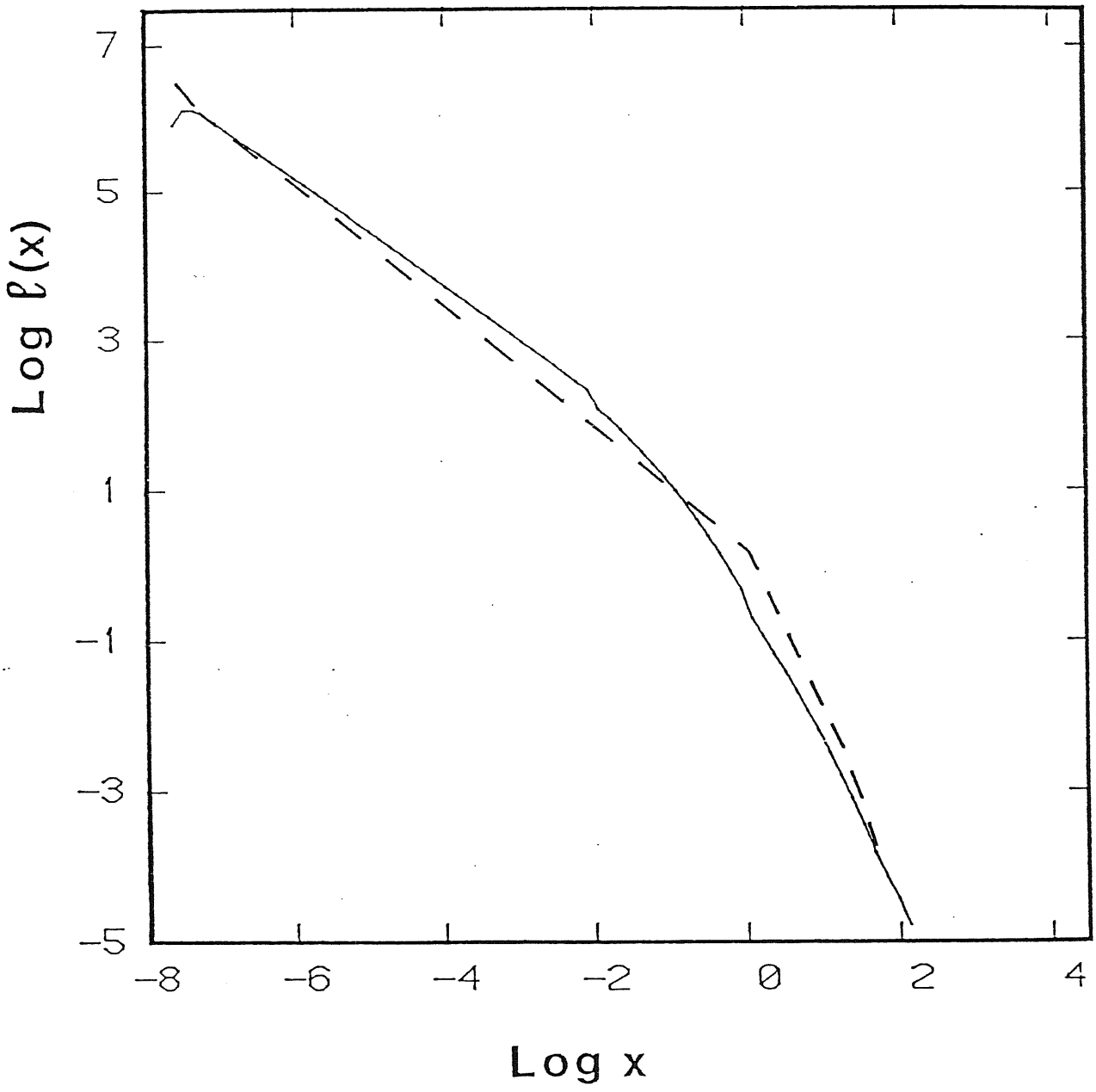

Figure 3.3. SSC spectrum, computed numerically for the same parameters of fig. 3.2, but including cool particle effects. The injected particles are assumed to be pairs, yielding a Thomson optical depth $\tau_T \sim 4.2$. The Compton equilibrium temperature is $\Theta_c \sim 10^{-2}$. The spectral indices are $\alpha_c \sim 0.75$ and $\alpha_\gamma \sim 1.7$. The overall spectrum of fig. 3.2 is reported (dashed line).

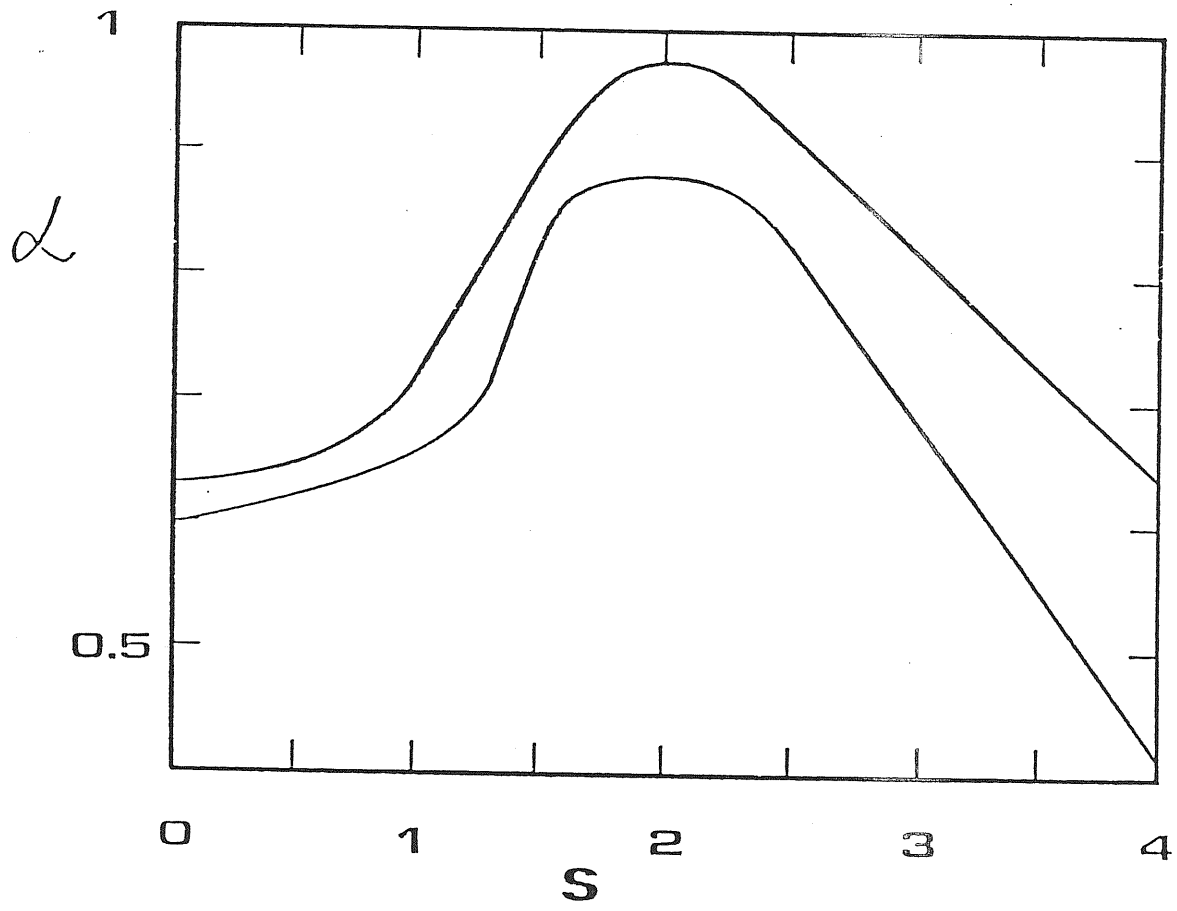

Figure 3.4. Spectral index α vs. injection slope s for $L_i = 10^{45}$ erg/s, $R = 10^{15}$ cm. *Upper line:* $U_B \sim U_r$. *Lower line:* $U_B \sim 10^{-2} U_r$ (for $s < 2$). For $s < 2$, the spectral index α refers to the synchrotron spectrum just above x_t, while for $s > 2$ it describes the overall spectrum up to $x \sim 1$. Cool particle effects are neglected.

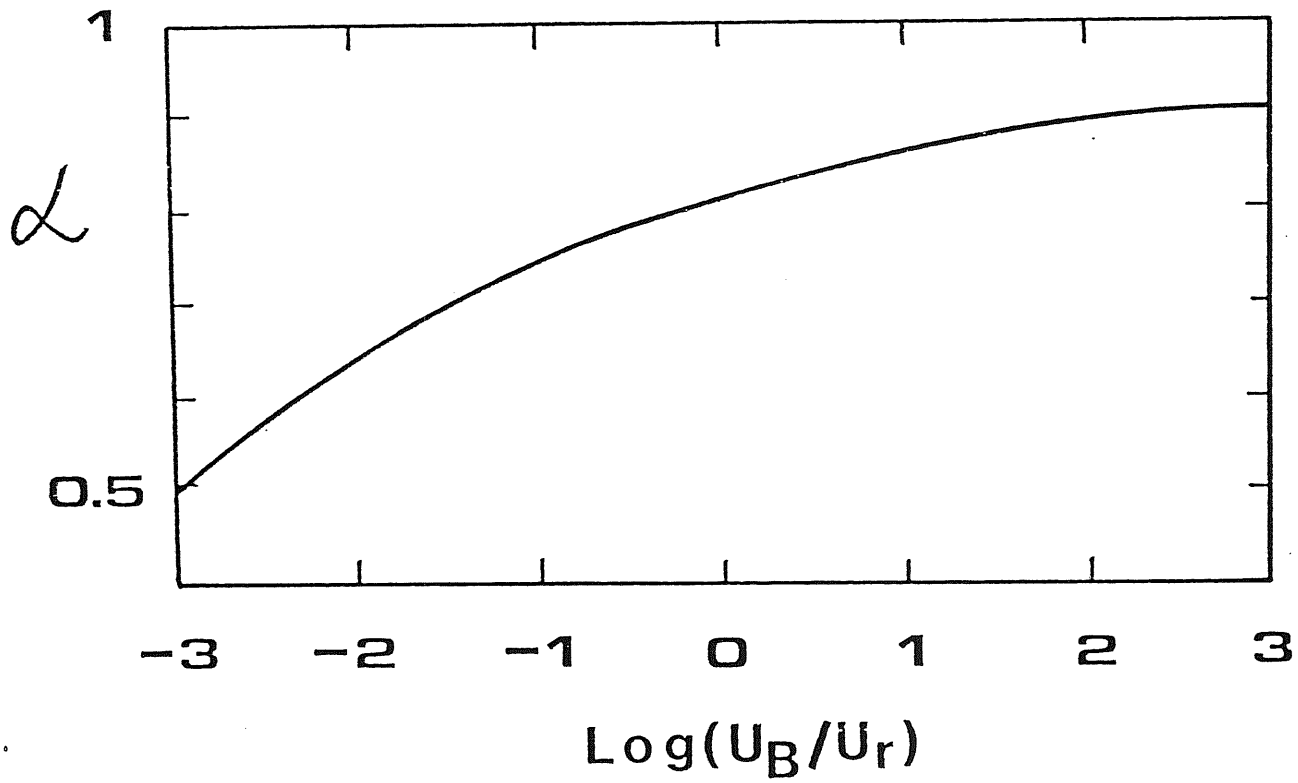

Figure 3.5. Spectral index α vs. the ratio U_B/U_r for $L_i = 10^{45}$ erg/s, $R = 10^{15}$ cm, and $s = 3$. Cool particles effects are neglected.

CHAPTER FOUR

A REVIEW OF PAIR PLASMAS

This thesis is mainly concerned with the SSC radiation process, but it seems worth, before including pair production processes in SSC models, to review the already wide literature about pair plasmas. The astrophysical relevance of electron positron pair production has long being recognized (Jelley 1966), but pioneering studies about both thermal (Bisnovatyi-Kogan, Zel'dovich, & Sunyaev 1971), and non- thermal (Bonometto & Rees 1971) plasmas needed about a decade to trigger a renewed interest in this field. If the ultimate source of power in active galactic nuclei is accretion onto a black hole, then in the potential well around the hole the mean energy per proton can reach 100 MeV. Part or all of this energy may be channeled into all particles equally, forming a thermal plasma, or into only a small fraction of the electrons (non-thermal plasma). The fundamental processes that produce pairs are particle-particle, particle-photon, and photon-photon interactions. To lowest order in the fine structure constant α_f

$\gamma\,\gamma \rightarrow e^+e^-$	$\dot{n}_+ = r_e^2 c n_{\gamma\gamma}^2 F_{\gamma\gamma}$	(4.1a)
$\gamma\,p \rightarrow e^+e^-p$	$\dot{n}_+ = \alpha_f r_e^2 c n_\gamma n_p F_{\gamma p}$	(4.1b)
$\gamma\,e \rightarrow e^+e^-e$	$\dot{n}_+ = \alpha_f r_e^2 c n_\gamma n_\pm F_{\gamma e}$	(4.1c)
$e\,e \rightarrow e^+e^-ee$	$\dot{n}_+ = \alpha_f^2 r_e^2 c (n_+ + n_-)^2 F_{ee}$	(4.1d)
$e\,p \rightarrow e^+e^-ep$	$\dot{n}_+ = \alpha_f^2 r_e^2 c (n_+ + n_-) n_p F_{ep}$	(4.1e)

Here γ, p, e^+, e^- denote photon, proton, electron and positron, respectively, and e may be either an electron or positron, n_γ, n_p, n_+, n_- are the corresponding number densities, r_e is the classic electron radius. The dependence on energy of the reaction rate $\dot{n}_+$ is included in the F terms.

The inverse process, pair annihilation, occurs at a rate

$$e^+ e^- \rightarrow \gamma\gamma \qquad \dot{n}_A = r_e^2 c n_+ n_- 2F_A \tag{4.1f}$$

Escape of pairs can be handled in a phenomenological way introducing a mean escape velocity $c\beta_{esc}$

$$\dot{n}_{esc} = r_e^2 c (n_+ + n_-)^2 F_{esc} \tag{4.1g}$$

4.1 Thermal plasmas

If the plasma is thermal, the F terms in eqs. (4.1) involving only particles can be found averaging the energy dependent part of the reaction probabilities over the Maxwellian energy distribution. To find the F terms involving photons, their energy distribution has to be specified. For temperatures close to, or above, relativistic values, blackbody radiators would require a prodigious amount of energy, and in addition would be uninteresting, since all the plasma properties would be known. The most likely photon emission mechanism are bremmstrahlung, eventually Comptonized, cyclo-synchrotron producing soft photons Comptonized by the hot electrons, giving rise to a power law spectrum ending in an exponential cut (unsaturated case), or to a Wien spectrum (saturated case). Alternatively, the soft photon distribution can be produced in a different volume of the source at a different temperature, and be Comptonized in the region of interest. Photon-particle processes are less important than the other processes, being overwhelmed by photon-photon interactions in highly luminous sources, or by particle-particle processes in low luminosity objects. I will neglect them in the following. The remaining F terms important for the discussion below are given in table 4.1 (e.g. Lightman 1982, Svensson 1982, Zdziarski 1985).

Here $\Theta \equiv kT/mc^2$, and $\tau_T \equiv \sigma_T(n_+ + n_-)R$. Note that for Comptonization to be important, $\tau_T > 1$ for subrelativistic temperatures. Note also that particle-particle

Table 4.1 Energy averaged F terms

	$\Theta \ll 1$	$\Theta \gg 1$		
$F_{\gamma\gamma}$	$\frac{\pi^2 e^{-2/\Theta}}{8\Theta^3}$	$\frac{\pi \ln \Theta}{2\Theta^2}$	Wien	4.2a
$F_{\gamma\gamma}$	....	$\frac{2}{3}\left(\frac{\Theta}{2}\right)^{2\alpha}$	power law ($\alpha > -1$)	4.2b
F_{ee}	....	$\frac{112}{27\pi}\ln^3(2\Theta)$		4.2c
F_{ep}	....	$\frac{\ln^3(2\Theta)}{\pi}$		4.2d
F_A	π	$\frac{\pi \ln \Theta}{2\Theta^2}$		4.2e
F_{esc}	$\frac{8\pi}{3\tau_T}\beta_{esc}$	$\frac{8\pi}{3\tau_T}\beta_{esc}$		4.2f

processes *increase* with temperature, while photon-photon and annihilation processes *decrease* with temperature. Pair equilibrium demands that pair production balances annihilation and escape, and if escape is not important, a thermal plasma can be in pair equilibrium only *below* the maximum temperature $\Theta_{max} \approx 24$. Above Θ_{max} annihilation cannot keep up with particle-particle pair production.

Considering pair dominated plasma, for which $n_p < n_+ + n_- = n_e$, the pair balance equation is

$$\left(\frac{n_\gamma}{n_e}\right)^2 = \frac{F_A + F_{esc} - \alpha_f^2 F_{ee}}{F_{\gamma\gamma}} \tag{4.3}$$

Neglecting escape, the maximum temperature is reached when $F_A = \alpha_f^2 F_{ee}$, and the ratio n_γ/n_e drops to zero, due to the overproduction of pairs. This was the classic result of Bisnovatyi-Kogan, Zel'dovich, & Sunyaev (1971). Including the escape term let the plasma reach arbitrary large temperatures, provided β_{esc} is great enough (Zdziarski 1985). Note that for subrelativistic temperatures ($\Theta < 1$), Comptonization

is important if $\tau_T > 1$, and in this case annihilation dominates over pair escape in the interesting range of compactnesses ℓ.

The other fundamental result of pair plasma studies is the inverse correlation between maximum compactness ℓ_{max} and temperature of the plasma Θ, for compact ($\ell > 1$) sources. It can be understood qualitatevely with very simple considerations. In fact, for pair free sources, ($\ell \ll 1$), an increase of the heating (luminosity) corresponds to an increase of temperature, since the total number of particles is fixed. Increasing the luminosity further, the temperature become relativistic, triggering pair-producing processes. When pairs outnumber primary electrons, the available power is shared amongst an increasing number of particles, their mean energy (temperature) decreases, and the plasma develops a *negative* specific heat. Then, for a given temperature, steady sources in pair equilibrium are either low luminosity, low density, and pair free objects, or high luminosity and pair dominated sources. A third branch of solutions, corresponding to complete thermodynamic equilibrium and Planck photon distribution occurs at compactness values far above those we are interested in. Assuming that the source is powered by accretion onto a black hole, we can write ℓ in terms of the Eddington luminosity $L_E = 4\pi m_p c GM/\sigma_T$ and the Schwartzschild radius $R_s = 2GM/c^2$

$$\ell = \frac{2\pi}{3}\frac{m_p}{m_e}\frac{L}{L_E}\frac{3R_s}{R} \tag{4.4}$$

and we derive the limit $\ell < \ell_E \sim 4000$.

In the range $1 < \ell < \ell_E$, the maximum compactness parameter ℓ_{max} achievable with a given temperature Θ can be estimated assuming a simplified radiative transfer equation

$$\dot{n}_\gamma(x) = \frac{n_\gamma(x)}{(R/c)(1+\tau_T)} \tag{4.5}$$

so that

$$\begin{aligned} \ell_{max} &= Vol\,\frac{\sigma_T}{R^2(1+\tau_T)}\int n_\gamma(x)dx \\ &= \frac{4\pi}{3}\frac{\tau_T}{1+\tau_T}\int \frac{n_\gamma(x)}{n_e}dx \end{aligned} \tag{4.6}$$

If the photon distribution function is a power law with an exponential cut off at $x \simeq \Theta$, as is the case for unsaturated Comptonization, then eq. (4.6) becomes (Svensson 1984a, Zdziarski 1985)

$$\ell_{max} = \frac{2\pi}{3}\Theta\frac{n_\gamma}{n_e}\Gamma(1-\alpha)\min(1,\tau_T) \tag{4.7}$$

and we have the remarkable result that, as far as $\tau_T > 1$, the luminosity depends on the *ratio* of photon to particle densities (Svensson 1984a), which, in pair equilibrium, is fixed by the pair balance equation. For the range of ℓ we are interested, eq. (4.3) simplifies further, since particle-particle interactions are unimportant.

At subrelativistic temperatures pair production occurs in the exponential tail of the photon distribution, established by Comptonization with a large τ_T. Then escape ($\propto 1/\tau_T$) is unimportant, and setting $n_\gamma/n_e = (F_A/F_{\gamma\gamma})^{1/2}$ yields (Svensson 1984a)

$$\ell_{max} = \frac{4\sqrt{2\pi}}{3}\Gamma(1-\alpha)\Theta^{5/2}e^{1/\Theta}, \qquad \Theta \ll 1 \tag{4.8}$$

For relativistic temperatures, and for unsaturated Comptonized spectra, $\tau_T < 1$ is required. From eq. (1.71) τ_T is related to the spectral index α by

$$\tau_T \approx (4\Theta)^{-2\alpha} \tag{4.9}$$

Escape dominates over annihilation if $\beta_{esc} > \beta_{min}$

$$\beta_{min} \approx \frac{3\ln\Theta}{(4\Theta)^{2-2\alpha}} \tag{4.10}$$

Then eq. (4.7), for $\Theta \gg 1$ and for $0.5 < \alpha < 1$ becomes

$$\ell_{max} \simeq \frac{\pi}{8^\alpha}\Gamma(1-\alpha)\Theta^{-3\alpha}, \qquad \beta_{esc} < \beta_{min} \tag{4.11}$$

$$\ell_{max} \simeq 2^{2-\alpha}\Gamma(1-\alpha)\beta_{esc}^{1/2}\Theta^{1-2\alpha}, \qquad \beta_{esc} > \beta_{min} \tag{4.12}$$

Fig. 4.1 shows ℓ_{max} versus Θ (Zdziarski 1985, Svensson 1986) in the case of Comptonization of soft photons with $\alpha = 0.7$ and Comptonized bremsstrahlung. Fig. 4.2 shows ℓ versus Θ (Svensson 1984a) in the case of bremsstrahlung, hence when no

sources of externally produced soft photons is present, and assuming no escape of pairs. The three branches of solutions discussed above (pair free, pair dominated, and complete thermodynamic equilibrium) can be seen. Thin and not Comptonized bremsstrahlung can be observed only for very low values of the compactness, due to the inefficiency of the process.

For subrelativistic and relativistic temperatures the bremsstrahlung luminosity is (Svensson 1984a)

$$\ell_{brem} \simeq \frac{16}{3}\alpha_f \sqrt{\frac{2}{\pi}} \tau_T^2 \Theta^{1/2}, \qquad \Theta \ll 1 \tag{4.13}$$

$$\ell_{brem} \simeq 18\,\alpha_f\,\tau_T^2\,\Theta \ln\Theta, \qquad \Theta \gg 1 \tag{4.14}$$

Defining an approximated y parameter $y = \tau_T\Theta(1+\tau_T)(1+\Theta)$ Comptonization is unimportant ($y < 1$) if

$$\ell_{brem} < \frac{\Theta^{-1/2}}{32}, \qquad \Theta \ll 1 \tag{4.15}$$

$$\ell_{brem} < 0.13\,\Theta^{-3} \ln\Theta, \qquad \Theta \gg 1 \tag{4.16}$$

Above these values the resulting spectrum is modified by Comptonization, and a Wien peak is expected to form.

The annihilation line produced by pairs is never expected to be seen in thermal plasmas in pair equilibrium: at low temperatures the line is broadened by the large optical depth of the pairs and absorbed by photon-photon interactions, at high temperatures the other emission processes dominate due to the decreased annihilation cross section (*cf.* F_A) and thermal broadening (Svensson 1984a).

4.2 Non thermal plasmas

In non thermal plasmas a small fraction of particles carries a substantial fraction of the total power. Consequently, pair production processes involving particle-particle

and photon-particle collisions are less important than the photon-photon interactions. The created pairs modify the energy distribution function of the emitting particles, which must be solved for self consistently. Usually, an injected particle spectrum of primary particles is assumed, while the steady distribution is found through the specification of the cooling processes.

Photon-photon collisions have a threshold

$$x_1 x_2 \geq \frac{2}{1-\cos\theta} \tag{4.17}$$

where θ is the angle between the two photons of energies x_1, x_2. The cross section peaks around $x_1 x_2 \sim 2$, and for this reason collisions preferentially take place between photons of energies x and $1/x$, respectively, as long as the photon number density distribution is a decreasing function of energy. It is easy to see that the dimensionless compactness ℓ directly measures the optical depth of the photon-photon interactions $\tau_{\gamma\gamma}(x)$. For power law photon distribution $\tau_{\gamma\gamma}(x)$ is given by

$$\tau_{\gamma\gamma}(x) = \eta(\alpha)\sigma_T R \frac{n(1/x)}{x} \tag{4.18}$$

where the function $\eta(\alpha)$ can be approximated by (Svensson 1987)

$$\eta(\alpha) = \frac{7}{6}(1+\alpha)^{-5/3}(2+\alpha)^{-1} \tag{4.19}$$

and the spectral index α has to be evaluated at the energy $1/x$. Then, apart from factors of order unity

$$\ell \approx 4\pi\,\tau_{\gamma\gamma}(1) \tag{4.20}$$

So γ-ray absorption and pair production are very important if $\ell > 4\pi$ in hard X-rays, corresponding to $L_x/R \geq 5 \times 10^{29}$ erg/s/cm, and, of course, if γ-ray photons are actually produced. Pair production starts to affect the emerging emission for $\tau_{\gamma\gamma}(x_{max}) \geq 1$ (corresponding to values of ℓ much below unity), while pair production saturates for $\tau_{\gamma\gamma}(1) \geq 1$ (virtually each γ-ray photon produce a pair). Note that $\tau_{\gamma\gamma}$ depends on the target photon density, and so on the X-ray luminosity.

From eqs. (4.20) and (4.4) we have that pairs are very important for sources emitting more than 1% of their Eddington limit in hard X-rays, which seems to be a

fairly typical value for AGNs (e.g. Wandel & Mushotzky 1986). Relativistic beaming, if present, strongly enhances the observed value of the compactness and consequently the derived $\tau_{\gamma\gamma}$

$$\tau_{\gamma\gamma}(x) = \delta^{p+1}\tau'_{\gamma\gamma}(x) \tag{4.21}$$

where the prime stands for the comoving frame, and $p = 2+\alpha$ or $3+\alpha$ according to the discussion in section 2.2. Note that the extra power in the exponent of δ comes from measuring the size with the minimum observed variability timescale ($R = ct\delta$). If beaming of radiation is not due to relativistic bulk motion, but to collimation effects (by e.g. a thick disk funnel) in the observer's direction, then $\tau_{\gamma\gamma}(x) \approx (4\pi/\Omega)\tau'_{\gamma\gamma}(x)$, where Ω is the solid angle of the beam.

A simple result, first noted by Svensson (1984b) can be achieved with the use of eqs. (1.18) and (4.18), and assuming that the internally produced radiation is power law distributed in the whole energy range. In this case $\tau_{\gamma\gamma}(x) \propto x^{\alpha}$, so that

$$\ell(x) = \frac{\epsilon(x)R}{\tau_{\gamma\gamma}(x)}\left(1 - e^{-\tau_{\gamma\gamma}(x)}\right) \propto \begin{cases} x^{-\alpha} & \tau_{\gamma\gamma}(x) \ll 1 \\ x^{-2\alpha} & \tau_{\gamma\gamma}(x) \gg 1 \end{cases} \tag{4.22}$$

The observed radiation will have a break at the energy for which $\tau_{\gamma\gamma}(x)$ becomes unity. Note that this break cannot be at energies below mc^2, for in this case depletion of target photons decreases the value of $\tau_{\gamma\gamma}$. Thus γ-ray emission is actually expected to be observed from highly compact sources of large optical depths, with a steep γ-ray spectrum coming from the outermost layers of the source.

The created pairs share the available energy of the interacting photons

$$\gamma_+ + \gamma_- = x + \frac{1}{x} \tag{4.23}$$

and it turns out that for power law spectra it is a good approximation to assume

$$\gamma_{\pm} = \frac{x}{2} \tag{4.24}$$

as long as $\alpha > 0.5$ (Bonometto & Rees 1971, Svensson 1987).

Given the photon production rate $\dot{n}(x)$, the pair production rate $P(\gamma)$ is

$$P(\gamma) = 4\,\dot{n}(2\gamma)\left[1 - \frac{1 - e^{-\tau_{\gamma\gamma}(2\gamma)}}{\tau_{\gamma\gamma}(2\gamma)}\right] \tag{4.25}$$

Once created, pairs radiate and cool before annihilating, and they can be thought of as an extra injection $P(\gamma)$, besides the injection of primary particles $Q(\gamma)$. Eventually, the energy of the pairs is large enough to produce γ-ray photons above the pair production threshold, thus yielding a new generation of pairs, and so on. The non linearity of the process does not allow a general analytic solution for the emergent equilibrium spectrum, and the steady particle distribution. To summarize:

i) The pair production rate depends on the photon production rates at the two energies x and $1/x$ (incident and target photons)

ii) These rates depend on the pair production rate (pairs make photons)

iii) The cool pair density can be large enough to increase the radiation energy density through diffusion.

iv) Cool pairs are heated by hard photons undergoing down scattering, and cooled by soft photons by upscattering, thus they can change the spectrum emitted by relativistic particles both in the soft and high energy bands.

The pioneering work on non non-thermal pair production is **Bonometto & Rees (1971)**. Since they considered SSC models, their results are here discussed in some detail. Their key hypotheses are:

1) Compton losses overcomes synchrotron losses ($\dot{\gamma}_c \gg \dot{\gamma}_s$)

2) The pair production is saturated [$P(\gamma) = 4\,\dot{n}(2\gamma)$]

3) The steady energy distribution of particles and photons are smooth power laws [$N(\gamma) \propto \gamma^{-p}$ and $\dot{n}(x) \propto x^{-\alpha-1}$]. The power law photon spectrum can be characterized by the two spectral indices α_x and α_γ for the X- and the γ-ray bands, respectively, since they take into account KN effects

4) The relation between the slopes of particle and photon distributions is the standard one ($p = 2\alpha_x + 1$) at X-ray energies

Furthermore, they neglect the effects of cool particles, assume a monoenergetic

primary particle injection for simplicity, and take into account KN effects by introducing a step function (*cf.* eq. 1.54) for the scattering cross section.

By point 1 above, most of the power emitted by primary particles is at high energies above the threshold for pair production. By point 2 most of the luminosity radiated above the energy for which $\tau_{\gamma\gamma}(x) = 1$ is absorbed and redistributed at lower energies. The authors then derive the equilibrium spectrum in the whole energy range writing the continuity equation

$$\frac{d}{d\gamma}\left[\dot{\gamma}N(\gamma)\right] = Q(\gamma) + P(\gamma) \tag{4.26}$$

and (by points 2, 3, 4) verify that a unique power law distribution is an approximate solution, for any p and α. To fix their values, they equate the *coefficients* of eq. (4.26) and find $p \simeq 3$ and $\alpha \simeq 1$. However, it can be argued that this result is not consistent with the above listed hypotheses. In fact, for $\alpha = 1$ for the entire spectrum, equal power is emitted in equal energy intervals, making the synchrotron luminosity L_s approximately equal to the IC one L_c. This in turn implies that most of the power absorbed by pair production is preferentially channeled into low energy synchrotron radiation. But this cannot happen, given the assumption of point 1). Redistribution of high into low energy radiation in fact strengthens the inequality $\dot{\gamma}_c \gg \dot{\gamma}_s$ (*cf.* eq. 1.62), making Compton losses even more dominant. Thus at least at high energies, the IC slope has to be significantly flatter than unity in order to have $L_c \gg L_s$.

At high energies, the primary particles always outnumber pairs, whose maximum energy is half as large as that of the primary electrons. Then the hypothesis of a unique power law equilibrium distribution is not correct. Furthermore, the τ_c parameter (*cf.* chapter 1), which measures the importance of higher orders of Compton scatterings at the same energy, becomes of the order of 0.1-1, making the assumption $p = 2\alpha_x + 1$ stated in point 4) above invalid.

More analytical details will be given in the next chapter, toghether with numerical results for the case of saturated pair production in weakly magnetized sources.

Kazanas (1984) discussed the same problem, deriving the same equilibrium spectral index $\alpha = 1$, but assuming complete Thomson cooling. This is an important

assumption, since in this case the first order IC photon production rate does not depend on the *slope* of synchrotron photons and thus, by eq. (1.53), if $\tau_{\gamma\gamma}(2\gamma) > 1$

$$P(\gamma) = 4\,\dot{n}(2\gamma) \propto \gamma^{-\frac{p+1}{2}} \tag{4.27}$$

Sobstituting in eq. (4.26), with $\dot{\gamma} \propto \gamma^2$ (Thomson regime)

$$\frac{d}{d\gamma}\gamma^{2-p} \propto \gamma^{-\frac{p+1}{2}} \tag{4.28}$$

The *exponents* in this expression are equal if $p = 3$. For this value, however, the coefficients in eq. (4.28) are not equal (Svensson 1987). Furthermore, since Compton losses are assumed to be dominant, we face the same problem, discussed above, for an overall spectral index $\alpha = 1$. Note that for $U_B \ll U_r$, as assumed, the cooling rate $\dot{\gamma} \propto \gamma^2[U_B/U_r + g(\gamma)] \sim \gamma^2 g(\gamma)$ should be used, instead of $\dot{\gamma} \propto \gamma^2$. In other words, the assumption of complete Thomson cooling is inconsistent with Compton dominating over synchrotron cooling.

Guilbert, Fabian, & Rees (1983), (see also **Phinney 1983**)) chose a different approach, not trying to self consistently derive the spectral slope of the emergent spectrum, but instead stressing the importance of the reprocessing of the radiation by the cool pairs. They demonstrate that, whenever $\tau_{\gamma\gamma}(1) \geq 1$, a population of cool pairs is formed, with optical depth $\tau_T \propto \ell^{1/2}$, of the same order of $\tau_{\gamma\gamma}(1)$ (pair production at threshold and pair annihilation of cool pairs both have a cross section of the order of the Thomson one). The created relativistic pairs Compton or synchrotron cool until they join a thermal distribution at a (minimum) temperature Θ to be found balancing heating (pairs down scatter hard photons) and cooling (by thermal Comptonization of photons softer than Θ). All photons above mc^2 are assumed to produce pairs. As a result of downscattering, a break is predicted to occur in the spectrum at $x_b \sim 1/\tau_T^2$. Since $\tau_T^2 \propto \ell$, more compact sources have lower x_b, resembling the $\ell - \theta$ dependence found for thermal pair plasmas.

A different class of models, in which particles Compton cool on a soft externally produced radiation field (so for negligible values of the magnetic field) has been considered, among others, by Fabian (1984), Zdziarski & Lightman (1985), Fabian *et al.*

(1986), Svensson (1986, 1987), and Lightman & Zdziarski (1987). In these models the problem partly simplifies because the soft photon radiation field is a priori fixed, and not affected by the emission of the pairs. Different models are characterized by the different approach (analytical or numerical), different values of the compactness ℓ_e (concerning the injected electron luminosity) and ℓ_s (concerning the injected soft photon luminosity), different treatments of the thermal Comptonization, and the inclusion of higher orders IC scatterings.

Zdziarski & Lightman (1985) discussed the case in which the scattering optical depth τ_T of cool pairs is less than unity, requiring $\ell_e < 30$. The injected soft photons have luminosities $\ell_s \gg \ell_e$. Only the first order IC flux is considered, and complete Thomson cooling is assumed. With these assumptions it is important to stress that the IC photon production rate is *independent* on ℓ_s, since $\tau_c \propto 1/\ell_s$ and $\dot{n}_c(x) \propto \tau_c \ell_s$. Note also that for $\ell_s > \ell_e$ the IC process mainly occurs in the Thomson regime, and in this case Kazanas' (1984) analysis becomes approximately valid for $\ell_e \gg 1$ and neglecting cool particle effects. On the other extreme ($\ell_e \leq 10$), pair production can be handled as a perturbation to the primary injection of particles. If, in addition, only one generation of pairs is possible (pairs do not produce photons energetic enough to produce further pairs) the problem simplifies considerably, since in this case the pair-producing photon rate depends only upon the primary particles, and the treatment can be kept analytic. In the range of compactness values considered, the X-ray slope changes from $\alpha_x = 0.5$ to $\alpha_x \sim 0.7$ for increasing ℓ_e.

Svensson (1987) discussed the case $\ell_e < 4000$ and $\ell_s \geq \ell_e$, including cool particle effects (for large values of ℓ_e) in a phenomenological way, introducing a break in the hard X-ray radiation at $1/\tau_T^2$ due to down scattering. Above this energy the emerging power law flux is assumed to steepen by a factor $\Delta\alpha = 0.5$, up to $x = 1$. Thermal upscattering of the assumed monoenergetic soft photon luminosity produces a steep tail with an index α_{th} given by eq. (1.69). The condition $\ell_s > \ell_e$ allows to consider only the first order IC scattering, and to neglect KN effects. For all his

displayed models, the soft monochromatic photons are injected at a rate $\ell_s = 4000$ and at the energy $x_0 = 2.7 \times 10^{-5}$, corresponding to a blakbody temperature of 10^5 K. The treatment is almost completely analytic, and the general behaviour of the self consistent solutions can be understood in a simple way, due to Svensson (1986) himself, in the case of *saturated* pair production. Contrary to what Zdziarski & Lightman (1985) and Kazanas (1984) assumed, the number of generation of pairs is never very large, if only the first order IC scattering is important. In fact, the highest energy ($\gamma \sim \gamma_{max}$) primary particles produce photons of energy $x_{max} = (4/3)\gamma_{max}^2 x_0$. They produce pairs of energy $x_{max}/2$, which in turn produce photons of $x_{max,1} = (4/3)(x_{max}/2)^2 x_0$, and so on, until $x_{max,N} \leq 2$, and the cascade stops. The maximum number N, of generation of pairs is (Svensson 1986, 1987)

$$N = \mathrm{Int}\left\{ \frac{\ln\left[\ln(2x_0/3)/\ln(2\gamma_{max}x_0)\right]}{\ln 2} \right\} \tag{4.29}$$

For monoenergetic injection the photon production rate of primary particles $\dot{n}(x) \propto x^{-1.5}$ at all energies, which gives (in the saturated regime) $P_1(\gamma) \propto \gamma^{-1.5}$. This first generation of pairs cools, and its steady energy distribution steepens by unity, giving $\dot{n}_1(x) \propto x^{-1.75}$. Repeating the argument, for the i_{th} generation we have $P_i(\gamma) \propto \gamma^{-s_i}$, $N_i(\gamma) \propto \gamma^{-p_i}$, $\dot{n}_i(x) \propto x^{-\alpha_i - 1}$, with $s_i = 2 - 2^{-i}$, $p_i = 3 - 2^i$, and

$$\alpha_i = 1 - 2^{-i-1} \tag{3.30}$$

where i is always less then 3 or 4, for any reasonable choice of the parameters, as long as $\gamma_{max}x_0 < 1$. Note that the slopes given above are appropriate only in the energy range where the $(i+1)_{th}$ generation overnumbers the i_{th} one, and thus the steady $N(\gamma)$ distribution is not a unique power law. However, if the radiation produced by different generation of pairs sufficiently overlaps, the overall photon spectrum is a smooth power law of limiting index $\alpha \simeq 1$ (neglecting thermal up and down scattering).

An important parameter, measuring the importance of pair production, is the pair yield ξ. It is defined as the fraction of the injected *kinetic* power that is converted

into pair rest mass

$$\xi = \frac{\int_1^{\gamma_{max,pairs}} P(\gamma)d\gamma}{\int_1^{\gamma_{max}} Q(\gamma)(\gamma-1)d\gamma} = \frac{\ell_A}{\ell_e} \tag{4.31}$$

where ℓ_A is the luminosity produced by the annihilating pairs, since steady state requires that pair creation and annihilation balance. Note that this luminosity may not be in the form of a narrow annihilation line, since most of it gets scattered out of the energy range close to mc^2 for $\tau_T > 1$. Energy conservation requires $\xi < 1$. Detailed calculations have shown that, for $\ell_e > 10$, $\xi \sim 0.1$ nearly independently on all the other parameters (*cf.* also Lightman & Zdziarski 1987). The value of ξ_{eq} at which pairs become important can be estimated evaluating when the total injection rates of primary particles and pairs are equal

$$\frac{\int P(\gamma)d\gamma}{\int Q(\gamma)(\gamma-1)d\gamma} = (<\gamma> -1)^{-1} \tag{4.32}$$

where $<\gamma>$ is the average energy of the injected distribution of primary particles. For monoenergetic injections $\xi_{eq} \sim \gamma_{max}^{-1}$.

Unsaturated pair production occurs when some γ-ray photons escape rather than produce pairs. This regime corresponds to compactness values $\ell_x < 10$ in hard X-rays (*cf.* eq. 4.20). For very low values of ℓ_e pair production is *completely* unsaturated, in the sense that $\tau_{\gamma\gamma} < 1$ at all energies. Then, if the photons produced by pairs are negligible, and in the case of monoenergetic injection

$$P(\gamma) \simeq 4\dot{n}(2\gamma)\frac{\tau_{\gamma\gamma}(2\gamma)}{2} \simeq \frac{27c}{(16\pi)^2\sigma_T}\eta(\alpha)\frac{\ell_e^2}{x_{max}R^2}\gamma^{-1} \tag{4.33}$$

where $x_{max} = (4/3)\gamma_{max}^2 x_0$ is the maximum photon energy emitted by the first order IC scattering. Eq. (4.33) gives the pair yield

$$\xi = 1.2 \times 10^{-2}\,\ell_e\frac{\ln(\gamma_{max})}{x_{max}}, \qquad \ell_e \ll 40 \tag{4.34}$$

Photon produced by pairs, increasing the number of target photons, starts to be important at $\ell_e \geq 6$, depending on the value of $\gamma_{max}x_0$. Since photons of energy x are absorbed colliding with target photons of energy $1/x$, the optical depth rapidly increases as soon as pairs significantly contribute to the emission above $1/x_{max}$. This

occurs for value of $\gamma_{max}x_0$ slightly lower than unity, and causes the pair yield to increase by orders of magnitude for ℓ_e around 5-10. Thus even a small redistribution of the highest energy radiation has a large effect on the (small) flux density at $x \sim x_{max}^{-1}$, with strong changes in the observed intensity and spectral shape. In fig. 4.3 the pair yield ξ versus ℓ_e is shown. As can be seen, $\xi \propto \ell_e$ for low ℓ_e and saturates at a value of about 10% for $\ell_e > 10$. For intermediate ℓ_e-values the transition from unsaturated to saturated pair production becomes sharp if $\gamma_{max}x_0 \sim 1$.

Fabian *et al.* (1986) discussed the case $1 < \ell_e < 10^3$, monoenergetic injection of primary particles at γ_{max} and monochromatic soft photons at $x_0 < \gamma_{max}^{-1}$. Comptonization of cool pairs, when important, is included by introducing a frequency shift per scattering $\Delta x/x = 4\theta - x/(1+x)$, allowing for up and down scattering. The approach is completely numerical, which allowed the authors to study the time dependent behaviours of the emerging radiation, caused by sudden changes in the primary electron injection rate. Steady solutions are presented for $0.1 < \ell_e/\ell_s < 10$. As noted by Svensson (1987), all their displayed spectra have values of $\gamma_{max}x_0$ such that only one pair generation is possible, and according to the simple estimate of eq. (4.30) the spectral index is $\alpha \sim 0.75$ if thermal Comptonization does not occur at the relevant (X-ray) energies. Note that their treatment of thermal Comptonization refers to the *internal* radiation field and overestimate the steepening of the *emerging* radiation above $1/\tau_t^2$. When thermal particles effects are not important, and for $\ell_s > \ell_e$, their results agree with the analytical findings of Svensson (1987).

An important result of their paper concerns the time dependent behaviour. Evaluating the annihilation timesale t_A from the annihilation rate gives $t_A = n_+/(\dot{n}_+)_A \sim (R/c)/\tau_T$. For $\tau_T > 1$, t_A is shorter than the light crossing time $t_{cross} = R/c$ or the escape time $t_{esc} = (1+\tau_t)R/c$. Then a decrease in the primary particle injection (injected luminosity) can let the source become thin before internal photons escape. Photons previously stored by diffusion can freely escape from the source producing an initial *increase* in the observed flux, before the steady state corresponding to the new rate ℓ_e is established. The reversed situation is similar: an increase in ℓ_e ini-

tially corresponds to a *decrease* in the observed flux, since photon trapping becomes more efficient. This situation can be the best oppurtunity to see the annihilation line, which (for the KN decline) is less affected by diffusion trapping. For the same reason, photons of energy above mc^2 do not follow this trend, and can always freely escape.

Lightman & Zdziarki (1987) further improve on the theory of non-thermal pair plasmas with the goal of comparing theory and observations. Instead of a monoenergetic soft photon field they assume a blackbody field at some temperature, and, including higher orders IC scatterings, can explore models of any value of the ratio ℓ_c/ℓ_s. They use the full Kompaneets equation to treat thermal Comptonization and introduce relativistic corrections to photon scattering and escape probabilities. In addition, monoenergetic as well as power law injected particle distributions are considered. The treatment is fully numerical, but analytical results in the case $\ell_c \gg \ell_s$ and steep power law injections were presented by Zdziarski & Lamb (1986). Note that their treatment of thermal Comptonization assumes that the spatial photon source distribution across the source obeys a sinusoidal law, being more concentrated in the center (Sunyaev & Titarchuck 1980). This partly accounts for the differences of their spectra with respect to those of Svensson, for the same model parameters. A second difference comes from the more detailed treatment of downscattering at high energies, where relativistic corrections are taken into account. Finally, assuming a blackbody soft photon source smoothes out some sharp features present in Svensson's displayed spectra. All these differences, however, only concern the spectra above $1/\tau_T^2$.

Here, I wish to give an analytical estimate (rather, a rule of thumb) of the resulting spectral index in the case $\ell_c \gg \ell_s$ and monoenergetic particle injection. Neglecting for the moment cool particle effects, the electron kinetic equation is in this case

$$N(\gamma) = \frac{3mc}{4\sigma_T} \frac{Q_0 + \int_\gamma P(\gamma)d\gamma}{\gamma^2\left[U_s + U_r g(\gamma)\right]} \tag{4.35}$$

which gives

$$\tau_c(\gamma) = \frac{1 + \xi\gamma_{max}\int_\gamma P(\gamma)d\gamma / \int_1 P(\gamma)d\gamma}{\gamma^2\gamma_{max}\left[\ell_s/\ell_c + g(\gamma)\right]} \tag{4.36}$$

For $\ell_s \ll \ell_e$ the parameter $\tau_c(1)$ is

$$\tau_c(1) \approx \xi \left(\frac{4}{3}\right)^{1-\alpha_x} \tag{4.37}$$

which is of the order of 0.1-0.2 for saturated pair production. Then we can approximate the normalization of the scattered spectrum fixing it at the top of the soft photon distribution, namely $\ell_s(x_0) \approx \ell_s/x_0 \approx \ell_c(x_0)$. If the scattered spectrum extends with the same spectral index α_x up to $x \sim 1$, and then breaks (for photon absorption) in a steep power law ($\alpha_\gamma > 1$) above, we can find α_x by the luminosity balance condition

$$\ell_e = \ell_s + \ell_c + \ell_\gamma \tag{4.38}$$

where ℓ_c is the total emerging luminosity produced by IC scatterings below mc^2, and ℓ_γ is the emerging γ-ray luminosity. Neglecting ℓ_γ, eq. (4.38) gives

$$\alpha_x \approx 1 - \frac{\ln\left[(1-\alpha_x)\ell_c/\ell_s\right]}{\ln(1/x_0)} \tag{4.39}$$

If the spectrum breaks at $1/\tau_T^2$, and above this energy a small fraction of the total poer is emitted ($\alpha_x > 0.5$), then the term $\ln(1/x_0)$ have to be replaced by $\ln\left[1/(\tau_T^2 x_0)\right]$.

This estimate of the spectral index at X-ray energies is rather crude, but helps in understanding the general behaviours of models with $\ell_e \gg \ell_s$, in which α_x *flattens* increasing the ratio ℓ_e/ℓ_s. Also in this case pair production redistribute energy from high to low frequencies, but since (for photon conservation) the scattered spectrum cannot exceed the primary soft photon spectrum at low energies, the power is redistributed at all energies up to $x = 1$ or $x = 1/\tau_T^2$. Eventually, the ratio ℓ_e/ℓ_s is great enough to yield spectral indices $\alpha_x < 0.5$. In this case the equilibrium Compton temperature could exceed the value $\Theta_c \sim 1/\tau_T^2$, yielding high values of the Comptonization y parameter, and making the reprocessing by subrelativistic thermal pairs very important.

4.3 Discussion

Thermal plasmas in pair equilibrium can exist only if their temperature does not exceed a maximum value, determined by their compactness ℓ. At this value, the electron-positron pair density outnumbers the ion density. Note that the classical Eddington limit for pair dominated sources is a factor $m_p/m_e = 1836$ smaller, but collective plasma effects or magnetic fields can trap the pairs for higher values of the luminosity. Assuming that each proton is effectively coupled to $1+2n_+/n_p$ electrons, Lightman & Zdziarski (1987) define the *pair reduced* Eddington limit L_E^*

$$L_E^* \equiv \frac{L_E}{1+2n_+/n_p} \tag{4.40}$$

and found $L_E^* \sim 0.1\, L_E$ as a typical value.

The likely locations of hot plasmas in which pair production can be important are two temperature ion tori or the corona of a thin disk or radiation supported torus. In the case of ion tori (Rees *et al.* 1982) protons are supposed to be close to their virial temperature $\Theta_{vir} = (m_p/m_e)r_g/R$, since the low densities involved make Coulomb collisions inefficient to mantain the coupling between ion and electrons.

In this scenario, Moskalik & Sikora (1986), adding phenomenological accretion terms to the time dependent energy equations, found limit cycle behaviours of the system, if ℓ is around 10. In fact the produced pairs increase the coupling between ions and electrons or positrons, and let the ions accrete on a shorter timescale while releasing the drained energy in a flare in hard X-rays. After the time needed to accumulate enough protons from the more external regions, the process can start again

Begelman, Sikora & Rees (1987) noted that in ion tori models in which pair production is important, also structural variations are expected, since the increased ions-pairs coupling decreases the ion pressure, allowing the ion torus to collapse in its internal part.

Pair production in non thermal plasmas has been studied intensively in recent

years, and the majority of the models examined so far assume that the injected primary particles and the produced pairs cool via Compton scattering on a soft radiation field, assumed to be externally produced by other means.

Pairs start to be important at a value of ℓ_e well below unity, while the efficiency ξ of converting the injected luminosity in pair rest mass saturates for $\ell_e \geq 10$. Independently on many parameters, the saturated value of ξ is found to be around 10%. In highly compact sources this fraction of luminosity is expected to be seen in a annihilation line. Thermal velocities and down scattering will broaden the line, making its width uncertain.

Different models can be classified (Lightman & Zdziarski 1987) by the injection mode (monoenergetic, steep or flat power laws) and by the ratio ℓ_s/ℓ_e.

$\ell_s \gg \ell_e$

For models in which primary particles are injected at one energy, or with a flat power law distribution ($Q(\gamma) \propto \gamma^{-s}$, $s < 1$), the power absorbed in the γ-ray band is redistributed at low energies, causing the spectrum below $1/\tau_T^2$ to steepen gradually from $\alpha = 0.5$ to $\alpha \sim 1$ as ℓ_e is increased. Since the X-ray compactness ℓ_x is also a function of ℓ_e, a correlation between α_x and ℓ_x is predicted, in the sense that more compact sources should be steeper. Note that in this class of models the flattest slope is $\alpha = 0.5$.

If the injected particle spectrum is a steep power law ($s > 2$), a small fraction of the luminosity is emitted in the γ-ray band, the importance of pairs is reduced, and the spectral index α depends on the slope s of the injected particles in the standard way: $\alpha = s/2$.

$\ell_s \ll \ell_e$

Also in this case a clear distinction can be made on the basis of the injection mode. For very flat ($s < 1$) or monoenergetic injected distribution, the power absorbed by γ-ray absorption cannot be completely redistributed at low energies, since there the equilibrium flux cannot exceed the luminosity of (primary) soft photons. Energy

conservation requires the overall spectrum be flatter than unity for saturated pair production, and to be correlated with the ratio ℓ_e/ℓ_s.

For steep ($s > 1$) injected distributions, the models are similar to the case discussed in Zdziarski & Lamb (1986) and in the third chapter of this thesis. Pairs are only marginally important, since Klein Nishina effects provide an intrinsic break at $x \sim 1$, and above this energy the spectrum is steeper than unity. At X-ray energies, below $x \sim 1/\tau_T^2$, the spectral index α is flatter than unity, and becomes smaller increasing the ratio ℓ_e/ℓ_s, possibly accounting for observed indices (e.g. 3C 273) flatter than 0.5 in the X-ray band.

Models in which the soft radiation field is produced by the Compton scattering particles themselves by synchrotron radiation are found to be not completely self consistent, and will be the subject of the next chapter.

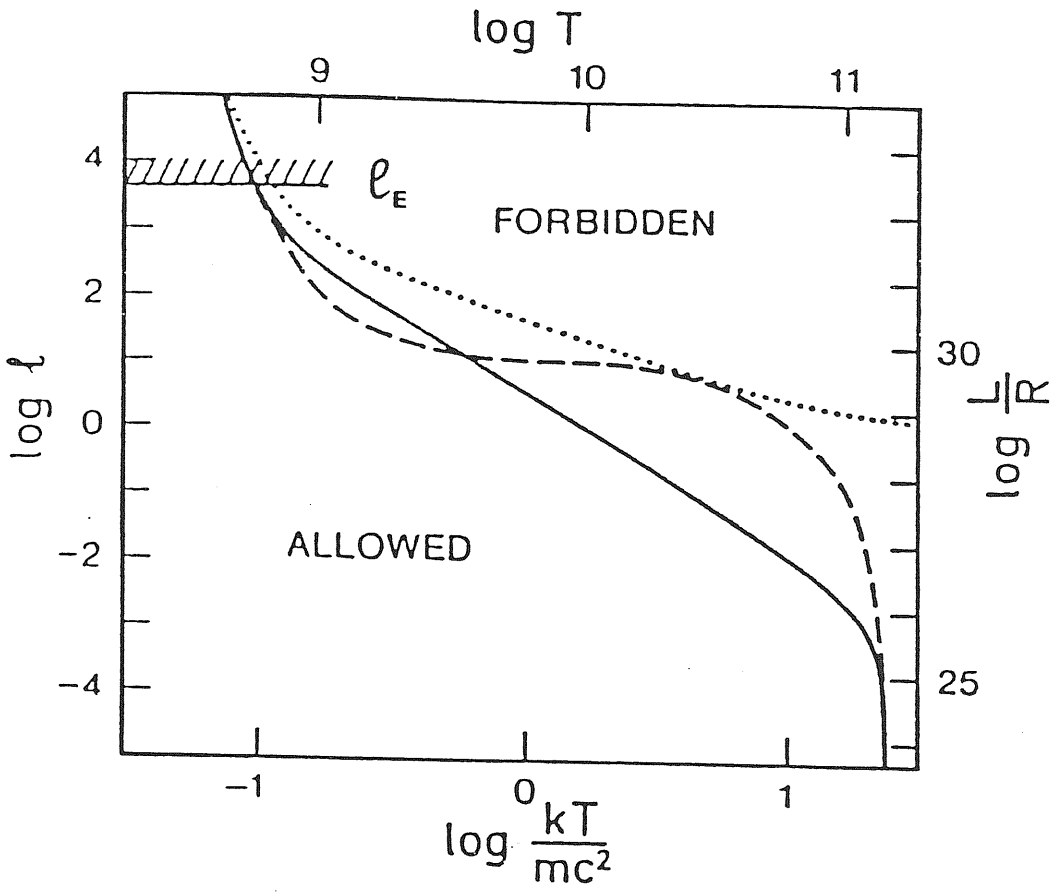

Figure 4.1. The maximum value of the compactness ℓ_{max} vs. the dimensionless temperature kT/mc^2, in the case of Comptonization of soft photons (yielding a spectral index $\alpha = 0.7$) with (dotted) and without (solid) pair escape, and in the case of Comptonized Bremsstralung (dashed). (From Svensson 1986).

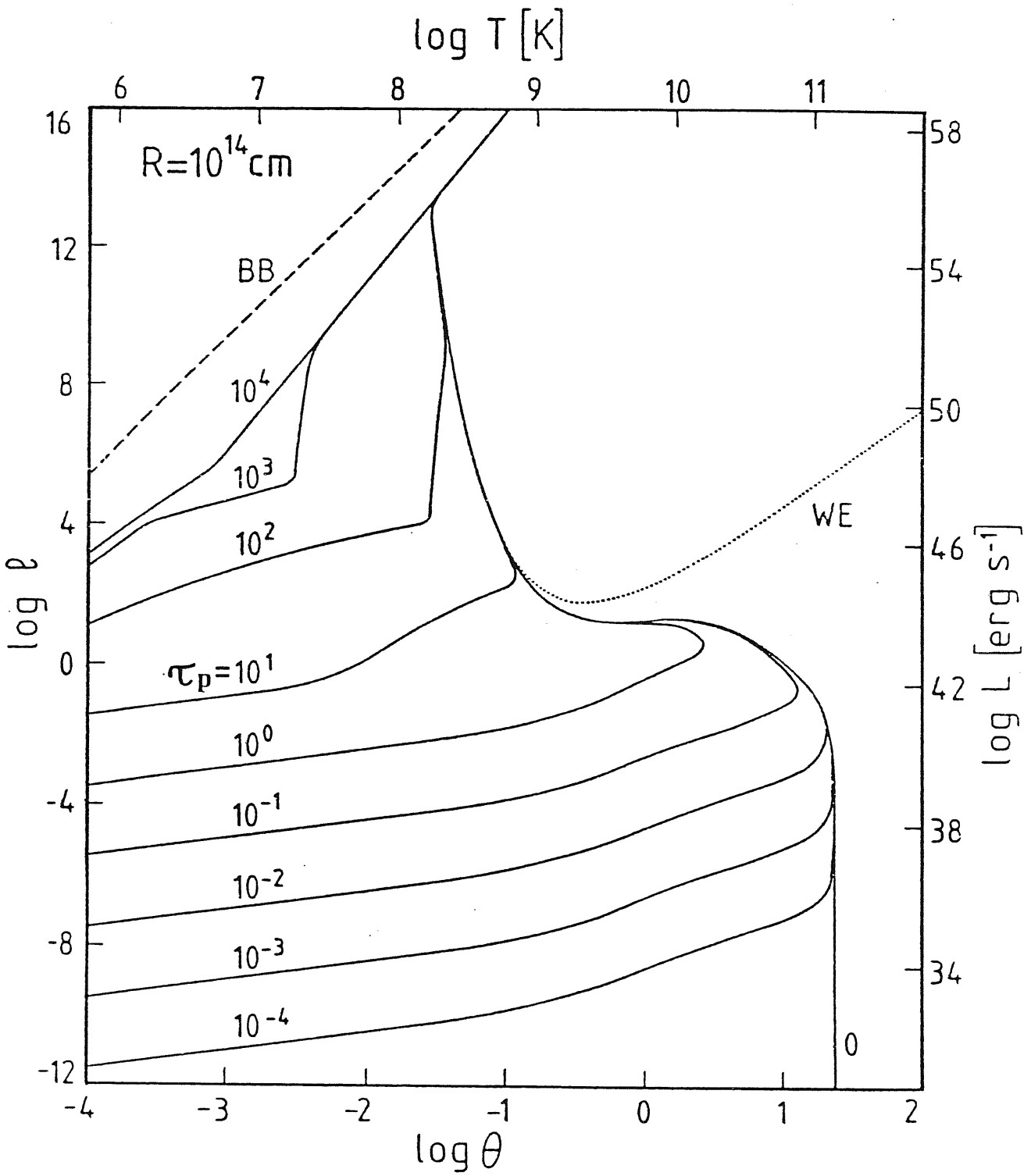

The compactness ℓ vs. the plasma dimensionless temperature Θ in the case of Bremsstrahlung. (from Svensson 1984).

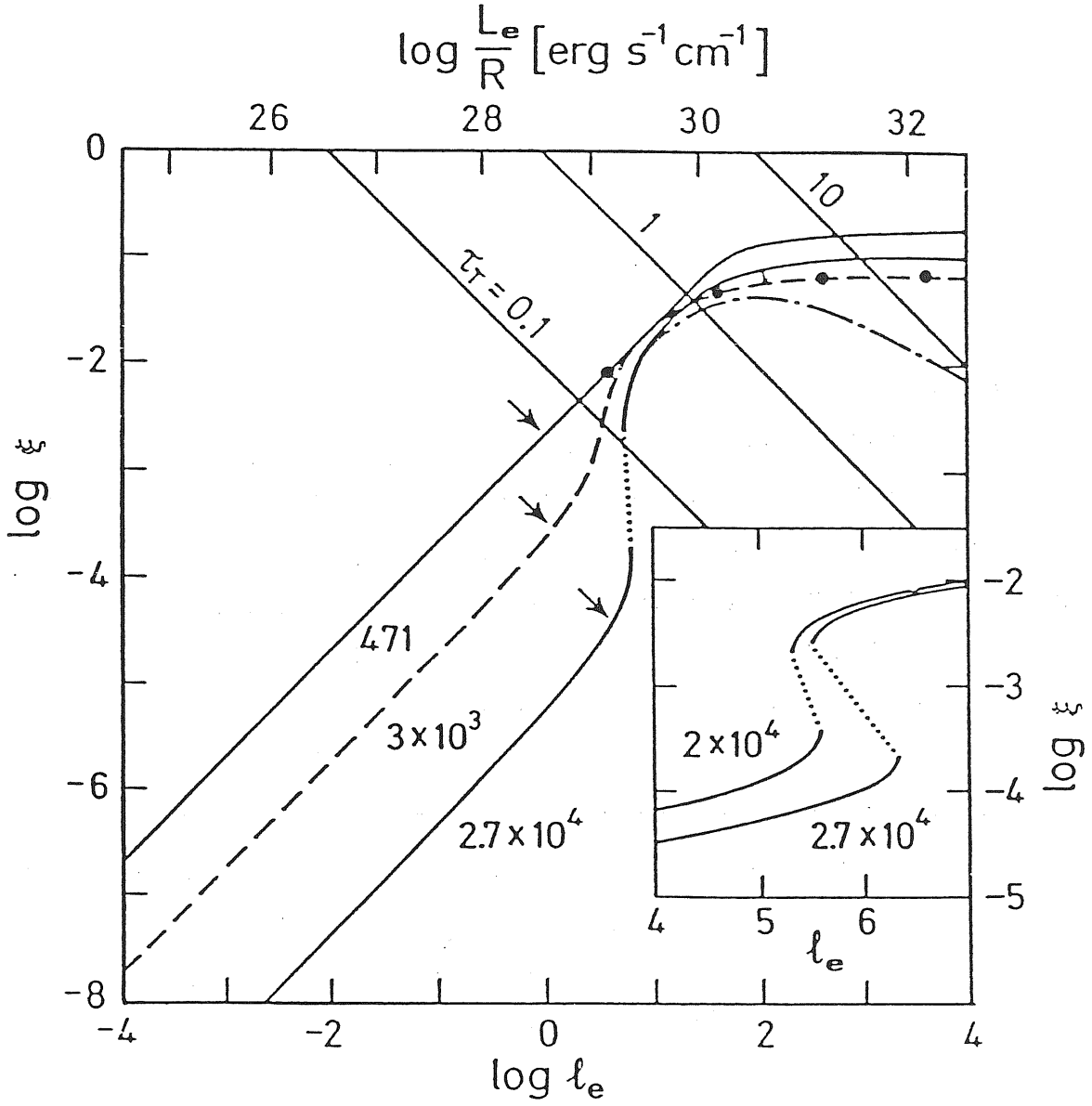

Figure 4.3. The pair yield ξ vs. the electron compactness ℓ_e for different choices of the maximum energy of the injected particles (from Svensson 1987).

CHAPTER FIVE

PAIR PRODUCTION IN SSC MODELS

5.1 Generalities

Most of the models reviewed in chapter four assumed that relativistic particles *and* soft photons are injected throughout the source. In SSC models, the soft photons are provided by the relativistic electrons and pairs themselves, by synchrotron emission. Thus the created pairs not only modify the emergent scattered spectrum, but also contribute to the soft photon radiation field to be scattered at X- and γ-ray energies. Their influence on the synchrotron spectrum is twofold: first, if the pairs are created by photons of large enough energy, they can emit thin synchrotron radiation, and second, since pair production reprocesses the entire spectrum, decreasing the radiation energy density above mc^2 and increasing it below, the inverse Compton cooling rate is increased, and consequently the steady relativistic particle distribution function is decreased. These two opposing effects do not balance, and are strongly dependent on the ratio U_B/U_r which determines the dominant cooling mechanism. If the energy of the injected primary particles is large enough, synchrotron photons are emitted above the pair production threshold, and so can directly produce pairs. If this is the case, and for particular choices of the other parameters, the inverse Compton process can be completely neglected. It turns out that a convenient approach to study pair production in SSC models is to think at the synchrotron mechanism as an inverse Compton process, in which the relativistic particles scatter the virtual magnetic photons monochromatically distributed at the cyclotron frequency. Then, in complete analogy with pure Compton models examined before, a dimensionless

magnetic compactness can be introduced

$$\ell_B = \frac{16\pi}{9}\frac{\sigma_T R U_B}{mc^2} = \frac{16\pi}{27}\alpha_f \frac{R}{\lambda_c} x_B^2 \tag{5.1}$$

where α_f is the fine structure constant, λ_c is the electron Compton wavelength, and x_B is the dimensionless cyclotron frequency, that is, the value of the magnetic field measured in units of the critical one B_c. In this way ℓ_B can replace the soft photon injection rate ℓ_s of pure Compton models.

Note, however, that ℓ_s is generally assumed to be a peaked (monochromatic or blackbody) distribution, the peak energy x_0 being a free parameter. Instead, ℓ_B is always monochromatic, and the cyclotron frequency x_B is obviously related to ℓ_B by eq. (5.1).

In real sources, relativistic particles cool both producing synchrotron and SSC photons, and scattering a soft, externally produced, radiation field of luminosity L_{ext}. For instance, thermal radiation produced in an accretion disk can supply soft photons to be scattered by non thermal electrons in a magnetized region of size R, localized at a distance d from the thermal emission region. Then synchrotron radiation provides the dominant soft photon energy density if

$$B > 390\frac{(Q\, L_{ext,45})^{1/2}}{R_{15}}\ \mathrm{G} \tag{5.2}$$

where $L = 10^{45} L_{45}$ erg/s, $R = 10^{15} R_{15}$ cm, and $Q = R^2/d^2$ is a dilution factor.

In the following, eq. (5.2) is assumed to hold, and the scattering on the externally produced photons neglected.

If primary particles are injected monoenergetically at the energy γ_{max}, at a rate corresponding to an electron compactness ℓ_e, then homogeneous SSC models are determined by four parameters: the compactnesses ℓ_B and ℓ_e, γ_{max}, and the size R of the source (assumed spherical). If the particles are injected with a power law distribution of slope s between γ_{min} and γ_{max}, the values of s and γ_{min} must be specified also. Different models are classified according to the ratio ℓ_B/ℓ_e, the mode of injection, the value of the maximum emitted synchrotron energy $x_{s,max} = (4/3)\gamma_{max}^2 x_B$, and the probability of γ-ray absorption.

I will call *synchrotron models* those models in which synchrotron photons are emitted above the pair production threshold. This requires

$$x_B > \frac{2}{3}\gamma_{max}^{-2} \tag{5.3}$$

In order to avoid quantum effects, I also assume

$$x_B < \gamma_{max}^{-1} \tag{5.4}$$

If, in addition, $\ell_B \gg \ell_e$, then the IC process is not important, and this model is analogous to the case analytically studied by Svensson (1987) (but see below).

Monoenergetically or *power law* injection models are defined according to the primary particles injection mode. In any case, it is assumed that all the injected power is converted into radiation and pairs. Since the case of steep injection has been discussed in chapter three, here I will concentrate on monoenergetic injection models, reminding that power law injection spectra flatter than γ^{-1} are almost equivalent to a monoenergetic injection.

Magnetic dominated or *radiation dominated* sources are defined according to the ratio U_B/U_r (greater or smaller than unity, respectively). Note that this ratio is not always equivalent to the ratio ℓ_B/ℓ_e, because photon diffusion in sources optically thick to scattering can enhance the photon energy density, and note also that the ratio U_B/U_r is not necessarily equivalent to the ratio of synchrotron to Compton losses, because of synchrotron self absorption and KN effects.

Saturated pair production occurs when a γ-ray photon produce a pair rather than escape. Since the photon-photon optical depth $\tau_{\gamma\gamma}(x)$ is an increasing function of energy x for usual photon spectra, *completely saturated* pair production occurs when $\tau_{\gamma\gamma}$ is greater than unity just above mc^2. Viceversa, when $\tau_{\gamma\gamma}$ is less than unity even at the maximum emitted energy γ_{max}, most of the photons escape rather than collide with softer photons, and the pair production regime will be called *completely unsaturated.*

5.2 Basic equations

Consider a source of radius R, embedded in a magnetic field B. Throughout the source, $Q(\gamma)$ primary particles of energy γmc^2 are injected per unit volume and per unit time, corresponding to the dimensionless luminosity ℓ_e

$$\ell_e = \frac{4\pi R^2 \sigma_T}{3c} \int Q(\gamma)(\gamma - 1) d\gamma \tag{5.5}$$

The source is assumed compact enough to let particles radiatively cool down to sub-relativistic energies before escaping or annihilating. Photon-photon collisions produce pairs at a rate $P(\gamma)$ which is considered as an extra injection of particles. The kinetic equation for primary particles and pairs can formally be solved for steady state yielding

$$N(\gamma) = \frac{3mc}{4\sigma_T} \frac{\int_\gamma [Q(\gamma) + P(\gamma)] d\gamma}{\gamma^2 \left[U_B f(\gamma, \gamma_t) + \int_{x_t}^{3/(4\gamma)} n(x) x mc^2 dx \right]} \tag{5.6}$$

where $f(\gamma, \gamma_t)$ takes into account synchrotron reabsorption effects and becomes unity above γ_t.

Synchrotron photons above the self absorption energy x_t are produced at a rate (Zdziarski 1986)

$$\dot{n}_s(x_s) = \frac{c}{8a_0} \frac{N(\gamma)}{\gamma}, \qquad \gamma = \left(\frac{3x_s}{4x_B} \right)^{1/2} \tag{5.7}$$

where $a_0 = 5.29 \times 10^{-9}$ cm is the Bohr radius. For power law particle distribution, eq. (5.7) gives eq. (1.7). The optically thick part of the synchrotron spectrum is here neglected for simplicity. The value of γ_t is given by (*cf.* eqs. 1.19, 3.25)

$$\gamma_t = \frac{3}{4} \left[\left(\frac{3}{2} \right)^{p_t} \frac{\sqrt{\pi}}{2\sqrt{3}} \frac{\sigma_t R N(\gamma_t)}{\alpha_f x_B} \right]^{1/4} \tag{5.8}$$

where p_t is the slope of $N(\gamma)$ at γ_t. Photons are produced by the IC process of the $(i+1)_{th}$ order at a rate (Zdziarski 1986)

$$\dot{n}_{i+1}(x_{i+1}) = \frac{\sigma_T c}{2x_{i+1}} \int_{x_1}^{x_2} n_i(x_i) N(\gamma) \gamma d\gamma, \qquad \gamma = \left(\frac{3x_{i+1}}{4x_i} \right)^{1/2} \tag{5.9}$$

where $x_2 = \min[3/(4x_{i+1}), x_{i,max}]$, x_1 can be evaluated from fig. 1.6, and where $n_0(x)$ is the synchrotron photon number density distribution.

Upscattering by thermal subrelativistic particles of temperature Θ and optical depth τ_T is treated as indicated in section 1.6, if this process is important. In the actual computations, Comptonization has been included if the spectral index α_{th} defined by eq. (1.69) is less than 5.

Radiative transfer is treated phenomenologically, following the results of Sunyaev & Titarchuck (1980) and the prescriptions of Svensson (1987). Photon diffusion caused by cool pairs is assumed to enhance the photon density by the factor $(1 + \tau_T/3)$. Above $x = 1/\tau_T^2$ downscattering is important in removing high energy photons, causing both the internal photon density distribution and the emerging flux to steepen. The degree of this steepening is different, however, being $\Delta\alpha = 0.5$ for the emerging radiation (if the scattering particles and the photon sources are uniformily distributed), and $\Delta\alpha = 1$ for the internal radiation. At energies close to mc^2 KN effects start to be important, reducing the (down) scattering probability, and the degree of the steepening (Lightman & Zdziarski 1987, Guilbert 1987), but detailed numerical calculations are needed in this case. In order to derive analytical solutions, I use the approximated treatment of Svensson (1987) which gives, for photon energies $x < 1$

$$n(x) = \frac{3R}{4c}\dot{n}(x)\left(1 + \frac{\tau_T}{3}\right)\left[1 - \exp\left(-\frac{3}{x\tau_T^2}\right)\right], \qquad x < 1 \qquad (5.10)$$

This equation assumes that the scattering cross section equal the Thomson one up to energies $x = 1$.

The probability of a photon to be scattered by the thermal and non thermal populations of particles is proportional to their densities. When $\tau_T > 1$, and thermal particle effects are important, thermal Comptonization and diffusion are calculated for each order IC photon densities before to compute the next order of the IC emission rate. In other words, the i_{th} IC emission rate $\dot{n}_i(x)$ is calculated according to eq.(5.9). Then $\dot{n}_{c,i}(x)$ is computed by eq. (1.70), and the radiative transfer (eq. 5.10) is used to compute $n_i(x)$ which in turn allows to calculate $\dot{n}_{i+1}(x)$ by eq. (5.9) again, and so on. In order to compute the first order IC emission, the synchrotron photon density

is computed in the same way.

The photon density above $x = 1$ need not to be known, since Compton scattering in the KN limit is neglected (*cf.* the upper limit in the integral of eq. 5.9 and discussion in section 1.5), and since the pair production rate depend on the target photon density (hence with $x < 1$) and on the γ-ray *emission* rate. However since downscattering effectively removes photons of high energies, it can compete with the pair production process, particularly at energies just above mc^2. Photon-photon collisions and downscattering act as an absorption process at energies $x > 1$, with a total absorption optical depth $\tau_{abs}(x)$

$$\tau_{abs}(x) = \tau_{\gamma\gamma}(x) + \tau_T \left[\frac{\sigma_{KN}(x)}{\sigma_T} \right] \tag{5.11}$$

Then the pair production rate $P(\gamma)$ is found computing the fraction $\tau_{\gamma\gamma}(x)/\tau_{abs}(x)$ of the total number of absorbed photons. This yields (Svensson 1987)

$$P(\gamma) = 4\,\dot{n}(2\gamma) \left[1 - \frac{1 - e^{-\tau_{abs}(2\gamma)}}{\tau_{abs}(2\gamma)} \right] \frac{\tau_{\gamma\gamma}(1\gamma)}{\tau_{abs}(2\gamma)} \tag{5.12}$$

The reverse process, pair annihilation, depends on the temperature Θ of the pairs, assumed to join a Maxwellian distribution after the relativistic cooling. The pair annihilation rate is

$$\dot{n}_A = r_e^2 c n_+ n_- F_A(\theta) \tag{5.13}$$

where (Svensson 1987)

$$F_A(\Theta) = \pi \frac{\left[1 + 0.5(4\pi\alpha_f^2/\Theta)^{0.6} + 4\pi\alpha_f^2/\Theta \right]^{1/2}}{1 + 2\Theta^2/\ln(1.12\Theta + 1.3)} \tag{5.14}$$

For temperatures of interest here, $F_A \sim \pi$.

Balancing pair production and annihilation the optical depth τ_T of the cool pairs can be found

$$\tau_T = \left[\frac{16\pi\sigma_T R^2}{3cF_A(\Theta)} \int_1^{\gamma_{max}/2} P(\gamma) d\gamma \right]^{1/2} \tag{5.15}$$

The annihilation timescale $t_A \equiv n_+/\dot{n}_A$ is

$$t_A = \frac{16}{3} \frac{R/c}{\tau_T} \tag{5.16}$$

which, as remarked in the last chapter, is shorter than the light crossing time if the source is thick to electron scattering. As in Svensson (1987), Lightman & Zdziarski (1987), the pair yield is here defined as the fraction of injected kinetic power going into pair rest mass

$$\xi \equiv \frac{\int_1^{\gamma_{max}/2} P(\gamma)d\gamma}{\int_1^{\gamma_{max}} Q(\gamma)(\gamma-1)d\gamma} = \frac{F_A(\Theta)}{4}\frac{\tau_T^2}{\ell_e} \tag{5.17}$$

The determination of the temperature Θ of the cool pairs is higly uncertain. A *minimum* value can be found by Compton balance, assuming that particles are heated by down scattering hard photons and cooled by thermal Comptonization. Other processes can heat pairs, however, and in particular synchrotron reabsorption. In the following I will neglect this possibility and use

$$\Theta = \Theta_c \simeq \frac{1}{4}\frac{\int_{x_t}^1 n(x)x^2dx}{\int_{x_t}^1 n(x)xdx} \tag{5.18}$$

which can be regarded as a mean photon energy of the internal radiation, but calculated up to $x = 1$, because heating effects due to very hard photons are negligible. Note that the implicit use of the Thomson cross section up to $x = 1$ somewhat overestimates the derived temperature.

The spectral shape of the emerging radiation is not the same as the photon emission rates, being modified by photon absorption and down scattering. I use the prescriptions of Svensson (1987) for the emerging luminosity

$$\ell(x) = \frac{4\pi\sigma_T R^2}{3c} x\,\dot{n}(x)\,C(x) \tag{5.19}$$

where $C(x)$ is given by

$$C(x) = \begin{cases} 1-\exp\left(-\dfrac{\sqrt{3/x}}{\tau_T}\right), & x<1 \\ \dfrac{1-\exp[-\tau_{abs}(x)]}{\tau_{abs}(x)}, & x>1 \end{cases} \tag{5.20}$$

This choice of $C(x)$ for $x < 1$ introduces a break $\Delta\alpha = 1/2$ close to $1/\tau_T^2$ when down scattering is important.

In the following the system of equations (5.5)-(5.20) is applied to specific cases, in order to find analytic approximations, before to solve them numerically.

5.3a Synchrotron models

As remarked before, in these models the maximum synchrotron energy $x_{s,max}$ is greater than the pair production threshold $x = 2$, and consequently Compton emission is important only in the energy range between $x_{s,max}$ and γ_{max}. For simplicity, I assume a monoenergetic injected distribution $Q(\gamma) = Q_0\delta(\gamma - \gamma_{max})$. These models strongly resemble those in which particles cool on an external radiation field ℓ_s by only IC emission, with two differences:

1) the synchrotron spectrum peaks at the selfabsorption energy $x_t = (4/3)\gamma_t^2 x_B$, while in the case of pure Compton cooling the scattered spectrum is not self absorbed.

2) The energy x_0 at which the external photon field peaks is assumed to be independent on ℓ_s. If thermal in origin, the flux at x_0 has not to exceed the blackbody limit, giving (Zdziarski 1987)

$$x_0 \geq \left(\frac{a_0 \ell_s}{\alpha_f R}\right)^{1/4} \simeq 5.2 \times 10^{-6}\left(\frac{\ell_s}{R_{15}}\right)^{1/4} \tag{5.21}$$

In synchrotron models, ℓ_B and x_B are related by eq. (5.1) which yields

$$x_B = \left(\frac{27\lambda_c \ell_B}{16\pi R \alpha_f}\right)^{1/2} = 1.7 \times 10^{-12}\left(\frac{\ell_B}{R_{15}}\right)^{1/2} \tag{5.22}$$

The relevant energy to be compared with x_0 is the self absorption energy x_t

$$x_t = 5.7 \times 10^{-9}\left(\frac{\gamma_t}{50}\right)^2\left(\frac{\ell_B}{R_{15}}\right)^{1/2} \tag{5.23}$$

Then in synchrotron models the spectrum extends down to lower energies with respect to pure Compton models, and larger values of γ_{max} are needed to produce synchrotron photons above the pair production threshold.

As in pure Compton models, the parameter $x_B\gamma_{max}$ is important here, because it controls the number and the relative importance of different generations of pairs.

For $\ell_B > \ell_e$, Compton emission is not energetically important, even if it is the only process producing pairs of energy greater than $x_{s,max}/2$. Neglecting IC emission for the moment, the number of pair generations is given by eq. (4.29), where x_0 must be replaced by x_B. Then a larger range of values of γ_{max} can yield only one generation of pairs, due to the small value of x_B. The maximum energy of the pairs is $\gamma_p = x_{s,max}/2$, and pairs are important if their steady energy distribution is above that of primary particles. This defines an energy $\tilde{\gamma}$ below which pairs outnumber primary particles

$$\int_{\tilde{\gamma}} \frac{P(\gamma)}{Q_0} > 1 \tag{5.24}$$

For energy conservation, $\tilde{\gamma} < \gamma_{max}$, and in synchrotron models with $\ell_B > \ell_e$, $\tilde{\gamma}$ is also smaller than γ_p, because the pair distribution is always steeper than that of primary particles. To proceed further, let assume that pair production is unsaturated, implying $\tau_{\gamma\gamma}(x_{s,max}) < 1$, and assume that pairs do not emit target photons for pair production (*no opacity feedback*) implying $(4/3)\tilde{\gamma}^2 x_B < 1/x_{s,max}$. In these conditions both incident and target photons that produce pairs are emitted by primary particles, whose distribution $N_0(\gamma)$ is known

$$\sigma_T R N_0(\gamma) \simeq \frac{\ell_e}{\ell_B}\frac{\gamma^{-2}}{\gamma_{max}}, \qquad \gamma > \gamma_t \tag{5.25}$$

where the condition $U_B > U_r$ allows to neglect KN effects, and to use $U_B/U_r = \ell_B/\ell_e$. Furthermore, if $\tau_{\gamma\gamma}(x_{s,max}) < 1$, pairs are produced at a rate

$$P(\gamma) \simeq 4\,\dot{n}(2\gamma)\frac{\tau_{\gamma\gamma}(2\gamma)}{2} \tag{5.26}$$

$$\tau_{\gamma\gamma}(2\gamma) = \eta(\alpha)\sigma_T R\frac{3R}{4c}\frac{\dot{n}(1/(2\gamma))}{2\gamma} \tag{5.27}$$

Both $\dot{n}(2\gamma)$ and $\dot{n}(1/(2\gamma))$ refer to synchrotron photons emitted by primary particles, hence above $\tilde{x} = (4/3)\tilde{\gamma}^2 x_B$. At these energies eq. (5.25) can be substituted into eq. (5.7) to have

$$P(\gamma) = \frac{27\eta(\alpha)}{16^2\pi}\frac{Q_0\ell_e}{x_B\gamma_{max}}\gamma^{-1} = \frac{9\eta(\alpha)}{64\pi}\frac{Q_0\ell_e\gamma_{max}}{x_{s,max}}\gamma^{-1} \tag{5.28}$$

Using eq. (5.28), the pair yield ξ is

$$\xi = \frac{9\eta(\alpha)}{128\pi}\ell_e \frac{\ln(x_{s,max}/2)}{x_{s,max}/2} \tag{5.29}$$

Inclusion of IC emission should not substantially modify eq. (5.29), at least if $\ell_B > \ell_e$, since most pairs are created by synchrotron photons in any case. The energy $\tilde{\gamma}$ where pairs and primary particle densities are equal is given by

$$\tilde{\gamma} = \frac{x_{s,max}}{2}\exp\left(-\frac{16^2\pi x_B x_{s,max}}{27\ell_e\eta(\alpha)}\right) \tag{5.30}$$

and a necessary condition to derive eq. (5.28) was that opacity feedbacks can be neglected, requiring

$$\tilde{\gamma} < \left(\frac{3}{2x_B x_{s,max}}\right)^{1/2} \tag{5.31}$$

Below $\tilde{x}$ the ratio $\ell_p(x)/\ell_0(x)$ of the luminosity produced by the pairs to that of primary particles is

$$\frac{\ell_p(x)}{\ell_0(x)} = \frac{9\eta(\alpha)}{64\pi}\frac{\ell_e\gamma_{max}}{x_{s,max}}\ln\left(\frac{\gamma_p}{\gamma}\right), \qquad \gamma = \left(\frac{3x}{4x_B}\right)^{1/2} \tag{5.32}$$

where $\gamma_p = x_{s,max}/2$.

Now consider IC losses, important above $x_{s,max}$. Considering only primary particles, the ratio of the extrapolation of the synchrotron spectrum to the IC emission, at a given energy x is

$$\frac{\ell_s(x)}{\ell_c(x)} \simeq \frac{\sqrt{3}\,\ell_e}{4\gamma_{max}\ell_B}\ln[\Lambda(x)], \qquad x > x_{s,max} \tag{5.33}$$

where

$$\Lambda(x) = \frac{3}{4x}\left[\max\left(x_t, \frac{3x}{4\gamma_{max}^2}\right)\right]^{-1} \tag{5.34}$$

The pairs produced by IC photons have maximum energy $\gamma_{max}/2$, but for γ approaching this energy the logarithmic cut off becomes important. However, the emission of the pairs produced by IC radiation can be important, providing target photons for synchrotron γ-rays, making the assumption of no opacity feedbacks invalid. More important, pairs produced by IC photons can in turn produce IC photons, making

the problem completely non linear, and eq. (5.33) is no longer indicative neither of the actual Compton emissivity nor of the pair production rate. Note that the *first* order IC emission is analogous to the *second* order in pure Compton models, and this problem has been dicussed by Svensson (1987). Here I follow a simplified approach, to determine the spectral index of the synchrotron radiation above $\tilde{x}$ in extreme cases.

At energies above unity, eq. (5.9) for the first order Compton emission reads

$$\dot{n}_c(x_c) = \frac{\sigma_T c}{2x_c}\int_{x_1}^{3/(4x_c)} N(\gamma)\gamma n_s(x)dx \qquad (5.35)$$

This equation assures that pairs created by synchrotron photons emit IC emission up to the energy $x_c \sim x_{s,max}$, and are therefore unimportant above. A pair created above this energy contribute to the IC emission of photons of half the energy than those that originated the original pair. If this contribution is greater than that of original particles, two extreme cases exist:

1) The absorption optical depth $\tau_{\gamma\gamma}(x)$ is less than unity in the whole energy range. Then eqs. (5.26) and (5.27) can be used yielding

$$P(\gamma) \propto \gamma^{-1}\,\dot{n}_s\Big(\frac{1}{2\gamma}\Big)\,\dot{n}_s(2\gamma), \qquad \gamma > \gamma_p \qquad (5.36)$$

Neglecting logarithmic factors, a self consistent solution of eq. (5.36) is $P(\gamma) \propto \gamma^{-1}$, corresponding to $\dot{n}_s(1/x)$ and $\dot{n}_c(x)$ having the same spectral index $\alpha = 0.5$ [$\dot{n}(x) \propto x^{-\alpha-1}$]. Note that complete unsaturated pair production requires

$$\tau_{\gamma\gamma}(\gamma_{max}) \simeq \frac{9\eta(\alpha)}{16\pi}\,\ell\Big(\frac{1}{\gamma_{max}}\Big) < 1 \qquad (5.37)$$

2) The optical depth $\tau_{\gamma\gamma}(x)$ is greater than unity above $x_{s,max}$, requiring

$$\tau_{\gamma\gamma}(x_{s,max}) \simeq \frac{9\eta(\alpha)}{16\pi}\,\ell\Big(\frac{1}{x_{s,max}}\Big) > 1 \qquad (5.38)$$

In this case the pair production above $x_{s,max}$ can be approximated with

$$P(\gamma) \simeq 4\,\dot{n}_c(2\gamma), \qquad \gamma > \gamma_p \qquad (5.39)$$

If the pairs outnumber primary particles above γ_p, $N(\gamma)$ can be approximated with

$$N(\gamma) \approx \frac{\gamma^{-2}}{\sigma_T R\gamma_{max}}\,\frac{\ell_e}{\ell_B}\int_{\gamma}^{\gamma_{max}/2}\frac{4\dot{n}_c(2\gamma)}{Q_0}d\gamma, \qquad \gamma_p < \gamma \ll \gamma_{max} \qquad (5.40)$$

Furthermore, if $P(\gamma)$ is a power law, $P(\gamma) \sim P_0\gamma^{-\alpha_\gamma-1}$ at these energies, than

$$P_0\gamma^{-\alpha_\gamma-1} \propto \gamma^{\frac{-\alpha_\gamma+3}{2}} \int_{x_1}^{3/(8\gamma)} x^{-\alpha_x-1} x^{\frac{\alpha_\gamma+1}{2}} dx \qquad (5.41)$$

where α_x is the spectral index below $x = 3/(8\gamma)$.

If the same pairs are responsible for the emission both of target and incident photons [below $x = 3/(8\gamma)$ for synchrotron, above $x_{s,max}$ for IC], then $\alpha_x \sim (\alpha_\gamma+1)/2$ and equating the exponents in eq. (5.41) yields $\alpha_\gamma \sim 1$ with a logarithmic cut off at high energies. Note that in this case $\alpha_x \sim 1$ also. On the other hand, if $\alpha_x < 1$, a smooth power law is not a solution of eq. (5.41). In general, a power law solution with $\alpha_\gamma \sim 1$ is possible when the integral in eq. (5.41) is a weak function of γ. This is the case if $\alpha_x \geq 1$.

For deriving the power law equilibrium solution, it is necessary that pairs produce photons which in turn create pairs in the same energy range of the original ones. The conditions of saturated pair production then allows to find the value of α in particular cases. Note that this result, although yielding the same limiting value of α obtained by pure Compton models with many generations of pairs (and considering only the first order IC spectrum), has a different origin. In pure Compton models $\alpha = 1$ is obtained when the emission by pairs of different generations sufficiently overlaps, and refers to the overall spectrum, up to mc^2 (neglecting downscattering). Each pair generation has different energy spectrum, increasingly steeper with generation number (see chapter four). Here $\alpha = 1$ can be obtained for a restricted range of energies, and is caused by the inclusion of an additional scattering order. In this conditions the concept of generation of pairs become ambigous, because even particles of very low energy can produce pair-producing photons by the IC process, if the maximum synchrotron energy $x_{s,max}$ is significantly less than γ_{max}. If, on the other hand, $x_{s,max} \sim \gamma_{max}$, the synchrotron process dominates in the whole energy range, and the IC mechanism is not important (see figs. 11a and 11b of Svensson 1987).

To summarize, depending on γ_{max}, x_B, and ℓ_e, different regimes are possible, with very different behaviours of the emerging radiation spectral shape.

For $1 \ll x_{s,max} \ll \gamma_{max}$ and $\ell \leq 1$, pair production is completely unsaturated,

and consequently a spectral index $\alpha = 0.5$ is predicted, even if the spectrum is not a smooth power law. Pairs produced by synchrotron photons dominate the emission at low energies (eq. 5.32) up to $x = \tilde{x}$, while pairs produced by the IC process can be dominant above.

For intermediate values of ℓ_e ($\sim 10 - 10^2$), $\tau_{\gamma\gamma}(x > x_{s,max})$ becomes greater than unity, while pair production is still unsaturated below $x_{s,max}$. In these regime $\alpha = 0.5$ below $\tilde{x}$, while $\alpha \sim 1$ is expected above, at least for appropriate values of γ_{max} and x_B.

For higher values of ℓ_e pair production is completely saturated, and becomes independent on the target photon density. As in pure Compton models, the maximum value of the pair yield ξ occurs for one generation of pairs produced by the synchrotron emission. In this case

$$\xi = \frac{1 - (x_{s,max}/2)^{-1/2}}{(x_{s,max}/2)^{1/2}} \tag{5.42}$$

which reaches the maximum value $\xi = 1/4$ for $x_{s,max} = 8$. Pairs created by such small values of $x_{s,max}$ emit self absorbed synchrotron radiation, and do not contribute to the thin spectrum, which is dominated by pairs created by the IC process and by primary particles. This has an important consequence, since opacity feedbacks introduced by the emission of pairs of low energies are completely lacking if $\gamma_p < \gamma_t$, and pair production by IC photons remains unsaturated for larger values of ℓ_e with respect to pure Compton models. Downscattering decreases the number of target photons below mc^2 in such a way that pair production just above this energy is never completely saturated, and $\tau_{\gamma\gamma}(1)$ is of order unity even for $\ell_e \gg 1$. Then the maximum pair yield ξ is decreased to a typical (saturated) value of 5-10%.

5.3b Examples and discussion

Fig 5.1 shows the $x_B - \gamma_{max}$ plane in the region appropriate for synchrotron models. Stars denote computed models whose spectra are shown in figs. 5.2-5.5. The

dashed dotted line corresponds to $x_{s,max} = 8$ for which ξ is maximized. The other labels indicate different values of $x_{s,max}$.

All the computed models have $\ell_B/\ell_e = 10$, $R = 10^{15}$ cm, and a monoenergetic electron injection at γ_{max} is assumed, with γ_{max} given by

$$\gamma_{max} = 3.743 \times 10^5 \, x_{s,max}^{1/2} \left(\frac{R_{15}}{\ell_e} \frac{10}{\ell_B/\ell_e} \right)^{1/4} \tag{5.43}$$

Each figure shows four spectra corresponding to a fixed value of $x_{s,max}$ and $\ell_e = 1, 10, 10^2, 10^3$. Cool particle effect are included as discussed in section 5.2. All models have been numerically computed, using the set of equations of section 5.2 and an iterative method. All the interesting parameters of the models are listed in table 5.1.

Fig. 5.2a shows the spectra for $x_{s,max} = 8$. As can be seen, for very different values of ℓ_e the spectral shape of the models is substantially the same, up to $x = \Theta$, where the kink in the spectrum for $\ell_e = 100$ and 1000 is due to the (assumed) abrupt cut off of the Comptonized spectrum. For all the four spectra, the self absorption energy γ_t is greater than the energy of the pairs created by synchrotron photons. Then their synchrotron emission is self absorbed, and do not increase the number of target photons for pair production by IC photons. Correspondingly, these pairs are marginally important, and only for $\ell_e = 10^3$ can outnumber primary particles above γ_t.

Fig 5.2b shows the primary particle and pair energy distributions, and their sum for the case $\ell_e = 10^3$ [note that the quantity $\gamma^2 \tau_c(\gamma)$ is plotted]. Below γ_t the distribution is calculated setting $\dot{\gamma}_s = 0$, and is not reliable (see chapter one). Note, however, that for $\ell_B > \ell_e$ and monoenergetic injections, a peaked distribution of particles is actually expected to be formed by synchrotron reheating, with the peak energy close to γ_t. Note also that when the synchrotron spectrum extends bejond $x \sim \gamma_t$, and for $\ell_B > \ell_e$, particles of energy $\gamma < \gamma_t$ do not contribute to the emission (they emit IC photons of energy smaller than $x_{s,max}$). As fig 5.2b shows, at γ_t pairs are only a factor ~ 3.5 more numerous than primary particles, and their

density is equal for $\tilde{\gamma} \sim 56$. At these energies, $N(\gamma) \propto \gamma^{-2.5}$. The expected break at $\tilde{x} = (4/3)\tilde{\gamma} x_B \sim 7 \times 10^{-7}$ is not seen, because thermal Comptonization has smoothed out the entire spectrum, up to $x \sim \Theta \sim 10^{-2}$. For high synchrotron energies, only primary particles contribute, yielding $\alpha \sim 0.5$ up to $x = 1/\tau_T^2$, above which $\alpha \sim 1$. The annihilation line is neglected as a source of photons, and is omitted in the figures. The kink in the spectrum at $x = 1$ for high values af ℓ_e is due to the approximated treatment of downscattering, to pair production, and to the fact that the annihilation line is neglected. As can be seen from table 5.1, the maximum value of the pair yield ξ is 5-6%, much below the value found neglecting downscattering. However, the numerical program correctly gives $\xi \sim 1/4$ for $\ell_e = 10^3$ if downscattering is neglected.

Fig. 5.3 shows the four models corresponding to $x_{s,max} = 10^2$. As can be seen, the overall spectra show much more features than before. Three main points have to been focussed:

1) The low energy synchrotron emission are emitted by pairs produced by synchrotron photons, which have maximum energy $\gamma_p = 50$ and which emit up to

$$x_p \simeq 1.8 \times 10^{-8} \ell_e^{1/2} \tag{5.44}$$

The energy range between γ_t and γ_p is small, and the logarithmic cut off in the energy distribution of these pairs (*cf.* eq. 3.12) is important, causing the the spectrum to be very steep at the corresponding synchrotron frequencies.

2) For all the values of ℓ_e considered in fig. 5.2a, pairs produced by IC emission are important, outnumbering primary particles in some energy range, and emitting synchrotron radiation above x_p. The spectral index just above x_p is $\alpha \sim 0.5$ for the $\ell_e = 1$, 10 models, and $\alpha \sim 0.8$ for the $\ell_e = 10^2$ model. For the $\ell_e = 1$ case, pair production saturates ($\tau_{\gamma\gamma}(x) > 1$) for $x > 3 \times 10^5$, and for $x > 10^4$ in the $\ell_e = 10^2$ case. Then at lower energies eq. (5.36) can be used, and consistently $P(\gamma) \propto \gamma^{-1}$ can be found, with a logarithmic cut off, which determines the steepening clearly visible in the $\ell_e = 10$ model. For $\ell_e = 10^2$, $\tau_{\gamma\gamma}$ becomes greater than unity just above $x_{s,max}$, and since below $x_{s,max}^{-1}$ the spectrum cannot be approximated with a power law of index one in any energy range, no simple analytical solution exists.

3) Instead, for $\ell_e = 10^3$, the spectrum between 10^{-5} and 6×10^{-4} is smooth and approximately of slope one. Then eq. (5.41) applies for particle energies $\gamma < 3 \times 10^4$. below this value, $P(\gamma) \propto \gamma^{-2}$ is expected, and consequently $\alpha \sim 1$ for synchrotron energies between x_p and $x \sim 0.2$.

Fig. 5.4 shows the four spectra corresponding to $x_{s,max} = 10^4$. In this case pairs created by synchrotron photons reach the maximum energy $\gamma_p = 5 \times 10^3$, and emit synchrotron photons up to $x_p \sim 1.8 \times 10^{-4} \ell_e^{1/2}$. Pairs created by the IC photons start to be important for $\ell_e = 10$, and for $\ell_e = 100$ eq. (5.41) applies because in the range $10^{-5} < x < 10^{-3}$ the spectrum is approximately a power law of index one. Consequently, for $10^3 < \gamma < 10^5$, $P(\gamma) \propto \gamma^{-2}$, and the synchrotron spectrum is dominated by the emission of this pairs between $\tilde{x}$ and $x \sim 0.2$. The same argument applies to the $\ell_e = 10^3$ model, but in this case downscattering steepens the high energy spectrum above $1/\tau_T^2 \sim 0.1$. For the low ℓ_e cases, the spectral index just above the self absorption energy x_t is $\alpha = 0.5$, since pairs emitting at these frequencies are created in the unsaturated regime, and $\dot{n}(x) \propto x^{-1.5}$ both at x and $1/x$, yielding (eq. 5.36) $P(\gamma) \propto \gamma^{-1}$ up to $\gamma \sim \gamma_p$. For models of fig. 5.4, thermal upscattering is not important, since the pair yield ξ is small, reaching $\sim 1\%$ for $\ell_e = 10^3$.

Fig. 5.5 shows the four spectra corresponding to $x_{s,max} = 10^6$. As can be seen from fig. 5.1, three of these models (the highest ℓ_e ones), lies in the region of the $x_B - \gamma_{max}$ plane where two generations of pairs occur. This can also be seen directly from fig. 5.5, where, for the $\ell_e = 1$ model, pairs created by synchrotron photons emit up to $x \sim 2$. For this model, as the arrows indicate, saturated pair production occurs above $x = 10^4$. Above this energy, primary particles emits a spectrum $\dot{n}(x) \propto x^{-1.5}$, and consequently $P(\gamma) \propto \gamma^{-1.5}$ also. In turn, synchrotron emission above $(4/3)x_B(10^4/2)^2 \simeq 10^{-4}$ is characterized by the spectral index $\alpha \simeq 0.75$. Below this energy, $\alpha \sim 0.5$, as indicated by eq. (5.36). The second generation of pairs mostly emit self absorbed syncrotron radiation, particularly for the $\ell_e = 10$ model. For higher ℓ_e, Comptonization starts to be important, smoothing out the spectrum at low

energies, where the second generation of pairs partly contributes. This explains the prevalence of $\alpha \sim 0.75$ as the mean spectral index for all the four models. At energies above $x = 10^3$, and below $x_{s,max}$, all models have a γ-ray spectral index $\alpha_\gamma \sim 1.25$. This can be explained considering that, for $\tau_{\gamma\gamma} \gg 1$, $\ell_e(x) \propto x\dot{n}(x)/\tau_{\gamma\gamma}(x)$. Since only primary particles contribute at the highest frequencies, $x\dot{n}(x) \propto x^{-0.5}$, while $\tau_{\gamma\gamma}(x) \propto \dot{n}(1/x)/x \propto x^{0.75}$, thus accounting for the observed high energy γ-ray slope.

Fig. 5.6 shows the pair yield ξ as a function of the injected luminosity ℓ_e, for the models shown in the previous figures. In addition, the dashed line refers to the models with $x_{s,max} = 8$, neglecting downscattering. The curves for the models with $x_{s,max} = 8$, 10^2, 10^4 show a similar behaviour, with the pair yield linearly increasing with ℓ_e until saturation is reached. Note, however, that synchrotron self absorption has the effect to reduce the importance of the opacity feedback, particularly for low values of $x_{s,max}$, and this reduces the pair yield with respect to pure Compton models with the same value of ℓ_e before saturation is reached. Furthermore, as remarked before, x_B or $\gamma_t^2 x_B$ is always below the value of x_0 assumed so far in pure Compton models, thus reducing further the pair opacity feedback for the same values of γ_{max}, and increasing the region in the parameter space where only one pair generation is allowed to be created by the synchrotron process. The effect of a second generation of pairs can be seen for the curve corresponding to $x_{s,max} = 10^6$, which increases faster than linearly as soon as the second generation is produced, and which is more sensitive to the pair opacity feedbak caused by low energy synchrotron photons produced by pairs.

Finally, fig. 5.7 shows the dependence of the spectral index α_{2-10}, calculated between 2 and 10 keV, on the compactness ℓ_e, for the models of figs 5.2-5.5. For high values of ℓ_e ($\ell_e > 300$) the value of α_{2-10} is influenced by other effects, besides pair emission, and care must be taken to interpret these spectral indices. In fact besides the steepening of the spectrum caused by pair emission, downscattering is important, and this energy range can be interested by cut off effects in the pair distribution.

In this case the spectrum is not a power law (see the high ℓ_e case in fig. 5.4). For $\ell_e < 300$, the spectral indices are in the range 0.5-1, and remains almost constant in the range $10 < \ell_e < 300$, for all but the $x_{s,max} = 8$ models.

The overall shape of all models is not a smooth power law, particularly for the cases in which only one pair generation is possible. All spectra have kinks, breaks and tails, and the equilibrium overall spectral shape with $\alpha \sim 1$ is never found in the synchrotron models here discussed.

Even if not important for the total energetics, the IC process drastically changes the shape of the spectrum in limited energy ranges, and for particular values of ℓ_e and $x_{s,max}$ an equilibrium spectrum with $\alpha \sim 1$ is appropriate, for different reasons from those responsible of the same value of α in pure Compton models with three-four generations of pairs which overlap in energy.

Models with $x_{s,max}$ around 8 are the most efficient in producing pairs, but synchrotron self absorption reduces their importance, inhibiting pair opacity feedbacks, until the density of the cool pairs is so high that the entire spectrum is reprocessed by them. In this case the major effect of pairs can be a drastic reduction of the linear polarization of the synchrotron flux. Note however that although the synchrotron models examined so far emit between the far infrared and high energy γ-ray band, they refer to the most compact regions of the source, which are likely to dominate the observed flux only at high energies, due to the presence of other, more extended components.

5.4a SSC models: the case of one generation of pairs

If $x_{s,max}$ is below the pair production threshold ($x_{s,max} < 2$), pairs are created only by the IC process. In order to derive the equilibrium photon and particle spectrum analytically, a number of assumptions are required, valid in a narrow region of the parameter space. However, these results can give useful insights about the general

problem.

Consider a model for which the magnetic energy desity U_B is larger than the synchrotron radiation energy density U_r^s. In this regime only the first order IC scattering is important, and higher orders can be neglected. Furthermore, since synchrotron cooling dominates, KN effects are not important in this case. Consider sources compact enough to absorb all photons above $x = 2$. The first order IC spectrum will extend above $x = 2$ if

$$x_B > \frac{9}{16}\gamma_{max}^{-4} \tag{5.45}$$

where γ_{max} is the energy at which primary particles are injected throughout the source. The created pairs do not produce photons above threshold if

$$x_B < \frac{9}{8}\gamma_{max}^{-10/3} \tag{5.46}$$

Even if this condition is violated, the emission by the pairs above $x = 2$ is not important as long as it is less than the emission by the primary electrons, and this occurs for a much larger value of γ_{max}. When x_B and γ_{max} satisfy these conditions, a parameter range will exist where: i) all γ-rays get absorbed, but still ii) higher orders IC scatterings can be neglected, and iii) only the first generation of pairs is relevant.

I assume here that IC radiation is responsible for the emission at high energies. Since $U_B > U_r^s$ is required, the total power of the produced pairs is much less than the injected one. Nevertheless pairs strongly influence the spectral shape and intensity at X-ray energies.

A delicate point which is relevant in this model is the assumed net synchrotron cooling rate for electrons energies $\gamma < \gamma_t$. To roughly estimate the effect of synchrotron self absorption the function $f(\gamma, \gamma_t)$ in eq. (5.6) is set to zero below γ_t. Above γ_t, self absorption can be neglected, and $f(\gamma, \gamma_t) = 1$. All the calculations are then repeated with $f(\gamma, \gamma_t) = 1$ in the whole energy range, to show the important modifications this function introduces in the IC spectrum.

Neglecting KN effects, not important if $U_B > U_r$ and if $x_{s,max} \ll 1$, the steady distribution of primary particles and pairs can be written as

$$\sigma_T R N(\gamma) = \frac{\gamma^{-2}}{\gamma_{max}} \left[\frac{\ell_B f(\gamma, \gamma_t)}{\ell_e} + \left(1 + \frac{\tau_T}{3}\right)\right]^{-1} \left[1 + \xi\gamma_{max}\frac{\int_\gamma^{\gamma_p} P(\gamma)d\gamma}{\int_1^{\gamma_p} P(\gamma)d\gamma}\right] \tag{5.47}$$

where $\gamma_p = (2/3)\gamma_{max}^2 x_{s,max}$ is the maximum energy of the produced pairs. The assumption of one generation of pairs prevents γ_p to be very large. This assumption assures also that only primary particles can emit pair-producing photons. The distribution of primary particles $N_0(\gamma)$ coincides with the total distribution above γ_p and is given by

$$\sigma_T R N_0(\gamma) = \frac{\gamma^{-2}}{\gamma_{max}} \left[\frac{\ell_B f(\gamma, \gamma_t)}{\ell_e} + \left(1 + \frac{\tau_T}{3}\right) \right]^{-1} \tag{5.48}$$

Furthermore, within our assumptions, synchrotron photons produced by the pairs are not energetic enough to be scattered above $x = 2$. Then the Compton flux $\dot{n}_c(x)$ above $x = 2$ is a power law, with a logarithmic high energy cut off, thus yielding

$$P(\gamma) = b\gamma^{-3/2} \ln(\gamma_p/\gamma) \tag{4.59}$$

The constant b depends on $f(\gamma, \gamma_t)$. If this function equals unity in the whole energy range

$$b = \frac{\sqrt{6}}{8} \left(1 + \frac{\tau_T}{3}\right) \frac{\ell_e}{\ell_B} \frac{Q_0}{x_{s,max}^{1/2}} \left[\frac{\ell_e}{\ell_B} + \left(1 + \frac{\tau_T}{3}\right) \right]^{-2} \tag{5.50}$$

in this case, the pair yield is

$$\xi = \frac{1}{2}\left(1 + \frac{\tau_T}{3}\right) \frac{\ell_e}{\ell_B} \left[\frac{\ell_e}{\ell_B} + \left(1 + \frac{\tau_T}{3}\right) \right]^{-2} \frac{2\gamma_p^{-1/2} + \ln \gamma_p - 2}{\gamma_p^{1/2}} \tag{5.51}$$

which has a maximum when $2/\gamma_p^{1/2} = 2 - \ln \gamma_p^{1/2}$, that is, $\gamma_p \approx 24.5$, or $x_{c,max} \approx 49$, which yields

$$x_B \simeq \left(\frac{21}{4}\right)^2 \gamma_{max}^{-4} \tag{5.51}$$

The maximum value of the pair yield here occurs at a larger value of γ_p than in synchrotron models, because pair production here always occurs in the tail of the Compton spectrum, where the logarithmic behaviour becomes important. Note the importance of photon diffusion of synchrotron photons, enhancing the radiation energy density and *decreasing* the steady density of relativistic particles. As long as $\ell_B/\ell_e > 1 + \tau_T/3$, the latter effect is of minor importance, and the maximum pair yield ξ_{max} has the approximate value (for $\tau_t \gg 1$)

$$\xi_{max} \approx \left(2\frac{\ell_e}{\ell_B}\right)^2 \frac{\ell_e}{10^3} \tag{5.52}$$

valid for saturated pair production ($\ell_e > 100$) and magnetic dominated sources ($\ell_B \gg \ell_e$).

Thermal Comptonization is never very important in these models, due to the assumption $\ell_B \gg \ell_e$. In fact, the bulk of the power is emitted by the synchrotron process, which extends to $x_{s,max} \ll 1$. A small fraction of the total luminosity is emitted bejond $x_{s,max}$, and consequently downscattering is not energetically important. Since the power absorbed by cool particles which downscatter hard photons must be emitted at lower energies by the Comptonization process, it can be concluded that also the latter process is not important, even if it can produce a steep power law tail above $x_{s,max}$ and up to $x \sim \Theta$. However, synchrotron reabsorption, increasing the equilibrium value of Θ with respect to the Compton value Θ_c, can change this picture. The role of synchrotron self absorption is twofold: first, modifying the steady energy distribution below γ_t, it affects the *relativistic* Compton spectrum between $x_{s,max}$ and $\gamma_t^2 x_{s,max}$, and second, increasing Θ, it increases the importance of the thermal Comptonization process. This problem has not been explored yet, and is presently under study (Ghisellini, Guilbert, & Svensson, in preparation).

Here, I limit myself to consider crudely two extreme situations, setting the function $f(\gamma, \gamma_t)$ in eq. (5.6) either equal to unity in the whole energy range (then neglecting self asorption effect on the particle distribution) or equal to zero below γ_t and one above it (corresponding to detailed balance between absorption and emission for *each* electron of energy $\gamma < \gamma_t$). Neither of the two above assumption is correct, but their comparison can illustrate the effects reabsorption can have for the IC flux.

5.4b Examples and discussion

The model is completely specified by four parameters: the size of the source R, the magnetic field strength B, the energy of the injected primary electrons γ_{max}, and the injected luminosity L_e, or equivalently, ℓ_e.

Fig. 5.8 shows $x\ell(x)$ vs. x for $R = 3 \times 10^{15}$ cm, $L_e = 10^{47}$ erg/s, $B = 4 \times 10^3$ G, and $\gamma_{max} = 10^3$, for the two choices of $f(\gamma, \gamma_t)$ discussed above. For this set of parameters, $\ell_e = 902$, and $\ell_B/\ell_e = 10$. This figure is the result of a numerical calculation of all the basic equations presented in section 5.2, using an iterative method.

The second order IC spectrum is not shown here, and is completely negligible (*cf.* fig. 5.9). Pairs are marginally important for the synchrotron emission, since they outnumber primary particles only below γ_t. The IC spectrum is the sum of four contributions, corresponding to the scattering between primary electrons or pairs with their synchrotron photons. The scattering of pairs off primary synchrotron photons dominates the IC spectrum up to $x \sim 10^{-2}$ (5 keV). Below this energy, $\alpha \sim 0.75$ for the $f(\gamma, \gamma_t) = 1$ case, and ~ 0.9 for the model with $f(\gamma, \gamma_t) = H(\gamma - \gamma_t)$, where $H(\gamma)$ is a step function. The resulting values of the optical depth τ_T and the pair yield ξ are $\tau_T \sim 2$ and $\xi \sim 0.5\%$ for both cases. The Compton temperature is $\Theta_c \sim 1.6 \times 10^{-3}$, and for this values Comptonization is not important, and has been neglected. The γ-ray spectrum emerges from the outermost layers of the source, from a depth at which $\tau_{\gamma\gamma}(x)$ becomes less than unity. Further absorption is expected for this high energy radiation passing through the X-ray photosphere, but it is neglected, as well as the annihilation line emission.

From fig. 5.8 it can be seen that self absorption effects play a dominant role for the IC emission up to $x \sim 0.1$. To evaluate the effects of pair production only, the model of fig. 5.8 with $f(\gamma, \gamma_t) = 1$ is compared in fig. 5.9 with a model of the same size and magnetic field, but with $L_e = 3.3 \times 10^{46}$ erg/s and $\gamma_{max} = 333$ (corresponding to the same number of primary injected particles as before).

The latter model cannot produce pairs by first order IC emission, and can be considered pair free (pairs produced by the second order IC photons give a pair yield $\xi \sim 3 \times 10^{-4}\%$). Below 5 keV, the two models have $\alpha_x = 0.5$ and 0.73, respectively, with a factor of about 3 difference in flux density. The dashed lines refers to the same models, for which photon absorption and pair production was completely neglected. It can be seen that below 5 keV the flux enhancement is completely due to pair emission. Supposing that in the source γ_{max} increases from 333 to 10^3, all other quantities

remaining the same, the emergent spectrum changes as in fig. 5.9, if synchrotron self absorption is not important. At 1 keV, the increase in flux density will be seen in a timescale $\sim$ 3 days, and spectral variability will be observed at the same energy. Further effects can occur on timescales shorter than the escape time, which however is always the minimum observable variability timescale. In fact, the enhanced photon trapping caused by pairs initially decreases the emerging luminosity in the previuos example, as shown by Fabian *et al.* (1986).

In fig. 5.10 the parameter space allowed for the model presented here is shown for $R = 3 \times 10^{15}$ cm and $\ell_e = 902$. It is constrained by the requirements: i) $\ell_B/\ell_e > (1 + \tau_T/3)$, ii) maximum energy of the first order IC spectrum greater than 2, iii) completly saturated pair production. Also shown is the function corresponding to $x_{s,max}\gamma_{max} = 3/4$, which is the limit for complete Thomson cooling for the first order IC scattering. Note that U_r^s is increased by the trapping pairs, so that the limit $U_r^s = U_B$ does not correspond to a straight line in fig. 5.10.

In general, for any given γ_{max}, the importance of pairs decreases increasing the value of the magnetic field as a larger fraction of the injected luminosity comes out at high energies. In particular, for $U_r/U_B < 1$, and low γ_{max}, very few pairs should be present in the source, produced by the second and higher orders IC scatterings, which become important only for $U_r > U_B$.

On the other hand, for high γ_{max}, and $U_B > U_r$, $\tau_{\gamma\gamma}$ becomes greater than unity only at $x \gg 2$. Furthermore, KN effects start depressing the radiation emitted at high energies, even for the first order IC. Both these effects decrease the number and so the importance of the produced pairs until $x_{s,max}$ can reach the pair production threshold, with all the effects discussed in section 5.3.

The region of parameter space for $U_B > U_r$ in which pairs are important fulfills the requirements to derive the final self-consistent spectrum analytically, by eqs. (5.43)-(5.41) and is enclosed by the dashed and dot-dot-dashed lines in fig. 5.10. In this region, pairs do not affect the part of the spectrum where most of the luminosity comes from, but have a great influence on the whole X-ray band. With only one

generation of pairs, the spectral index in narrow energy bands can be steeper than unity, either because of logarithmic dependences of $P(\gamma)$ or because of up- and down-scattering.

In fig. 5.10 the "threshold" (dash-dotted) line marks the boundary between a region in which the source is almost pair free, and a region in which a large density of pairs can be reached. Starting from this pair free region, a small change in γ_{max} can produce large changes in the X-ray band. For particular values of x_B, a change in γ_{max} can even change the dominant cooling mechanism, producing large variability also in the synchrotron spectrum, besides the changes induced by the synchrotron radiation emitted by the pairs.

The derived analytic solution is valid for a small region of the parameter space, due to the requirement of having U_r/U_B less than, but close to, unity, in order to have enough X-ray compactness to absorb all photons above threshold, still neglecting higher orders IC scatterings. However this solution helps the understanding of the results in other regions of the parameter space, particularly those corresponding to $U_r > U_B$, where pairs are expected to play a dominant role.

5.5 SSC models: the case of $\ell_e \gg \ell_B$

If the power injected in primary particles exceeds that in virtual magnetic photons, Compton losses are responsible of the bulk of the emitted luminosity. In this case the particle distribution function is not affected by synchrotron reabsorption effects and can be derived for the whole energy range. The effects due to the KN decline of the scattering cross section, on the other hand, becomes very important, and were one of the key ingredients to derive the self consistent equilibrium spectrum in the case of the injection of a steep power law of primary particles, discussed in chapter three. Here, I consider monoenergetic injections at the energy γ_{max}.

To disantangle the different effects due to the KN decline, pair production and

relativistic pair emission, and reprocessing by the cool pairs, it is convenient to start neglecting for the moment all the effects due to pairs. In this case the scattering optical depth $\tau_c(\gamma)$ of the relativistic particles is

$$\tau_c(\gamma) = \frac{\gamma^{-2}}{\gamma_{max}\left[\ell_B/\ell_e + g(\gamma)\right]} \tag{5.53}$$

The factor $g(\gamma)$ is given by eqs. (3.15) and (3.16). In fig. 3.1 an example of spectrum was given, for $\ell_e/\ell_B \sim 15$ and $\gamma_{max} = 10^4$. Increasing the value of ℓ_e/ℓ_B let KN effects be important for lower values of γ. Without pair production, the energy density above mc^2 is dominant, and as a consequence the function $g(\gamma)$ will depend on γ_{max}. For a smooth power law spectrum of index $\alpha < 1$ up to $x \sim \gamma_{max}$

$$g(\gamma) \sim \left(\frac{4\gamma_{max}\gamma}{3}\right)^{\alpha-1}$$

Then, even for $\ell_e/\ell_B \gg 1$, only *low values* of γ_{max} allow the term ℓ_B/ℓ_e to be neglected in eq. (5.53).

If, instead, saturated pair production occurs, a small fraction of the total energy density is above mc^2. Neglecting down scattering, and for a smooth power law spectrum

$$g(\gamma) \sim \left(\frac{4\gamma}{3}\right)^{\alpha-1}$$

independently on γ_{max}. Pair production and pair emission redistribute the bulk of the radiation energy density toward energies below mc^2, increasing the fraction available for scattering, and thus the Compton cooling rate of an electron of a given energy γ. This in turn makes the term $g(\gamma)$ easily be greater than ℓ_B/ℓ_e, in the whole energy range. Unfortunately, the assumption of a unique power law spectrum oversimplifies the real case, in which the synchrotron spectrum or its extrapolation always lies above the IC one, even if both were characterized by the same spectral index. Then only approximate relations can be derived for $\tau_c(\gamma)$, and in restricted energy ranges.

Another difficulty which arises considering models with copious pair production concerns the importance of higher orders IC scatterings, even when the maximum energy emitted by the first order is close to γ_{max}. Neglecting cool particle effects,

the particle distribution is given by eq. (4.37), with ℓ_B replacing ℓ_s. Since $\tau_c(1)$ is of the order of the pair yield ξ, the second (and higher) order IC scattering gives a substantial contribution to the emission, for models yielding the saturated value of ξ. Since the synchrotron spectrum is not peaked, and is modified by pair emission, the simple estimate of the spectral index given in chapter four for the case $\ell_e \gg \ell_s$ cannot be applied here. However, for the reasons outlined when discussing the Bonometto & Rees (1971) paper, the spectral index at X-ray energies is expected to be flatter than unity, to let Compton cooling dominate over the synchrotron one.

For energy conservation, pairs cannot outnumber primary particles at the highest energies of the steady $N(\gamma)$ distribution, which can even be flatter than γ^{-2} close to γ_{max}, due to KN effects. As a consequence, the bulk of the synchrotron luminosity is emitted close to the highest energy $x_{s,max}$. Fixing γ_{max} and x_B, and increasing ℓ_e (so the ratio ℓ_e/ℓ_B), the synchrotron luminosity *decreases*. Then the only way Compton radiation has to release the injected luminosity is to flatten its spectrum. Without cool particle effect, the bulk of the total luminosity is emitted around mc^2 (for saturated pair production), and α_x decreases for increasing value of the ratio ℓ_e/ℓ_B.

As an example, fig 5.11a shows the SSC spectra numerically computed for the case $\ell_e = 10^3$, $\ell_e/\ell_B = 10^2$, $\gamma_{max} \simeq 180$ and $R = 10^{15}$ cm. In the spectrum labelled 1 pair production is completly neglected (dashed line), while for the spectrum labelled 2 cool particles effects are neglected. For the spectrum labelled 3 cool particles effect are included. Table 5.2 lists the interesting parameters of models 2 and 3.

The value of γ_{max} is chosen according to the relation

$$\gamma_{max} \simeq 756\, x_{c,1}^{1/4} \left(\frac{R_{15}}{\ell_e} \frac{\ell_e}{\ell_B} \right)^{1/8} \tag{5.54}$$

where the maximum emitted energy of the first order IC spectrum $x_{c,1}$ has been set equal to 10^{-2}. Then pairs are created by photons produced by the second and higher orders IC scatterings.

Fig. 5.11b shows the particle distribution functions in the form $\gamma^2\tau_c(\gamma)$ vs. γ, for the three cases of fig. 5.11a. Dashed lines refers to pairs.

Neglecting pair production, most of radiation is produced by the second order IC spectrum, at energies close to γ_{max}. Due to KN corrections, the particle distribution is a quasi-power law of index $p \sim 1.85$. Between $x = 10^{-6}$ and 10^{-3} the resulting spectral index is $\alpha \sim 0.43$. The particle distributions of models 1 and 2 nearly coincides at high energies, and since $\gamma_t \sim 77$ for both models, their thin synchrotron spectra are nearly identical. For this reason, also the first order IC spectra are similar at energies close to $x_{c,1}$, where primary particles mostly contribute. Below $x_{c,1}$, $\alpha \sim 0.75$ for model 2. For this model, note the increased importance of the second order IC emission above $x_{c,1}$, with respect to model 1. As expected, the bulk of the luminosity in model 2 is emitted around mc^2.

For model 3, where cool particle effects have been taken into account, the radiation energy density below $1/\tau_T^2$ is enhanced both by thermal Comptonization and photon diffusion. As a result, the steady particle distribution function is decreased with respect to model 1 and 2 (fig. 5.11b). Again, primary particles are dominant at high energies, producing a very flat thermally Comptonized synchrotron spectrum, whose total luminosity is much smaller than those of models 1 and 2. Above $1/\tau_T^2 \sim 10^{-2}$, the spectrum is steepened by downscattering, and above mc^2 by photon-photon absorption. Then the spectral index between $x_{s,max}$ and $1/\tau_T^2$ has to be flatter than in model 2, because most of the luminosity is emitted in this restricted energy range. Between $x = 10^{-5}$ and 10^{-2} (5 eV-5 keV) $\alpha \sim 0.6$. The equilibrium Compton temperature $\Theta_c \sim 5 \times 10^{-3}$, yielding $y = 4\Theta_c\tau_T^2 \sim 2$ and $\alpha_{th} \sim 1$.

Note that $1/\tau_T^2 \sim \Theta_c \sim x_{c,1}$: the highest energies of both first order relativistic and thermal Comptonization roughly coincides with the break due to downscattering, thus producing the hump at $x \sim 10^{-2}$, which is artificially enhanced by the only approximated treatment of thermal Comptonization adopted here.

To understand the general behaviour of the relation of the spectral index to the input parameters, a very crude derivation can be put forward, taking advantage, once more, of the luminosity balance condition. Consider models in which saturated pair production occurs, with $\ell_e \gg \ell_B$. Then:

1) The $\tau_c(1)$ parameter is of the order 0.05-0.2, being proportional to ξ. Higher orders IC scatterings are important, helping to smooth out any sharp feature of the spectrum.

2) Thermal Comptonization is important, further smoothing the transition below and above $x_{s,max}$ in the spectrum.

3) KN effects flattens the particle distribution at high energies, responsible of the thin synchrotron emission $\ell_s(x)$. Most of the synchrotron luminosity is emitted close to $x_{s,max} \ll 1/\tau_T^2$.

4) Downscattering limits the energy range where most of the radiation comes from to energies below $1/\tau_T^2$.

These considerations suggest to approximate the spectrum between $x_{s,max}$ and $1/\tau_T^2$ with a unique power law of index α_x, normalizing it at $x_{s,max}$ with the synchrotron flux density $\ell_s(x_{s,max})$. The synchrotron to the total injected luminosity ratio is

$$\frac{\ell_s}{\ell_e} \approx \frac{\ell_B}{\ell_e(1+\tau_T/3)} \left(\frac{4}{3}\gamma_{max}\right)^{1-\alpha_x} \left[\frac{\frac{1}{2-\alpha_x} + \xi\gamma_{max}^{1-\alpha_\gamma} \frac{1-\gamma_{max}^{\alpha_x+\alpha_\gamma-2}}{2-\alpha_x-\alpha_\gamma}}{1+\xi\frac{\gamma_{max}^{1-\alpha_\gamma}-1}{1-\alpha_\gamma}}\right] \qquad (5.55)$$

where $P(\gamma) \propto \gamma^{-1-\alpha_\gamma}$ has been assumed. Note that the term in square brackets is always of the order of unity. The luminosity balance condition

$$\ell_e(1-\xi) = \ell_s + \ell(x_{s,max} < x < 1/\tau_T^2) + \ell(x > 1/\tau_T^2)$$

gives, neglecting $\ell(x > 1/\tau_T^2)$

$$\alpha_x \approx 1 - \frac{1}{\ln\left[1/(\tau_T^2 x_B \gamma_{max})\right]} \ln\left[\frac{\ell_e}{\ell_B}\left(1+\frac{\tau_T}{3}\right)(1-\alpha_x)\right] \qquad (5.56)$$

For the parameters of model 3 in fig. 5.11a, eq. (5.56) gives $\alpha_x \sim 0.69$, which well agrees with the average spectral index between $x_{s,max}$ and $1/\tau_T^2$.

Fig. 5.12 shows three spectra computed for $\ell_e/\ell_B = 30$, $\gamma_{max} = 10^3$, $R = 10^{15}$ cm, and $\ell_e = 1, 10, 10^2, 10^3$. For the low luminosity model (see the corresponding stars in fig. 5.10) pairs are produced by second order IC photons, while they are

created mainly by the first order in the high ℓ_e models. Thermal Comptonization is not important for the $\ell_e = 10$ model, and has been neglected. For the $\ell = 10^3$ model, thermal Comptonization and higher orders IC scatterings are sufficiently important to yield a smooth spectrum. Applying eq. (5.56) we derive $\alpha \sim 0.76$ to be compared with the average value $\alpha \sim 0.8$ of the computed model, between $x_{s,max}$ and $1/\tau_T^2$. All synchrotron spectra are flat ($\alpha \sim 0.5$) since the emission by the pairs is reabsorbed, or smoothed out by Comptonization.

Fig. 5.13 and fig. 5.14 shows three spectra computed for the same parameters of fig. 5.12, except for γ_{max} which is 10^4 in fig. 5.13 and 10^5 in fig. 5.14. As indicated in fig. 5.10, for these models $\gamma_{max} x_{s,max} \gg 1$, so that KN effects are important even for the first order scattering. The general behaviour of the models of figs. 5.12-5.14 is the same for equal values of ℓ_e, and it is remarkable that the spectra for $\ell_e = 10^3$ are nearly identical, independent on the value of γ_{max}. In this case all the $x\ell(x)$ spectra peak at $x \sim 10^{-2}$, corresponding to ~ 5 keV, and are quasi-power law before, with $\alpha \sim 0.6 - 0.7$, which is also the range suggested by eq. (5.56).

5.6 Summary and discussion

In this chapter I tried to show the effects of pair production in steady SSC models both by analytical and numerical means. The injection mode of the primary relativistic particles was always assumed to be monoenergetic at the energy γ_{max}.

For $\gamma_{max}^2 x_B > 3/2$, synchrotron photons are emitted above $x = 2$, and mostly contribute to the pair production rate. This case is analogous to pure Compton models, with the important differences due to synchrotron self absorption and to the small value of x_B, compared to the typical energy of the injected soft photons in models where the magnetic field is neglected. Synchrotron photons with energy $x < x_t$ emitted by low energy pairs are reabsorbed, and do not contribute to the

enhancement of the target photons (opacity feedback) of γ-rays of energy $x > 1/x_t$. Then the transition from unsaturated to saturated pair production for models with $\gamma_{max} x_t \sim 1$ is smoother than the corresponding pure Compton models. Due to the small value of x_B, a large region of the parameter space corresponds to models with only one generation of pairs produced by the synchrotron photons.

Even if not important to the total energy budget, inclusion of IC losses modifies the spectral shape in narrow energy bands, particularly for intermediate values of ℓ_e $(10-10^2)$, and for models with $x_B \gamma_{max} < 1$. High energy pairs created by IC photons can dominate the synchrotron emission above $\sim x_B x_{s,max}^2$. If below this energy the spectrum can be approximated with a power law of index one in particular bands, then it is analytically found that the equilibrium spectral index above $\sim x_B x_{s,max}^2$ must be one also.

The spectral index α_{2-10} between 2 and 10 keV is found to be sensitive to the chosen value of $x_{s,max}$ and ℓ_e in a complex way, and to depend only on x_{smax} between $10 < \ell_e < 300$. For $\ell_e > 300$ downscattering and/or the steep tail of the pair distribution cause α_{2-10} to steepen. For values of $x_B \gamma_{max}$ corresponding to two generations of pairs, and for saturated pair production, the overall spectrum $x\ell(x)$ is smooth and peaks at $x \sim 5$ keV.

For $\gamma_{max}^2 x_B < 3/2$, pairs are produced by IC photons. A clear distinction can be made on the basis of the ratio ℓ_e/ℓ_B.

For $\ell_e/\ell_B < 1$, the synchrotron process emits the bulk of the injected power (for flat injections), but pairs can play a dominant role at X-ray energies for values of ℓ_e yielding saturated pair production. In a narrow region of the $x_B - \gamma_{max}$ parameter space, and for $\ell_e >\sim 300$, an analytical model can be, and has been, constructed. Pairs redistribute the luminosity produced at γ-ray energies towards X-rays, changing both intensity and spectral shape with respect to a pair free model. Particularly interesting is the case in which a source is characterized by a value of γ_{max} just below the "threshold" line in fig. 5.10. A small increase in γ_{max} can let the source change

from a pair free to a pair dominated state. However, it is stressed that the derived spectra at X-ray energies are highly uncertain, due to the ignorance of the effects synchrotron reabsorption can have on the particle distribution below γ_t.

For $\ell_e/\ell_b \gg 1$, synchrotron reabsorption play a minor role, and the reabsorbed energy can be neglected. For these models it is found that the spectral index below mc^2 or below $1/\tau_T^2$ (when downscattering is important) is always less than unity, contrary to earlier estimates by Bonometto & Rees (1971) and Kazanas (1984). In this case higher orders IC scatterings are never negligible, and give a substantial contribution to the emission at all energies. When important, thermal Comptonization smoothes out the spectrum at energies close to $x_{s,max}$, and between this energy and $1/\tau_T^2$ it can be approximated with a power law whose index is found analytically, and in agreement with the numerical results. Independent on the chosen values of γ_{max}, models of high compactnesses and same ℓ_e/ℓ_B ratio looks very similar, peaking in $x\ell(x)$ plots at $x \sim \Theta \sim 10^{-2}$. For most of these models the spectrum between 2 and 10 keV is not a power law, and α_{2-10} is not a measure of the resulting spectrum. The adopted approximate treatment of thermal up- and down- scattering breaks down for $y \gg 1$, i.e. when $\Theta > 1/\tau_t^2$. In this case a Wien peak is expected to develop at $x \sim \Theta > 10^{-2}$. For this to occur, high values of both ℓ_e and ℓ_e/ℓ_B are required, and the spectrum below $x = \Theta$ will be characterized by an average spectral index $\alpha < 0.5$.

Table 5.1

ℓ_e	γ_t	Θ	τ_T	α_{th}	ξ	α_{2-10}	x_{smax}
1	12.8	7×10^{-2}	0.05	-	1.94×10^{-3}	0.5	8
10	10.6	7×10^{-2}	0.44	-	1.53×10^{-2}	0.51	8
100	10.8	4.1×10^{-2}	2.41	1.44	4.64×10^{-2}	0.49	8
1000	10.6	1.3×10^{-2}	8.3	0.7	5.86×10^{-2}	0.82	8
1	23.1	5.9×10^{-2}	0.024	-	4.57×10^{-4}	0.54	10^2
10	27.4	5.6×10^{-2}	0.23	-	4.26×10^{-3}	0.46	10^2
100	30.4	2.36×10^{-2}	1.9	2.9	2.95×10^{-2}	0.62	10^2
1000	26.4	5.4×10^{-3}	6.82	1.76	4.1×10^{-2}	0.78	10^2
1	11.6	3.82×10^{-2}	0.0014	-	2×10^{-6}	0.48	10^4
10	19.9	1.55×10^{-3}	0.053	-	2.85×10^{-4}	0.885	10^4
100	22.31	$2. \times 10^{-3}$	0.47	-	2.2×10^{-3}	0.904	10^4
1000	21.07	2.35×10^{-3}	3.03	7.8	8.9×10^{-3}	1.85	10^4
1	12.3	2.6×10^{-2}	0.054	-	2.3×10^{-5}	0.74	10^6
10	19.1	2.6×10^{-2}	0.1	-	7.45×10^{-4}	0.79	10^6
100	17.5	3×10^{-2}	1.42	3.3	1.64×10^{-2}	0.80	10^6
1000	19.1	9×10^{-3}	6.3	1.3	3.41×10^{-2}	1.37	10^6

Derived values of the selfabsorption energy γ_t, temperature Θ, optical depth τ_T, Comptonization spectral index α_{th}, pair yield ξ and the 2-10 kev spectral index α_{2-10} for the models shown in Figs. 5.2-5.5. $R = 10^{15}$cm and $\ell_B/\ell_e = 10$ is assumed for all models.

Table 5.2

ℓ_e	ℓ_e/ℓ_B	γ_{max}	γ_t	Θ	τ_T	α_{th}	ξ	Fig.
1000	100	180	76.6	3.3×10^{-2}	-	-	1.28×10^{-1}	5.11a (2)
1000	100	180	58.	5×10^{-3}	10.1	1.	8.96×10^{-2}	5.11a (3)
10	30	10^3	80.7	3×10^{-2}	0.23	-	4.25×10^{-3}	5.12
100	30	10^3	64.1	2.5×10^{-2}	2.52	2.	5.18×10^{-2}	5.12
1000	30	10^3	49.6	5.6×10^{-3}	8.7	1.2	6.7×10^{-2}	5.12
10	30	10^4	75	2.2×10^{-2}	0.25	-	4.9×10^{-3}	5.13
100	30	10^4	63	1.9×10^{-2}	2.33	2.74	4.2×10^{-2}	5.13
1000	30	10^4	48	4.8×10^{-3}	9.86	1.15	8.7×10^{-2}	5.13
10	30	10^5	75.4	1.5×10^{-2}	0.24	-	4.93×10^{-3}	5.14
100	30	10^5	64	1.8×10^{-2}	3.1	2.15	3.82×10^{-2}	5.14
1000	30	10^5	49.1	7.2×10^{-3}	7.56	1.23	4.94×10^{-2}	5.14
10	1	10^3	62.5	1.2×10^{-2}	0.05	-	2.3×10^{-4}	6.1
100	1	10^3	42.5	1.5×10^{-2}	0.8	-	5.3×10^{-3}	6.1
1000	1	10^3	31.2	3.4×10^{-3}	6.12	2.83	3.5×10^{-2}	6.1

Input and derived parameters for the models shown in Figs. 5.11-5.14. For all but the last three models $R = 10^{15}$cm. For the last three models $R = 10^{17}, 10^{16}, 10^{15}$cm, respectively.

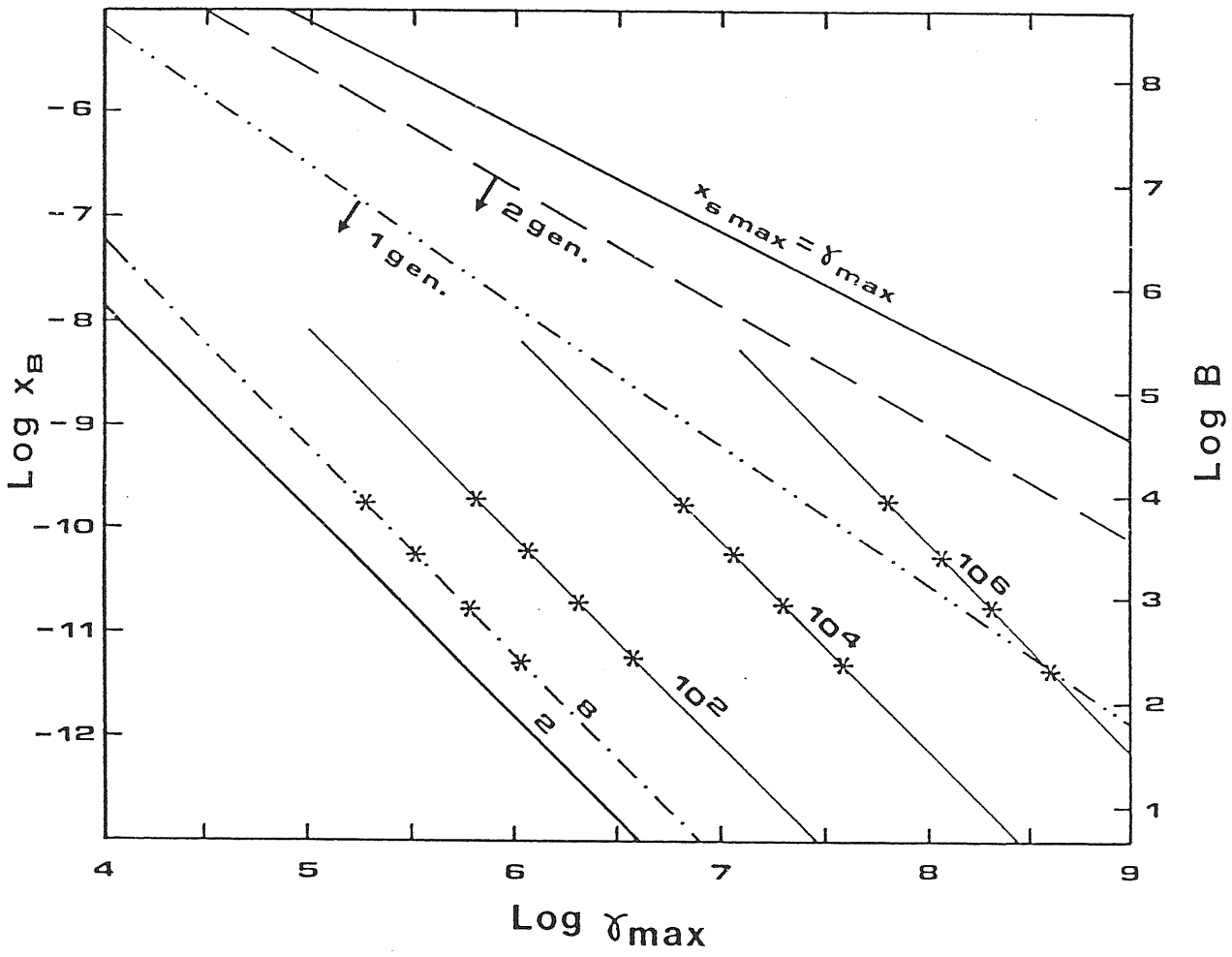

Figure 5.1. The parameter space $x_B - \gamma_{max}$ for models in which synchrotron photons create pairs. Labels indicate the maximum emitted synchrotron energy $x_{s,max}$, and the line $x_{s,max} = \gamma_{max}$ above which quantum effects are important. Below the dot-dot-dashed line only one generation of pairs created by synchrotron photons is possible, while two generations are possible between this line and the dashed one. Stars indicate the values of x_B and γ_{max} used for the models shown in figs. 5.2–5.5. Models with $x_{s,max} = 8$ correspond to those giving the maximum pair yield ξ_{max}.

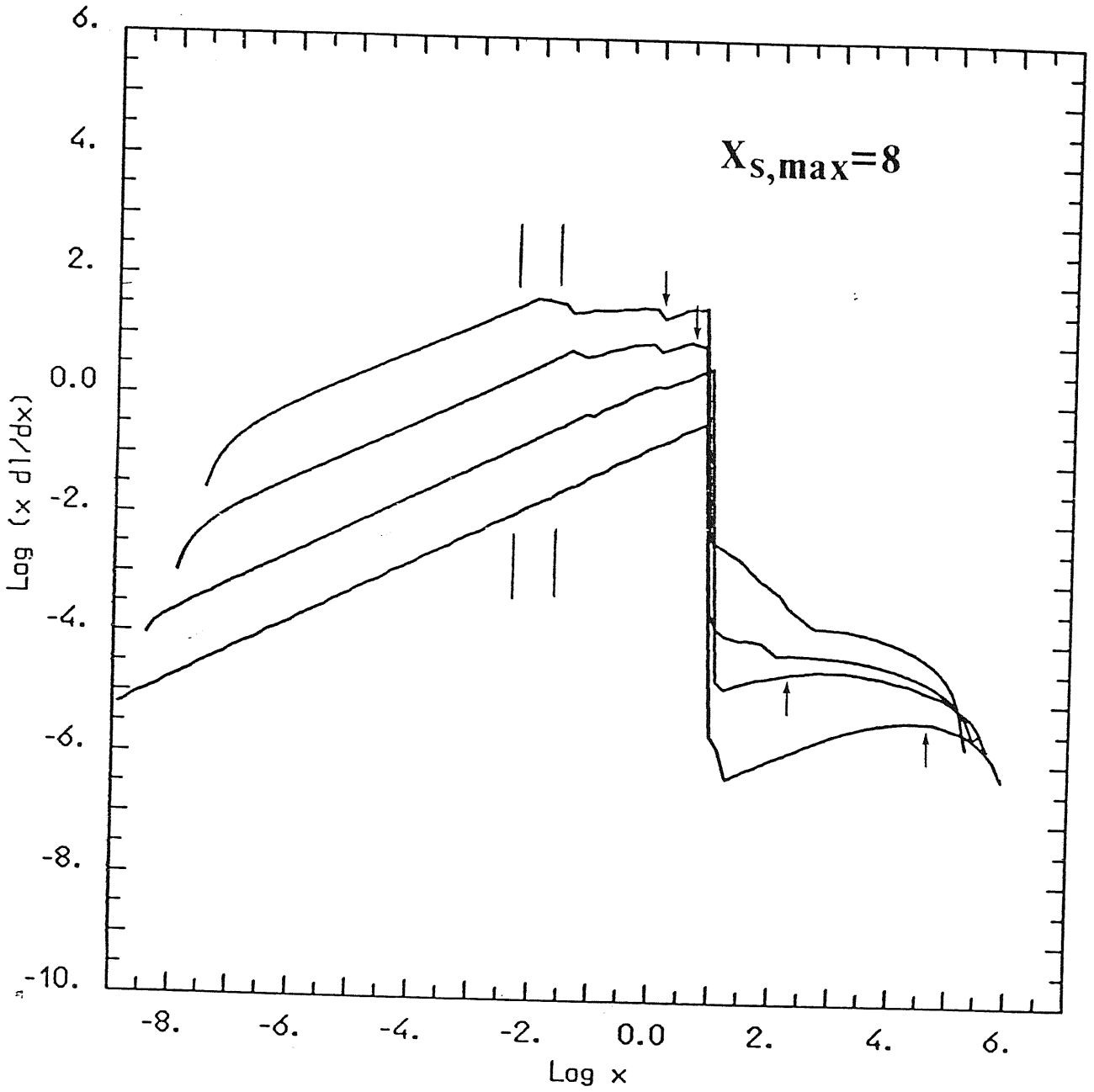

Figure 5.2a. SSC spectra computed for $\ell_e = 1$, 10, 10^2, and 10^3 (from bottom to top), $x_{s,max} = 8$, $R = 10^{15}$ cm, and $\ell_B/\ell_e = 10$. Primary particles are injected monoenergetically. Vertical segments indicate the range 2–10 keV. Arrows indicate the energy x at which $\tau_{\gamma\gamma}(x) = 1$. Input and derived parameters are listed in table 5.1.

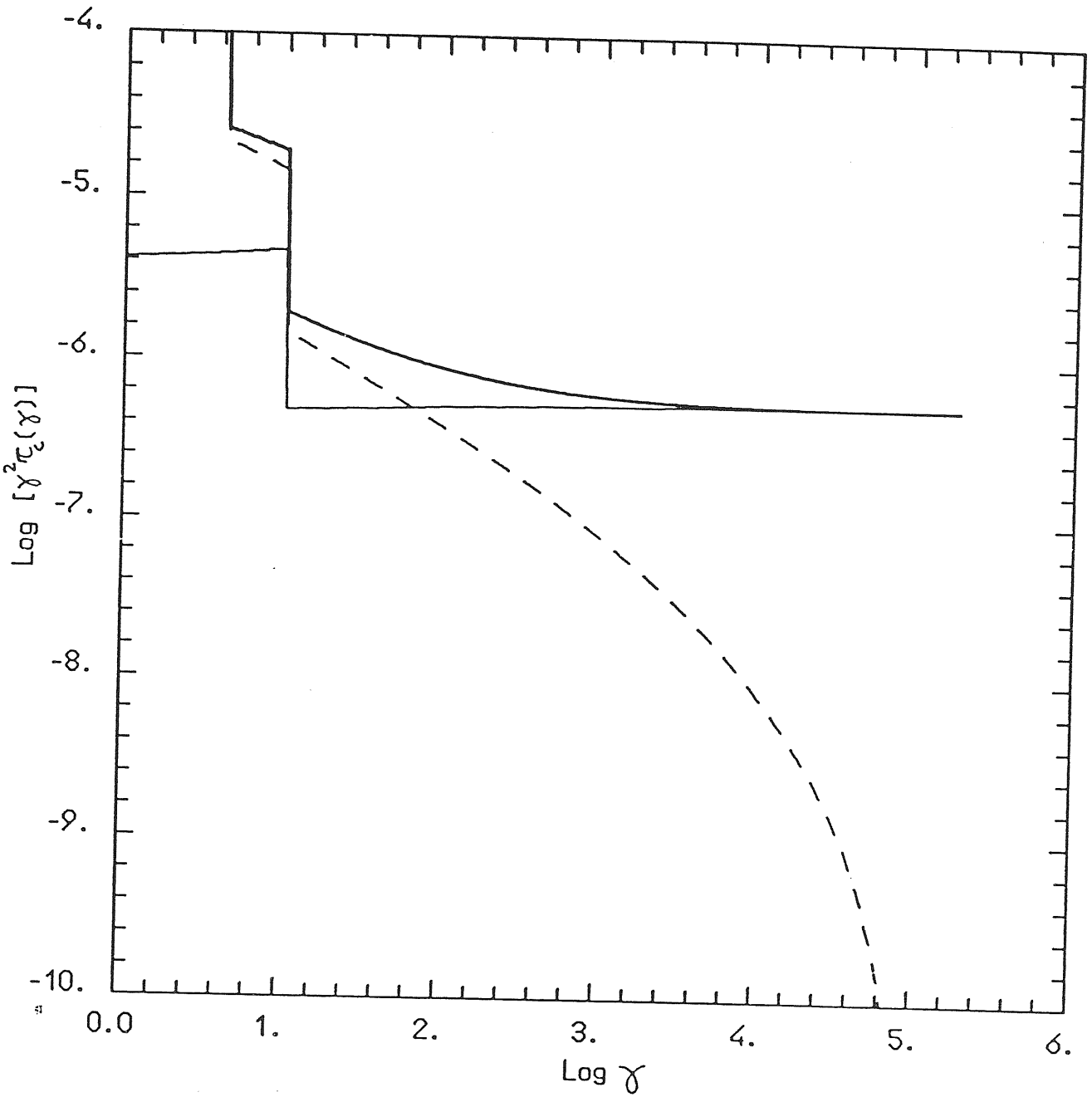

Figure 5.2b. The steady equilibrium energy distribution of pairs (dotted line), primary particles (thin line) and their sum (thick line) for the model with $\ell_e = 10^3$ of fig. 5.2a. Note that $\gamma^2\tau_c(\gamma) \equiv \sigma_T R\gamma^2 N(\gamma)$ is plotted. The discontinuity at $\gamma_t \sim 10$ is caused by the assumed synchrotron cooling rate in the selfabsorbed regime. This discontinuity, and the particle distribution below γ_t is not reliable.

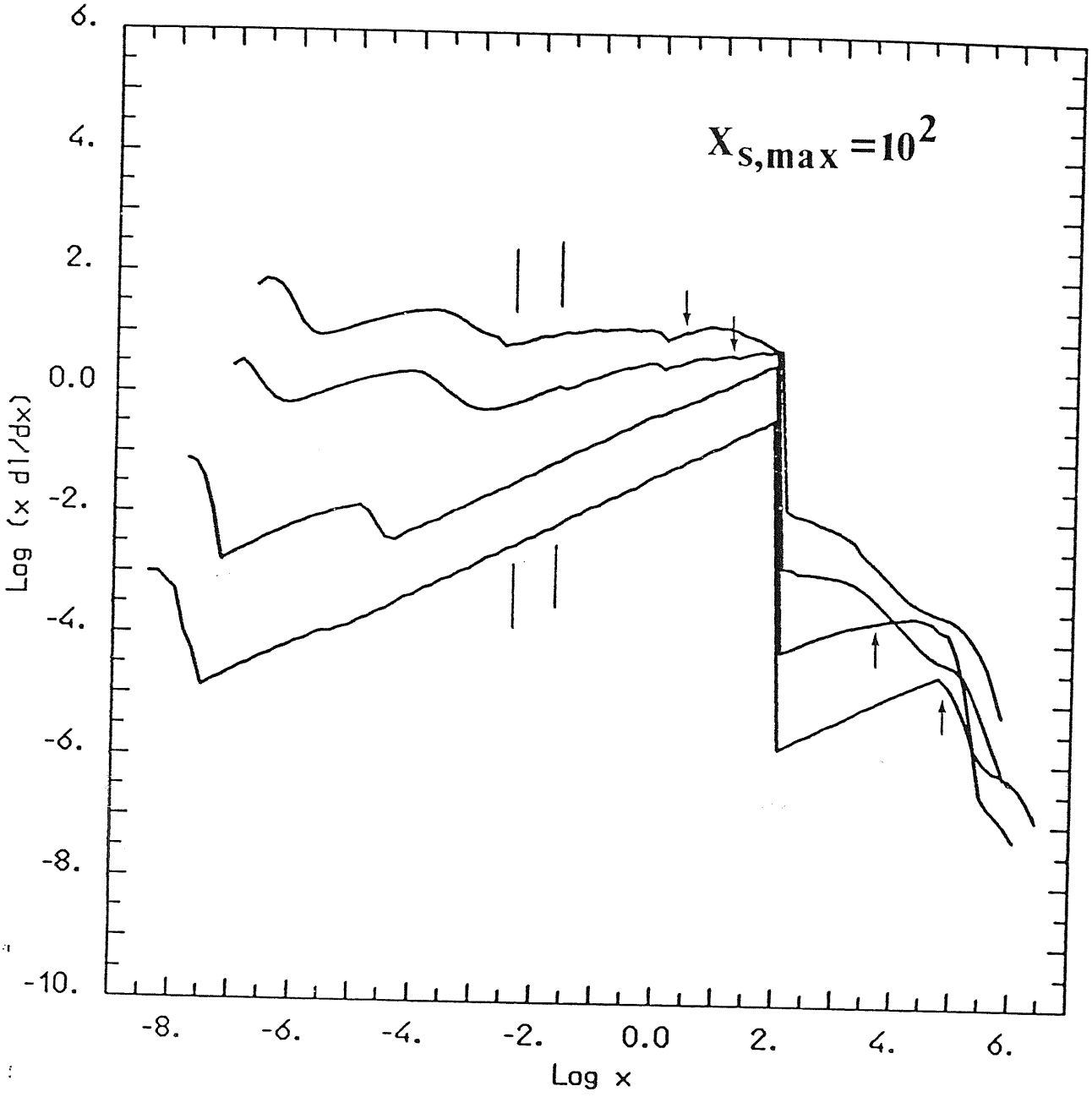

Figure 5.3. Same as fig. 5.2a, but for $x_{s,max} = 10^2$.

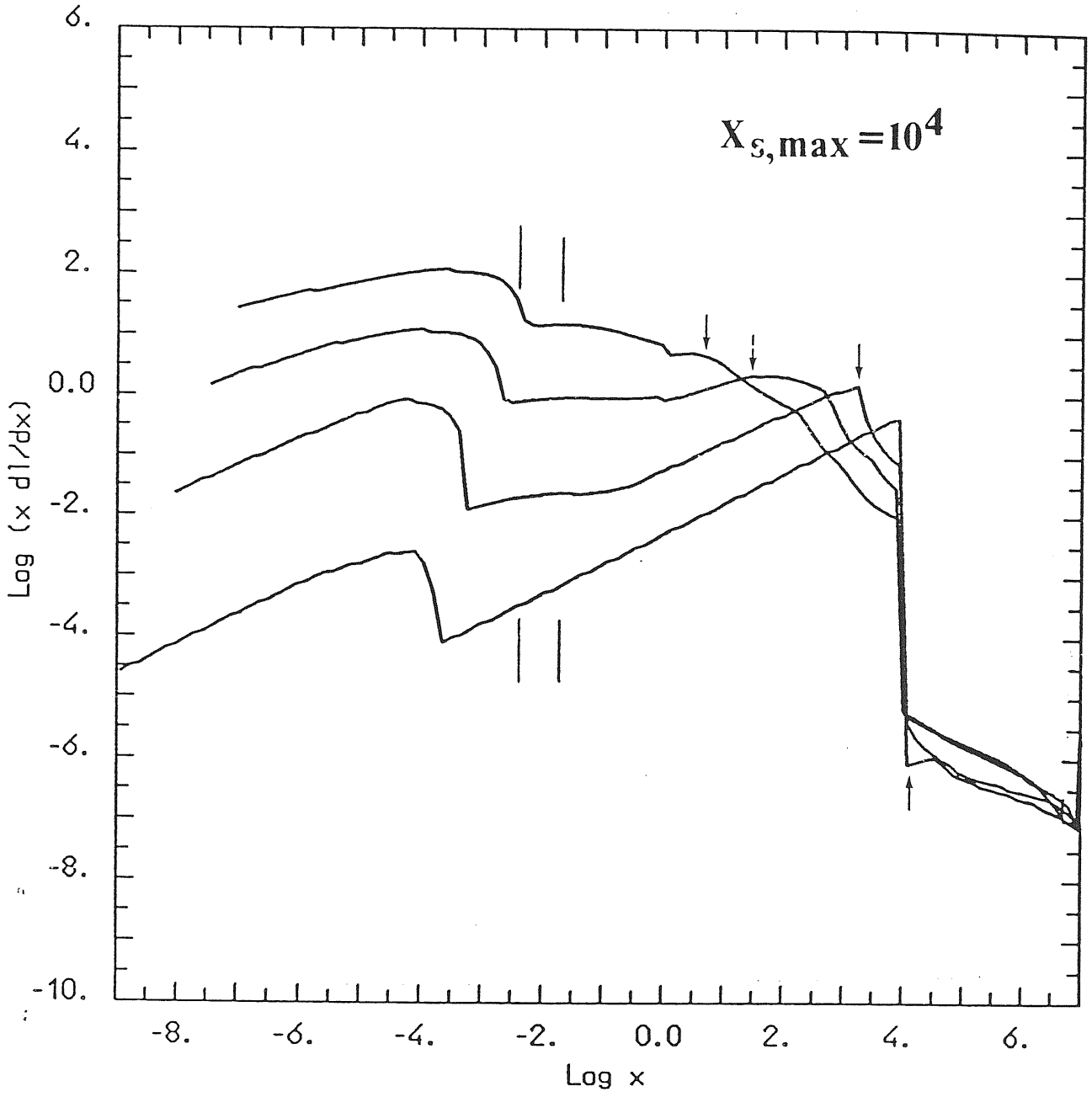

Figure 5.4. Same as fig. 5.2a, but for $x_{s,max} = 10^4$.

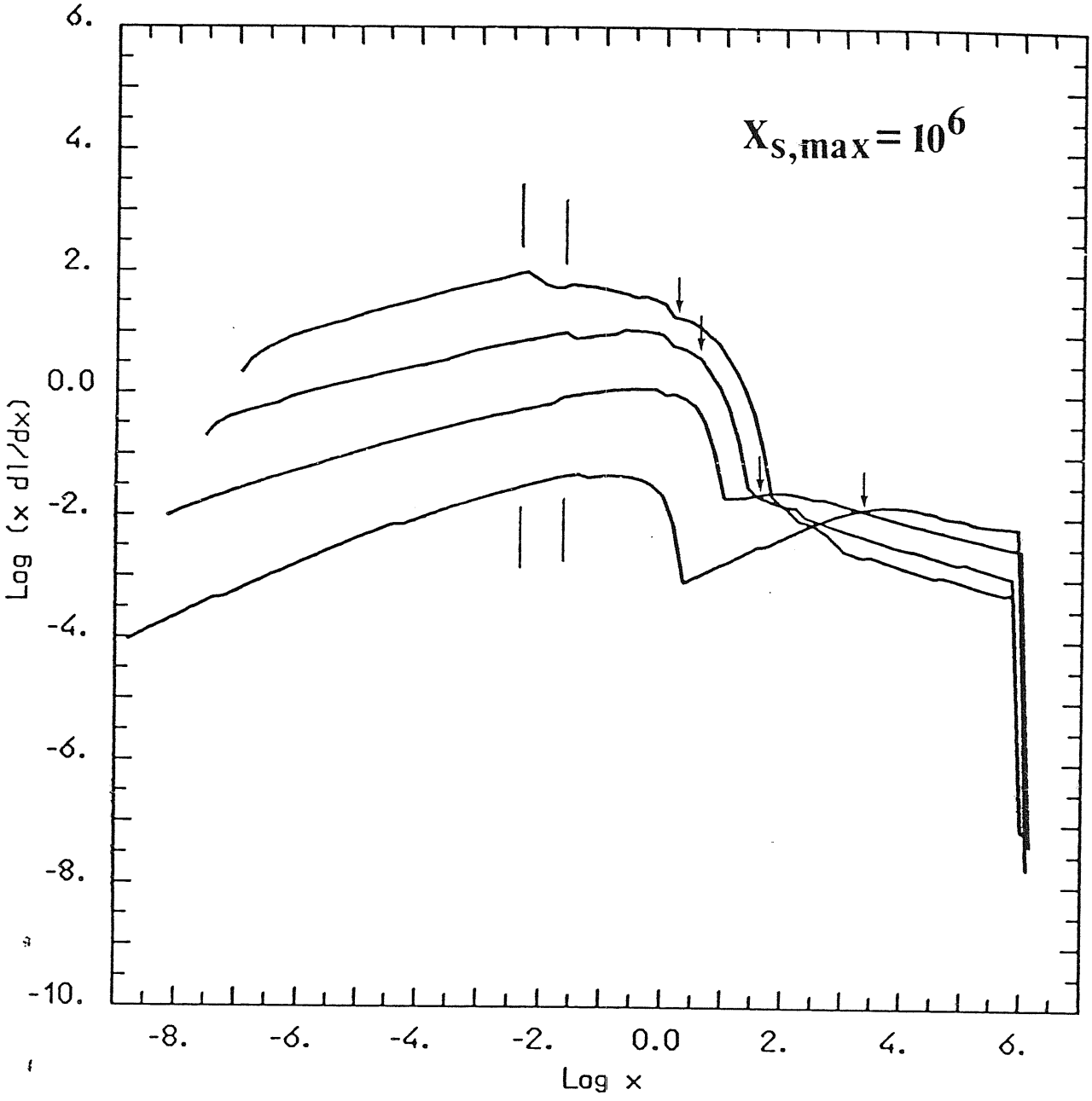

Figure 5.5. Same as fig. 5.2a, but for $x_{s,max} = 10^6$. As shown in fig. 5.1, all but the $\ell_e = 1$ models produce two generations of pairs by synchrotron photons.

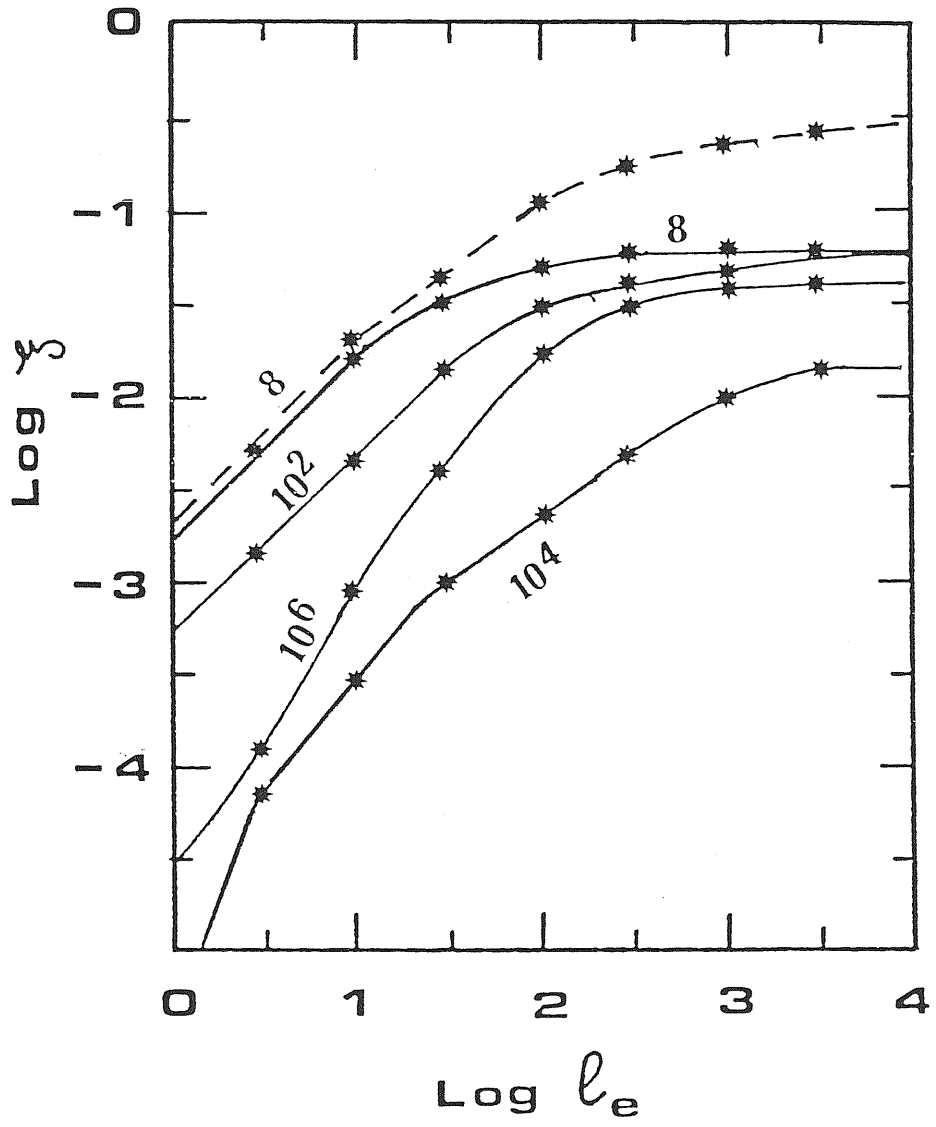

Figure 5.6. The pair yield ξ vs. the injected luminosity ℓ_e for different (labelled) values of the maximum synchrotron energy. Stars indicate values from computed models, lines are a guide to the eye. The dashed line corresponds to models with $x_{s,max} = 8$ in which cool particle effects have been neglected.

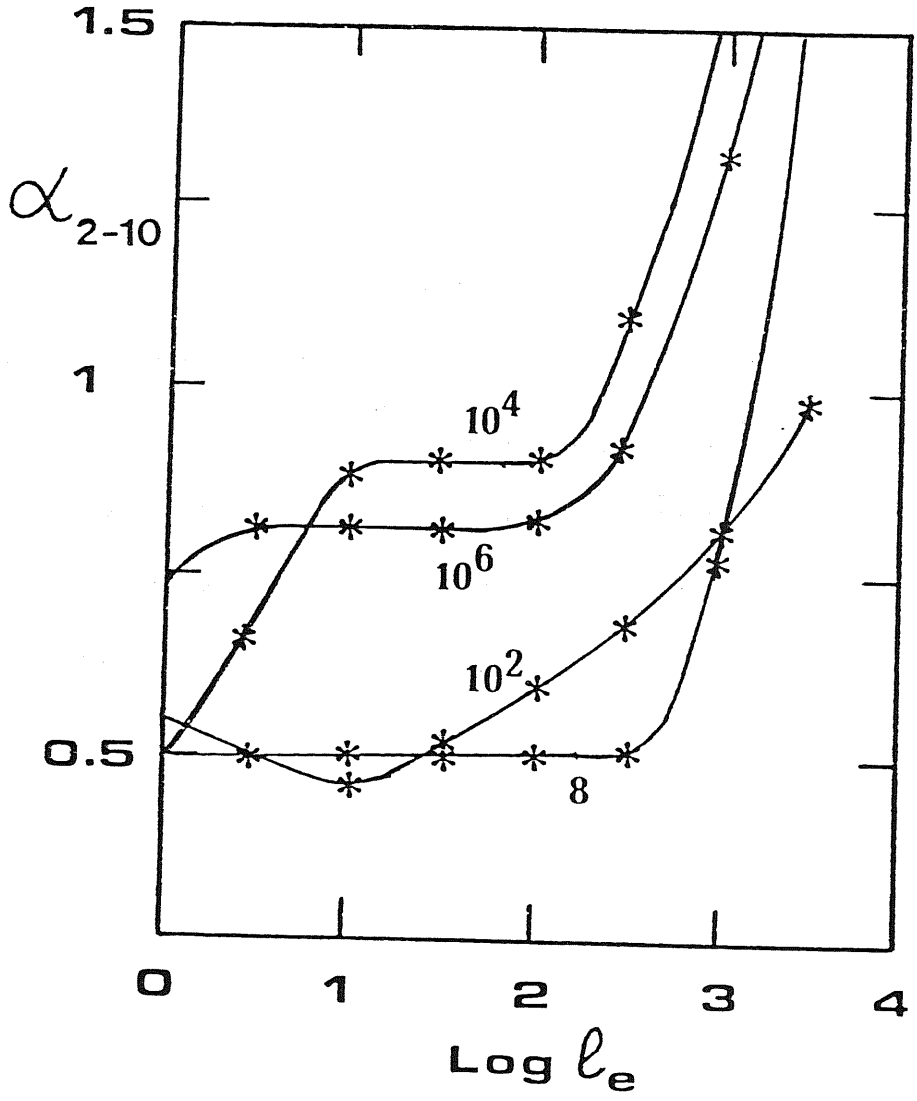

Figure 5.7. The spectral index α_{2-10} between 2 and 10 keV vs. the injected luminosity ℓ_e for different (labelled) values of the maximum synchrotron energy. Stars indicate values from computed models, lines are a guide to the eye.

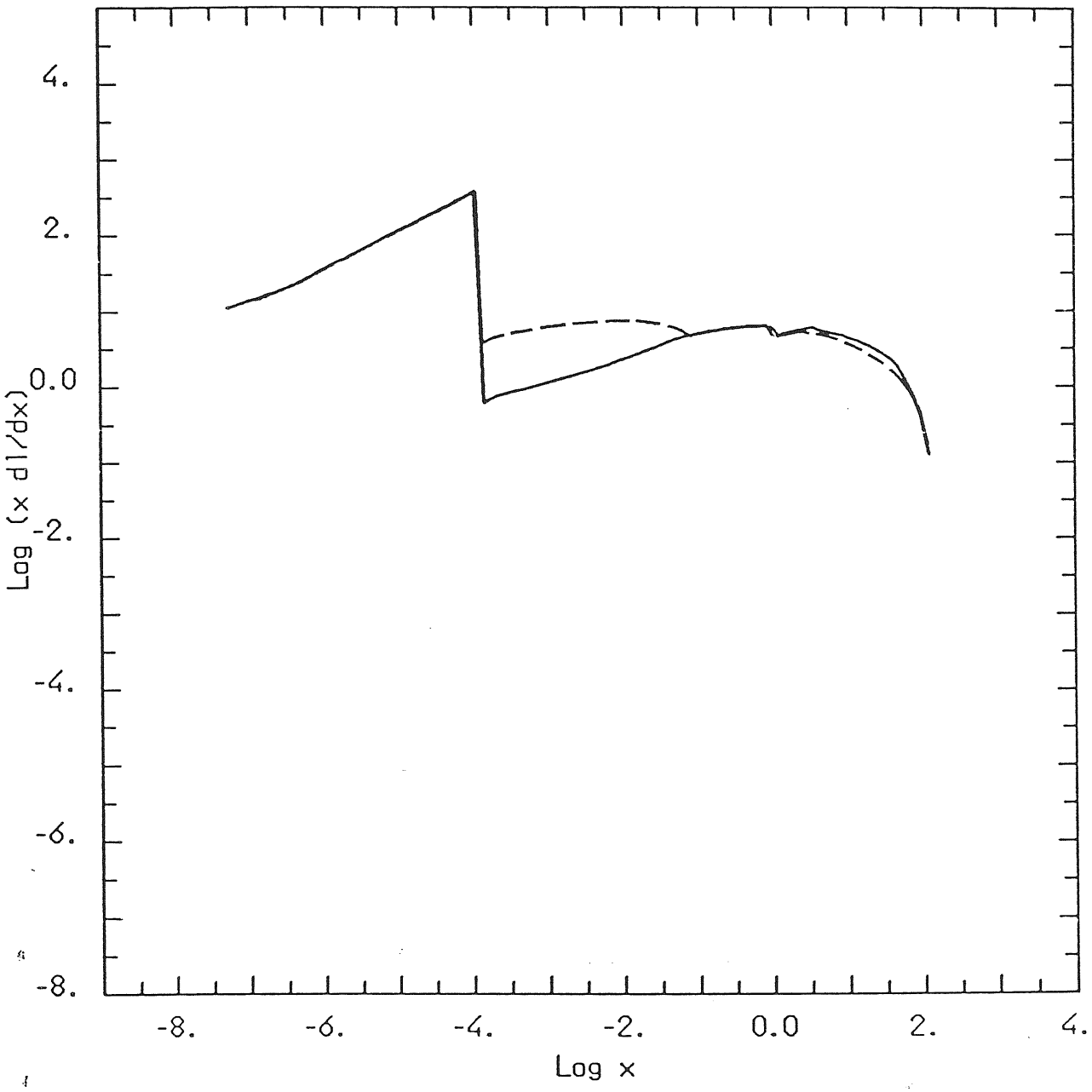

Figure 5.8. SSc spectra computed for $\ell_e = 902$, $R = 3 \times 10^{15}$ cm (corresponding to $L = 10^{47}$ erg/s), monoenergetic particle injection at the energy $\gamma_{max} = 10^3$, and $\ell_B/\ell_e = 10$. *Solid line*: no synchrotron reabsorption is considered for the cooling rate of the particles. *Dashed line*: the net synchrotron cooling rate below the self absorption energy γ_t has been assumed to vanish.

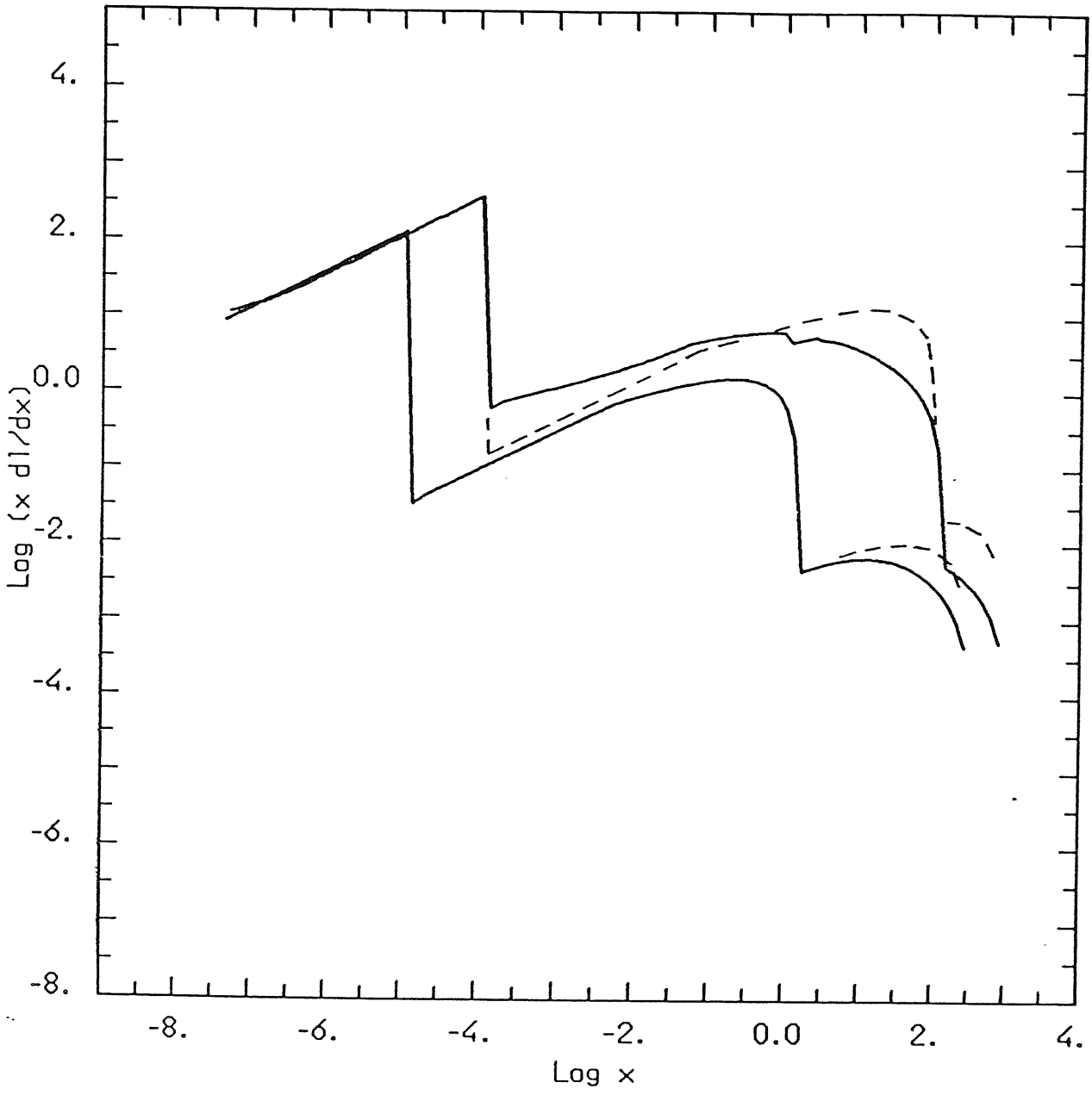

Figure 5.9. SSC spectra computed for the same parameters of fig. 5.8 (upper solid line), and for a model of same size, magnetic field, and number of primary injected particles per unit time, but at the energy $\gamma_{max} = 333$ (lower solid line). The luminosity of the second model is consequently 1/3 of that of the first. Due to the reduced value of γ_{max}, in the second model a small pair production place, at the highest energies emitted by the second order IC scattering. Dashed lines refer to models with the same parameters, but completely neglecting pair production.

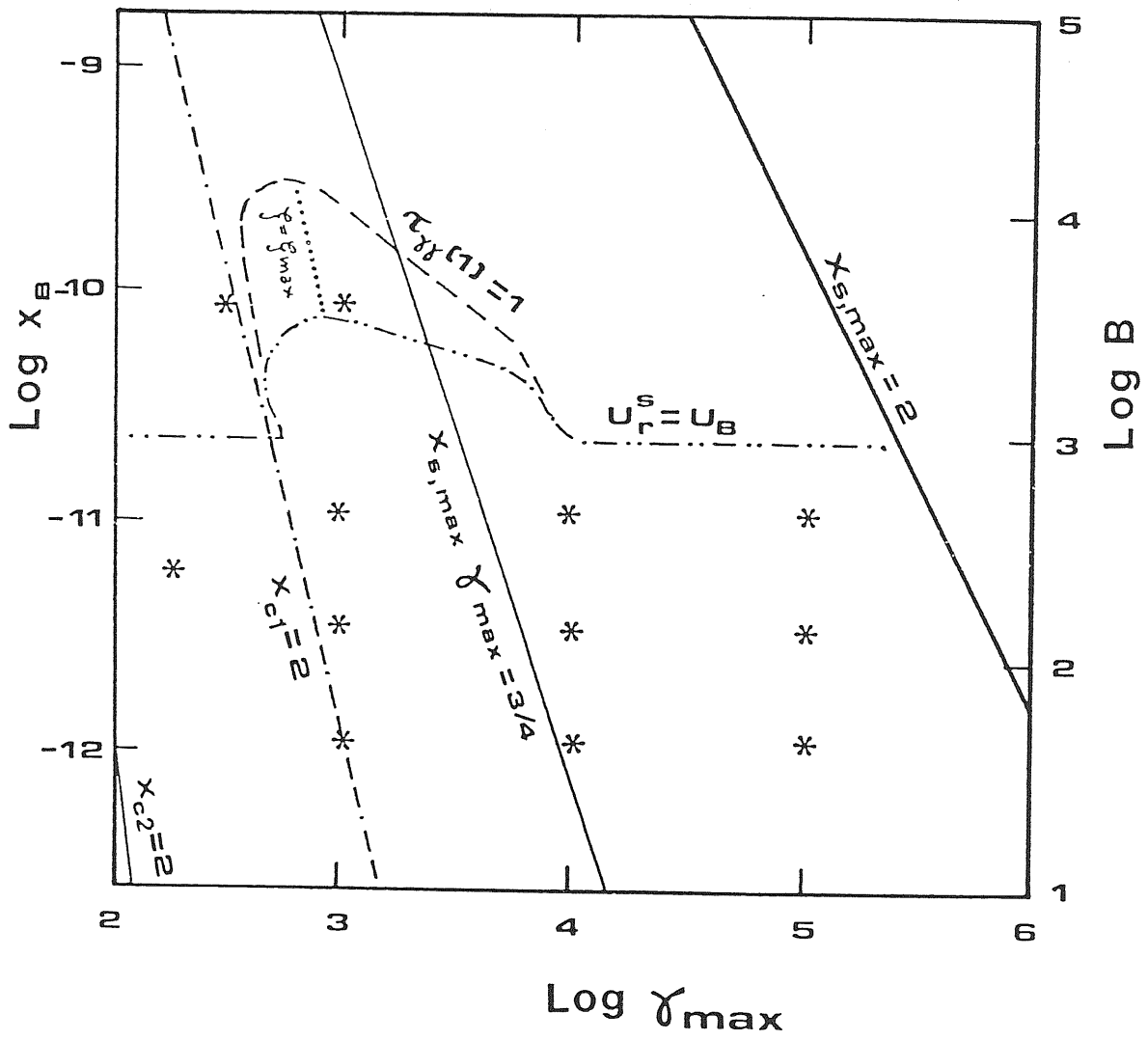

Figure 5.10. The parameter space $x_B - \gamma_{max}$ for models in which pairs are created by photons produced by the inverse Compton process. Stars indicate the values used in the models shown in figs. 5.8, 5.9, and 5.11–5.14. Between the lines labelled $x_{c,1} = 2$ and $x_{c,2} = 2$ pairs are created by the second order IC photons. In the triangle- shaped region between the dashed and dot-dot-dashed lines the assumptions of section 5.4 are valid. This region, and the line $U_r^s = U_B$ have been drawn assuming $R = 3 \times 10^{15}$ cm and $\ell_e = 902$. The other lines are independent of size and luminosity.

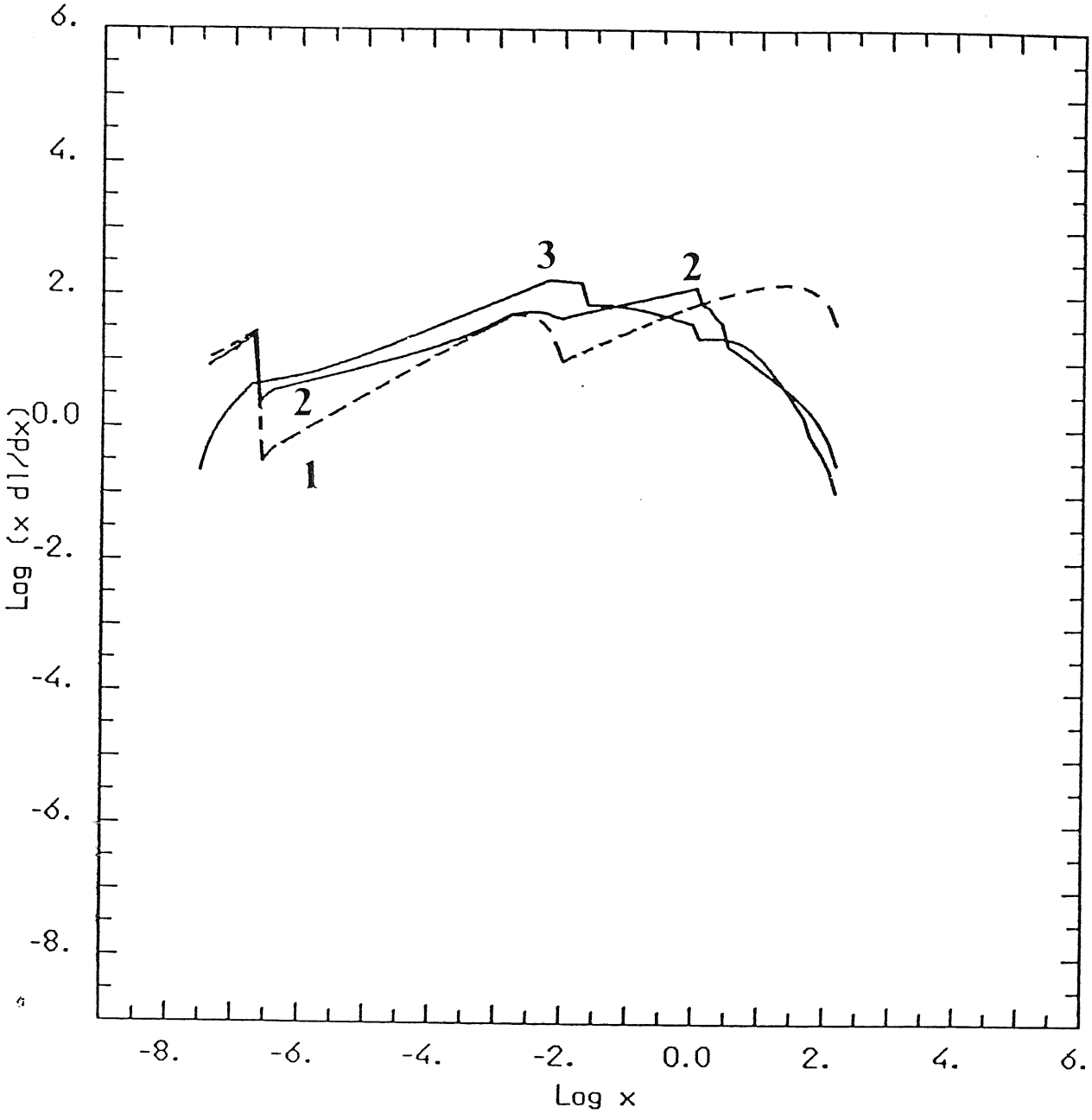

Figure 5.11a. SSC spectra for $R = 10^{15}$ cm, $\ell_e = 10^3$, $\ell_e/\ell_B = 10^2$, and monoenergetic injection of primary particles at $\gamma_{max} = 180$. For the spectrum labelled 1 (dashed line) pair production is completely neglected. Model 2 includes pair production, but cool particle effects are neglected, while they are included in model 3. Input and derived parameters are listed in table 5.2.

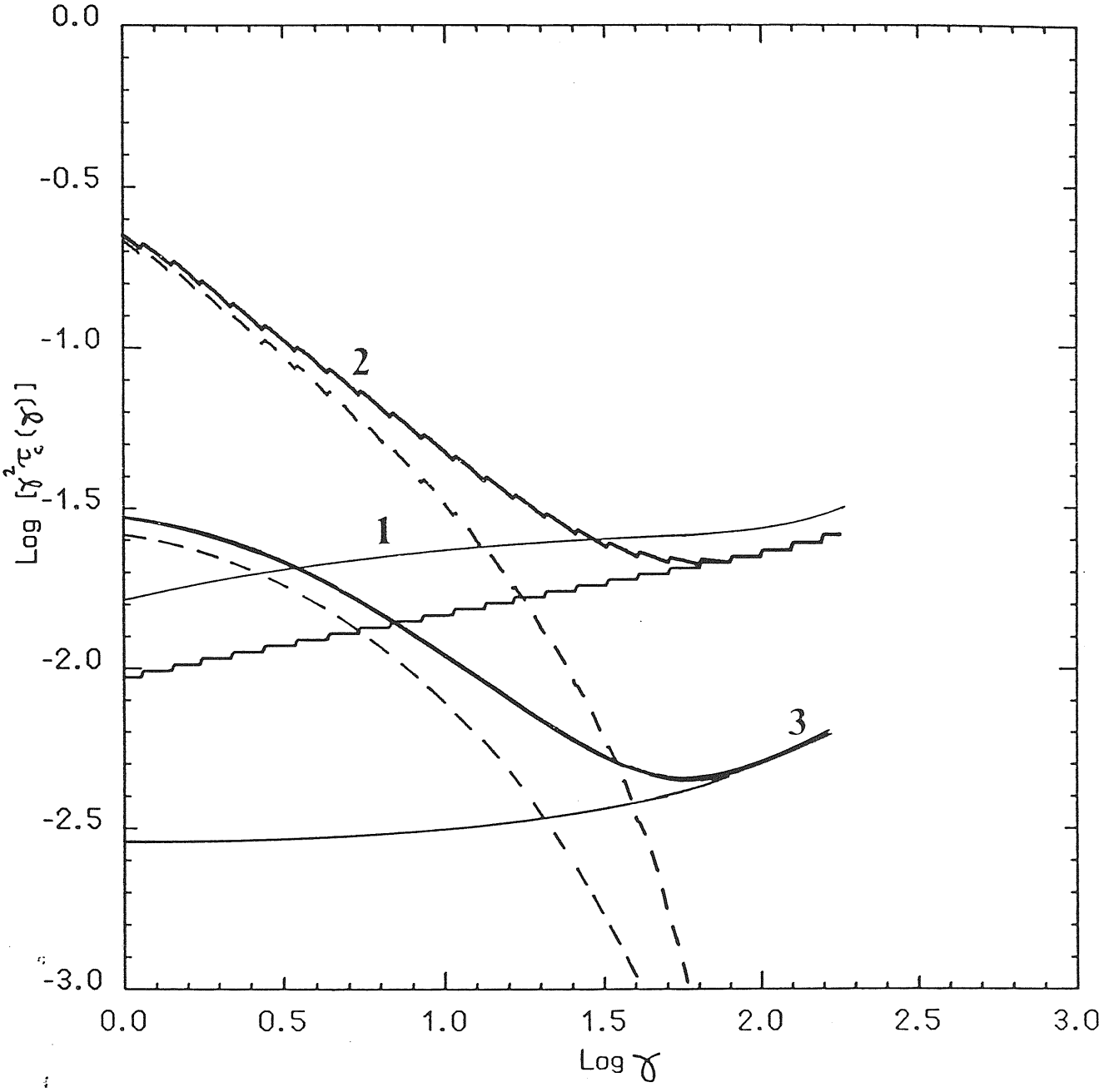

Figure 5.11b. The steady particle energy distributions of the models shown in fig. 5.11a. Labels indicate the corresponding models of fig. 5.11a. Dashed lines refer to pairs, thin solid lines to primary particles, thick solid line to their sum. Note that $\gamma^2\tau_c(\gamma) \equiv \sigma_t R\gamma^2 N(\gamma)$ is plotted.

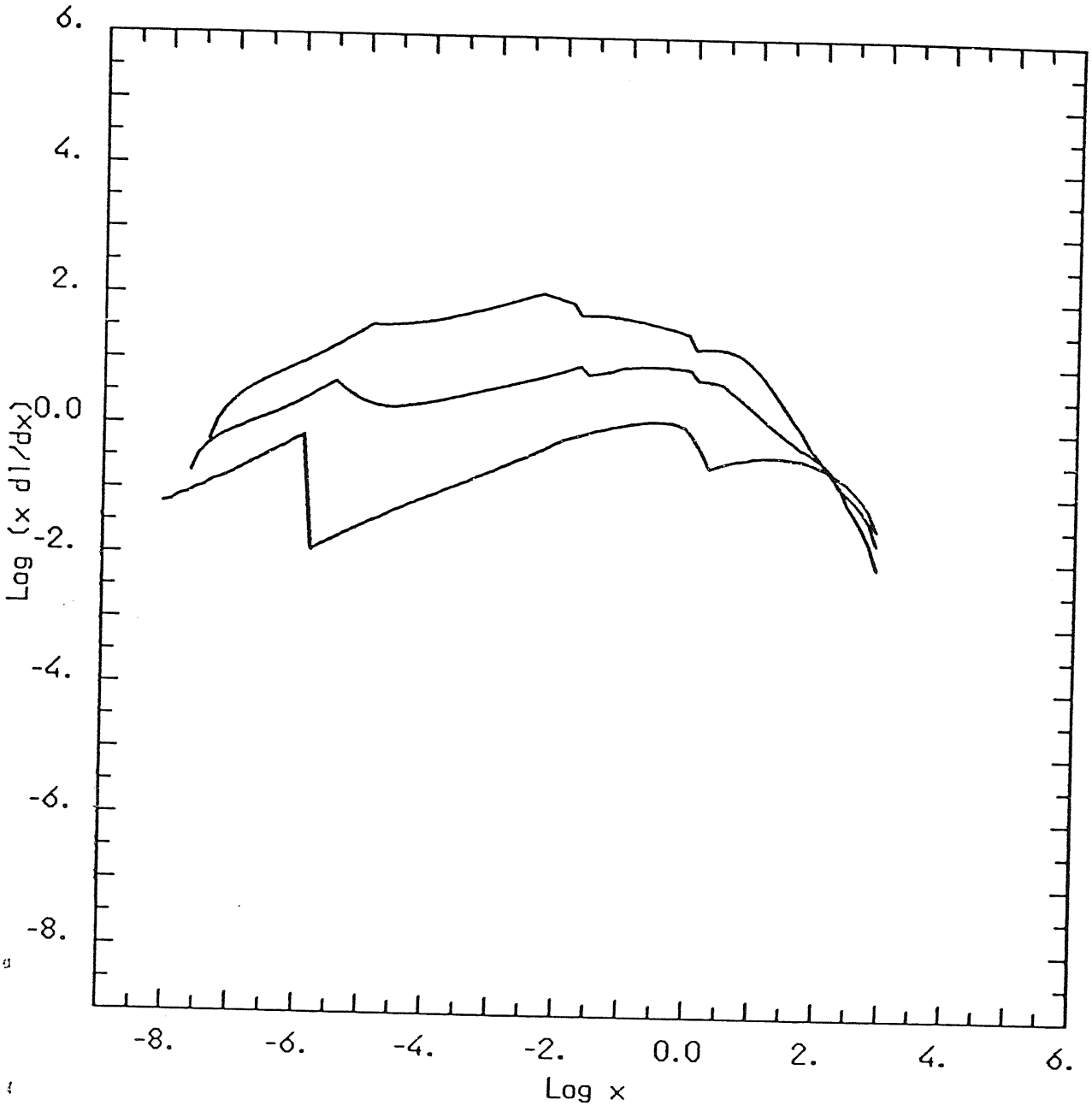

Figure 5.12. SSC spectra for $R = 10^{15}$ cm, $\ell_e/\ell_B = 30$, monoenergetic injection of primary particles at $\gamma_{max} = 10^3$, and for $\ell_e = 10,\ 10^2,\ 10^3$ (from bottom to top). Input and derived parameters are listed in table 5.2.

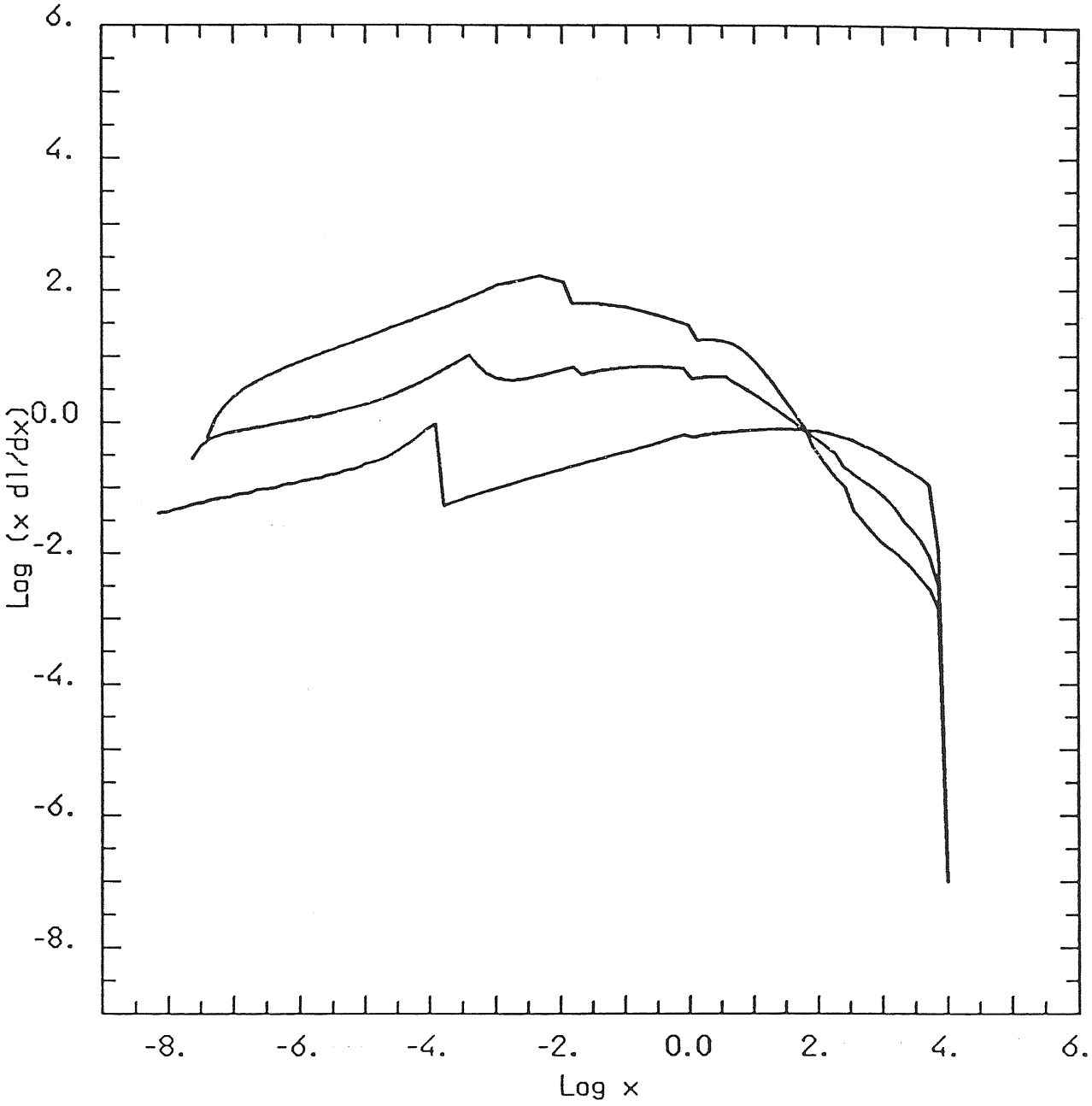

Figure 5.13. Same as fig. 5.12, but for $\gamma_{max} = 10^4$.

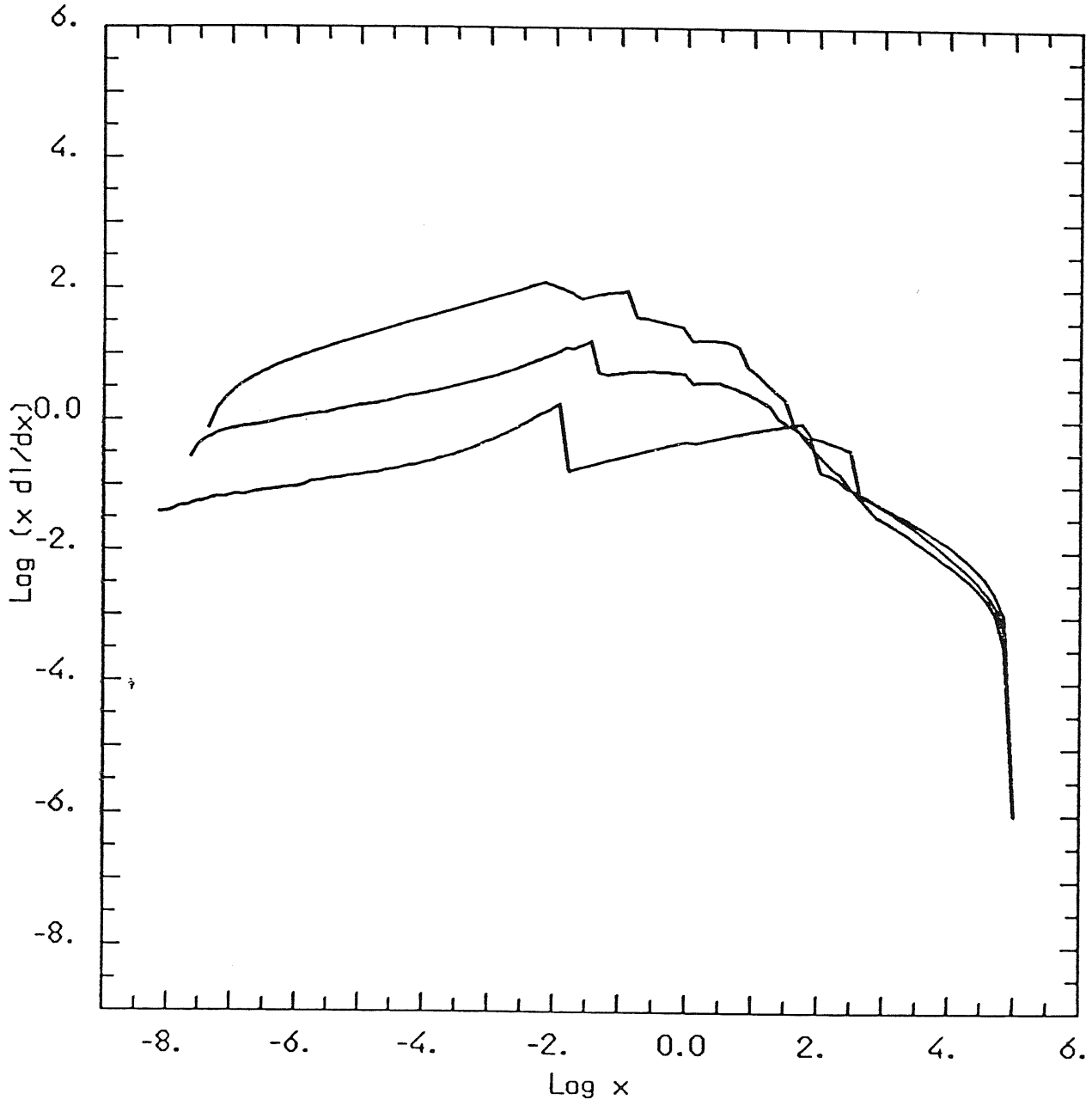

Figure 5.14. Same as fig. 5.12, but for $\gamma_{max} = 10^5$.

DISCUSSION

Synchrotron self Compton models for compact sources cover the whole energy range from the far infrared to the γ-ray band. Apart from the spectra calculated in the second chapter of this thesis, all the spectra shown so far refer to homogeneous models, and have to be considered as the spectra emitted by a single component of a real source, which can contain different emitting regions. The UV bump and the extended radio emission in quasars are two examples of contributions coming from different emission regions. Furthermore, the observed variability timescales are generally shorter at higher frequencies, suggesting that larger components dominate the emission in the lower energy bands. Though this may happen due to the contribution of different processes, it is also plausible that the SSC mechanism is active on different spatial scales in the same source, possibly yielding an overall spectrum different from that of a single region. Specific examples are considered in the second chapter.

Figure 6.1 illustrates the latter point in a general way. It is assumed that three components emit the same luminosity $L_e = 3.7 \times 10^{46}$ erg/s, but from different volumes, of radius $R = 10^{15}$, 10^{16}, and 10^{17} cm, corresponding to $\ell_e = 10^3$, 10^2, and 10, respectively. In all three cases $\ell_B = \ell_e$ and the injection of particles is monoenergetic at $\gamma_{max} = 10^3$. For such a model, the convolution of the three individual spectra yields $\alpha \sim 0.5$ in the submillimeter-far IR band, $\alpha \sim 1$ in the optical, $\alpha \sim 2.2$ in the extreme UV and soft X-rays, $\alpha \sim 0.6$ at 1 keV, $\alpha \sim 0.8$ between 2 keV and 0.5 Mev, and $\alpha \sim 1.6$ in the γ-ray band. The spectral index between 2 μ and 2 keV is $\alpha_{IRX} \sim 1.1$. Note, from table 5.2, that only the most compact region is optically thick to scattering by the cool pairs, which lengthens the minimum variability timescale to $\sim$ 1 day, and reduces the polarization of the synchrotron radiation only in the energy band where the most compact component dominates.

It is gratifying that the simple assumptions made can qualitatively account for the overall non thermal energy distribution of a typical AGN.

However, other possibilities exist, and the choice of the parameters is not unique. What is important, and has to be stressed, is that the most compact region of the source gives the major contribution to the overall spectrum at X-ray energies. For this component, all the effects described in the third and fifth chapter are likely to play a dominant role. I will therefore concentrate the discussion on the X-ray band.

AGNs show a variety of X-ray spectral indices. Wilkes & Elvis (1987) have shown that for the 33 sources in their sample α_x between 0.3 and 3.5 keV ranges from -0.2 to 1.8. A correlation is found between α_x and radio loudness, in the sense that for radioquiet and radioloud quasars the average values of α_x are about 1 and 0.5, respectively. Few sources (like PG $1211+143$) show evidences for a steep soft X-ray excess below ~ 1 keV.

On the other hand, the sample of a dozen sources (mostly nearby Seyfert galaxies) of Rothschild *et al.* (1983) observed between 2 and 165 keV show an average value $\alpha_x \sim 0.62$, with a small scatter around the mean.

BL Lacs usually have steep X-spectra (see e.g. Urry 1984, Urry, Mushotzky & Holt 1986), with α_x between 1 and 2 below a few keVs. Possibly, a hard tail is present above ~ 10 keV.

Only handful of AGNs have been detected above a few hundred keV (for review see e.g. Bassani *et al.* 1985). These observations indicate that the X-γ-ray spectrum breaks at 1-10 MeV. More tight constraints can be derived from the cosmic γ-ray background, which shows a hump at ~ 3 MeV, and has a power law shape of slope $\alpha_\gamma \sim 2$ at higher energies (Rothschild *et al.* 1983), indicating that the mean γ-ray spectrum (if any) of AGNs must be steep.

Recent data on AGNs (Wandel & Mushotzky 1986, and references therein) seem to suggest a range of observed ℓ clustering around a mean value of about 10. Note that the use of time variability yields an upper limit of the source size, and then a lower limit of ℓ.

In standard SSC models, any value of α_x can be accounted for by an appropriate

slope of the ad hoc assumed power law particle distribution.

More correctly, and more interestingly, the observed values of α_x can however be produced by "self consistent" SSC models with a minimum of required parameters. In table 6.1 a schematic classification of the the type of models discussed in the third and fifth chapter is given.

Table 6.1

Mod. type	ℓ_e/ℓ_B	Inj. mode	Pairs by
1	any	steep pow. law	few pairs by IC
2	≤ 1	monoen.	synchro.
3	≤ 1	monoen.	1st order IC
4	$\gg 1$	monoen.	1st, 2nd order IC

Consider, for the moment, only models in which the maximum synchrotron energy is well below mc^2. In chapter three we discussed the case of the injection of a steep particle distribution, extending in energy down to $\gamma_{min} \sim 1$. These models yield *flat* ($\alpha \leq 1$) spectral indices below mc^2, or up to the energy $x \sim 1/\tau_T^2$ where down scattering starts to be important. Below this energy, the overall spectrum is smooth, and any discontinuity in the observed spectrum must be due to the superposition of different emitting regions, and not to different emission mechanisms (i.e. synchrotron at low, and IC at high photon energies). For low values of the compactness ($\ell_e < 10$) and for flat injected distributions, the resulting spectrum has a flat slope too, and related to the slope of the injected particle distribution, because pairs do not play a major role.

For higher value of the compactness ($\ell_e > 10$) and for monoenergetic (or flat) injection modes, pairs are important, at least in the X-ray band, even if $\ell_B \gg \ell_e$ (type 3 models), i.e. even if most of the injected luminosity is emitted at low energies

by the synchrotron process. In this particular case $\alpha_x \sim 0.7 - 1$ or even steeper, if the logarithmic high energy cut off of the pair distribution is important, and affects the X-ray emission. Down scattering is not important in these models, and an X-ray concave spectrum is predicted, flattening towards higher energies, where emission from pairs is not important.

An interesting feature of type 4 models is the similarity of different spectra characterized by high compactness ($\ell_e > 300$), same value of the ratio ℓ_e/ℓ_B and different γ_{max}. No matter if X-rays are produced by synchrotron emission, first, or second IC radiation, the X-ray spectral index below $\sim$ 5 keV is approximately the same, and is constrained in the narrow range $0.6 < \alpha_x < 0.8$ for the models shown in figs. 5.12-5.14. As shown by these figures, above 5 keV a concave spectrum is predicted.

Fig. 5.7 summarizes the derived spectral indices between 2 and 10 keV for type 2 models, in which synchrotron photons produce pairs. The important result is that α_{2-10} is constant for $10 < \ell_e < 300$ for almost all models, depending only on the maximum synchrotron energy, and constrained in the range $0.5 < \alpha_x < 0.8$. Steeper spectra are caused by down scattering and/or high energy cut off of the pair distribution, and correspond to $\ell_e > 300$.

For all models where pairs are important, a spectrum breaking at energies $x \sim 1/\tau_T^2 > 10^{-2} \sim 5$ keV into a steeper spectrum suggests that down scattering is important. If this is the case, the value of τ_T can be derived, and consequently the product of the pair yield and the compactness estimated ($\xi\ell_e \approx \tau_T^2$). On the other hand, a steep spectrum at keV energies and flatter above is indicative of the importance of thermal Comptonization, or high energy cut off in the pair distribution.

This steep component can be relevant for interpreting the soft X-ray excess observed in some AGN. As an example, fig. 6.1 shows a steep soft X-ray spectrum, flattening above $\sim$ 0.3 keV.

Thermal Comptonization, producing a steep power law tail in X-rays above the maximum synchrotron frequency may be relevant also for interpreting the steep soft X-ray spectrum of BL Lac objects. Future polarization measurements in X-rays are

the key observation to confirm or rule out this interpretation for BL Lacs. Note also that the convolution of the spectra in fig. 6.1 explains the spectrum of a typical BL Lac, and does not contrast the observed polarization properties of this class of objects. In fact, the highly polarized IR-optical continuum can come from large and pair-free volumes different from those responsible of the X-ray emission.

Models for which $\ell_e \gg \ell_B$ (type 1 and 4) are the only ones that can produce an X-ray spectrum flatter than 0.5, no matter the particle injection mode (monoenergetic, flat or steep power law). These models are then particularly important for interpreting the continuum in those sources which have a flat X-ray spectrum. The best studied source of this kind is the quasar 3C 273. For this source, the spectrum between 2 and 60 keV is characterized by $\alpha_x \sim 0.4$ (Worral *et al.* 1979). Observations by Bezler *et al.* (1984) between 18 and 240 keV gave $\alpha_x \sim 0.2$, suggesting spectral and intensity variations. No high energy steepening or cut off was observed. Marshall *et al.* (1981) reported an X-ray variability timescale of about 1/2 day.

The absence of a high energy steepening is indicative of the absence of cool particles, whose scattering optical depth must be less than unity. This argues in favour of type 1 models, for which pairs are unimportant, and suggests the possibility that the cool particles are reaccelerated. In order to have $\alpha_x \leq 0.5$, the ratio ℓ_e/ℓ_B must exceed 10^3 (*cf.* fig. 3.5), and the injected particle distribution must be a power law of slope s steeper than 3. If the X-ray luminosity is emitted isotropically, then an upper limit to the strength of the magnetic field can be derived:

$$B < 74.5 \left(\frac{\ell_e}{R_{15}} \frac{\ell_B}{\ell_e} \right)^{1/2} \text{ G}$$

where $R = 10^{15}$ cm corresponds to the reported X-ray variability timescale, and $\ell_e \sim 10^3$ to the observed compactness.

For what concerns the γ-ray band, it has to be stressed that all the discussed SSC models predict that γ-ray emission is not negligible, though the γ-ray spectrum is steep ($\alpha_\gamma > 1$), at least for $\ell_e > 10$. This is due to photon-photon absorption, when pair production is important, or to Klein Nishina effects, for models characterized

by a steep power law of injected particles (type 1). This is consistent with the few existing detections or upper limits in the γ-ray band of AGNs. As fig. 6.1 shows, the more extended regions of a source can produce γ-rays. As a consequence, the variability behaviour of γ- and X-rays can be different, and care must be taken when using the observed (or, hopefully, soon observable) α_γ to constrain models of the most compact X-ray component.

The last point I wish to discuss concerns the expected behaviour of SSC spectra in response to variations of the maximum energy γ_{max} of the injected particles, for constant ℓ_e, and to variations in the injection rate ℓ_e, for constant γ_{max}. Unless otherwise specified, the size and the magnetic field strength are assumed to be constant.

Variations in the maximum energy γ_{max}

For models of type 1 most of the power is injected in low energy particles. Then no change in the overall spectrum (at least at X-ray energies) is expected if γ_{max} is changed.

Also for models of type 4 and high compactness ($\ell_e > 300$) no change is predicted, according to figs. 5.12-5.14.

Instead, a dramatic change can occur in models of type 3, for two reasons. First, a change in γ_{max} can let the source switch from a pair-free state to a state in which copious pair production takes place (figs. 5.9 and 5.10), with important consequences on the X-rays produced by the *relativistic* Compton process. Second, as shown in fig. 6.1, *thermal* Comptonization can be important, producing a steep power law tail above the maximum synchrotron energy $x_{s,max}$ ($\propto \gamma_{max}^2$). If the range of variation of γ_{max} yields important pair production anyway, then a change in γ_{max}, will shift in energy the whole steep tail, dramatically changing the observed intensity at a given frequency, for roughly constant (and steep) spectral shape.

Spectral variations in models of type 2 subsequent to changes in γ_{max} are summarized in fig. 5.7 ($x_{s,max} \propto \gamma_{max}^2$), where a non monotonic behaviour of the X-ray

spectral index is indicated, due to the contribution of the second generation of pairs for the models with the highest value of $x_{s,max}$.

Variations in the injected luminosity ℓ_e

Fig. 5.7 shows the relation of the X-ray spectral index on the injected luminosity ℓ_e, for *constant* value of the ratio ℓ_e/ℓ_B. However, as long as $\ell_e/\ell_B < 1$, this figure approximately describes the expected spectral behaviour for models of type 2. In this case, the flux density is roughly proportional to ℓ_e, but its variations depend also on the other parameters of the models.

In models of type 1 and 4 an increase in luminosity corresponds to an increased ratio ℓ_e/ℓ_B, and then to a flatter spectrum (and viceversa. See eqs. 3.30, 3.32, 5.56). If, instead, ℓ_e is constant and the magnetic field increases, then a steepening of the spectrum is predicted by models of type 4 and (less pronounced) of type 1. In this latter case, intensity variations are such to let the total emitted luminosity be constant: the intensity increases at low frequencies, and decreases at higher ones. Depending on the frequency of observations, either a direct or an inverse correlation $\alpha - \ell(x)$ is possible.

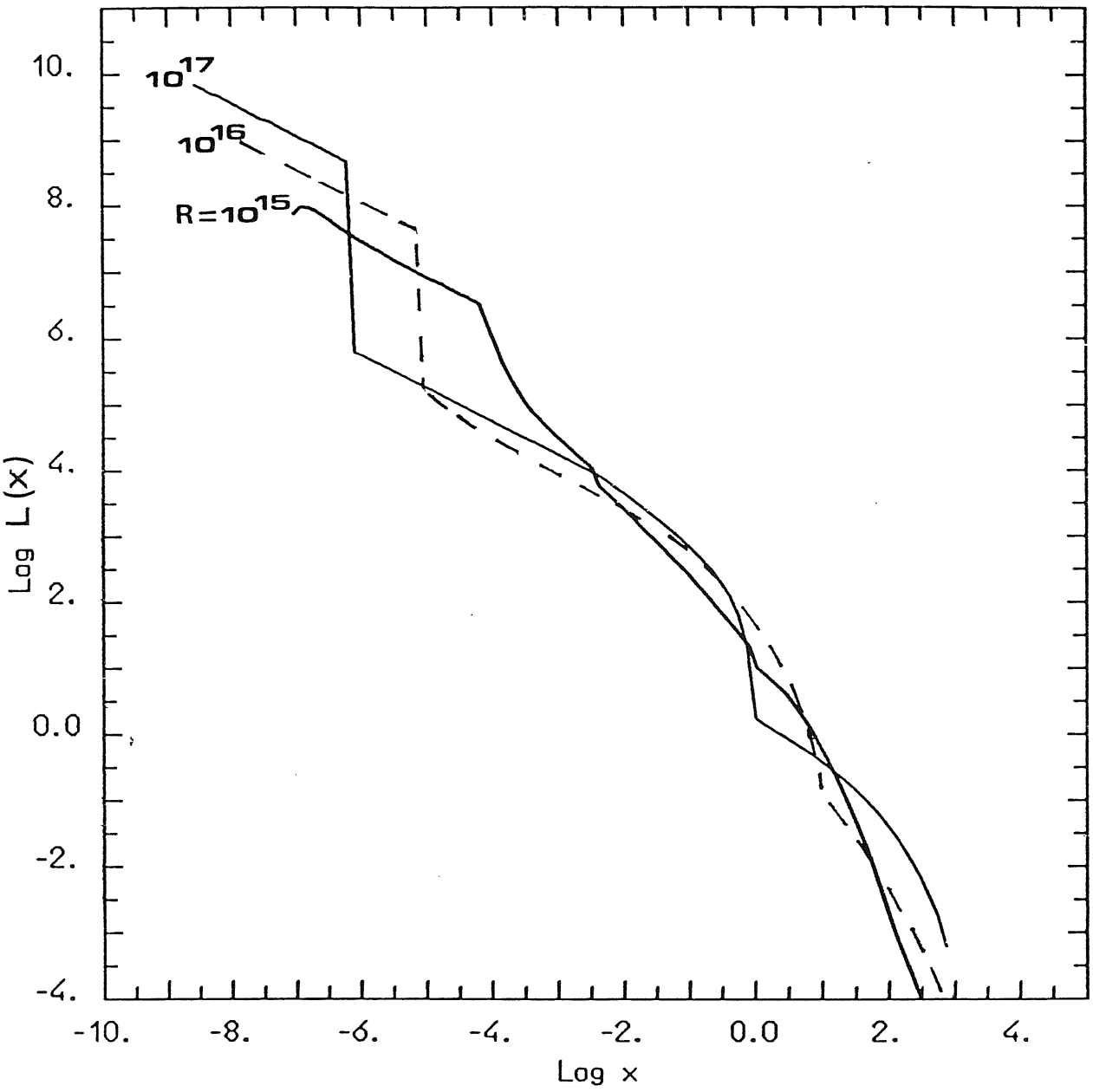

Figure 6.1. SSC specta for $\ell_e = \ell_B$, monoenergetic injection of primary particles at $\gamma_{max} = 10^3$, luminosity $L = 3.7 \times 10^{46}$ erg/s and different sizes $R = 10^{15}$, 10^{16}, 10^{17} cm (indicated by the labels). For these parameters, $\ell_e = 10$, 10^2, and 10^3, respectively. The most compact region dominates the emission only at X-ray energies. Note that $L(x)$ vs. x is plotted.

REFERENCES

Antonucci, R.J. & Ulvestad, J.S., 1985. *Astrophys. J.*, **294**, 158.

Bååth, L.B., Elgered, G., Lundqvist, G., Graham, D., Weiler, K.W., Seielstad, G.A., Tallqvist,G.A. & Schilizzi, R.T., 1981. *Astron. Astrophys.*, **96**, 316.

Bååth, L.B., 1984. *IAU Symp. 110, VLBI and Compact radio Sources*, p.127, eds. Fanti, R., Kellermann, K.I. & Setti, G., Reidel, Dordrecht, Holland.

Begelman, M.C., Sikora, M. & Rees, M.J., 1987. *Astrophys. J.*, **313**, 689.

Bassani, L., Dean, A.J., Di Cocco, G., & Perotti, F., 1985. in *"Active galactic nuclei"*, p. 252, ed. Dyson, J.E., Manchester Univ. press.

Bezler, M., Kendziorra, E., Staubert, R., Hasinger, G., Pietsch, W., Reppin, C., Trumper, J., & Voges, W., 1984. *Astron. Astrophys.*, **136**, 351

Bisnovatyi–Kogan, G.S., Zel'dovich, Ya.B. & Sunyaev, R.A., 1971. *Soviet Astr.–A.J.*, **15**, 17.

Blandford, R.D. & Rees, M.J., 1978, *Pittsburgh Conference in BL Lac Objects*, p.328, Ed. Wolfe, A.N., University of Pittsburgh Press.

Blandford, R.D. & Konigl, A., 1979. *Astrophys. J.*, **23**, 34.

Blumenthal, G.R. & Gould, R.J., 1970. *Rev. of Mod. Physics*, **42**, 237.

Bonometto, S. & Rees,M.J., 1971. *Mon. Not. R. astr. Soc.*, **152**, 21.

Bregman, J.N. *et al.*, 1986. *Astrophys. J.*, **276**, 454.

Brown, R.L., Johnston, K.J., Briggs, F.H., Wolfe, A.M., Neff, S.G. & Walker, R.C., 1981. *Astrophys. J. Lett.*, **21**, 105.

Cavaliere, A., Giallongo, E. & Vagnetti, F., 1986. *Astron. Astrophys.*, **156**, 33.

Cavaliere, A. & Morrisonn, P., 1980. *Astrophys. J. Lett.*, **238**, L63.

Charugin, V.M. & Tsvetanov, Z.I., 1980. *Astrophys. and Space Sci.*, **67**, 309.

Cohen, M.H. & Unwin, S.C., 1984. *IAU Symp. 110, VLBI and Compact Radio Sources*, p.95, eds. Fanti, R., Kellermann, K.I. & Setti, G., Reidel, Dordrecht.

Cruz-Gonzales, I. & Huchra, J.P., 1984. *Astron. J.*, **89**, 441.

Eckart, A., Hill, P., Johnston, K.J., Pauliny-Toth, I.I.K., Spencer, J.H. & Witzel, A.A., 1982. *Astron. Astrophys.*, **108**, 157.

Ennis, D.J., Neugebauer, G. & Werner, M., 1982. *Astrophys. J.*, **262**, 460.

Fabian, A.C., 1984. In: *X-ray and UV Emission From Active Galactic Nuclei*, p.232, eds. Trümper,J. & Brinkmann, W., Max Planck, Garching.

Fabian, A. C., Blandford, R.D., Guilbert, P.W., Phinney, E.S. & Cuellar, L., 1986, *Mon. Not. R. astr. Soc.*, **211**, 931.

Gear, W.K., Robson, E.I., Ade, P.A.R., Griffin, M.H., Brown, L.M.J., Smith, M.G., Nolt, I.G., Rodostitz, J.V., Veeder, G. & Lebofsky, L., 1985. *Astrophys. J.*, **291**, 511.

Ginzburg, V.L. & Syrovatskii, S.I., 1965. *Ann. Rev. A. A.*, **3**, 297.

Ghisellini, G., 1987. *Mon. Not. R. astr. Soc.*, **224**, 1.

Ghisellini, G., Maraschi, L. & Treves, A., 1985, *Astron. Astrophys.*, **146**, 204.

Ghisellini, G., Maraschi, L., Tanzi, E.G. & Treves, A., 1986. *Astrophys. J.*, in press.

Gould, R.J., 1979, *Astron. Astrophys.*, **76**, 306.

Guilbert, P.W., Fabian, A.C. & Rees, M.J., 1983. *Mon. Not. R. astr. Soc.*, **205**, 593.

Hoyle, F.R.S., Burbidge, G.R. & Sargent, W.L.W., 1966. *Nature*, **209**, 751.

Jelley, J.V., 1966. *Nature*, **211**, 472.

Jones, F.C., 1968. *Phys. Rev.*, **167**, 1159.

Jones, T.W., O'Dell, S.L., & Stein, W.A., 1974. *Astrophys. J.*, **188**, 353.

Kardashev, N.S., 1962, *Soviet Astr. - A.J.*, **6**, 317.

Katz, J.I., 1976. *Astrophys. J.*, **206**, 910.

Kazanas, D., 1984. *Astrophys. J.*, **287**, 112.

Kellermann, K.I., Jauncey, D.L., Cohen, M.H., Shaffer, B.B., Clark, B.G., Broderick, J., Ronnang, B., Rydbeck, O.E.H., Matveyenko, L., Moiseyev, I., Vitkevitch, V.V., Cooper, B.F.C. & Batchelor, R., 1971. *Astrophys. J.*, **169**, 1.

Kellermann, K.I., *et al.*, 1977. *Astrophys. J.*, **211**, 658.

Kōnigl, A.P., 1981. *Astrophys. J.*, **243**, 700.

Landau, R., Jones, T.W., Epstein, E.E., Neugebauer, G., Soifer, B.T., Werner, M.W., Puschell, J.J. & Balonek, T.J., 1983. *Astrophys. J.*, **268**, 68.

Lawrence, C.R., Readhead, A.C.S., Linfield, R.P., Payne, D.G., Preston, R.A., Schilizzi, R.T., Porcas, R.W., Booth, R.S. & Burke, B.F., 1985. *Astrophys. J.*, **296**, 458.

Ledden, J.E. & O'Dell, S.L., 1985. *Astrophys. J.*, **298**, 630.

Lightman, A.P., 1982. *Astrophys. J.*, **253**, 842.

Lightman, A.P. & Zdziarsky, A.A., 1987. *Astrophys. J.*, **319**, 643.

Madau, P., Ghisellini, G. & Persic, M., 1986. *Mon. Not. R. astr. Soc.*, ???, ???.

Madejsky, G.M. & Schwartz, D.A., 1983. *Astrophys. J.*, **275**, 467.

Maraschi, L., Ghisellini, G., Tanzi, E.G. & Treves, A., 1986. *Astrophys. J.*, in press.

Maraschi, L., 1987. *"Variability of Galactic and Extragalactic X-ray Sources"*, p.101, Ed. Treves, A.

Marshall, N., Warwick, R.S., & Pounds, K.A., 1981. *Mon. Not. R. astr. Soc.*, **194**, 987

Marscher, A.P., 1977. *Astrophys. J.*, **216**, 244.

McCray, R., 1969. *Astrophys. J.*, **156**, 329.

Moore, R.L. & Stockman, H.S., 1984. *Astrophys. J.*, **279**, 465.

Moskalik, P. & Sikora, M., 1986. *Nature*, **319**, 649.

Orr, M.J.L & Browne, I.W.A., 1982. *Mon. Not. R. astr. Soc.*, **200**, 1067.

Pacholczyk, A.G., 1970, *"Radio Astrophysics"*, Freeman, San Francisco.

Pauliny-Toth, I.I.K, Preuss, E., Witzel, A., Graham, D., Pearson, T.J. & Readhead, A.C.S., 1981. *Astrophys. J.*, **248**, 61.

Pearson, T.J. & Readhead, A.C.S., 1981. *Astrophys. J.*, **248**, 61.

Phinney, E.S., 1983. *Ph. D. Thesis*, University of Cambridge.

Pozdnyakov, L.A., Sobol', I.M. & Sunyaev, R.A., 1977. *Soviet Astr. - A.J.*, **21**, 708.

Pozdnyakov, L.A., Sobol', I.M. & Sunyaev, R.A., 1979, *Soviet Astr. Letters*, **5**, 149.

Preuss, E. & Fosbury, R.A.E., 1983. *Mon. Not. R. astr. Soc.*, **204**, 783.

Rees, M.J., 1967a. *Mon. Not. R. astr. Soc.*, **136**, 279.

Rees, M.J., 1967b. *Mon. Not. R. astr. Soc.*, **137**, 429.

Rees, M.J., Begelman, M.C., Blandford, R.D. & Phinney, E.S., 1982. *Nature*, **295**, 17.

Reynolds, S.P., 1982. *Astrophys. J.*, **256**, 13.

Rybicki, G.B. & Lightman, A.P., 1979, *Radiative Processes in Astrophysics*, New York, Wiley Interscience.

Rothshild, R.E., Mushotsky, R.F., Baity, W.A., Gruber, D.E., Mattheson, J.L. & Peterson, L.E., 1983. *Astrophys. J.*, **269**, 423.

Shapiro, S.L., Lightman, A.P. & Eardley, D.M., 1976. *Astrophys. J.*, **204**, 187.

Shever, P.A.G. & Readhead, A.C.S., 1979. *Nature*, **277**, 182.

Sunyaev, R.A. & Titarchuk, L.G., 1980. *Astron. Astrophys.*, **86**, 121.

Svensson, R., 1982. *Astrophys. J.*, **258**, 335.

Svensson, R., 1984a. *Mon. Not. R. astr. Soc.*, **209**, 175.

Svensson, R., 1984b. In: *X-ray and UV Emission From Active Galactic Nuclei*, p.152, eds. Trümper, J. & Brinkmann, W., Max Planck, Garching.

Svensson, R., 1986. In *Radiation Hydrodynamics in Stars and Compact Objects, IAU Coll. No. 89*, in press.

Svensson, R., 1987. *Mon. Not. R. astr. Soc.*, **227**, 403.

Terrel, J., 1959. *Phys. Rev.*, **116**, 1041.

Unwin, S.C., Cohen, M.H., Pearson, T.J., Seielstad, C.A., Simon, R.S., Linfield, R.P. & Walker, R.C., 1983. *Astrophys. J.*, **271**, 536.

Unwin, S.C., Cohen, M.H., Biretta, J.A., Pearson, T.J., Seielstad, C.A., Walker, R.C., Simou, R.S. & Linfield, R.P., 1985. *Astrophys. J.*, **289**, 109.

Urry, C. M., 1984. *Ph.D. Thesis*, University of Maryland.

Urry, C.M. & Shafer, R.A., 1984. *Astrophys. J.*, **280**, 569.

Urry, C.M., Mushotsky, R.F. & Holt, S.S., 1986. *Astrophys. J.*, **305**, 369.

Wandel, A., Mushotsky, R.F., 1986. *Astrophys. J. Lett.*, **306**, L61.

Weiler, K.W. & Johnston, K.J., 1980. *Mon. Not. R. astr. Soc.*, **190**, 269.

Weistrop, D., Shaffer, D.B., Hintzen, P. & Romanishin, W., 1985. *Astrophys. J.*, **292**, 614.

Wilkes, B.J., & Elvis, M., 1987. to appear in *the Astrophys. J.* December 1.

Wood, K.S. *et al.*, 1984. *Ap. J. Suppl.*, **56**, 507.

Worral, D.M., Mushotzky, R.F., Boldt, E.A., Holt, S.S., & Serlemitsos, P.J., 1979. *Astrophys. J.*, **232**, 683.

Zdziarsky, A.A. & Lightman, A.P., 1985, *Astrophys. J. Lett.*, **294**, L79.

Zdziarsky, A.A., 1985. *Astrophys. J.*, **289**, 514.

Zdziarsky, A.A., 1986a. Harvard preprint n. 2177

Zdziarsky, A.A., 1986b. *Astrophys. J.*, **305**, 45.

Zdziarksy. A.A. & Lamb, D.Q., 1986. *Astrophys. J. Lett.*, **309**, L79.

Zdziarsky, A.A., 1987. *"Variability of Galactic and Extragalactic X-ray Sources"*, p.121, Ed. Treves, A.

Zensus, J.A., Porcas, R.W. & Pauliny-Toth, I.I.K., 1984. *Astron. Astrophys.*, **133**, 27.